Evaluating Salmonid and Stream Ecosystem Response to Conservation Measures and Environmental Stressors in the Columbia River Basin: Annual Report 2024

publication date: May 1, 2023

Authors: Casey Justice, Matthew Kaylor, Anna Ringelman, Ben Staton, Marshall Wolf, and David Graves

Technical Report 25-03

Columbia River Inter-Tribal Fish Commission

700 NE Multnomah St, Ste 1200, Portland OR 97232 · (503)238-0667 · www.critfc.org

Evaluating Salmonid and Stream Ecosystem Response to Conservation Measures and Environmental Stressors in the Columbia River Basin

BPA Project # 2009-004-00

Report covers work performed under BPA contract # 94441

Report was completed under BPA contract # 96464

Report covers work performed from: January 2024– December 2024

Authors: Casey Justice, Matthew Kaylor, Anna Ringelman, Ben Staton, Marshall Wolf and David Graves

Columbia River Inter-Tribal Fish Commission, Portland, OR

Report Created: May 1, 2025

This report was funded by the Bonneville Power Administration (BPA), U.S. Department of Energy, as part of BPA's program to protect, mitigate, and enhance fish and wildlife affected by the development and operation of hydroelectric facilities on the Columbia River and its tributaries. The views in this report are the author's and do not necessarily represent the views of BPA.

Table of Contents

List of Common Abbreviations

Abbreviation	Description
AqI	Aquatic Inventories Project
BPA	Bonneville Power Administration
BSR	Biologically Significant Reach
CC or CAT	Catherine Creek
CHaMP	Columbia Habitat Monitoring Program
CRB	Columbia River basin
CRITFC	Columbia River Inter-Tribal Fish Commission
CTUIR	Confederated Tribes of the Umatilla Indian Reservation
CTWSRO	Confederated Tribes of the Warm Springs Reservation of Oregon
DEQ	Oregon Department of Environmental Quality
EPA	Environmental Protection Agency
FL	Fork Length
GR	Grande Ronde River
GRMW	Grande Ronde Model Watershed
(SS)LCM	(State-Space) Life Cycle Model
LOS	Lostine River
MFJD	Middle Fork John Day River
MIN	Minam River
NOAA	National Oceanic and Atmospheric Administration
NPCC	Northwest Power and Conservation Council
ODFW	Oregon Department of Fish and Wildlife
OSU	Oregon State University
OWRD	Oregon Water Resources Department
PNAMP	Pacific Northwest Aquatic Monitoring Program
RM&E	Research, Monitoring, and Evaluation
UAS	Unmanned Aircraft System
UGR	upper Grande Ronde River
USBR	U.S. Bureau of Reclamation
USFS	U.S. Forest Service
USGS	U.S. Geological Survey
USWCD	Union Soil and Water Conservation District

EXECUTIVE SUMMARY

Background and objectives

This project employs a comprehensive and interdisciplinary approach to guide restoration planning and management actions in the Grande Ronde River and broader Columbia River basins by addressing the following key objectives: 1) Assess current habitat conditions relative to historical or reference target values; 2) Identify and evaluate factors limiting salmonid populations at multiple spatial and temporal scales; 3) Determine whether the current pace of restoration efforts can mitigate habitat degradation and climate change effects; 4) Examine life stage-specific fish responses to habitat conditions, food web dynamics, and land use changes; 5) Integrate life stage-specific responses to population-level impacts using life cycle models; and 6) Support CRITFC Tribes and other regional partners in addressing emerging concerns throughout the Columbia River Basin.

Below we provide abbreviated summaries of progress made in 2024 and key findings for individual project components. We group individual project components into four categories: 1) Habitat monitoring and remote sensing; 2) Fish ecology, productivity, and limiting factors; 3) Biological responses to restoration and habitat change; and 4) RM&E coordination and adaptive management. Note that aspects of many individual project components fall within two or more of these broad categories.

Progress and key findings

1. Habitat monitoring and remote sensing

1.1 Habitat surveys using the Tributary Habitat Assessment Protocol (TribAP)

- In 2021 and 2022, we worked collaboratively with the GRMW (funded partly by USFS) to survey fish habitat across a total of 105 stream kilometers surveys using CRITFC's Tributary Habitat Assessment Protocol (TribAP). Surveys covered the current extent of Chinook Salmon spawning and rearing habitat within the Grande Ronde Atlas Tier 1 and 2 priority areas.
- In 2024, we completed the QAQC and metric calculation process and provided a summary of the data as well as links to the final datasets.
- A summary of selected habitat limiting factors (side channels, riparian cover, pools, and large wood) indicated relatively high values in some metrics associated with recent restoration projects, but sub-optimal conditions remain within many biologically significant reaches (BSRs).

1.2 Water temperature monitoring

- CRITFC actively maintains 86 water temperature monitoring sites in the upper Grande Ronde, Catherine Creek, and Minam River watersheds where hourly, year-round water

temperature data is collected. Additionally, we maintain an SQL database which computes a suite of daily, weekly, and annual water temperature metrics for each site.

- In 2024, we downloaded data from 76 of our 86 temperature sites and summarized a subset of annual water temperature metrics at the biologically significant reach (BSR) and stream scale over the recent 10 year time period, and in 2024 specifically.
- Maximum weekly maximum temperature (MWMT) exceeded the EPA temperature standard of 16 °C for salmon and trout core rearing in 92% of the streams currently monitoring by CRITFC, while 67% of the streams exceeded the non-core rearing and migration standard of 18 °C. Additionally, the number of days > 18 °C averaged 43 and was as high as 102 in some locations. These data clearly indicate that high water temperature continues to be a serious limiting factor for salmonid recovery in the upper Grande Ronde basin and that management actions aimed at reducing summer water temperatures, increasing thermal heterogeneity, and improving climate change resiliency should be prioritized.

1.3 Thermal imagery acquisition (UAS)

- During August 2024, we collected thermal and true color RGB imagery using a UAS (drone) at three sites in the Meadow Creek watershed that are planned for restoration totaling 110.7 acres of floodplain area.
- The objective of this work was to test the feasibility and accuracy of UAS-based thermal imagery for assessing changes in stream thermal heterogeneity (particularly cold-water refugia) in response to river restoration in a temperature-impaired watershed. Should this technology prove effective, it could provide a cost-effective approach to assess both spatial and temporal (i.e., multiple flights per year) patterns in water temperature as it relates to restoration efforts and climate change.
- Data analysis from this effort is still in progress, but preliminary results indicate this methodology will likely provide fine-scale (5-10 cm/pixel resolution) maps of water temperature with sufficient precision to identify and delineate thermal refugia in locations with relatively open riparian canopy. Absolute accuracy of the thermal imagery is still under investigation, but manufacturer specifications for the UAS used in this study (Mavic 3T) suggest an average accuracy of < 2 °C can be expected.

1.4 Thermal imagery acquisition (FLIR)

- We contracted NV5 to acquire airborne thermal infrared (TIR) and true color imagery data during the summer of 2024 covering a total of 570 km of stream including the Grande Ronde lower tributaries, Upper Grande Ronde River, Lostine River, Catherine Creek, and Minam River. This imagery acquisition was cosponsored by the Grande Ronde Model Watershed (GRMW) and Union Soil and Water Conservation District (USWCD).
- A summary report documenting the contract specifications, data acquisition procedures, processing methods, and analysis of the final datasets is provided in Appendix B.

- These data will be used by CRITFC to quantify the spatial distribution and amount of cold-water refugia within the project extent and to evaluate how thermal heterogeneity has changed over time at both the watershed and restoration site scales. Additionally, these data are being used by basin partners (GRMW and USWCD) to guide restoration prioritization through the ATLAS process and to assess project impacts to water temperature.

2. Fish ecology, productivity, and limiting factors

2.1 Juvenile salmonid distribution in the Middle Fork John Day River

- We conducted watershed-wide snorkel surveys across the Middle Fork John Day in 2024 in collaboration with Confederated Tribes of the Warm Springs Reservation of Oregon (CTWSOR) and the Oregon Department of Fish and Wildlife (ODFW).
- The goal of this study is to build a long-term juvenile salmonid distribution data set to evaluate how salmonid distributions respond to climate conditions, restoration, and disturbance.
- This was the third year of watershed-scale surveys (along with 2021 and 2023), and we surveyed 46 mainstem reaches (10.6 km) and 110 tributary reaches (8.1 km) across 18 tributaries. We plan to conduct surveys across the same extent in July 2025 with project partners.

2.2 Spatial Relative Reproductive Success study

- We developed a study to expand the utility of the Relative Reproductive Success genetic approach to assess spatial patterns of female Chinook Salmon reproductive success.
- In 2024, we supplemented spawning ground surveys in MFJD, Catherine Creek, and Lookingglass Creek to increase the number of sampled and genotyped adults with known spawning locations. Adults were also sampled using the same approach in 2023 for MFJD and Catherine Creek.
- Offspring from 2023 parents have been sampled from screw traps since fall 2024 and will continue to be sample through spring 2025. Offspring from 2024 parents will be sampled in fall 2025 and spring 2026.
- Adult and offspring tissue samples will be sent to Hagerman Genetics Lab and genotyped, followed by PBT analyses to assign offspring to female parents. We will then evaluate spatial patterns of the number of offspring assigned to each female parent relative to other females.

2.3 Juvenile Chinook Salmon dispersal study

- We published a manuscript quantifying patterns and drivers of juvenile Chinook Salmon dispersal from their redd of origin to summer rearing habitats across the Middle Fork John Day (MFJD) basin using genetic parentage-based tagging (Kaylor et al. 2025 *Movement Ecology*)

- We are also evaluating fry dispersal from redds to floodplain habitats in collaboration with ODFW and CTWSOR. In 2024, we sampled fry from floodplain habitats across the MFJD that will be paired to parents sampled in 2023. Samples were sent to Hagerman Genetics Lab in winter 2025 for genotyping and parentage assignments. Fry dispersal was also evaluated in 2021 and we plan to analyze 2021 and 2024 fry dispersal data in 2025 and submit a manuscript in 2026.

3. Biological responses to restoration and habitat change

3.1 Meadow Creek historical outmigrant trap data and riparian vegetation analyses

- We analyzed the historic juvenile *O. mykiss* outmigration trap data from the Meadow Creek watershed collected by the USFS from 1987-1999. We produced yearly outmigration estimates for *O. mykiss* along with proportional basin production estimates.
- Analysis was conducted on riparian vegetation height change between 2009 and 2020 following the 2013-2014 large wood and riparian planting restoration actions. We utilized the previously collected LiDAR data within the Meadow Creek watershed with particular focus placed on the Starkey Experimental Forest and Range.
- These two datasets along with the analysis of juvenile fish abundances and their habitat published in the 2024 annual report were presented at Oregon AFS in February of 2025: Wolf, J.M., Justice, C., Flitcroft, R. L. Synthesizing three decades of Steelhead focused restoration and research in Oregon's Blue Mountains. ORAFS, Feb 28, 2025.

3.2 Meadow Creek response to watershed-scale restoration – pilot year

- We conducted a pilot study of aquatic biota in the Meadow Creek watershed in 2024 in collaboration with Confederated Tribes of the Umatilla Indian Reservation (CTUIR) and the Oregon Department of Fish and Wildlife (ODFW) to evaluate salmonid recapture rates and relative densities to inform the finalized study design for restoration monitoring and evaluation.
- Pilot study data was analyzed and findings utilized to refine the Meadow Creek aquatic biota study design and sampling methods in preparation for the next several years of pre-restoration monitoring.

3.3 Evaluation of IGF1 as a tool for assessing growth in juvenile salmonids in Lookingglass Creek

- We conducted a paired mark-recapture and insulin-like growth factor (IGF1) field pilot study in 2024 in Lookingglass Creek to evaluate the feasibility of using IGF1 concentration as a metric of growth.
- Blood plasma IGF1 assays were completed in April 2025, and exploratory data analysis is currently ongoing to evaluate the relationship between individual growth rates and IGF1 values using a mixed effects model.

3.4 LCM Phase I: Development of spring Chinook statistical estimation Life Cycle Model

- We have finalized development of the statistical life cycle model for Grande Ronde spring Chinook salmon and have made significant progress on a manuscript documenting it. The draft manuscript text/figures are included in Appendix C and complete mathematical details are in Appendix D.
- A state-space model integrated biological and environmental data from throughout the Chinook salmon life cycle.
- Early-life survival and growth were density-dependent for all populations.
- Later survival was linked to growth, indicating delayed effects of density dependence.
- Many populations displayed synchronous dynamics, indicating shared external drivers.
- Output will aid in evaluating potential outcomes of habitat restoration actions.

4. RM&E coordination and adaptive management

4.1 Adaptive management

- We continued our involvement and contributions towards the Grande Ronde Atlas, a collaborative process to prioritize restoration effort through Adaptive Management.
- In 2024, we participated in the Grande Ronde State of the Science meeting hosted by GRMW to discuss restoration progress, RM&E findings, and emerging uncertainties/questions pertinent to management efforts in the basin.
- We regularly attended and participated in monthly Middle Fork John Day Intensively Monitored Watershed (MFIMW) meetings, as well as the broader Joint John Day Basin Partnership/MFIMW meeting.

4.2 RM&E coordination and assistance

- We worked with CTUIR, ODFW, and USFS to formalize a study design to evaluate fish, invertebrate, and ecosystem response to watershed-scale restoration in the Meadow Creek watershed and we led efforts to finalize study protocols.
- We conducted a pilot field season in the Meadow Creek watershed along with CTUIR and ODFW to evaluate salmonid growth, salmonid diet, fish community composition and distribution, and food web characteristics, which was used to inform the feasibility of future restoration RM&E.
- We worked closely with OSU, CTUIR, and ODFW to develop a study and assist data collection for a master's student project evaluating juvenile Chinook dispersal in Catherine Creek.
- We worked with CTWSOR and ODFW to develop and implement a study assessing spatial patterns of adult Chinook Salmon relative reproductive success and another study evaluating Chinook fry dispersal to floodplain habitats. We also collaborated with CTWSOR and ODFW to conduct snorkel surveys across nearly 20 km, which were shared with CTWSOR to evaluate response to recent restoration.

- We worked closely with ODFW and NOAA to finalize a state-space life cycle model for Grande Ronde spring Chinook Salmon, which will be used to assess potential response to restoration scenarios that will be collectively developed by basin partners.

4.3 Development and refinement of RM&E methodology

- We made progress on updating the CRITFC-developed snorkel detection model (Staton et al. 2022) by incorporating paired snorkel survey and mark-recapture data collected in 2023.
- We made substantial progress towards assessing the feasibility and reliability of IGF1 to evaluate juvenile salmonid growth with a single capture event. This method may be particularly useful and broadly applicable to assessing growth in highly complex habitat conditions that are typically associated with large-scale floodplain restoration (e.g., Stage 0), where recapture of individuals is challenging.
- We are working with CTWSOR, CTUIR, and ODFW to extend the utility of Relative Reproductive Success and Parentage-Based Tagging as tools to evaluate spatial patterns of adult Chinook Salmon reproductive success within and among three watersheds. We plan to outline lessons learned and identify methodological considerations that we can document and share to provide a road map for others interested in implementing this approach.
- We are evaluating the use of two emerging technologies to better map and quantify thermal heterogeneity in riverscapes and response to restoration: 1) thermal imagery mapping using unmanned aircraft systems (UAS) and 2) mobile temperature and depth (TAD) devices to efficiently collect fine-scale, three-dimensional temperature data, which may identify sub-surface temperature anomalies, thereby complimenting the UAS imagery mapping.

Dissemination of project findings

- Staff from CRITFC's River Ecology group delivered 8 scientific presentations during 2024 describing project findings.
- We produced 5 peer-reviewed publications and 2 technical reports during the 2024 reporting period.

Conclusions

This report highlights significant research and monitoring accomplishments completed in 2024 by the Columbia River Inter-Tribal Fish Commission's River Ecology Group. We implemented advanced monitoring methods including helicopter-based thermal imagery, drone-based (UAS) thermal imagery, and field sampling using the Tributary Habitat Assessment Protocol (TribAP) in the upper Grande Ronde and Wallowa River basins to provide high-resolution datasets characterizing habitat complexity, water temperature, and cold-water refugia—key indicators of salmonid habitat quality. Results show measurable improvements in several restored areas, yet many reaches remain below ecological targets, especially on private lands, emphasizing the need for continued investment and strategic restoration planning.

We conducted several field studies and finalized prior studies focused on salmonid responses to environmental conditions and habitat changes. Studies revealed that juvenile salmonid dispersal is strongly influenced by stream temperature gradients, with many individuals relocating to cooler tributaries. Long-term snorkel surveys in the Middle Fork John Day River (MFJD) highlighted how thermal and hydrologic variation drives shifts in summer rearing distribution for Chinook Salmon, potentially increasing density-dependence in addition to thermal-induced stress. A parentage-based tagging study was launched to understand how spawning location affects female reproductive success, aiming to pinpoint high-value spawning habitats and be used as an RM&E tool to assess trends in productivity over time and in response to restoration and other management actions.

Finalizing the state-space life cycle model for Grande Ronde Chinook was a key modeling milestone. This model integrates empirical data from habitat, demographic, and environmental variables to simulate population dynamics and assess management interventions. Preliminary results indicate strong early-life density dependence and positive effects of increasing rearing habitat quantity and quality on juvenile growth and survival. A companion simulation framework is underway to test future restoration and management scenarios, making this a powerful tool for guiding basin-wide salmon recovery.

We made substantial progress on several projects focused on evaluating aquatic ecosystem response to restoration and habitat change. An analysis of historic *O. mykiss* outmigrant trap data from the Meadow Creek watershed produced robust estimates of abundance and productivity that provides historical context and pre-treatment data to support on-going RM&E efforts evaluating restoration effectiveness. We also worked closely with CTUIR, ODFW and USFS to implement a pilot field season, characterizing fish distribution, relative abundances, growth, and consumption across the watershed which culminated in the development of a collaborative aquatic biota RM&E study design. Lastly, we evaluated empirical *O. mykiss* growth rates in Lookingglass Creek relative to blood plasma IGF1 concentrations, which showed promising results for using IGF1 to evaluate growth response in complex habitat conditions – such as anticipated for Meadow Creek post-restoration – where recapturing individuals may be preclusive.

We supported CRITFC member tribes and regional partners through multiple avenues in 2024. We contributed to Adaptive Management planning through the Grande Ronde Model Watershed partnership and the Middle Fork John Day Intensively Monitored Watershed, and we actively participated in several other science forums (e.g., PNAMP). We collected or coordinated the acquisition of spatial data (e.g., thermal imagery, habitat conditions, salmonid abundance and distribution) that we provided to partners to inform restoration prioritization under climate change. Our collective collaboration with tribal, state, and federal partners strengthened cross-basin RM&E integration, supporting consistent methodologies and data sharing across the Columbia River Basin.

Overall, our 2024 accomplishments reflect a coordinated, data-rich approach to inform salmon recovery efforts in the Columbia River Basin at local and regional scales. The integration of cutting-edge remote sensing, directed field studies, and predictive modeling provides robust tools for adaptive, climate-resilient restoration strategies. These efforts support informed decision-making by land managers, funding agencies, and Tribal partners, and enhance our collective ability to restore and sustain culturally and ecologically vital fish populations.

INTRODUCTION

A tremendous amount of effort and mitigation funding have been dedicated towards recovering depleted salmon and steelhead stocks within the Columbia River Basin, and habitat restoration and protection remains the largest funding category within the Northwest Power and Conservation Council's Fish and Wildlife Program. RM&E is a crucial component of the adaptive management process to iteratively improve restoration efficacy and maximize positive impacts towards recovery goals. The Columbia River Inter-Tribal Fish Commission (CRITFC) River Ecology Group is conducting a research, monitoring, and evaluation (RM&E) project that provides robust, data-driven evaluation of restoration effectiveness and critical analyses, data products, targeted studies, and decision-support tools to aid in strategic planning of restoration and management actions.

This project employs a comprehensive and interdisciplinary approach to guide restoration planning and management actions by addressing the following key objectives: 1) Assess current habitat conditions relative to historical or reference target values; 2) Identify and evaluate factors limiting salmonid populations at multiple spatial and temporal scales; 3) Determine whether the current pace of restoration efforts can mitigate habitat degradation and climate change effects; 4) Examine life stage-specific fish responses to habitat conditions, food web dynamics, and land use changes; 5) Integrate life stage-specific responses to population-level impacts using life cycle models; and 6) Support CRITFC Tribes and other regional partners in addressing emerging concerns throughout the Columbia River Basin.

Since its inception in 2009, the project has continuously evolved to better serve CRITFC member Tribes and regional stakeholders while adapting to new scientific advancements and emerging environmental challenges. In particular, our work has increasingly emphasized climate change effects and approaches to mitigate for these impacts, food web dynamics as an essential component of habitat quality, the development and refinement of monitoring methodologies that capitalize on advancements in remote sensing technology, and the application of a holistic analytical framework that assesses ecological responses across entire life cycles and at the population scale. These project components and RM&E efforts complement and enhance other Fish and Wildlife Program-funded projects and Tribal RM&E initiatives by integrating remote sensing technologies (e.g., bathymetric LiDAR, thermal imagery, drone-based habitat assessments), application and refinement of analytical/methodological approaches (e.g., life cycle models, genetics, stable

isotopes, and IGF-1 growth hormone), and scalable modeling frameworks that translate localized fish and ecosystem response into population- and watershed-scale outcomes.

Geographically, this project is largely focused on the Grande Ronde River basin (tributary of the Snake River in the Columbia River basin) and the John Day River basin, but with applications and testing of research, monitoring, and evaluation approaches also occurring in other Columbia River tributaries.

Study Area

This project is occurring primarily in the Grande Ronde River and its tributaries, which originates in the Blue Mountains of NE Oregon and flows 334 km to its confluence with Snake River (Figure 1). Focal study watersheds include the upper Grande Ronde River (UGR) upstream of the town of La Grande, Catherine Creek (CAT), and to a lesser extent the Minam River (MIN). Spring Chinook Salmon populations in these basins were listed as threatened under the Endangered Species Act in 1992. Population declines over the past century were due in part to overharvest, hydropower impacts, and degraded habitat conditions resulting from intensive anthropogenic disturbances including timber harvest, cattle grazing, levee and road construction, stream diversions for irrigation, and removal of beaver populations (*Castor canadensis*). Specifically, stream temperature, streamflow, habitat diversity, large wood structures, and quantity of key habitats such as large pools, have been identified as key limiting factors for recovery of salmonid populations in these basins. The Minam River is a designated wilderness area and represents a minimally impacted reference stream. We additionally conduct limited research in nearby basins with similar biophysical conditions and land use history, such as Lookingglass Creek (Grande Ronde basin) and the Middle Fork John Day River.

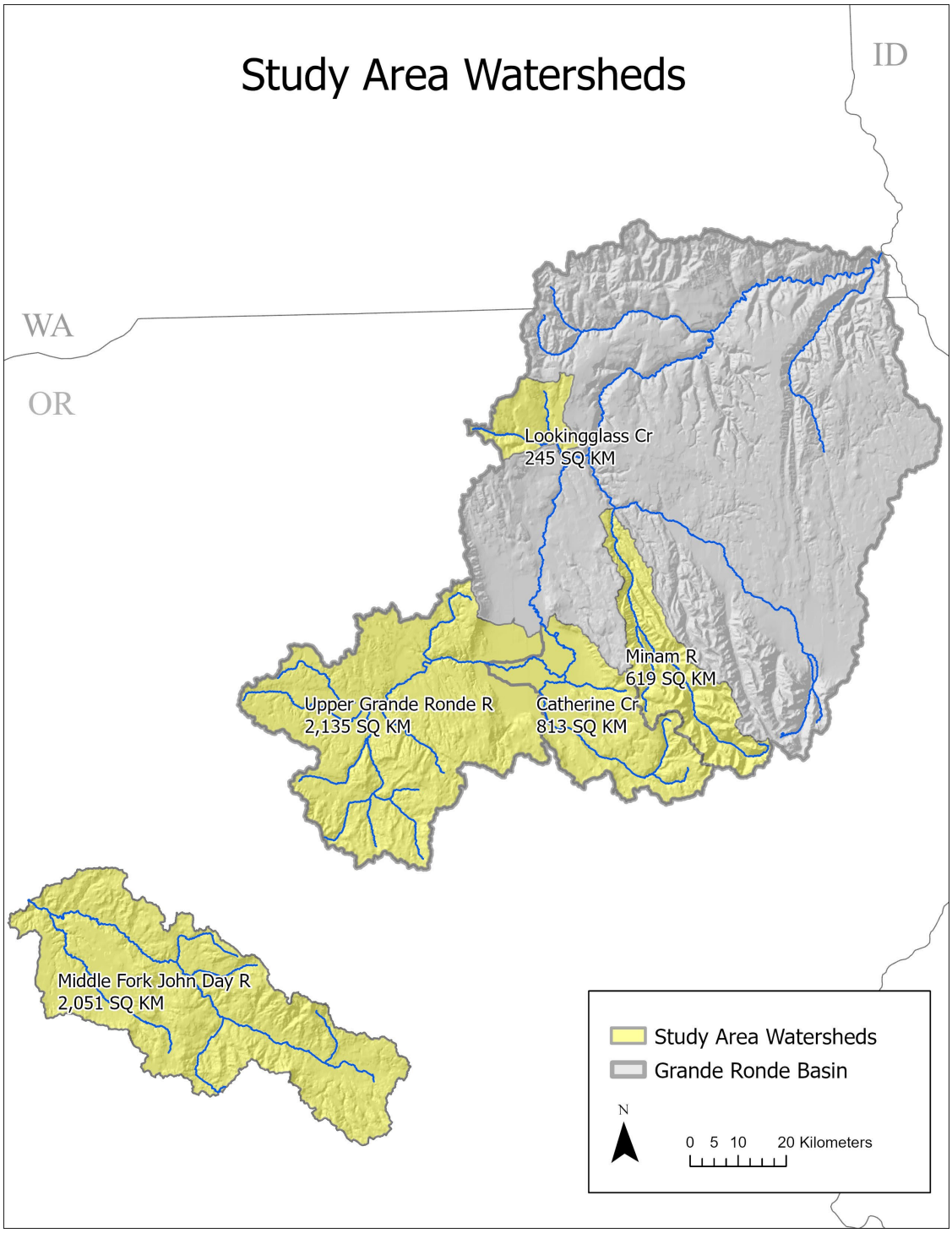

Figure 1. Study area in the Grande Ronde River basin, NE Oregon. Focal watersheds include the upper Grande Ronde River, Catherine Creek, and Minam River. The upper Grande Ronde and Catherine Creek are basins with significantly impacted habitat, currently undergoing restoration in various locations. The Minam River basin is the local reference area that has far less anthropogenic impact.

PROJECT COMPONENTS

1. Habitat monitoring and remote sensing

1.1 Habitat surveys using the Tributary Habitat Assessment Protocol (TribAP)

Introduction

CRITFC began monitoring fish habitat conditions in the upper Grande Ronde River, Catherine Creek, and Minam River in 2009. After initially drafting our own agency stream monitoring protocol, CRITFC supported the development and implementation of the Columbia Habitat Monitoring Program (CHaMP 2016). Data collected from these programs (2011-2017) provided the basis for describing status and trends of limiting habitat factors for salmonids in the study basins. In 2017, Bonneville Power Administration (BPA) commissioned a review of the Columbia Habitat Monitoring Program (CHaMP) which highlighted potential problems or shortcomings concerning repeatability, efficiency, and validity of some monitoring methods, and with extrapolation of metrics to unsampled portions of the basin. In response to these concerns and feedback from the Independent Science Review Panel (ISRP), our project reassessed the components that would ensure the success and longevity of a new monitoring approach and allow for the continuation of status and trends analysis. We identified four major considerations when reconceptualizing a new monitoring strategy: 1) the methods used should be based on regionally accepted practices, which are both repeatable and could reliably be used for comparison to previously-derived metrics from other protocols, 2) it should incorporate measures of long-term impacts of land use and climate change, 3) it increases efficiency of previous fish habitat survey methodologies by reducing the intensity of ground-based measurements and integrating data collected by unmanned aircraft systems (UAS), and 4) it promotes partnership and garners regional support as a means for funding and continued long-term monitoring.

Using these considerations as a guide, we developed the Tributary Habitat Assessment Protocol (Justice et al. 2020). This protocol includes a pared-down list of metrics identified as having minimal observer bias, clear linkage to common ecological concerns in Columbia basin tributaries (i.e., water temperature, channel and floodplain complexity, pool habitats, fine sediment, etc.), and consistency (i.e., cross-walkability) with previously-collected habitat monitoring data. This protocol was tested during the 2018 field season and implemented during summer of 2021 and 2022. The methods outlined in this protocol are based on widely accepted and previously implemented monitoring methods used throughout the Pacific Northwest (i.e., CHaMP, ODFW Aquatic Inventories Project [AqI]). Acknowledging previous criticisms, the monitoring approach outlined within the CRITFC Tributary Habitat Assessment Protocol aims to cover more ground with less effort and cost, while obtaining high resolution aerial imagery using UAS that will provide a rich, georeferenced dataset with numerous current and future analytical opportunities. Our application of this monitoring protocol corresponds to biologically significant reaches (BSRs)

in the project areas, with a specific focus on areas designated as high or medium priority for habitat restoration (i.e., Tier 1 and 2 BSRs; Atlas partners 2015). However, the protocol is flexible enough to be tailored to specific limiting factors or needs of a particular basin such as prioritization of stream segments with active or planned restoration.

The Tributary Habitat Assessment Protocol was designed to provide a comprehensive and continuous riverscape perspective of the status and trends in fish habitat by merging datasets from multiple spatial scales (channel unit ~ 1-100m, reach ~ 100-1000 m, segment ~ 1000-10,000m, watershed) and components of the riverscape (hydrology, geomorphology, biology). The major components of this protocol are split into ground- and aerial-based methods. The ground-based methods are a fusion of two widely used and accepted protocols within the CRB including AqI (Moore et al 2019) and CHaMP (CHaMP 2016), while the aerial-based portion of the protocol utilizes drones. Drones have become ubiquitous in monitoring throughout a range of disciplines within the CRB. Drones are used in this protocol to collect imagery of the stream channel and floodplain and to develop georeferenced orthomosaics, digital surface models, and digital terrain models. To increase efficiency and repeatability, we reduced the frequency and total number of measurements collected within habitat units (i.e., channel units) by ground crews compared with previous CHaMP surveys. We attempted to reduce the reliance on qualitative or visually estimated metrics to the degree possible with the intention of producing metrics that are robust enough to provide meaningful evaluations of habitat change over time.

Methods

Prior to conducting field surveys, the stream network was classified into segments to set the spatial boundaries for measurements of fish habitat and biota and to help organize the survey workflow into units of manageable size. We delineated stream segments using the National Hydrography Dataset High Resolution flowlines (NHDPlus HR, 1:24K scale; USGS 2016) as a starting point. Similar to the U.S. Forest Service (USFS) Region 6 Level I Stream Inventory Handbook (USDA 2018), segment boundaries were based on the presence of large tributary junctions (Strahler order ≥ 4) or significant changes in valley confinement and gradient. Stream reaches falling between these break points were lumped together into a 'segment' and assigned a unique identification number. With a few exceptions, we used a minimum segment length of 1 km, consistent with the spacing of Generalized Random Tessellation Stratified (GRTS) master sample points used by CHaMP and other programs to characterize broad-scale status and trends in fish habitat conditions. Segments were grouped by 12-digit hydrologic unit code (HUC) watershed boundaries, consistent with the National Watershed Boundary Dataset (WBD; USGS et al. 2015) to facilitate data tracking and management.

In 2021, we worked collaboratively with the GRMW (funded by USFS) to survey a total of 37.1 km (mainstem length) and 0.26 km² of stream habitat in the upper Grande Ronde River basin using the Tributary Habitat Assessment Protocol. Surveys were intended to cover the current extent of Chinook Salmon spawning and rearing habitat within the Grande Ronde Atlas Tier 1 area (Figure

2; Atlas 2015) which was comprised of 21 unique river segments. Unfortunately, some locations could not be surveyed due to landowner denial—most notably the Vey Meadows portions of Sheep Creek and the Grande Ronde River (~ 19.8 km). Additionally, portions of some segments (notably GR0007, GR0014, and GR0020) were surveyed by drone but the corresponding ground-based habitat data was lost or was lacking sufficient clarity to tie it to the drone imagery.

In 2022, we worked collaboratively with the GRMW (funded partly by USFS) and a subcontractor (Foresight Drone Services) to survey a total of 67.9 km (mainstem length) and 172 acres of stream habitat in the upper Grande Ronde River basin using the Tributary Habitat Assessment Protocol. Surveys were intended to cover the current extent of Chinook Salmon spawning and rearing habitat within the Grande Ronde Atlas Tier 2 priority areas and small portions of Tier 1 areas that were not surveyed in 2021 (Figure 2; Atlas Partners 2015).

Within each segment, we collected aerial imagery (standard red/green/blue [RGB] and multispectral) using a variety of unmanned aircraft systems. Surveys conducted by CRITFC utilized a DJI Matrice 600 Pro drone outfitted with a dual payload including a Zenmuse X5 RGB camera (16 MP resolution) and Micasense Rededge MX multispectral sensor (1.2 MP) flown at an altitude of 90 m (295 ft) above ground level. We used DJI Map Pilot Pro on an Apple iPad mini for flight planning and control. Front and side image overlap was set to 80% and flight speed was generally below 8 m/s. Aerial targets consisting of bright spray paint or painted bucket lids were surveyed with an EOS Arrow 100 GNSS receiver (sub-meter accuracy) and used for georeferencing the aerial imagery. A detailed summary of the UAS imagery acquisition conducted by Foresight Drone Services was provided in Justice et al. (2023).

Ground-based measurements such as channel unit number, type (pool, fast turbulent, fast non-turbulent, etc.), large wood count, water depth, etc. were recorded using ArcGIS Survey123 on iPad mini or Samsung Galaxy tablets. To tie ground-based measurements to aerial imagery, we surveyed the boundaries of channel units and the edge of water using an EOS Arrow 100 GNSS receiver (Figure 4). The Arrow 100 typically achieved submeter accuracy except in rare cases with deep canyon walls (e.g., Dark Canyon Creek). Data collection with the Arrow 100 receiver was managed using ArcGIS Field Maps on an iPad mini or Samsung Galaxy tablet. Detailed survey methods are available on monitoringresources.org at:

http://www.monitoringresources.org/Document/Protocol/Details/3554.

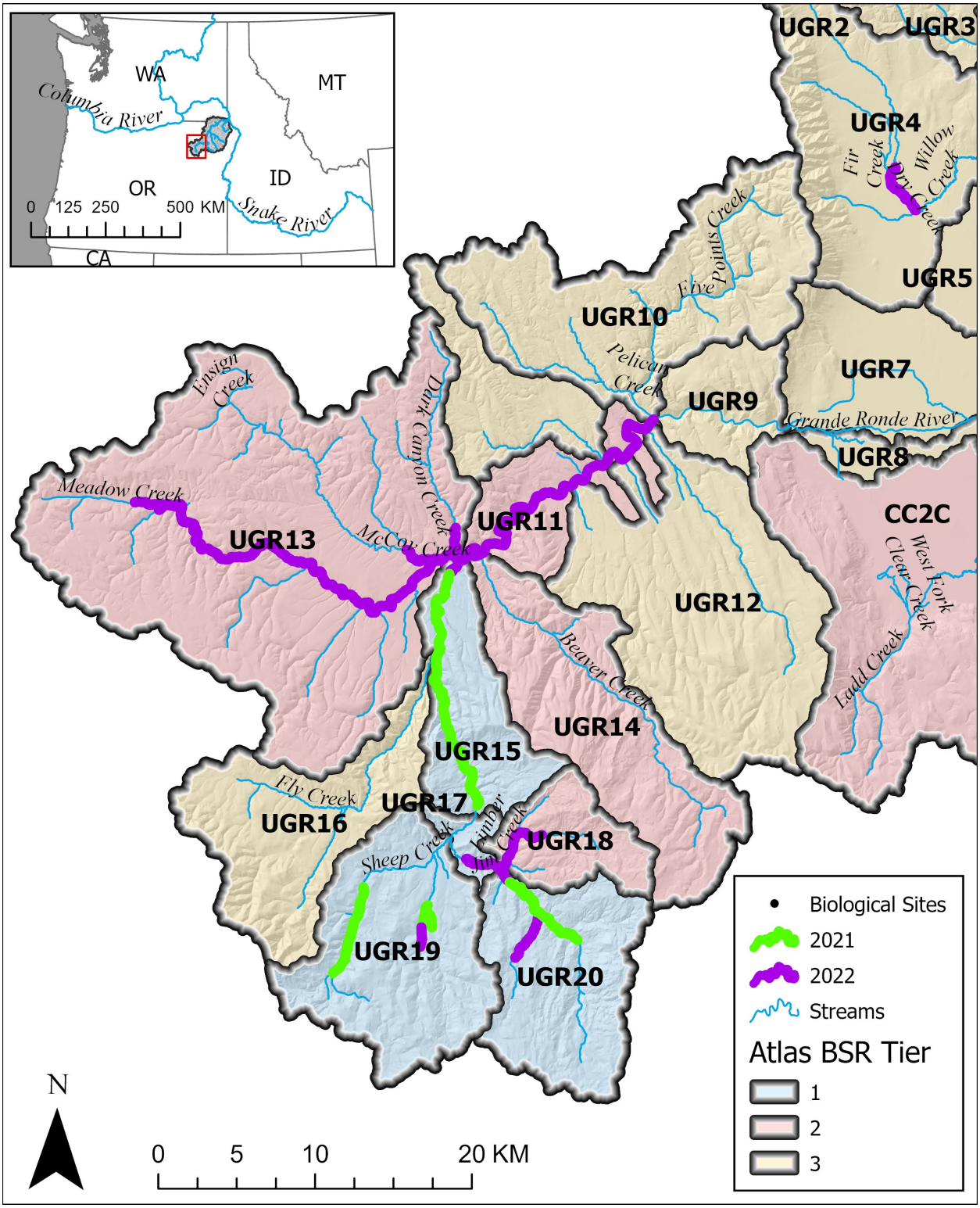

Figure 2. Survey area in the upper Grande Ronde River basin in NE Oregon

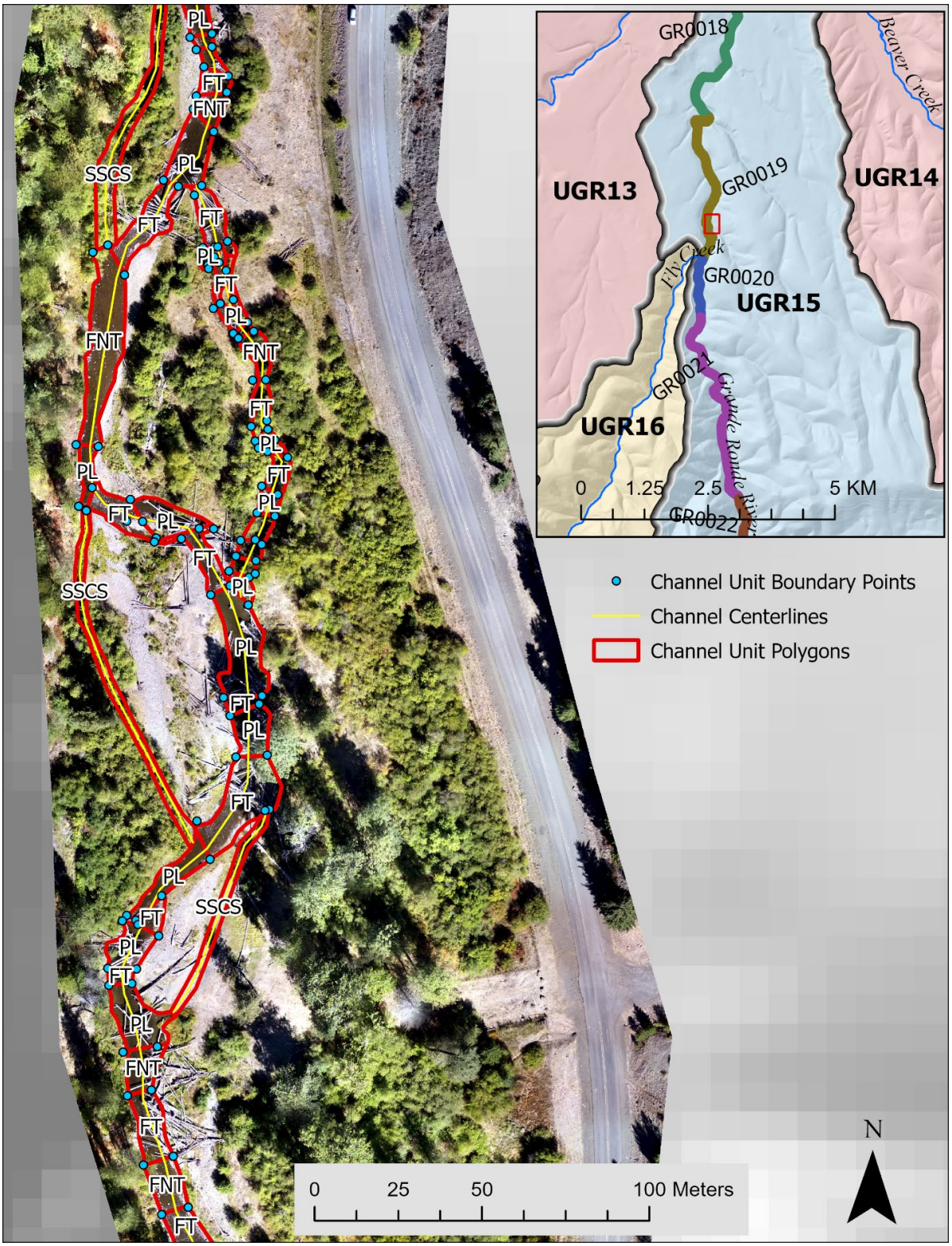

Figure 3. Example of spatial data collected within each survey segment including the unmanned aircraft system (UAS) orthomosaic, channel unit boundary points and polygons and channel centerlines.

Table 1. Description of stream habitat metrics derived from the Tributary Habitat Assessment Protocol.

Primary metric type	Secondary metric type	Metric	Description	Data source
Habitat quality/ diversity	Floodplain/ side channels	River complexity index (*RCI*)	River complexity index (RCI) = S*(1+J) where S = stream sinuosity, J = # of side channel junctions (Brown 2002)	Field/LiDAR /UAS
	Floodplain/ side channels	Side channel ratio (*SCRatio*)	Length of side channels divided by length of main channel during base flow (Beechie et al. 2017)	Field/LiDAR /UAS
	Riparian condition	Riparian tree cover (*RipTreeCov*)	Average percent tree canopy cover in the riparian zone (50 m stream buffer)	UAS/LiDAR
	Riparian condition	Riparian tree height (*RipTreeHt*)	Average tree height (m) in the riparian zone (50 m stream buffer)	UAS/LiDAR
	Riparian condition	*Riparian vegetation departure index (*RVD*)	Average percentage departure of current vegetation from simulated historical vegetation reference conditions in the riparian zone (Macfarlane et al. 2017)	Satellite/ Modeled
	Riparian condition	Normalized difference vegetation index (*NDVI*)	Average NDVI index in the riparian zone (50 m stream buffer) calculated as the ratio between visible and near-infrared reflectance of vegetation cover (Bhandari et al. 2012). NDVI is used as an index of vegetation greenness or health.	NAIP Satellite imagery
	River channel (cover)	Large wood area percentage (*LWAreaPct*)	Percentage of stream surface area covered by large wood during base flow.	UAS/LiDAR
	River channel (cover)	Large wood frequency bankfull (*LWFreqBF*)	Number of large wood pieces (> 3m length and 0.15 m diameter) within the bankfull channel per 100 m stream length (Moore et al. 2017)	Field

Primary metric type	Secondary metric type	Metric	Description	Data source
	River channel (cover)	Large wood frequency wetted (*LWFreqWet*)	Number of large wood pieces (> 3m length and 0.15 m diameter) within the wetted channel during base flow per 100 m stream length	Field
	River channel (cover)	Overhanging vegetation cover (*OverVegCov*)	Percentage of stream surface area covered by vegetation during base flow	UAS/LiDAR
	River channel (cover)	Undercut bank percentage (*UcutBankPct*)	Percentage of the total bank length that is undercut	Field/UAS
	River channel (pools)	Residual pool depth (*PoolResidDpth*)	Mean residual pool depth (max depth – pool tail depth in meters; Mossop and Bradford 2006)	Field/LiDAR
	River channel (pools)	Large pool frequency (*PoolFreqLg*)	Number of large pools (> 20 m² area and > 0.80 m max depth) per km stream length (McIntosh et al. 2000)	Field/UAS/ LiDAR
	River channel (pools)	Medium pool frequency (*PoolFreqMd*)	Number of medium- or larger-sized pools (> 20 m² area and > 0.50 m max depth) per km stream length	Field/UAS/ LiDAR
	River channel (substrate)	Median sediment particle size (*D50*)	Median sediment particle size on the streambed surface in riffles (Wolman 1954)	Field
	Water quality	*Coldwater refuge density (*ColdRefDen)*	Number of cold-water refuges per km stream length (Dugdale et al. 2015)	FLIR
	Water quality	*Coldwater refuge density (*ColdRefArea)*	Surface area (m²) of cold-water refuges	FLIR
	Water quality	Maximum weekly maximum temperature (*MWMT*)	Maximum 7-day running average of daily maximum temperature (EPA 2003)	Field/Modeled

Primary metric type	Secondary metric type	Metric	Description	Data source
	Water quality	*Observed/Expected benthic macroinvertebrates (*BenOE*)	Ratio of observed to expected (O/E) benthic macroinvertebrate taxa as predicted by the River Invertebrate Prediction and Classification System (RIVPACS, Hawkins et al. 2000)	Field
Habitat quantity	Floodplain/ side channels	Off-channel habitat base flow (*OCHabBase*)	Surface area (m²) of connected off-channel habitat during base flow	LiDAR/UAS
	Floodplain/ side channels	Side channel length (*SCLength*)	Length (m) of side channels during base flow	Field/UAS
	River channel (fast water)	Fast water area (*FastArea*)	Surface area (m²) of fast water habitat (e.g., fast turbulent, fast non-turbulent, fast small side channels) during base flow	Field/UAS
	River channel (pools)	Slow water area (*SlowArea*)	Surface area (m²) of slow water habitat (e.g., pools, off-channel units, slow small side channels) during base flow	Field/UAS
	River channel (total length)	*Length accessible main channel anadromous fish habitat (*MCLength*)	Length (km) of accessible main channel habitat that is currently used by anadromous fish for spawning, rearing, or migration	Field/ Modeled

Results

Habitat surveys conducted in 2021 and 2022 provided a nearly complete census of Grande Ronde Atlas Tier I and II habitats (Atlas Partners 2015) in the upper Grande Ronde River basin with the notable exception of the Vey Meadows property, which we did not have permission to survey except for a 1.5 km section downstream of Limber Jim Creek. These data provide a critical snapshot of recent habitat conditions that can be compared with past and future survey data and with restoration target values to track progress in recovery of key limiting habitat factors for Chinook Salmon.

Habitat metrics summarized at the biologically significant reach level are provided in Table 2, while segment- and channel unit-scale data are provided as spatial layers available upon request. Because some surveys within a given BSR spanned multiple years, we combined both survey years to provide a more complete estimate of habitat conditions for the entire BSR. All metrics were computed as weighted averages of the segment-scale metrics where the weight was given by the length of main channel within each segment. Here we've highlighted a subset of these metrics spanning a range of habitat categories but encourage interested parties to examine the accompanying data layers to assess conditions at specific sites of interest or to evaluate spatial patterns across the riverscape.

Side channel ratio (i.e., side channel length/main channel length), an index of channel complexity, was generally low across the study area, ranging from 0.02 to 0.43 (weighted mean = 0.10; Table 2) at the BSR scale. The highest side channel ratio was observed in UGR11, which included two recently-completed floodplain restoration projects sponsored by the Bureau of Reclamation (Bird Track Springs [completed 2018-19] and Longley Meadows [completed 2021-22]). Side channel ratio summarized at the NHD 1:24K segment scale ranged from 0-1.18 with the highest values observed in UGR11 (Bird Track Springs and Longley), and moderate values observed in portions of UGR20 (Mine Tailings Reach) (Figure 4).

Riparian tree cover (i.e., percentage of riparian area [50 m buffer] covered by trees > 3m tall) summarized at the BSR scale ranged from 15 to 54% (weighted mean = 29.4%; Table 2). Tree cover was generally highest near the headwaters (e.g., UGR20) and was relatively low in lower-elevation portions of the basin and in areas of private land ownership (e.g., UGR11; Figure 5). A notable exception to this pattern was observed in Willow Creek (UGR4), where despite having relatively short tree height (weighted mean 6.7 m), tree canopy cover was moderately high (weighted mean 45%).

Large pools (> 20 m² surface area and 0.8 m max depth) were relatively rare within the upper Grande Ronde watershed, with large pool frequency ranging from 0-16.6 pools/km (weighted mean = 3.2; Table 2). Large pools density was highest in the restored section of Willow Creek (UGR4) and was lowest in the surveyed portion of Vey Meadows (UGR17). Despite its small size, large pool frequency was surprising high in the upper portion of Chicken Creek (Figure 6), a direct result of intensive habitat restoration implemented by the U.S. Forest Service in 2020. A study by McIntosh (1994) showed that large pool frequency in the Grande Ronde River decreased from approximately 6.1 to 2.1 pools/km between 1934-42 and 1990-92. Our more recent data suggests that large pool frequency has increased somewhat since the early 1990s but is still lower than it was in the late 1930s. Given that the 1930s surveys occurred well after many land use activities had already degraded river conditions (e.g., splash damming, road and railroad construction, beaver trapping), these data suggest that significant work remains to increase large pool habitats in the upper Grande Ronde basin to levels approximating a relatively undisturbed reference condition.

Frequency of medium size pools (> 20 m² and > 0.5 m max depth) ranged from 3.5 pools/km in the Grande Ronde mainstem between Pelican and Meadow Creek (UGR11) to 33.5 pools/km in Willow Creek (UGR4; weighted mean = 10.5 pools/km; Table 2). These pool frequencies were generally low compared with restoration target values developed by CRITFC (Justice et al. 2023), which ranged from 17.1 to 33.8 depending on geomorphic channel type (e.g., cascade/step, pool riffle, plane bed, etc.; Table 3).

Large wood frequency in the wetted channel summarized at the BSR scale ranged from 2.6 – 27.7 pieces/100 m (weighted mean = 9.7 pieces/100 m; Table 2). Large wood was generally most abundant in the headwaters and lowest in the lower elevation/privately owned portions of the basin (Figure 7). Additionally, large wood frequency tended to be highest in recently restored areas of the basin including upper Sheep and Chicken Creeks (UGR19), lower Limber Jim Creek (UGR18), the upper Grande River near Clear Creek (i.e., Woodley reach; UGR20), the middle upper Grande Ronde (MUGR) reach near Fly Creek (UGR15) and the Bird Track Springs and Longley Meadows restoration project areas (UGR11). Large wood frequency in BSRs UGR18-20 is near or above the target values for restoration (Table 3, mean target value across channel types = 25.6 pieces/100 m), while additional restoration work is needed in other BSRs (particularly in privately-owned reaches) to increase wood abundance to levels approximating reference conditions.

Overall, these data indicated relatively high values in selected key limiting habitat metrics (side channels, riparian cover, pools, and large wood) associated with recent restoration projects, but sub-optimal conditions remain within most biologically significant reaches (BSRs).

Next Steps

We intend to combine the 2021 and 2022 habitat survey data with previous data collected using the Columbia Habitat Monitoring Program (CHaMP) from 2011-2017, and Oregon Department of Fish and Wildlife's Aquatic Inventories Project (AqI) (1990s-2000s) to evaluate temporal trends in key limiting habitat factors (e.g., pools, large wood, channel complexity, water temperature) at the watershed scale. We expect to complete this analysis during 2025.

Following the 2022 season, we discontinued sampling of habitat in the Grande Ronde basin using the Tributary Habitat Assessment Protocol for the following reasons: 1) the majority of Tier 1 (i.e., high priority) stream segments had been surveyed recently either by CRITFC or ODFW (AqI program), 2) we are increasing emphasis on large-scale remote sensing data such as LiDAR and FLIR collected on a decadal basis, and 3) private landowners have been frequently complaining of excessive research and monitoring activity on their property and the use of UAS (drones) is particularly problematic. We intend to seek feedback from restoration implementors and collaborators in the basin regarding future needs for comprehensive habitat monitoring.

Table 2. Habitat metrics summarized by biologically significant reach (BSR) for survey years 2021 and 2022. All metrics were computed as weighted averages of the segment-scale metrics where the weight was given by the length of main channel within each segment except for metrics describing absolute quantities such as total stream length or area (denoted by superscripts).

BSR	UGR4	UGR11	UGR13	UGR15	UGR17	UGR18	UGR19	UGR20
Year_Range	2022 - 2022	2022 - 2022	2022 - 2022	2021 - 2022	2022 - 2022	2022 - 2022	2021 - 2021	2021 - 2022
RCI	5.7	16.6	3.3	14.7	4.4	40.4	8.9	8.4
SCRatio	0.02	0.43	0.04	0.13	0.07	0.08	0.04	0.12
RipTreeCov	45	15	20	42	21	24	51	54
RipTreeHt	6.7	11.9	11.2	13.9	10.8	9.5	13.5	13.1
RVD	56	51	50	50	51	46	42	40
NDVI	0.28	0.25	0.30	0.16	0.21	0.31		0.29
LWFreqBF	16.2	12.2	6.9	14.4	4.1	41.8	41.8	28.2
LWFreqWet	11.1	6.3	4.4	7.5	2.6	27.7	27.2	18.1
OverVegCov	27	19	20	20	15	50	34	24
UcutBankPct	1.4	0.3	1.7	0.8	4.9	2.7	1.1	1.6
PoolResidDpth	0.49	0.68	0.36	0.41	0.26	0.28	0.36	0.39
PoolFreqLg	16.6	3.0	2.9	2.3	0.0	1.4	3.9	4.1
PoolFreqMd	33.5	3.5	11.6	7.7	12.9	13.5	12.4	15.4
D50		67	51	74	73	46	43	66
ColdRefArea[1]	0	2993	2072	508	0	0	0	12
ColdRefDen	0.0	162.8	56.2	25.7	0.0	0.0	0.0	1.4
MWMT		28.3		27.3		15.8	20.4	19.6
BenOE		0.35	0.37	0.36		0.71	0.42	0.67
OCHabBase[1]	237	43525	12634	10477	731	1038	898	5866
SCLength[1]	48	7967	1597	2390	104	541	257	1105
FastArea[1]	3890	306238	129083	181889	6412	6897	15512	43057
SlowArea[1]	8055	85665	80779	36365	4540	11847	11917	20995
MCLength[1]	2779	18383	36846	19502	1476	6506	6378	8847

Table 3. Restoration target values for medium pool frequency and large wood frequency derived from the 90th percentile of habitat measurements collecting using the Columbia Habitat Monitoring Program (CHaMP) protocol across the Columbia River Basin and originally reported in Justice et al. (2023).

Channel Type	Medium Pools/km	Large Wood Pieces/100 m
Cascade/Step	17.1	33.4
Plane Bed	26.6	21.0
Pool/Riffle	33.8	18.4
Straight	28.3	26.5
Meandering	30.5	24.0
Confined	22.9	27.3
Braided	23.5	28.4
Mean	26.1	25.6

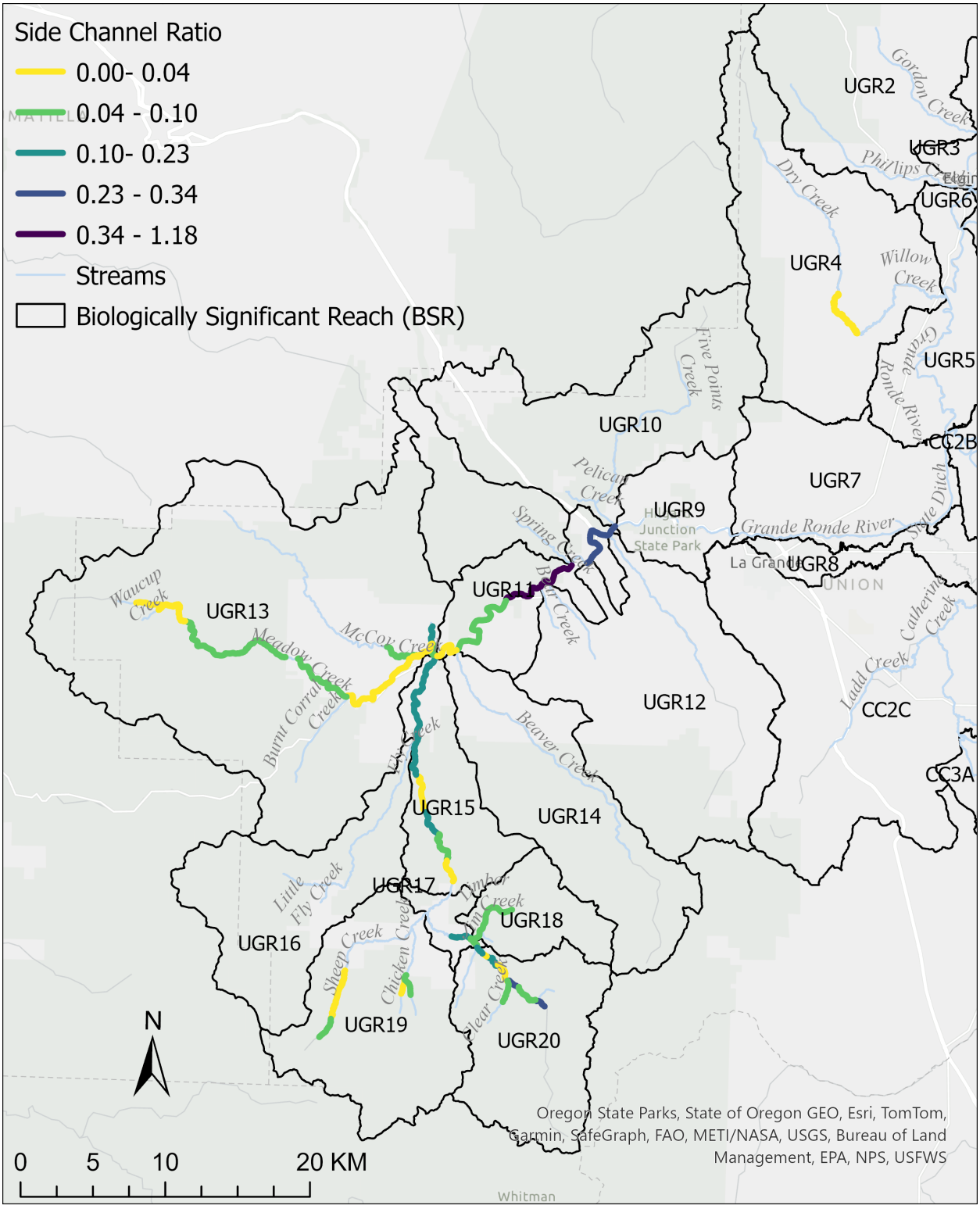

Figure 4. Segment-scale measurements of side channel ratio in Atlas Tier 1 and II areas of the upper Grande Ronde River basin during 2021 and 2022.

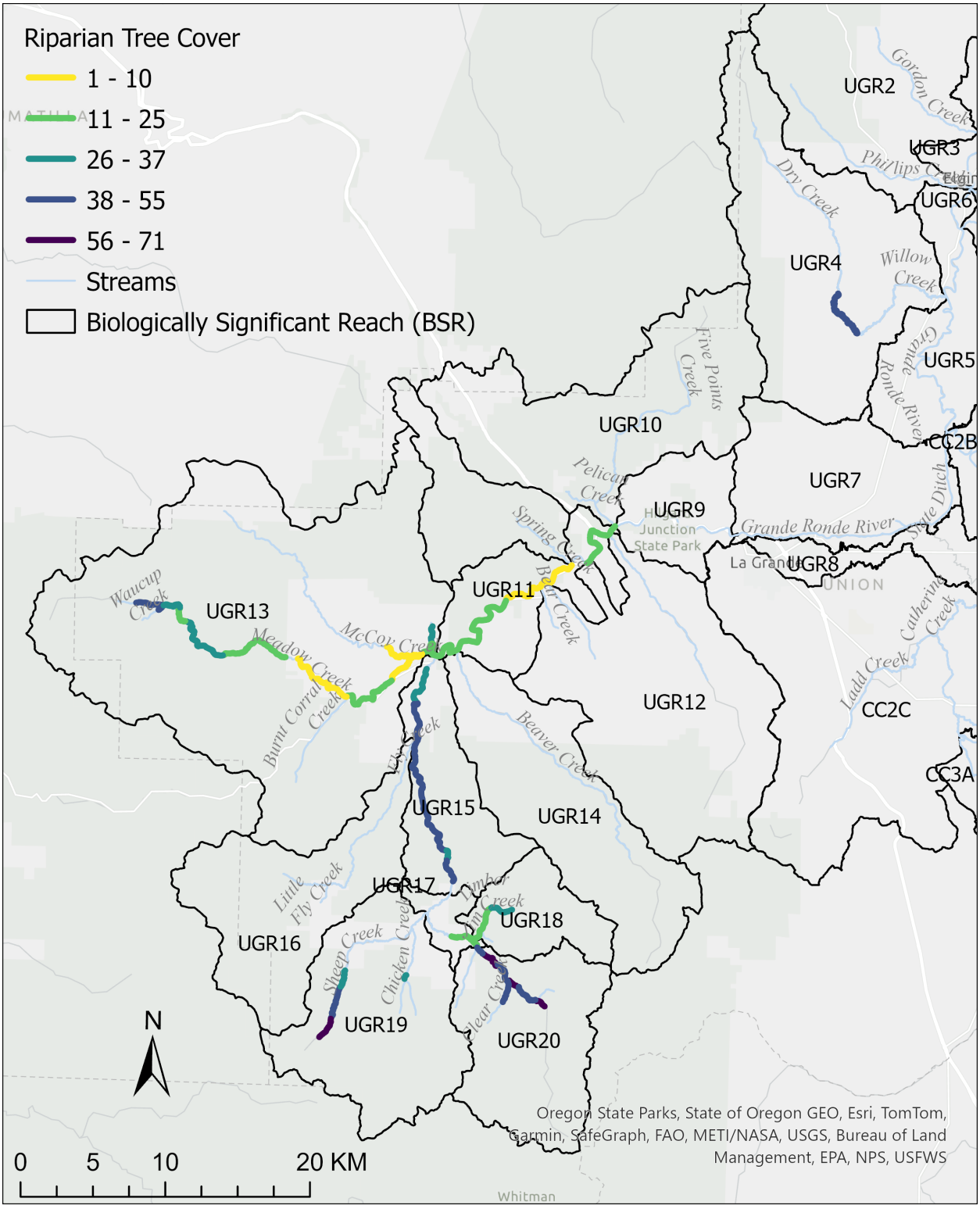

Figure 5. Segment-scale measurements of riparian tree cover in Atlas Tier 1 and II areas of the upper Grande Ronde River basin during 2021 and 2022.

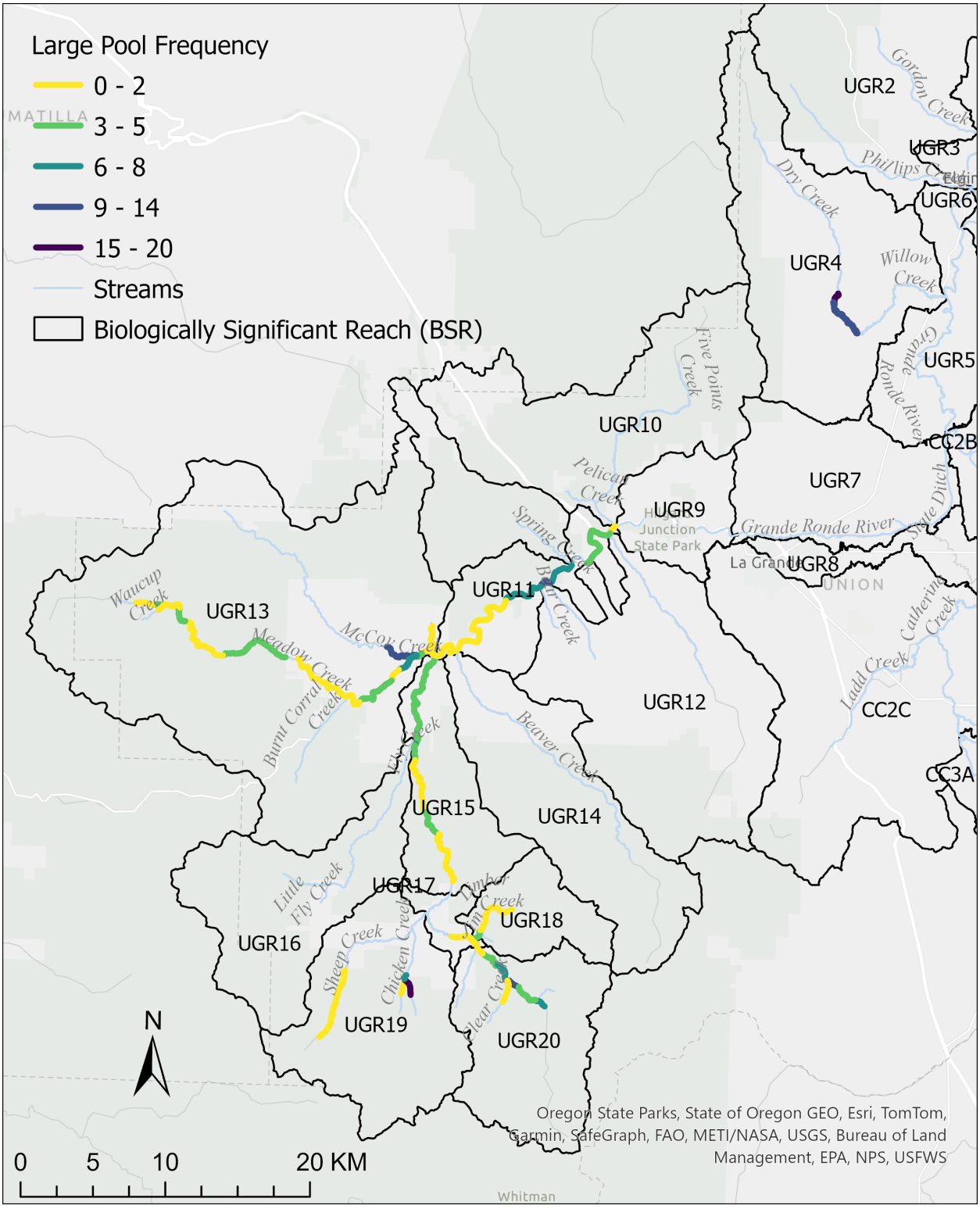

Figure 6. Segment-scale measurements of large pool frequency in Atlas Tier 1 and II areas of the upper Grande Ronde River basin during 2021 and 2022.

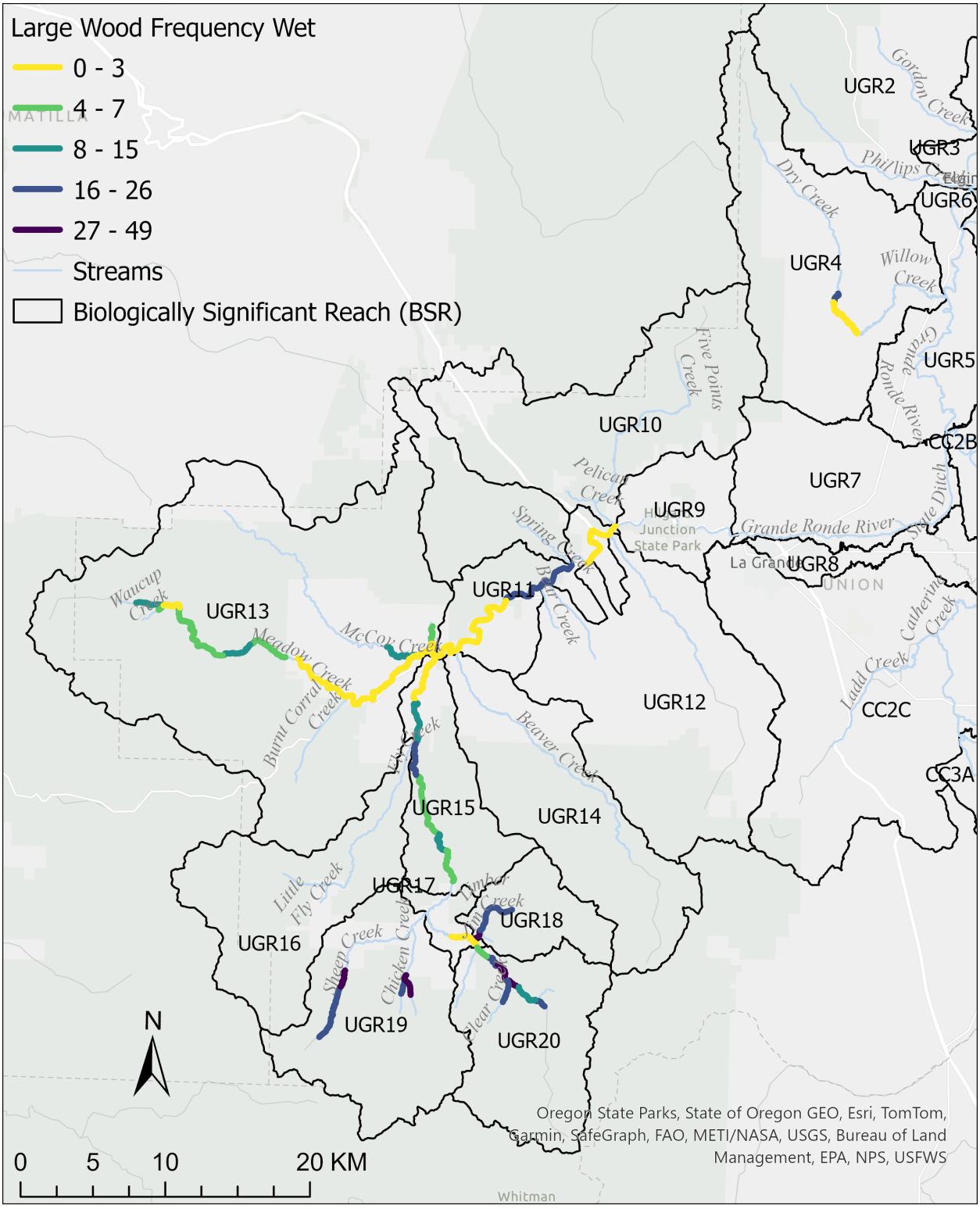

Figure 7. Segment-scale measurements of large wood frequency in the wetted channel in Atlas Tier 1 and II areas of the upper Grande Ronde River basin during 2021 and 2022.

References

Atlas partners. 2015. Atlas implementation guidelines - Catherine Creek and upper Grande Ronde River. Page 17. https://www.grmw.org/static/documents/atlas/Atlas%20Implementation%20Guidelines%20(6-8-15).pdf

Beechie, T. J., O. Stefankiv, B. Timpane-Padgham, J. E. Hall, G. R. Pess, M. Rowse, M. Liermann, K. Fresh, and M. J. Ford. 2017. Monitoring Salmon Habitat Status and Trends in Puget Sound: Development of Sample Designs, Monitoring Metrics, and Sampling Protocols for Large River, Floodplain, Delta, and Nearshore Environments. U.S. Department of Commerce, NOAA Technical Memorandum NMFSNWFSC-137. https://doi.org/10.7289/V5/TM-NWFSC-137.

Bhandari, A. K., A. Kumar, and G. K. Singh. 2012. Feature Extraction using Normalized Difference Vegetation Index (NDVI): A Case Study of Jabalpur City. Procedia Technology 6:612–621.

Brown, A. G. 2002. Learning from the past: palaeohydrology and palaeoecology. Freshwater Biology 47(4):817–829.

CHaMP (Columbia Habitat Monitoring Program). 2016. Scientific protocol for salmonid habitat surveys within the Columbia Habitat Monitoring Program.

Dugdale, S. J., N. E. Bergeron, and A. St-Hilaire. 2015. Spatial distribution of thermal refuges analysed in relation to riverscape hydromorphology using airborne thermal infrared imagery. Remote Sensing of Environment 160:43–55.

EPA (U.S. Environmental Protection Agency). 2003. EPA region 10 guidance for Pacific Northwest state and tribal temperature water quality standards. Page 49. U.S. Environmental Protection Agency, EPA 910-B-03-002, Region 10 Office of Water, Seattle, Washington.

Hawkins, C. P., R. H. Norris, J. N. Hogue, and J. W. Feminella. 2000. Development and evaluation of predictive models for measuring the biological integrity of streams. Ecological Applications 10(5):1456–1477.

Justice, C., L. Burns, S. White. 2020. Tributary Habitat Assessment Protocol v2.0. Monitoring Resources.org. http://www.monitoringresources.org/Document/Protocol/Details/3554

Justice, C., M. Kaylor, S. Ringelman, A., and B. Staton. 2023. Evaluating salmonid and stream ecosystem response to conservations measures and environmental stressors in the Columbia River basin. Page 93. Columbia River Inter-Tribal Fish Commission, BPA Project # 2009-004-00, Portland, OR.

Macfarlane, W. W., J. T. Gilbert, M. L. Jensen, J. D. Gilbert, N. Hough-Snee, P. A. McHugh, J. M. Wheaton, and S. N. Bennett. 2017. Riparian vegetation as an indicator of riparian

condition: Detecting departures from historic condition across the North American West. Journal of Environmental Management 202:447–460.

McIntosh, B. A., J. R. Sedell, Smith, J.E., R. C. Wissmar, S. E. Clarke, G. H. Reeves, and L. A. Brown. 1994. Historical changes in fish habitat for select riiver basins of Eastern Oregon and Washington. Northwest Science 68(Special Issue):36–52.

McIntosh, B. A., J. R. Sedell, R. F. Thurow, S. E. Clarke, and G. L. Chandler. 2000. Historical changes in pool habitats in the Columbia River basin. Ecological Applications 10(5):1478.

Moore, K., K. Jones, J. Dambacher, C. Stein, and et al. 2019. Aquatic Inventories Project: methods for stream habitat and snorkel surveys. Page 89. Oregon Department of Fish and Wildlife, Version 29.1, Corvallis, OR.

Mossop, B., and M. J. Bradford. 2006. Using thalweg profiling to assess and monitor juvenile salmon (Oncorhynchus spp.) habitat in small streams. Canadian Journal of Fisheries and Aquatic Sciences 63(7):1515–1525.

U.S. Department of Agriculture (USDA). 2018. Stream inventory handbook Level I and II. Page 142. U.S. Department of Agriculture, Forest Service, Pacific Northwest Region, Region 6, Version 2.18.

U.S. Geological Survey (USGS), U.S. Department of Agriculture – Natural Resource Conservation Service (NRCS), U.S. Environmental Protection Agency (EPA), et al. 2015. National Watershed Boundary Dataset (WBD). Downloaded as part of the NHDPlus HR dataset from https://www.usgs.gov/core-science-systems/ngp/national-hydrography/access-national-hydrography-products on 6/16/2020.

U.S. Geological Survey (USGS). 2016. BETA - USGS National Hydrography Dataset Plus High Resolution (NHDPlus HR) Best Resolution for HU4-0101 (Subregion) Publication Date 20160512 HU-4 Subregion FileGDB 10.1. Downloaded from https://www.usgs.gov/core-science-systems/ngp/national-hydrography/access-national-hydrography-products on 6/16/2020.

Wolman, M. G. 1954. A method of sampling coarse river-bed material. Transaction of the American Geophysical Union 35:951–956.

1.2 Water temperature monitoring

Introduction

CRITFC has maintained an extensive network of year-round water temperature loggers in the Grande Ronde basin since 2009 with the goal of tracking long-term trends in water temperature related to land use, restoration, and climate change. These data have also been used to develop

fish-habitat relationships and parameterize water temperature models such as Heat Source. Temperature data has also been shared widely with basin partners and others to aid in assessment of site-specific restoration effectiveness or development of large-scale temperature models (e.g., NorWeST, DEQ TMDL).

Methods

CRITFC actively maintains 86 water temperature monitoring sites in the upper Grande Ronde, Catherine Creek, and Minam River watersheds, but has monitored up to 192 sites in past years (Figure 8). Temperature data is measured hourly and loggers are deployed year-round. Additionally, we maintain a database of external agency temperature loggers for data collected between 1988 and 2017 totaling 452 unique sites. External agencies included the Bureau of Land Management (BLM), CTUIR, Oregon Department of Environmental Quality (DEQ), GRMW, Nez Perce Tribe, ODFW, Oregon Water Resources Department (OWRD), Union Soil and Water Conservation District (USWCD), USFS, and U.S. Geological Survey (USGS). We visited all active sites during fall (late September to early October) to download data, check the status of logger batteries, and assess deployment conditions.

Raw hourly temperature measurements were checked for errors using a combination of automated and manual/visual inspection QAQC routines. Any hourly measurements that exceeded 30 °C, were less than -1 °C, had an absolute hourly change > 3 °C, or had an absolute field audit temperature difference > 0.5 °C were flagged as potential errors and were subsequently verified manually by CRITFC staff. For each temperature monitoring site, we generated a suite of daily, weekly, and annual water temperature metrics using SQL scripts within CRITFC's centralized database management system (CDMS) that describe key components of stream thermal regimes (e.g., magnitude, variability, frequency, duration, and timing) using guidance from Heck et al. (2018) (Table 4). To avoid errors associated with missing data, metrics were only computed for sites that had valid measurements for at least 90% of the total possible records for a given time period as per Isaak et al. (2017).

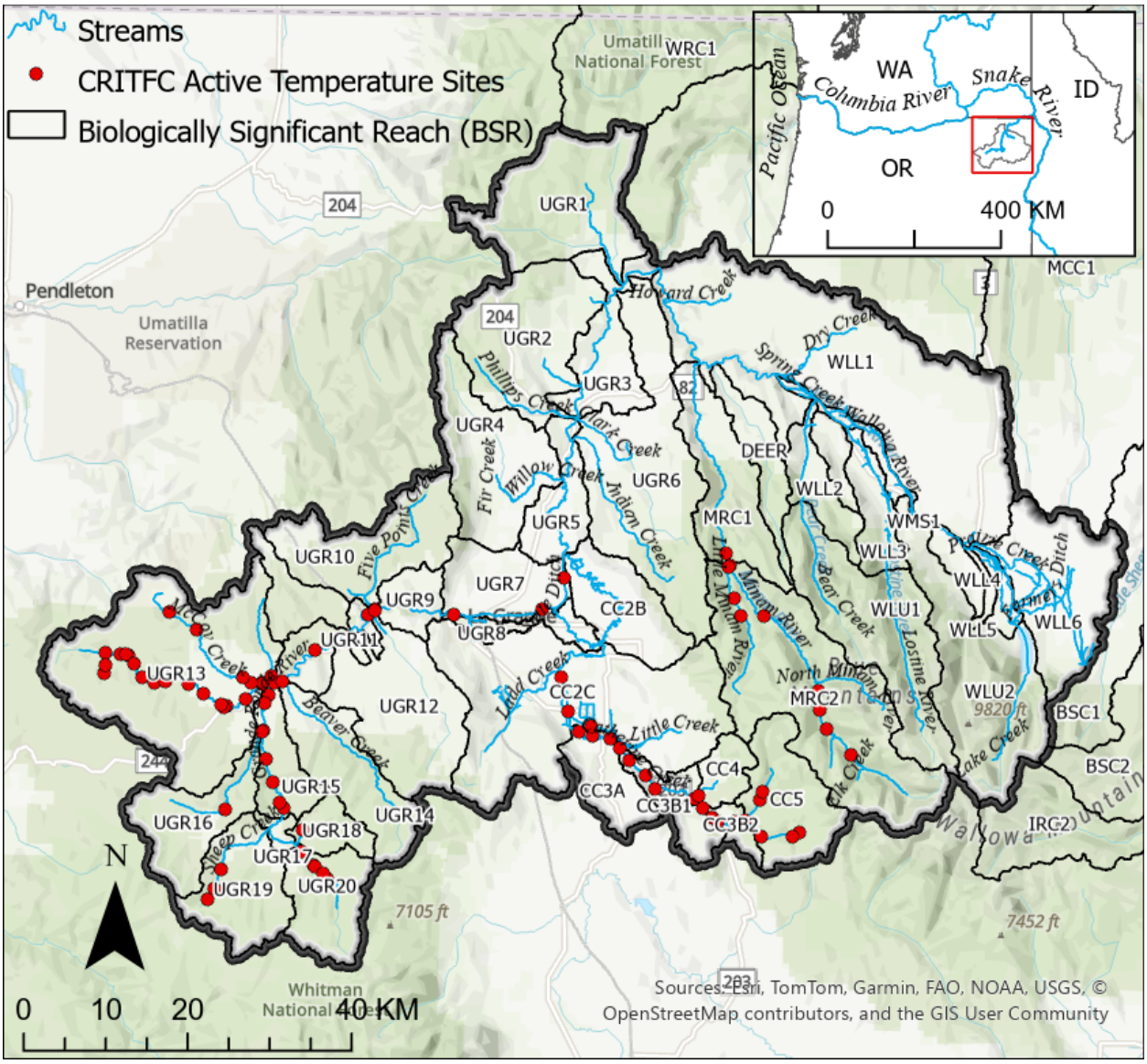

Figure 8. Water temperature monitoring sites in the Grande Ronde River basin from 2009 to 2024.

Table 4. Annual water temperature metrics calculated in the CRITFC water temperature database. Metrics based on Heck et al. (2018) with some additions.

Category	Metric	Definition
Magnitude (°C)	*Maximum*	Warmest temperature of the year
	MWMT	Maximum Weekly Maximum Temperature (i.e., highest 7-day average of daily maximum temperatures in summer [Jul. 1 - Aug. 31])
	MWAT	Maximum Weekly Average Temperature (i.e., highest 7-day average of daily mean temperatures in summer [Jul. 1 - Aug. 31])
	DegreeDays	Sum of daily mean temperatures > 0 °C in a year
	JuneAvg	Average of daily mean temperatures in June
	JulyAvg	Average of daily mean temperatures in July
	AugAvg	Average of daily mean temperatures in August
	SeptAvg	Average of daily mean temperatures in September
Variability (°C)	*MeanRange*	Difference between the highest and lowest daily mean temperature in a year
	MaxRange	Difference between the highest and lowest daily maximum temperature in a year
	MeanVariance	A statistical measure of deviations from the mean among daily mean temperatures in a year
	MaxVariance	A statistical measure of deviations from the mean among daily maximum temperatures in a year
Frequency (n)	*Days16*	Number of days in a year where the daily maximum temperature exceeded 16 °C
	Days18	Number of days in a year where the daily maximum temperature exceeded 18 °C
	Days20	Number of days in a year where the daily maximum temperature exceeded 20 °C
Duration (n)	*CD16*	Consecutive number of days in a year where daily maximum temperature exceeded 16 °C
	CD18	Consecutive number of days in a year where daily maximum temperature exceeded 18 °C
	CD20	Consecutive number of days in a year where daily maximum temperature exceeded 20 °C
Timing	*CTD50_Day*	Day of year of attaining 50% of the cumulative degree days in a given year
	CTD75_Day	Day of year of attaining 75% of the cumulative degree days in a given year

Results

We summarized a subset of annual water temperature metrics by biologically significant reach (BSR) and stream using all active CRITFC temperature monitoring sites over the recent 10-year time period (2015-2024; Table 5). Ten-year average maximum weekly maximum temperature (MWMT) ranged from 13.7 to 28.6 °C (mean = 21.0 °C), with the highest peak temperatures occurring in the lower portion of the upper Grande Ronde River between Five Points Creek and Meadow Creek (UGR11) and the lowest temperatures occurring in Middle Fork Catherine Creek (CC5). MWMT was similar in 2024 compared to the 10-year mean (mean difference = 0.0 °C).

Maximum range, a measure of annual variability in daily max temperature, ranged from 14.3 to 29.8 °C (mean = 21.9 °C). Temperature variability tracked very closely with MWMT in terms of spatial patterns across the basin. The number of days exceeding 18 °C ranged from 0 to 102 (mean = 42.9), with the highest number of days over 18 °C occurring in McCoy Creek (UGR13) and lowest in Middle Fork Catherine Creek (CC5). The frequency of days over 18 °C was also very high in the lower portion of the Grande Ronde River (UGR11), Meadow Creek (UGR13), and lower Catherine Creek (CC2C). The consecutive number of days exceeding 18 °C followed a similar pattern as the number of days over 18 °C (range = 0 – 79.9, mean = 30.8). The day of year corresponding to the 50^{th} percentile of cumulative degree days, a measure of how quickly streams warm up, ranged from 192-215 (July 10 – August 2). McCoy Creek reached its median degree days fastest, while Little Catherine Creek warmed the slowest.

The summary presented here represents a small subset of the available water temperature data collected and managed through this project. Raw temperature measurements as well as daily, weekly, and annual water temperature metrics are stored in CRITFC's Centralized Database Management System (CDMS) and are available to the public upon request. We intend to conduct an analysis of temporal trends in water temperature over the duration of this project (2009-current) along with other key limiting habitat factors for dissemination in the 2025 Annual Report.

Table 5. Selected annual water temperature metrics from 2015-2024 summarized by biologically significant reach (BSR) and stream. Missing values represent sites/years with fewer than 90% of the total potential measurements for a given time period.

			10-Year Mean (2015-2024)					2024
BSR	Stream	Sites	MWMT	MaxRange	Days18	CD18	CTD50_Day	MWMT
CC2C	Catherine Creek	2	26.2	28.6	80.0	75.5	211.5	26.8
CC2C	Little Creek	1	22.6	23.3	69.5	60.5	210.5	23.3
CC3A	Catherine Creek	2	23.0	24.0	65.8	53.6	208.7	23.3
CC3B1	Catherine Creek	6	22.3	23.2	58.0	39.4	208.2	22.7
CC3B2	Catherine Creek	4	19.3	19.9	21.8	9.4	209.8	19.3
CC4	Little Catherine Creek	1	18.0	20.3	21.8	16.3	214.3	18.5
CC5	Middle Fork Catherine Creek	1	13.7	14.3	0.0	0.0	208.9	13.7
CC5	North Fork Catherine Creek	3	16.4	17.2	3.4	1.6	210.3	16.3
CC5	South Fork Catherine Creek	4	15.2	15.7	1.1	0.7	208.8	14.5
MRC1	Minam River	1	19.6	20.6	27.0	15.5	211.0	
MRC2	Little Minam River	3	17.0	17.9	4.9	2.1	210.0	
MRC2	Minam River	6	17.4	18.2	10.7	5.9	211.6	
UGR10	Five Points Creek	1	23.1	23.9	67.5	40.0	205.0	23.1
UGR11	Grande Ronde River	4	28.6	29.8	97.2	79.9	202.3	28.0
UGR13	Burnt Corral	1	20.6					
UGR13	McCoy Creek	3	26.5	27.8	102.0	71.7	191.7	26.7
UGR13	Meadow Creek	14	26.5	27.5	93.8	58.8	197.1	26.3
UGR15	Grande Ronde River	7	25.7	26.4	77.2	51.6	205.8	25.4
UGR16	Fly Creek	2	24.0	24.8	70.0	45.2	200.7	23.3
UGR18	Limber Jim Creek	1	16.3	17.1	1.8	1.2	208.0	16.3
UGR19	Sheep Creek	3	19.4	20.4	26.0	14.0	208.4	19.0
UGR20	Clear Creek	1	17.7	18.7	9.6	3.0	212.0	17.4
UGR20	Grande Ronde River	4	18.3	18.9	13.5	6.7	211.1	18.1
UGR7	Grande Ronde River	3	26.4	26.0	64.8	57.0	207.8	27.4
	Min	1	13.7	14.3	0.0	0.0	191.7	13.7
	Max	14	28.6	29.8	102.0	79.9	214.3	28.0
	Mean	3.3	21.0	21.9	42.9	30.8	207.5	21.5

References

Heck, M. P., L. D. Schultz, D. Hockman-Wert, E. C. Dinger, and J. B. Dunham. 2018. Monitoring stream temperatures—A guide for non-specialists. Page 76 U.S. Geological Survey Techniques and Methods, book 3, chapter A25.

EPA (U.S. Environmental Protection Agency). 2003. EPA region 10 guidance for Pacific Northwest state and tribal temperature water quality standards. Page 49. U.S. Environmental Protection Agency, EPA 910-B-03-002, Region 10 Office of Water, Seattle, Washington.

Isaak, D. J., S. J. Wenger, E. E. Peterson, J. M. Ver Hoef, D. E. Nagel, C. H. Luce, S. W. Hostetler, J. B. Dunham, B. B. Roper, S. P. Wollrab, G. L. Chandler, D. L. Horan, and S. Parkes-Payne. 2017. The NorWeST Summer Stream Temperature Model and Scenarios for the Western U.S.: A Crowd-Sourced Database and New Geospatial Tools Foster a User Community and Predict Broad Climate Warming of Rivers and Streams: Stream climates in the Western U.S. Water Resources Research 53(11):9181–9205.

McCullough, D., S. Spalding, D. Sturdevant, and M. Hicks. 2001. Issue paper 5: summary of technical literature examining the physiological effects of temperature on salmonids. Page 113. U.S. Environmental Protection Agency, EPA-910-D-01-005.

1.3 Thermal imagery acquisition (UAS)

Introduction

We conducted a small pilot study in the Meadow Creek watershed of the Grande Ronde basin during August of 2024 to assess the feasibility of using unmanned aircraft systems (UAS, drones) to assess spatial patterns in water temperature and availability of cold-water refugia. This work was focused on stream reaches that are planned for floodplain restoration beginning in 2028, offering an opportunity to assess how thermal heterogeneity changes in response to river restoration. With peak stream temperatures exceeding 25 °C (the approximate incipient lethal temperature for salmonids) in many portions of this watershed and climate change predicted to increase water temperatures in the future, it's critical to understand how management actions are influencing this key limiting habitat factor for target species such as steelhead (*O. mykiss*) and Chinook Salmon (*O. tshawytscha*).

Methods

We used a DJI Mavic 3T UAS equipped with both an RGB (standard red, green, blue spectral bands) and thermal camera. The RGB wide angle camera included a ½-inch CMOS sensor with a 48 MP effective resolution and 24 mm lens with electronic shutter. The thermal camera utilized an uncooled radiometric VOx microbolometer thermal imager with a 640 X 512 pixel resolution and approximate accuracy of ±2°C. We surveyed three locations in the Meadow Creek watershed including two reaches in the McCoy Meadows area (reach 5B [survey area = 0.12 km², 29.4 acres]

and 5D [survey area = 0.19 km², 47.6 acres]) and one reach in the Starkey Experimental Forest (reach 4C [survey area = 0.14 km², 33.7 acres], Figure 9).

UAS flight missions were conducted during August 20-22 near mid-day (11 AM – 2 PM) to capture peak summer water temperatures and minimize the influence of shadows in the imagery. The UAS was operated at an altitude of approximately 40 – 55 m at a speed of 3 m/s with front and side image overlap of 90 and 85%, respectively. Images were captured using a gimble pitch of 90° (i.e., straight down or "nadir"). The relatively low altitude, high image overlap and slow speed of these flight missions was intended to maximize thermal image quality and minimize ground sampling distance (target < 5 cm/pixel). We deployed 3-5 HOBO TidbiT v2 water temperature loggers (accuracy < 0.2 °C) with a logging interval of 5 minutes within each reach to assess accuracy of the thermal imagery.

We processed the UAS imagery using the cloud-based DroneDeploy software (https://www.dronedeploy.com/). This software was selected because of its ability to process large numbers of images for a single project (up to 10,000) and generate radiometric thermal orthomosaics from DJI imagery, which our previous software (Pix4DMapper) was not capable of doing. Outputs generated from DroneDeploy for each project area included an RGB orthomosaic, digital surface model (DSM; highest elevation of all surfaces included ground, vegetation and structures), digital terrain model (DTM; bare earth elevation), visible atmospherically resistant index (VARI, an index of vegetation health similar to NDVI), and radiometric thermal orthomosaic (surface temperature in °C).

Results

Analysis of these data is in progress and a summary of the results from 2024 combined with additional thermal imagery data from 2025 will be presented in the 2025 Annual Report. Preliminary results from two of the reaches show promise in terms of characterizing reasonably accurate water temperature maps (~ ± 2 °C based on manufacturer specifications) at the reach scale (1-2 km; Figure 10), although image accuracy relative to water temperature loggers has not been completed yet. Additionally, the UAS thermal imagery appeared suitable for identifying fine-scale relative differences in water temperature indicative of thermal features or cold-water refuges formed by cold seeps, hyporheic upwelling, or springs (Figure 11). However, there were some apparent errors or nonuniformities in the imagery which appeared as streaking or vertical lines (also known as strip noise) in some locations (Figure 11). This issue, and other types of vignetting is common in uncooled UAS-based microbolometers and is thought to be caused by temperature variations in the camera components during flight (thermal drift; Yuan and Hua, 2022). Various methods have been utilized to correct for these nonuniformities in UAS-based thermal imagery (Redana et al. 2024; Yuan and Hua 2022; Torres-Rua 2017), and we are currently assessing these options to determine if it would be worth the time and effort to do so.

References

Redana, M., L. T. Lancaster, X. Y. Chong, Y. Y. Lip, and C. Gibbins. 2024. An open-source method for producing reliable water temperature maps for ecological applications using non-radiometric sensors. Remote Sensing Applications: Society and Environment 34:101184.

Torres-Rua, A. 2017. Vicarious Calibration of sUAS Microbolometer Temperature Imagery for Estimation of Radiometric Land Surface Temperature. Sensors 17(7):1499.

Yuan, W., and W. Hua. 2022. A Case Study of Vignetting Nonuniformity in UAV-Based Uncooled Thermal Cameras. Drones 6(12):394.

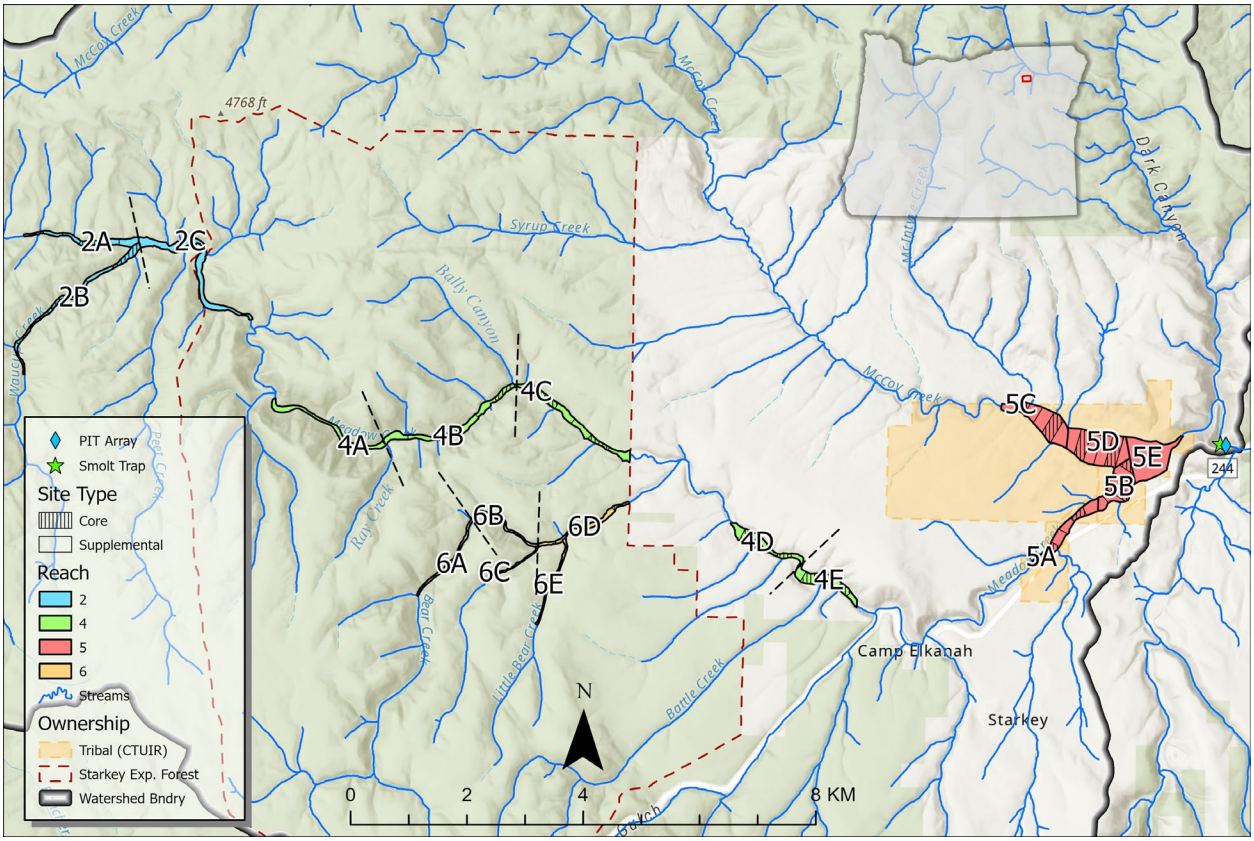

Figure 9. Study area map showing planned floodplain restoration and monitoring sites in the Meadow Creek watershed.

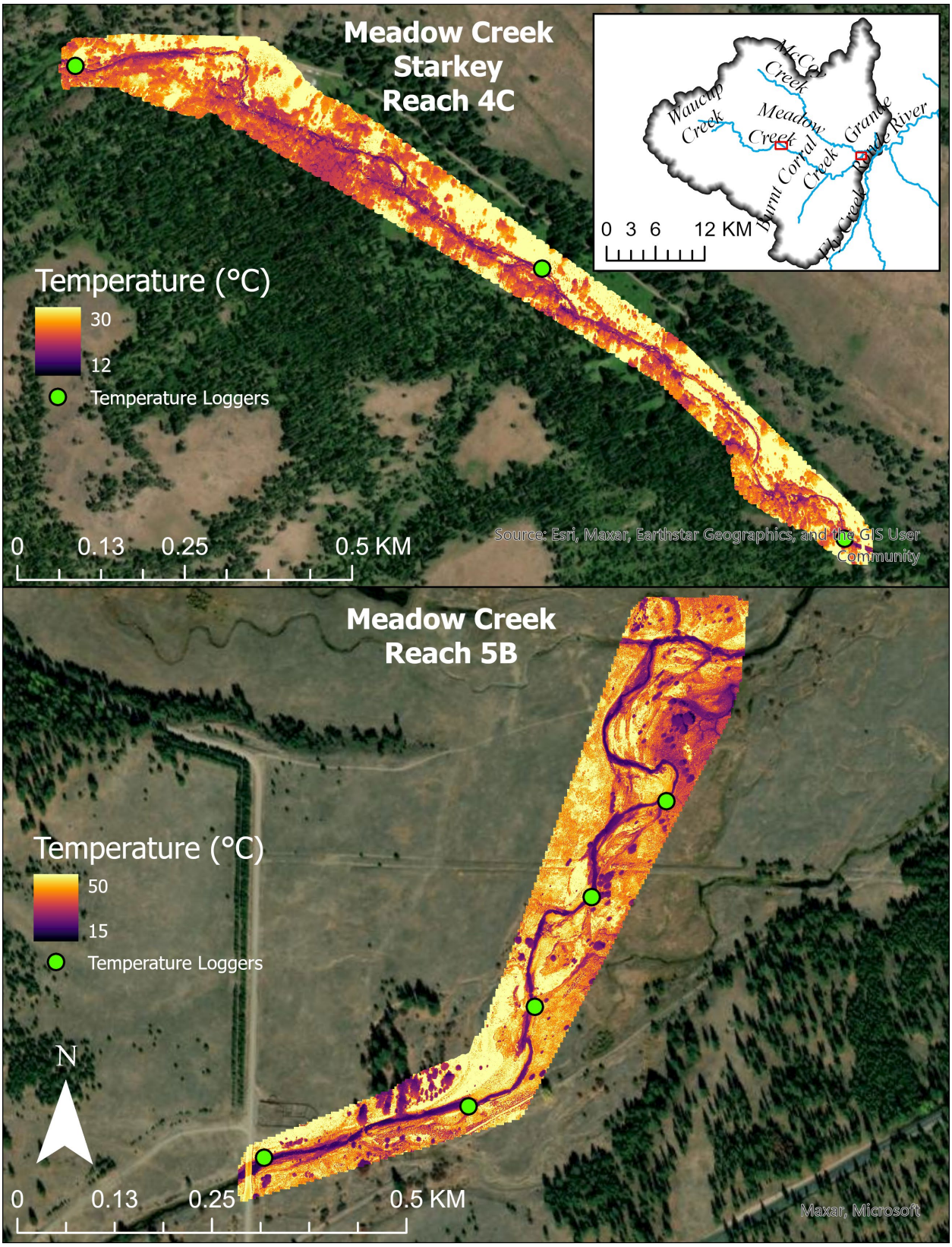

Figure 10. Thermal imagery collected using unmanned aircraft systems (UAS) at two sites in the Meadow Creek watershed during August 2024.

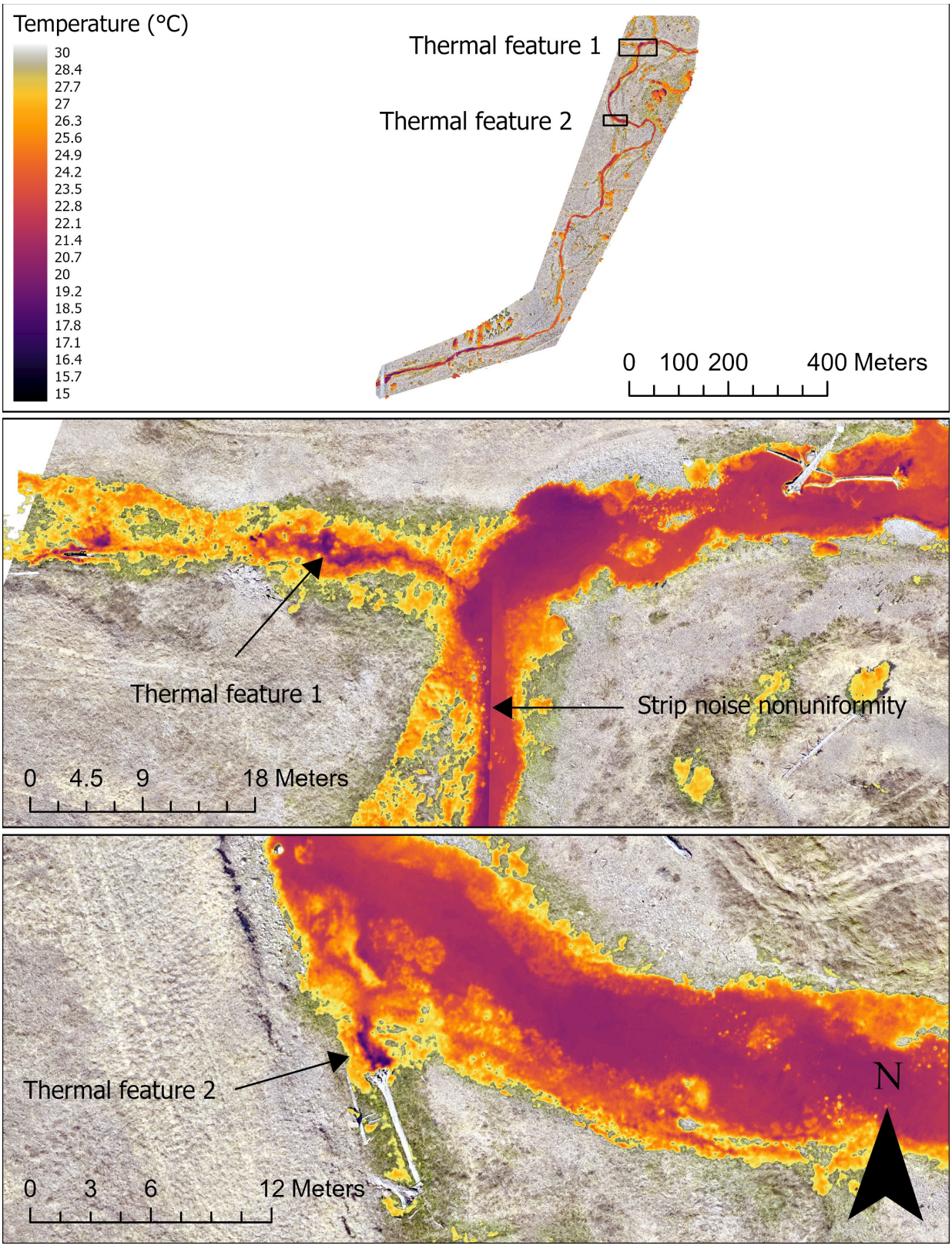

Figure 11. Example of thermal features or potential cold-water refuges from UAS thermal imagery in reach 5B of Meadow Creek during August 2024.

1.4 Thermal imagery acquisition (FLIR)

We contracted NV5 Geospatial to acquire airborne thermal infrared (TIR) and true color imagery data during the summer of 2024 for the Grande Ronde River area of interest (AOI) in northeastern Oregon. This imagery acquisition was co-sponsored by the Grande Ronde Model Watershed (GRMW) and Union Soil and Water Conservation District (USWCD). The survey was conducted between August 16 and August 19, 2024, covering a total length of 570 kilometers (km) of the Grande Ronde Lower Tributaries, Upper Grande Ronde River, Lostine River, Catherine Creek, and Minam River (Figure 12). Prior to the TIR data collection, NV5 field crew deployed 28 data loggers throughout the survey area to record water temperature during the TIR acquisition time frame.

A summary report documenting the contract specifications, data acquisition procedures, processing methods, and analysis of the final datasets is provided in Appendix B. Contracted deliverables including imagery and support files (Table 6) are available upon request.

These data will be used by CRITFC to quantify the spatial distribution and amount of cold-water refugia within the project extent. We will compare these data with availability of cold-water refuge habitats delineated from the 2010 FLIR data to assess how thermal heterogeneity has changed over time at both the watershed scale and at selected restoration sites. Additionally, these data are being used by basin partners (GRMW and USWCD) to guide restoration prioritization through the ATLAS process and to assess project impacts to water temperature.

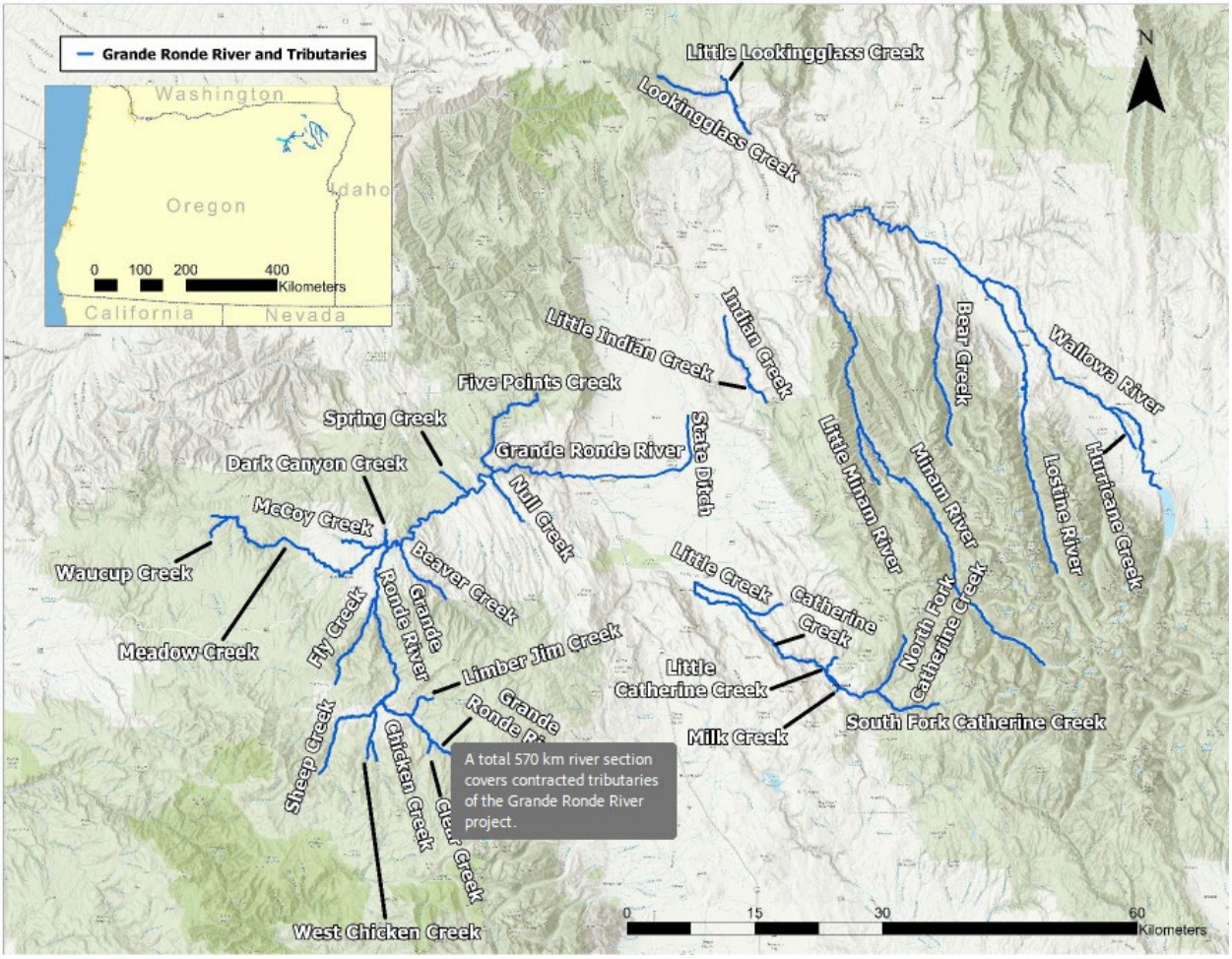

Figure 12. Map of the Grande Ronde, OR thermal infrared survey area.

Table 6. Products delivered to CRITFC for the 2024 Grande Ronde thermal imagery acquisition project.

Product Type	File Type	Product Details
Rasters	**Thermal infrared Imagery** 0.5m GeoTIFF (*.tif) **3-Band (RGB) Digital Imagery** 20 cm GeoTIFF (*.tif) 20 cm GeoTIFF (*.tif) 20 cm MrSID (*.sid)	**Thermal infrared Imagery (cell values = Celsius x 10)** • Calibrated, rectified images • Calibrated, rectified imagery mosaics **3-Band (RGB) Digital Imagery** • Orthorectified Frames • Tiled Imagery Mosaics • AOI Imagery Mosaic
Vectors	Shapefiles (*.shp)	• Stream centerlines • Temperature accuracy assessments • TIR image center points and sensor exterior orientation (EO) • Longitudinal temperature profile (LTP) • Significant thermal features (STF) • RGB Mosaic Tile Index • RGB Orthorectified Frames Index
Supplemental	MS Excel Format (*.xlsx) Layer Files (*.lyr)	• "xlsx" folder contains longitudinal temperature profiles (LTP) and significant thermal features (STF) in MS Excel format (*.xlsx) • "Color ramps" folder contains customized layer files (*.lyrx) for visualization in ArcGIS Pro
Metadata	Extensible Markup Language (*.xml)	• FGDC (CSDGM) compliant Metadata
Reports	Adobe Acrobat (*.pdf)	• Technical Data Report

2. Fish ecology, productivity, and limiting factors

2.1 Juvenile salmonid distribution in the Middle Fork John Day River

Background

The extent and quality of juvenile salmonid rearing habitat is an important limiting factor controlling population carrying capacity and productivity through density-dependent processes (Quinn 2007). As reproductive output increases (e.g., number of spawners) the corresponding production of offspring does not increase linearly; instead, the amount of additional offspring production for each unit increase in reproductive output decreases as juveniles experience greater competition for prey resources and high-quality habitats. Salmon populations across the Columbia River Basin are highly suppressed relative to historic returns, yet density-dependent effects on population dynamics remain persistent (Walters et al. 2013). This may be attributed, in part, to changes in the extent and quality of rearing habitats. For example, if reproductive output remained constant but the spatial extent (or quality) of rearing habitat was contracted, density-dependent effects would increase as juveniles experience greater competition for limited resources. Consequently, a main goal of habitat restoration efforts is to increase the amount and quality of rearing habitats and thereby decrease density dependence.

Density dependence is not only a function of the total number of individuals within a population or watershed, but also how juveniles are distributed at finer spatial scales (e.g., spread out uniformly versus clusters of high densities). The extent of thermally suitable summer rearing habitat within watersheds is projected to contract through time as climate change intensifies (Isaak et al. 2015; Carlson et al. 2025). In thermally heterogeneous watersheds, this contraction may transition from continuous summer rearing extents to a patchwork of thermally suitable rearing habitats nested within warmer habitats (O'Sullivan et al. 2021). These "core" rearing areas are critical in supporting salmonids in warmer years and will be increasingly important with climate change. Evaluating juvenile salmonid distributions in response to inter-annual variation in environmental conditions is an effective tool to identify "core" rearing areas (Flitcroft et al. 2014), providing important information to prioritize the locations of restoration efforts to maintain or enhance summer rearing habitats.

Project overview

This study examines how annual variations in environmental conditions and spawning distributions influence the expansion or contraction of juvenile Chinook Salmon rearing habitat in the Middle Fork John Day River (MFJD). The project is a collaborative effort between the Columbia River Inter-Tribal Fish Commission (CRITFC), the Confederated Tribes of the Warm Springs Reservation of Oregon (CTWSOR), the Oregon Department of Fish and Wildlife (ODFW), and other partners associated with the Middle Fork John Day Intensively Monitored Watershed.

Our initial surveys in 2021 were part of a broader study evaluating juvenile Chinook Salmon dispersal from redds to summer rearing habitats across the MFJD (Kaylor et al. 2025). These surveys took place during a year of record-breaking summer temperatures and low discharge, which appeared to restrict juvenile salmon distribution. Watershed-scale abundance estimates combined with data on dispersal patterns revealed that 1) parr tributary use was high (~27% of all MFJD parr), 2) parr within the mainstem were concentrated in sections with cooler July average maximum daily temperature, and 3) parr originating in warmer mainstem sections generally moved to cooler mainstem sections (such as within the Oxbow Conservation Area) or to tributaries (see Kaylor et al. 2025). Previous survey efforts conducted from 2014-2016 showed a broader distribution of parr as far as 25 km downstream of our 2021 mainstem extent and that temperature was also associated with parr presence (Handley and Ruzycki 2015), a result consistent with other evaluations of juvenile salmonid distribution and temperature in the MFJD (Torgersen et al. 1999, 2006). Cumulatively, these findings suggest that parr distribution across the MFJD at broad spatial scales largely depends on temperature and that inter-annual variation in thermal and flow conditions likely results in expansion (cool, higher flow years) and contraction (warm, lower flow years) of the parr distribution.

We aim to build a long-term dataset of adult spawning and juvenile rearing distributions across the MFJD that encompasses broad variability in environmental conditions and adult run sizes. To date, we have conducted snorkel surveys in 2021, 2023, and 2024, corresponding to spawning distributions from 2020, 2022, and 2023, respectively. A detailed description of the 2021 survey design and methodology is available in Kaylor et al. (2025), whereas details of 2023 surveys can be found in Justice et al. (2024). Beginning in 2023, we refined our sampling approach to ensure a comprehensive and repeatable assessment of rearing extent across varying conditions. This framework will be used in future surveys, including those planned for 2025.

Methods

Spawning ground surveys—led by ODFW and supported by multiple partner agencies and volunteers—are conducted annually across the MFJD spawning extent (Bare et al. 2021). Surveys are performed weekly during peak spawning in mid-September, typically comprising three full surveys each year. In 2020, wildfire smoke delayed the first survey, resulting in only two completed surveys (9/16 and 9/23), whereas three full surveys were conducted in 2022 (9/14, 9/19, 9/26) and 2023 (9/11, 9/18, 9/25). Surveyors walk along opposite stream banks, marking new redds with flagging to prevent duplicate counts, and use GPS to record redd locations during the final survey.

The 2021 sampling design focused on characterizing parr abundance across the rearing extent of that summer, which was contracted due to abnormally warm conditions. In 2023, we expanded and standardized the design to encompass the full potential rearing extent, making it repeatable across years regardless of environmental conditions. Mainstem survey reaches were extended from the 2021 range (rkm 83.8–117.5) to a broader range in 2023 and 2024 (rkm 54.7–122.3). Similarly,

tributary surveys expanded from the 2021 range (rkm 79.8–112.8) to 2023 (rkm 58.3–112.8) and 2024 (rkm 53.6–112.8 after the addition of Slide Creek), informed by previous Chinook Salmon parr distribution studies (Handley et al. 2011; Handley and Ruzycki 2015).

To account for variability in survey effort across years, we categorized mainstem reaches and tributaries into priority tiers. Tier 1 reaches are to be surveyed annually, while Tier 2 reaches are supplementary and surveyed as time and crew availability allows. We used a Generalized Random Tessellation Stratified (GRTS) design to select mainstem sites spanning from Slide Creek (rkm 54) to Phipps Meadows (rkm 122). Of 64 available GRTS points, we identified 30 Tier 1 reaches and 18 Tier 2 reaches that were selected to maximize spatial coverage. In both 2023 and 2024, we leveraged CTWSOR planned sampling to conduct more intensive snorkel surveys from Caribou Creek (rkm 105) to Vinegar Creek (rkm 110) and in Phipps Meadows at the upstream mainstem extent (rkms 120-122). These CTWSOR reaches (11 in 2023; 12 in 2024) overlapped with and replaced four Tier 1 and two Tier 2 reaches. We expanded the number of tributaries from 9 in 2021 to 20 in 2023 (11 Tier 1). In 2024, we largely implemented the same tributary sampling design, but we revised the categorization of Tier 1 and Tier 2 tributaries based on 2023 survey data and feedback from project partners (Table 8) and we added Slide Creek (not previously surveyed) as a Tier 1 tributary after a private landowner granted access.

For 2023 surveys, we scaled mainstem survey reaches with river width (approximately 15x bankfull width), increasing linearly from 200 m at the farthest upstream site (rkm 120.8) to 400 m at the farthest downstream site (rkm 55). We adjusted mainstem reach lengths to 150–300 m for 2024 based on partner feedback that shorter lengths would allow for more sites to be surveyed. To standardize methodology and accommodate the increased effort to survey more tributaries, we established discrete reaches at predetermined intervals. We applied shorter intervals between reaches closer to tributary mouths (typically every 250 m from 0-1 km) and longer distance intervals farther upstream (typically every 500 m upstream of 1 km). We made alterations to this design to navigate around private properties lacking access and to accommodate tributaries where parr are known to move over three kilometers upstream (e.g., Big Creek and Camp Creek; every 500 m from 0-2 km, then every 1000 m). Planned reach lengths for 2023 were 50 m for smaller tributaries (n = 13) and 100 m for larger tributaries (n = 7), but in 2024 we modified reach lengths for larger Tier 1 tributaries to decrease with distance upstream (100 m for first km; 75 m between 1-2 km; and 50 m upstream of 2 km). In both 2023 and 2024, we surveyed reaches from downstream to upstream until zero parr were observed in a reach, which we considered the upstream extent of Chinook parr. To validate this assumption, in 2024 we sampled an additional upstream reach after no fish were observed in a reach when time allowed.

Snorkel surveys were conducted at the habitat unit-level, in which snorkelers recorded counts of Chinook Salmon parr and juvenile *O. mykiss* (except 2021) observed from the reach GPS location upstream until the predetermined survey length was exceeded. We visually delineated habitat units as pools, fast-non-turbulent (FNT; i.e., runs, glides), and fast-turbulent (FT; i.e., riffles). We sampled all pools and FNTs in all years. In 2021, we sampled alternating FTs in mainstem sites

and every fourth FT in tributaries, whereas in 2023 and 2024 we sampled a minimum of 25% of FTs by length for both mainstem and tributary reaches.

To adjust for imperfect detection, we recorded habitat attributes affecting visibility and applied the detection model from Staton et al. (2022) to estimate detection probabilities. Attributes included channel unit type, average depth, large wood density, and observer visibility ratings. We used model-based detection probabilities to expand raw counts into abundance estimates with 80% confidence intervals. For unsurveyed FTs, densities were imputed using mean values from similar units within the same reach. However, in this report, we only present Chinook parr counts scaled by the linear length of reaches (total count/total length in meters) as we plan to update the detection model with additional data collected in 2023.

Results

Snorkel surveys were conducted from 7/17 to 7/26 in 2023 and from 7/1 to 7/18 in 2024. Below, we update the summary of sampling efforts and preliminary results that we previously presented for 2021 and 2023 data (Justice et al. 2024) with survey details and findings from the summer 2024. Notably, in summer 2023, we collected paired snorkel count and mark-recapture data to refine parameter estimates in the Staton et al. (2022) snorkel detection model. These updated estimates will be applied to count data from all survey years, potentially modifying abundance estimates. Therefore, the expanded counts reported here should be considered preliminary.

The spatial distribution of adult spawning extents varied among years, as did the total number of redds, with 162, 237, and 343 total redds in 2020, 2022, and 2023, respectively (Figure 13). While the downstream extent of spawning was similar in all three years (near rkm 70), the upstream extent was contracted in 2020 (max rkm = 114), whereas adults spawned to the farthest possible upstream extent in Phipps Meadows in 2022 and 2023 (~rkm 121). Other notable differences include: 1) A lower proportion of redds from Camp Creek to Big Boulder Creek (rkm 80-88.1) in 2022 (11%) relative to 2020 (20%) and 2023 (19%); 2) A higher proportion of redds within the Oxbow Conservation Area (rkms 92-98.5) in 2022 (38%) relative to 2020 and 2023 (~19% each); and 3) no spawning from the upstream end of Voight's Meadow (rkm 115.7) to the headwaters in Phipp's Meadow in 2020, but 3.4% and 5.2% of redds in 2022 and 2023, respectively.

Survey efforts expanded across years to better capture the full spatial extent of juvenile Chinook Salmon rearing. In 2021, surveys encompassed 7.5 km of the mainstem and 6.1 km of four tributaries, with electrofishing conducted over 2.6 km in five smaller tributaries. In 2023, we surveyed 39 mainstem reaches covering 11.2 km (Table 7) and 88 reaches of 18 tributaries totaling 8.6 km (Table 8). In 2024, we reduced mainstem and tributary reach lengths, which facilitated surveying more reaches, including 49 mainstem reaches across 10.6 km (Table 7) and 110 reaches of 18 tributaries totaling 8.1 km (Table 8).

In 2021, Chinook Salmon parr distribution across the mainstem was highly contracted compared to later years (Figure 14; Figure 15), likely due to extreme summer temperatures and low flows (Kaylor et al. 2025). The highest estimated densities within the mainstem were within the Oxbow

Conservation Area (rkms 91–96) and Forrest Conservation Area (rkms 100–106). In contrast, few parr were observed downstream of Big Boulder Creek (rkm 88.1) or upstream of the confluence with Clear Creek (rkm 112), despite these areas accounting for approximately 35% of 2020 redds. Tributary use was high, and we estimated that ~27% of all parr across the MFJD were within the nine sampled tributaries, of which the four largest – Big Boulder, Granite Boulder Creek, Vinegar Creek, and Clear Creek – accounted for 18.3% of all parr (Kaylor et al. 2025).

In 2023, Chinook Salmon parr were distributed across a broad spatial extent (Figure 14). Parr were observed in 36 of 39 mainstem reaches, absent only from the farthest downstream (rkms 55 & 60) and upstream (rkm 122) reaches. Relative to 2021, parr densities were more broadly distributed along the mainstem from a ~rkm 80 to ~rkm 113, but with several apparent peaks including near rkm 95, rkm 102, and rkm 110. Parr were present in all tributaries surveyed except Lick Creek, a small tributary of Camp Creek. The upstream extent within tributaries was highly variable, with parr detected at least 1 km upstream in eight tributaries, including 3.0 km in Davis Creek, 3.5 km in Vinegar Creek, and 6.5 km in Camp Creek (Figure 16; Figure 17).

In 2024, parr distribution in the mainstem was similar to 2023 with a more continuous distribution from rkm 80 to rkm 112 rather than the distinct bimodal distribution observed in 2021 (Figure 15). Also similar to 2023, parr were present but at low densities from Big Creek to Camp Creek (rkms 64-80) and from Clear Creek to the headwaters in Phipps Meadows (rkms 112-122). In 2023, we identified the downstream extent of parr rearing within the mainstem (two sites with no parr observed). While the farthest downstream reach surveyed in 2024 (rkm 60) had parr present, only two parr were observed over 300 m, suggesting few, if any, parr occupied mainstem habitats farther downstream. Tributary surveys in 2024 largely resembled the patterns observed in 2023, but with several deviations (Figure 16; Figure 17): In 2024 1) parr densities (count/m) were considerably higher in Big Creek, Dead Cow Gulch, and Bridge Creek, but lower in Big Boulder Creek and Vinegar Creek; and 2) parr were observed farther upstream in Big Creek, Butte Creek, Granite Boulder Creek, Clear Creek, Lick Creek, and Ruby Creek, but not as far upstream in Little Boulder Creek and Caribou Creek. Notably, Slide Creek, newly surveyed in 2024 after access to private property was granted, supported a substantial number of parr up to 2 km upstream. Slide Creek will remain a priority tributary to sample in future years to capture downstream tributary rearing extent.

Comparing 2021 to later years highlights the influence of inter-annual variability in environmental conditions on rearing distributions (i.e., Figure 14 and others). The 2021 distribution was more contracted, likely due to extreme temperatures and low summer flows. Temperature thresholds identified in 2021 (mean July daily maximum >25 °C) were exceeded in downstream mainstem reaches, likely limiting parr presence. Consequently, the distribution of redds was poorly associated with parr distribution the following year (Figure 18), which instead tracked longitudinal temperature patterns (Kaylor et al. 2025). In contrast, 2023 and 2024 distributions reflected broader rearing extents and were better associated with the distribution of prior year redds (Figure 18). This is potentially attributed to more favorable thermal and flow conditions that necessitated

less movement and dispersal from emergence locations. Additional years, particularly those with extreme climate conditions, will be critical to further elucidate how environmental variability drives annual rearing distributions (Carlson et al. 2025).

Next steps

Our goal is to assess inter-annual variability in summer rearing distributions of Chinook Salmon parr and juvenile *O. mykiss*, particularly how environmental (e.g., temperature, discharge) and biological (adult spawning distributions) factors influence this variability and how localized response to restoration scale up to shape distribution at the population scale. To achieve this, we will continue building upon this multi-year data set, thereby encompassing a broader range of environmental and biological conditions through time. Once additional data, including those from 2024, are incorporated into updated detection models, we plan to predict parr abundance across the mainstem and tributaries of the MFJD using Spatial Stream Network (SSN) models incorporating biophysical variables as well as spatial autocorrelation to improve network-scale prediction. These analyses will enhance our understanding of how climate variability and restoration efforts shape juvenile salmonid distributions in the MFJD.

References

Bare, C. M., I. A. Tattam, and J. R. Ruzycki. 2021. Chinook Salmon productivity and escapement monitoring in the John Day River basin. Oregon Department of Fish and Wildlife, John Day, OR.

Carlson, S. M., K. C. Pregler, M. Obedzinski, S. P. Gallagher, S. J. Rhoades, C. Woelfle, N. Queener, S. E. Thompson, and M. E. Power. 2025. Anatomy of a range contraction: Flow–phenology mismatches threaten salmonid fishes near their trailing edge. *PNAS* 122(14).

Flitcroft, R., K. Burnett, J. Snyder, G. Reeves, and L. Ganio. 2014. Riverscape Patterns among Years of Juvenile Coho Salmon in Midcoastal Oregon: Implications for Conservation. *Transactions of the American Fisheries Society* 143(1): 26–38.

Handley, K. A., C. James, J. R. Ruzycki, and R. W. Carmichael. 2011. Fish population monitoring in the Middle Fork John Day River intensively monitored watershed - Annual Technical Report 2011. Oregon Department of Fish and Wildlife, Technical Report, La Grande, OR.

Handley, K. A., and J. R. Ruzycki. 2015. Fish Population Monitoring in the Middle Fork John Day River Intensively Monitored Watershed. Page 51. Oregon Department of Fish and Wildlife, Technical Report 212-920–10249, La Grande, OR.

Isaak, D. J., M. K. Young, D. E. Nagel, D. L. Horan, and M. C. Groce. 2015. The cold-water climate shield: Delineating refugia for preserving salmonid fishes through the 21st century. *Global Change Biology* 21.

Justice, C., M. Kaylor, A. Ringelman, B. Staton, and M. Wolf. 2024. Evaluating salmonid and stream ecosystem response to conservation measures and environmental stressors in the Columbia River basin: Annual report 2023. Columbia River Inter-Tribal Fish Commission, Portland, OR.

Kaylor, M. J., L. R. Ciepiela, M. Feden, J. T. Lemanski, C. Justice, B. A. Staton, J. B. Armstrong, S. Kelly, S. R. Narum, I. A. Tattam, and S. M. White. 2025. Watershed-scale dispersal patterns of juvenile Chinook Salmon (*Oncorhynchus tshawytscha*) revealed through genetic parentage analysis. *Movement Ecology* 13(1). https://doi.org/10.1186/s40462-024-00524-3

O'Sullivan, A. M., E. Corey, R. A. Cunjak, T. Linnansaari, and R. A. Curry. 2021. Salmonid thermal habitat contraction in a hydrogeologically complex setting. *Ecosphere* 12(10):e03797.

Quinn, T. P. 2007. The Behavior and Ecology of Pacific Salmon and Trout. University of British Columbia Press.

Staton, B. A., C. Justice, S. White, E. R. Sedell, L. A. Burns, and M. J. Kaylor. 2022. Accounting for uncertainty when estimating drivers of imperfect detection: An integrated approach illustrated with snorkel surveys for riverine fishes. *Fisheries Research* 249:106209.

Torgersen, C. E., D. M. Price, H. W. Li, and B. A. McIntosh. 1999. Multiscale thermal refugia and stream habitat associations of Chinook Salmon in northeastern Oregon. *Ecological Applications* 9(1):301–319.

Walters, A. W., T. Copeland, and D. A. Venditti. 2013. The density dilemma: limitations on juvenile production in threatened salmon populations. *Ecology of Freshwater Fish* 22(4):508–519.

Tables and Figures

Table 7: Characteristics of MFJD mainstem reaches in our sampling design and survey details for 2023 and 2024. We plan to sample Tier 1 reaches in each survey year, whereas Tier 2 reaches are considered supplementary and will be surveyed in future years if time allows.

Reach ID	Rkm	Priority		Planned length (m)		Sampled (y/n)		Sampled length (m)		Comments
	-	2023	2024	2023	2024	2023	2024	2023	2024	-
MFJD_55	54.7	Tier 1	Tier 1	400	300	Y	N	380	-	
MFJD_57	57.7	-	Tier 2	-	300	N	N	-	-	
MFJD_60	60.6	Tier 1	Tier 1	400	300	Y	Y	280	300	
MFJD_63	63.2	-	Tier 2	-	300	N	N	-	-	
MFJD_67	66.6	Tier 1	Tier 1	400	300	Y	Y	335	306	
MFJD_68	68.1	-	Tier 2	-	300	N	N	-	-	
MFJD_69	69.4	Tier 1	Tier 1	400	300	Y	Y	339	355	
MFJD_72	72.0	Tier 1	Tier 2	400	300	Y	Y	428	300	
MFJD_73	73.5	-	Tier 1	-	300	N	N	-	-	
MFJD_75	74.6	Tier 1	Tier 2	400	300	Y	Y	264	300	
MFJD_76	76.5	-	Tier 1	-	300	N	N	-	-	
MFJD_78	78.5	Tier 1	Tier 2	400	300	Y	Y	234	319	
MFJD_80	79.7	-	Tier 1	-	300	N	Y	-	250	
MFJD_83	82.7	Tier 1	Tier 2	400	250	Y	Y	449	256	
MFJD_84	83.8	Tier 1	Tier 1	350	250	Y	Y	433	259	
MFJD_85	85.3	Tier 1	Tier 2	350	250	Y	Y	431	250	
MFJD_86	86.5	Tier 2	Tier 1	350	250	N	Y	-	323	
MFJD_88	87.9	Tier 1	Tier 2	350	250	Y	Y	318	250	
MFJD_89	88.9	Tier 1	Tier 1	350	250	Y	Y	290	247	
MFJD_90	90.4	Tier 1	Tier 2	350	250	Y	Y	268	258	
MFJD_91	91.5	Tier 2	Tier 1	350	250	N	N	-	-	
MFJD_92	92.4	Tier 1	Tier 2	350	250	Y	Y	427	245	
MFJD_93	93.5	Tier 1	Tier 1	300	250	Y	Y	360	267	
MFJD_95	94.6	Tier 1	Tier 1	300	250	Y	Y	288	258	
MFJD_97	97.0	Tier 1	Tier 1	300	250	Y	Y	334	201	
MFJD_98	98.3	Tier 2	Tier 1	300	200	N	Y	-	202	
MFJD_99	99.1	Tier 1	Tier 2	300	200	Y	Y	314	238	
MFJD_100	99.8	Tier 2	Tier 1	300	200	N	Y	-	206	
MFJD_101	100.9	Tier 2	Tier 2	300	200	N	Y	-	197	
MFJD_102	101.6	Tier 1	Tier 2	300	200	Y	Y	398	289	
MFJD_103	102.6	Tier 1	Tier 1	300	200	Y	Y	290	197	
MFJD_104	104.5	Tier 1	Tier 1	250	200	Y	Y	235	202	
MFJD_106	105.9	Tier 2	Tier 1	250	200	Repl.	Repl.	427	420	Replaced by 2 reaches
MFJD_107	106.6	Tier 1	Tier 2	250	200	Repl.	Repl.	212	207	Replaced by 1 reach
MFJD_108	107.7	Tier 1	Tier 1	250	200	Repl.	Repl.	225	207	Replaced by 1 reach
MFJD_109	108.8	Tier 2	Tier 1	250	200	Repl.	Repl.	562	485	Replaced by 2 reaches

Reach ID	Rkm	Priority		Planned length (m)		Sampled (y/n)		Sampled length (m)		Comments
	-	2023	2024	2023	2024	2023	2024	2023	2024	-
MFJD_110	109.7	Tier 1	Tier 2	250	200	Repl.	Repl.	523	488	Replaced by 2 reaches
MFJD_110_2	110.4	Tier 2	Tier 1	250	200	N	Y	-	198	
MFJD_111	111.1	Tier 1	Tier 2	250	200	Y	Y	265	205	
MFJD_112	112.2	Tier 1	Tier 1	250	200	Y	Y	224	198	
MFJD_113	113.1	Tier 1	Tier 2	200	200	Y	Y	191	151	
MFJD_114	114.1	Tier 1	Tier 1	200	150	Y	Y	203	150	
MFJD_116	115.6	Tier 1	Tier 1	200	150	Y	Y	174	157	
MFJD_117	117.4	Tier 2	Tier 1	200	150	N	Y	-	213	
MFJD_118	118.1	Tier 2	Tier 1	200	150	Y	Y	158.6	200	
MFJD_119	119.3	Tier 1	Tier 1	200	150	Y	Y	188.7	209	
MFJD_121	120.8	Tier 1	Tier 1	200	150	Repl.	Repl.	719	796	Replaced by 4 reaches
Total	-	-	-	-	-	38 reaches	49 reaches	11.17 km	10.56 km	

Table 8. Characteristics of MFJD tributaries in our sampling design and survey details for 2023 and 2024. Planned length indicates the predetermined target length for individual reaches; Sampled length indicates the summed length of all sampled reaches; Max reach indicates the farthest upstream reach that was surveyed.

Tributary	Rkm	Priority		Planned length (m)		Surveyed (Y/N)		# reaches sampled		Sampled length (m)		Max reach (m)	
		2023	2024	2023	2024	2023	2024	2023	2024	2023	2024	2023	2024
Slide	53.6	-	Tier 1	-	100	N	Y	-	7	-	378	-	2000
Indian	58.3	-	Tier 2	100	50	Y	Y	2	3	200	155	250	500
Big	64.1	Tier 1	Tier 1	100	100	Y	Y	5	7	600	977	3500	4000
Bear	74.7	Tier 2	Tier 2	50	50	Y	Y	3	4	308	201	750	750
Camp	79.7	Tier 1	Tier 1	100	100	Y	Y	8	8	936	745	6500	7500
Lick	79.7	Tier 2	Tier 2	50	50	Y	Y	1	3	107	159	0	500
Big Bldr.	88.1	Tier 1	Tier 1	100	100	Y	Y	7	7	766	629	2000	2000
Beaver	92.8	Tier 2	P/A	50	-	N	N	-	-	-	-	-	-
Ruby	94.2	Tier 2	Tier 2	50	50	Y	Y	4	6	395	307	750	1500
Granite Bldr.	95.1	Tier 1	Tier 1	100	100	Y	Y	5	8	558	816	1000	2500
Butte	96.4	Tier 1	Tier 1	50	50	Y	Y	5	7	364	393	1500	2000
Little Butte	101.1	Tier 2	Tier 2	50	50	Y	N	3	-	315	-	750	-
Little Bldr.	103.1	Tier 2	Tier 2	50	50	Y	Y	4	4	457	205	750	750
Deerhorn	104.0	Tier 2	Tier 2	50	50	Y	Y	3	3	302	158	500	500
Caribou	105.4	Tier 2	Tier 2	50	50	Y	Y	3	1	313	51	500	250
Dead Cow	108.3	Tier 1	Tier 1	50	50	Y	Y	4	5	201	341	1000	1000
Vinegar	110.0	Tier 1	Tier 1	100	100	Y	Y	10	11	1075	893	3500	4000
Davis	110.7	Tier 1	Tier 1	100	50	Y	Y	9	10	523	570	3000	3500
Bridge	112.0	Tier 1	Tier 1	50	50	Y	Y	4	6	231	307	1500	2000
Clear	112.8	Tier 1	Tier 1	100	100	Y	Y	8	10	951	819	2500	3500
Summit	123.5	Tier 2	P/A	50	-	N	N	-	-	-	-	-	-
Total	-	-	-	-	-	18	18	88	110	8.6 km	8.1 km	-	-

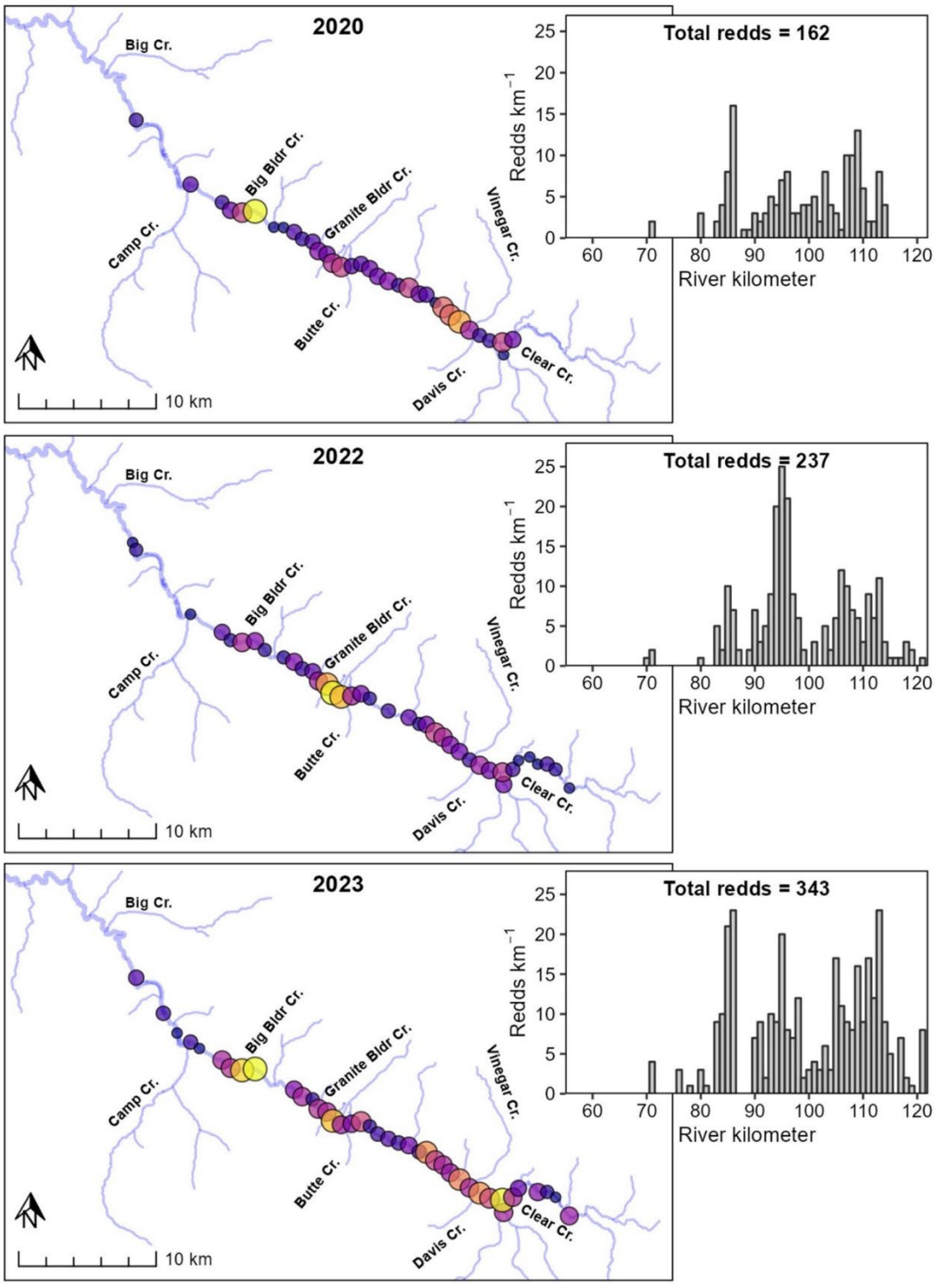

Figure 13: Map of redd density (redds km-1) across the MFJD in 2020, 2022, and 2023 and the distribution of redds by river kilometer in each year (insets). Offspring of these adults were sampled in 2021, 2023, and 2024.

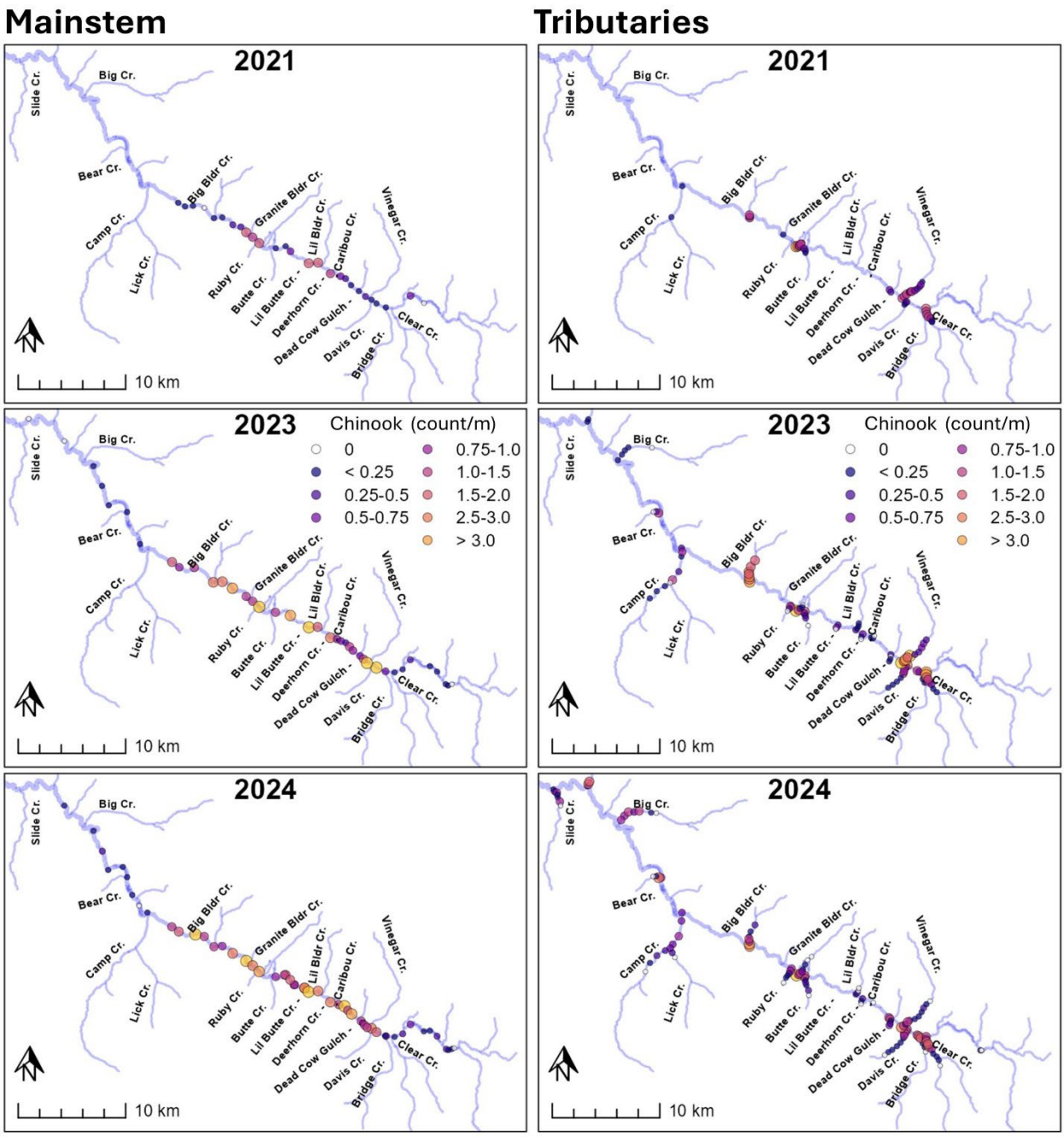

Figure 14: Parr densities at surveyed mainstem (left panels) and tributary (right panels) reaches across the MFJD in the summers of 2021 (top panels), 2023 (middle panels), and 2024 (bottom panels).

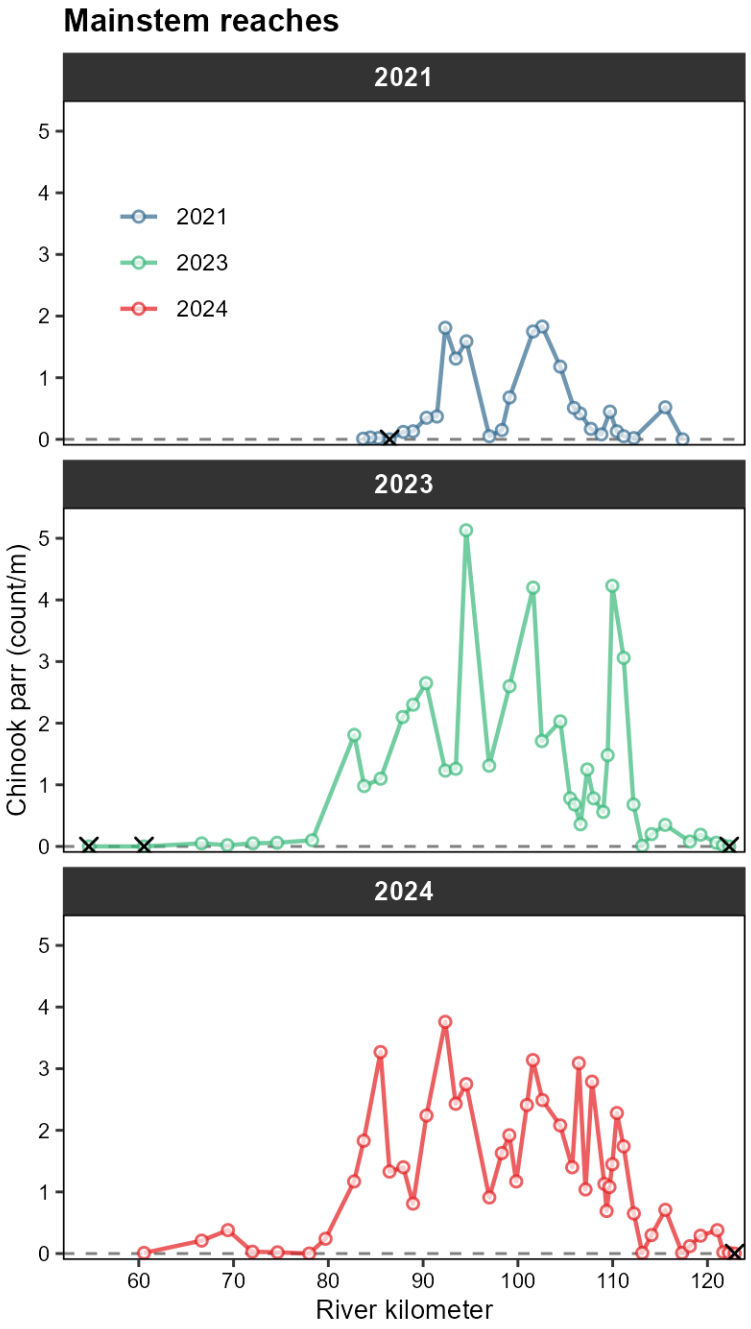

Figure 15: Chinook parr observed (count/m) in mainstem reaches across the MFJD in 2021 (blue lines and points), 2023 (green), and 2024 (red).

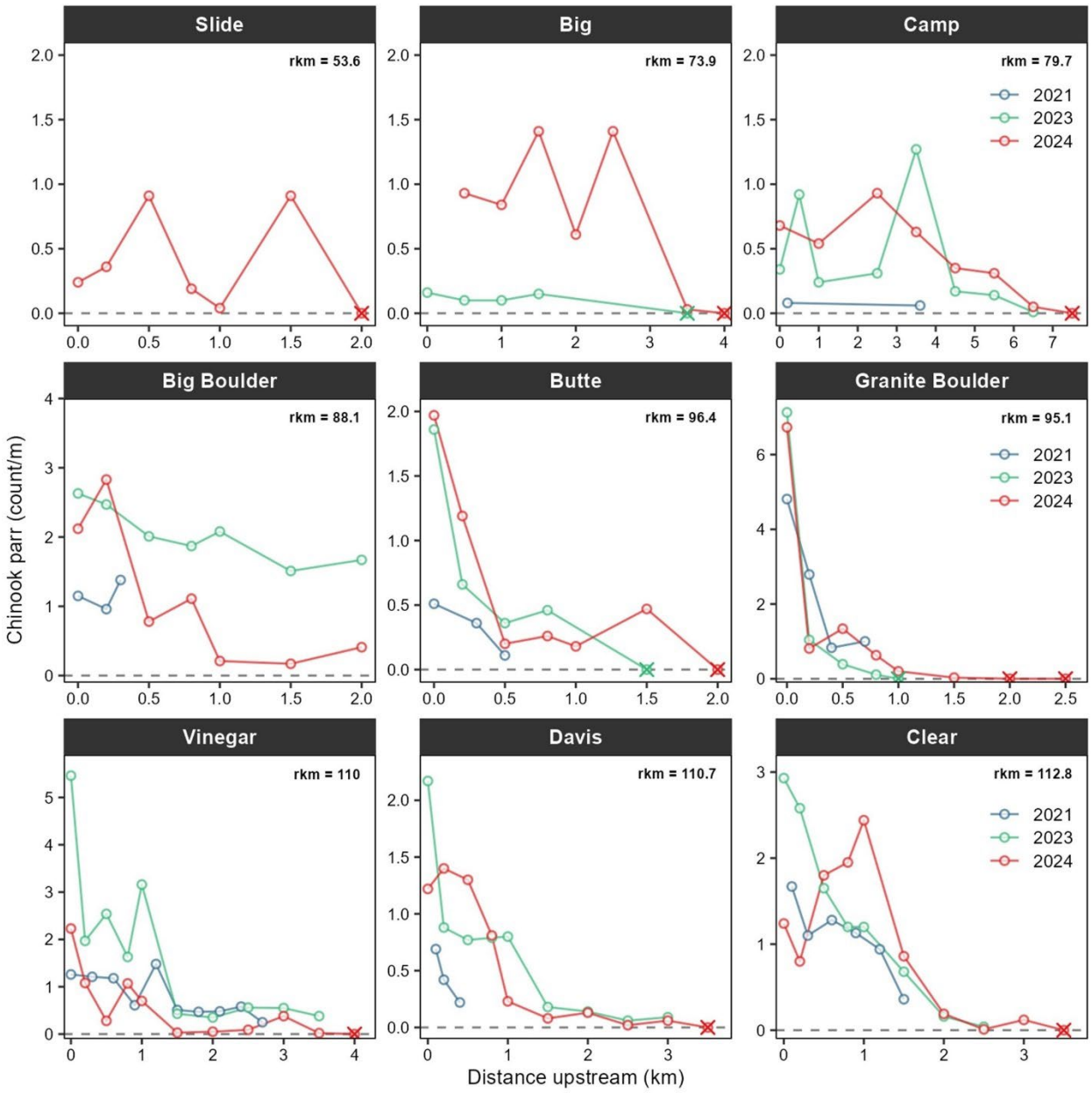

Figure 16: Chinook parr (count/m) in nine of the largest MFJD tributaries from rkm 50 to the headwaters near rkm 121 in 2021 (blue), 2023 (green), and 2024 (red). Counts are not corrected for imperfect detection. X's indicate reaches where no chinook parr were observed.

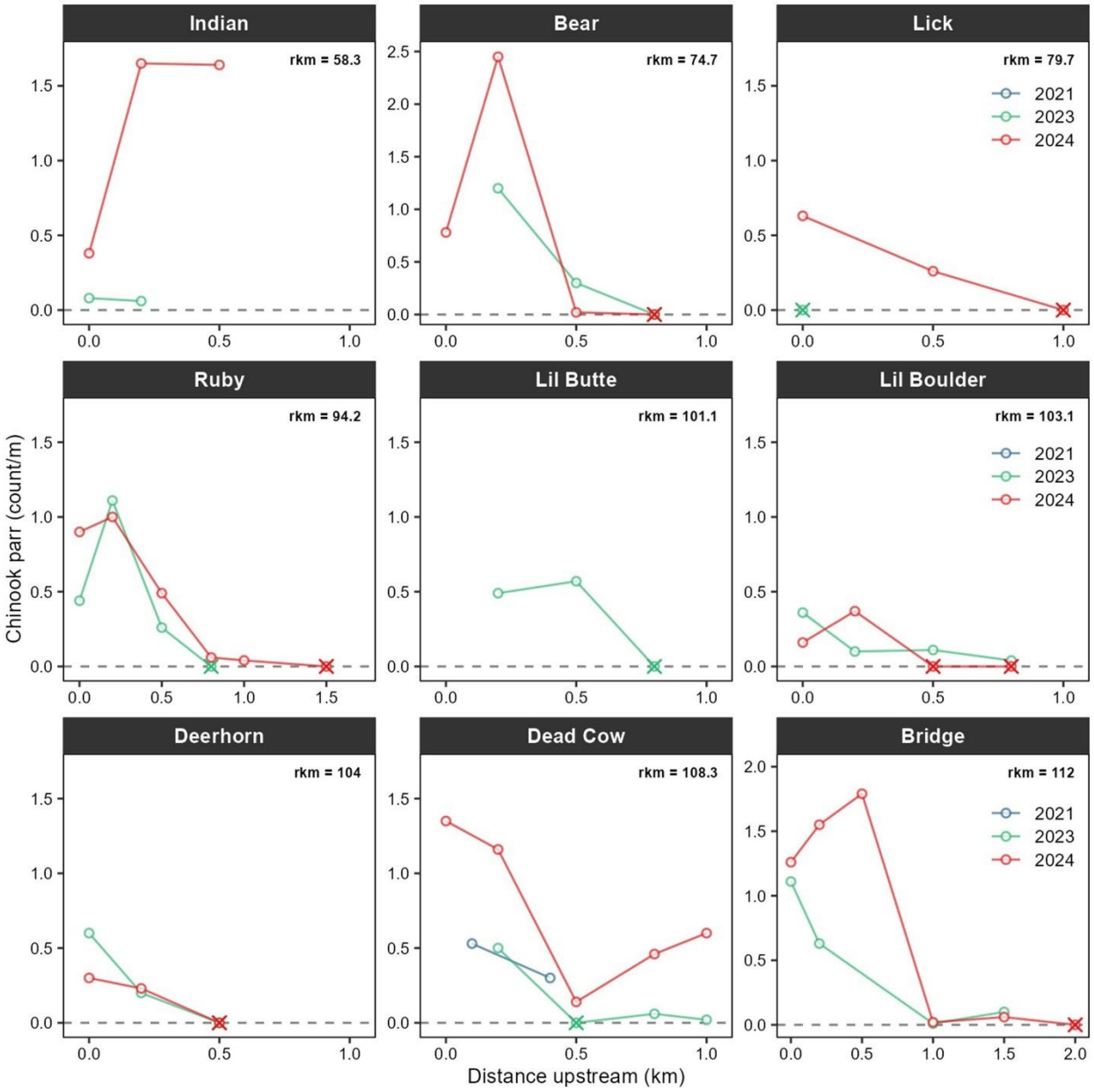

Figure 17: Chinook parr (count/m) in nine of the smaller MFJD tributaries from rkm 50 to the headwaters near rkm 121 in 2021 (blue), 2023 (green), and 2024 (red). Counts are not corrected for imperfect detection. X's indicate reaches where no chinook parr were observed.

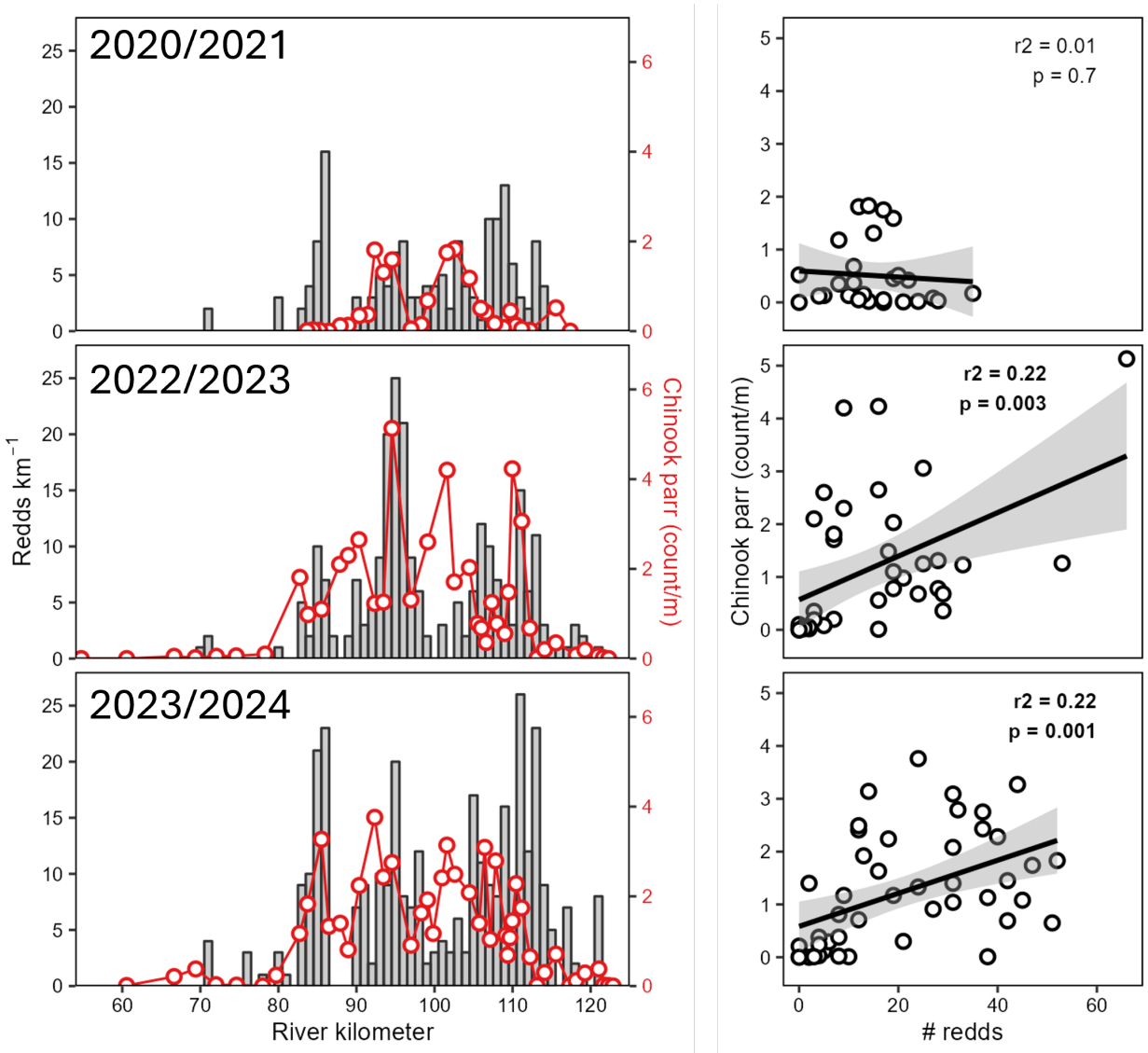

Figure 18: The distribution of redds across the MFJD in 2020, 2022, and 2023 (grey bars) relative to the distribution of their offspring (parr; red points and lines) the following summers in 2021, 2023, and 2024. The right panels show the linear relationship between the number of redds (within 2 km upstream and 1 km downstream of parr survey reaches) and the number of parr observed in mainstem reaches (count/m).

2.2 Spatial Relative Reproductive Success study

Background

Relative Reproductive Success (RRS) studies have proved to be an important tool to evaluate anadromous salmon population trends and the efficacy of hatchery supplementation actions (Koch et al. 2022; Nuetzel et al. 2023). RRS studies use genetic parentage-based tagging (PBT) to evaluate spawner success through comparing the number offspring – either as juveniles or returning adults – that are genetically-assigned to individual adults relative to other adults or groups of adults (e.g., hatchery-origin vs. natural-origin spawners). In RRS studies, adults are typically sampled at weirs as they return to natal streams and their offspring are sampled as out-migrating juveniles at screw traps or as returning adults to weirs several years later. With this approach, the spawning locations of individual adults are typically unknown, precluding evaluation of how and why adult reproductive success may vary spatially and temporally throughout a watershed.

We plan to extend the utility of RRS and PBT as tools to evaluate female spring-run Chinook Salmon reproductive success as a function of spawning location throughout watersheds. This approach requires 1) genotyping adults with known spawning locations, 2) obtaining and genotyping a random sample of their offspring, either as summer-rearing parr, out-migrants captured at screw traps, or returning adults to the weir, and 3) performing PBT to genetically assign offspring to maternal parents, thus determining individual locations of origin. In subbasins where RM&E efforts already include adult trapping and handling at weirs, regular spawning ground surveys (SGS), and summer parr sampling or juvenile out-migrant sampling using rotary screw traps, the minimum sampling requirements to evaluate spatial RRS are already in place if collecting tissue samples for genotyping are also being collected or could be collected. Relatively small increases in additional sampling effort could increase data resolution and sample sizes; for example, by supplementing spawning ground surveys to increase the number of spawners with known locations; PIT tagging adults captured and released above the weir (not required but highly beneficial); and bolstering the number of tissue samples collected from offspring (if they are not already being collected).

We believe this approach could be an important tool to assess watershed-scale habitat-productivity relationships, assess limiting factors across multiple life stages, evaluate response to management actions (e.g., restoration and hatchery supplementation), and inform population responses to climate change and disturbances (e.g., drought, fire). This approach could be particularly powerful because the key metric – the relative number of offspring produced by individual female spawners – integrates numerous processes (e.g., growth, survival) across multiple life stages, providing a cumulative metric to assess spatial patterns of productivity across freshwater life stages.

Preliminary analyses on previously collected data demonstrate the feasibility of this approach and provide an example of the analyses and results that can be achieved (Figure 19). We sampled post-spawn Chinook Salmon across the Middle Fork John Day River (MFJD) in 2020, sampled the

offspring of these adults in summer of 2021 (parr life stage), and used PBT to assign maternal parent-offspring pairs (see Kaylor et al. 2025). We then were able to estimate the number of offspring (from our samples rather than the total number of offspring present within the watershed) that were assigned to each individual female as a function of assumed spawning location (i.e., river kilometer of sampled carcass; Figure 19). However, our 2021 offspring sampling approach – capturing ~3300 parr across 21 mainstem reaches and nine tributaries – required substantial sampling and analytical effort, including additional surveys to estimate watershed-scale abundance used to adjust for sampling bias and better represent a random sample of the population (see Kaylor et al. 2025). To evaluate spatial patterns of reproductive success (rather than watershed-scale dispersal patterns as in the above study), offspring sampling could be conducted with considerably less effort by leveraging already-established summer parr capture and tagging efforts as well as screw traps and associated out-migrant sampling, which has the additional benefit of better representing a random sample of the juvenile population surviving to that life stage.

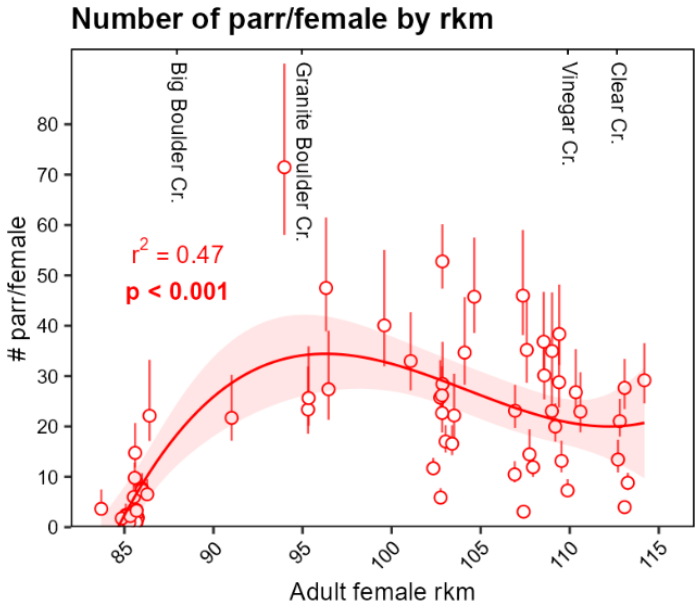

Figure 19: Spatial patterns of estimated relative reproductive success (number of parr/female) across the Middle Fork John Day River. Unpublished data. See Kaylor et al. 2025 for sampling methods and analytical approach to account for sampling bias.

Project overview

The goals of this study are 1) to evaluate spatial patterns of Chinook Salmon reproductive success (with an emphasis on females) across watersheds and in relation to thermal/hydrologic conditions, physical habitat, restoration, and parental attributes (e.g., natural- vs hatchery-origin, length, timing of weir capture, etc.), and 2) to refine the methodological and analytical approaches (e.g., required sample sizes, accounting for temporal patterns, detection, etc.) It is our intent to provide the information and lessons learned from this study as guidance for other research personnel and resource managers interested in applying this approach to other populations, locations, and species.

We are implementing this study across three subbasins– the Middle Fork John Day River (MFJD), Catherine Creek (CC), and Lookingglass Creek (LKG) – in collaboration with the Oregon Department of Fish and Wildlife (ODFW), the Confederated Tribes of the Umatilla Indian Reservation (CTUIR), the Confederated Tribes of the Warm Springs Reservation of Oregon (CTWSOR). These watersheds exhibit distinct thermal and hydrologic regimes, providing an opportunity to evaluate whether and to what degree spatial patterns of reproductive success are shaped by thermal/hydrologic characteristics of watersheds. Further, these watersheds differ in hatchery supplementation practices and associated RM&E infrastructure (e.g., use of weirs for adult trapping), providing an opportunity to assess potential differences in spatial patterns of productivity between hatchery- and natural-origin adults.

We completed adult sampling in brood years (BYs) 2023 and 2024 for MFJD and CC and in BY 2024 for LKG*. Offspring from each BY migrate out of the headwaters to areas lower in the system starting in the fall of BY+1 (e.g., fall 2024 for BY 2023) through the spring of BY+2 (e.g., spring 2025 for BY 2023). Rotary screw traps are operated by ODFW in all three subbasins and BY 2023 outmigrant sampling began in the fall of 2024 and will continue through June 2025 for CC and MFJD (see Table 9). BY 2024 outmigrant sampling will occur from fall 2025 through spring 2026 for CC, MFJD, and LKG.

(* Data presented in this report only pertains to BY 2024 adult sampling.)

Table 9: Gantt chart showing the timeline for weir sampling, adult sampling during spawning ground surveys, and juvenile/offspring sampling at screw traps. Note that there is no weir present for MFJD. Green fill indicates BY 2023 sampling and blue fill indicates BY 2024 sampling. *Note that rotary screw traps are typically pulled during winter, but some trapping may occur in portions of winter months (e.g., December, January, February) when flow conditions are favorable for trapping.

		2023				2024				2025				2026			
Subbasin	Sampling	Sp	Su	Fa	W	Sp	Su	Fa	W	Sp	Su	Fa	W	Sp	Su	Fa	W
CC	Adults-weir																
	Adults-SGS																
	Out-migrants												*				
LKG	Adults-weir																
	Adults-SGS																
	Out-migrants												*				
MFJD	Adults-weir																
	Adults-SGS																
	Out-migrants												*				

Methods

Weirs are installed on CC and LKG and operated by CTUIR to capture returning adults, obtain broodstock, and record data on adults passed upstream. For each fish passed upstream to spawn, data such as length, sex, and origin were recorded, tissue samples were taken for genetics, and a

PIT-tag was inserted into the dorsal sinus. The unique PIT-tag code allowed surveyors to scan carcasses recovered on spawning ground surveys and link individuals to the genetic sample taken at the weir, providing a higher quality genetic sample than typically sampled from carcasses. For the MFJD, which lacks a weir or adult trapping, tissue samples could only be collected from post-spawn carcasses.

Adults were sampled from spawning locations across CC in 2023 and 2024, MFJD in 2023 and 2024, and Lookingglass Creek in 2024. In each subbasin and year, carcasses were sampled through a combination of standard spawning ground surveys (SGS) and additional supplemental surveys. Standard SGSs are led by CTUIR in LKG and ODFW in MFJD and CC but are carried out by staff and volunteers representing numerous agencies. Standard SGSs are implemented across most of the accessible spawning extent and typically occur once a week for 2-4 consecutive weeks. Supplemental surveys were conducted by a smaller group of 1–4 surveyors, targeting locations of live adults on redds to increase the sample size of adults with known spawning locations. We implemented more intensive supplemental spawning ground surveys for MFJD, typically sampling reaches with high spawning activity every 2-3 days, because tissues samples could only be obtained from carcasses, and DNA degrades rapidly resulting in unsuccessful genotyping of older or more degraded samples. Newly encountered carcasses were surveyed using the established SGS protocols of each subbasin, which typically involved measuring length (fork length and/or middle of eye to posterior scale; MEPS), recording presence of adipose clip and opercle marks, examining body cavity for sex and percent eggs retained, a GPS point was recorded, and the unique PIT-tag code (if present) was recorded.

For LKG (BY 2024) and to a lesser extent CC (BY 2024), we also scanned the PIT-tag of post-spawn, moribund adults to obtain fish locations that could be linked back to weir metadata and genetic samples. This was necessary in LKG due to extremely poor carcass recovery rates, likely attributed to the combination of high scavenging rates and greater stream flow than the other subbasins. We used an approximately 2 m wood handle with an HPR-Lite PIT-tag reader attached at the end to scan the dorsal area of moribund fish. We only attempted to scan live fish that were clearly post-spawn; in most cases, live adults were tucked against the bank or under cover and could be scanned without them noticing or responding. If an adult swam away due to our presence, and appeared in good condition, we moved on and then returned 1-3 days later.

In 2024, standard SGSs were conducted on 8/27, 9/4, and 9/10 for CC, for LKG, and 9/9, 9/16, and 9/23 for MFJD. Supplemental surveys were conducted over an additional 7 days in CC (8/28-9/12), 8 days in LKG, and 6 days in MFJD (9/17-9/30).

Results (2024 only)

Catherine Creek

There were 149 redds identified in CC during 2024 SGSs (note that this is not an estimate of the total number of redds in Catherine Creek in 2024). A total of 195 carcasses were sampled during standard and supplemental SGSs, with ~25% (n = 48) of carcasses collected during supplemental

surveys. In addition, the dorsal-implanted PIT-tags of 74 moribund adults were scanned, providing assumed spawning locations that can be linked to weir metadata and genetic samples. Of the 74 live-scanned adults, 28 were later surveyed as carcasses, whereas 46 were not and no carcass survey data (e.g., fork length, field-confirmed sex and origin) is available. Collectively between sampled carcasses and passive live-scanning, 241 individual adults were surveyed, of which 230 had retained a PIT-tag they received at the weir. Supplemental surveys accounted for 39% of adults with known locations (94 out of 241).

Of the 241 surveyed adults, we collected data from nearly three times more hatchery-origin (n = 167) than natural-origin adults (n = 67), which is roughly consistent with the proportion of hatchery and natural origin adults release above the weir to spawn. Note that the number, proportion, and distribution of SGS-sampled NOR and HOR adults presented in this report may differ from those of ODFW; for live-scanned adults and degraded carcasses with unknown sex and/or origin, we used their unique PIT-tag to pair to data collected at the weir to obtain sex and origin. Ultimately, we plan to use the genetically-determined sex and origin of all adults for all analyses. The distribution of sampled adults generally reflected the distribution of redds (Figure 20); however, the spatial distribution of HOR and NOR adults differed throughout the watershed, with proportionally more HOR adults sampled farther upstream and more NOR adults sampled farther downstream (Figure 20). Natural-origin adults comprised 77%, 37%, 21%, and 10% of sampled adults between rkms 70-75, 75-80, 80-85, and 85-90, respectively, with an opposite trend for HOR adults. The numbers of male and female adults were similar for both HOR (77 males, 85 females) and NOR (34 males, 31 females) adults.

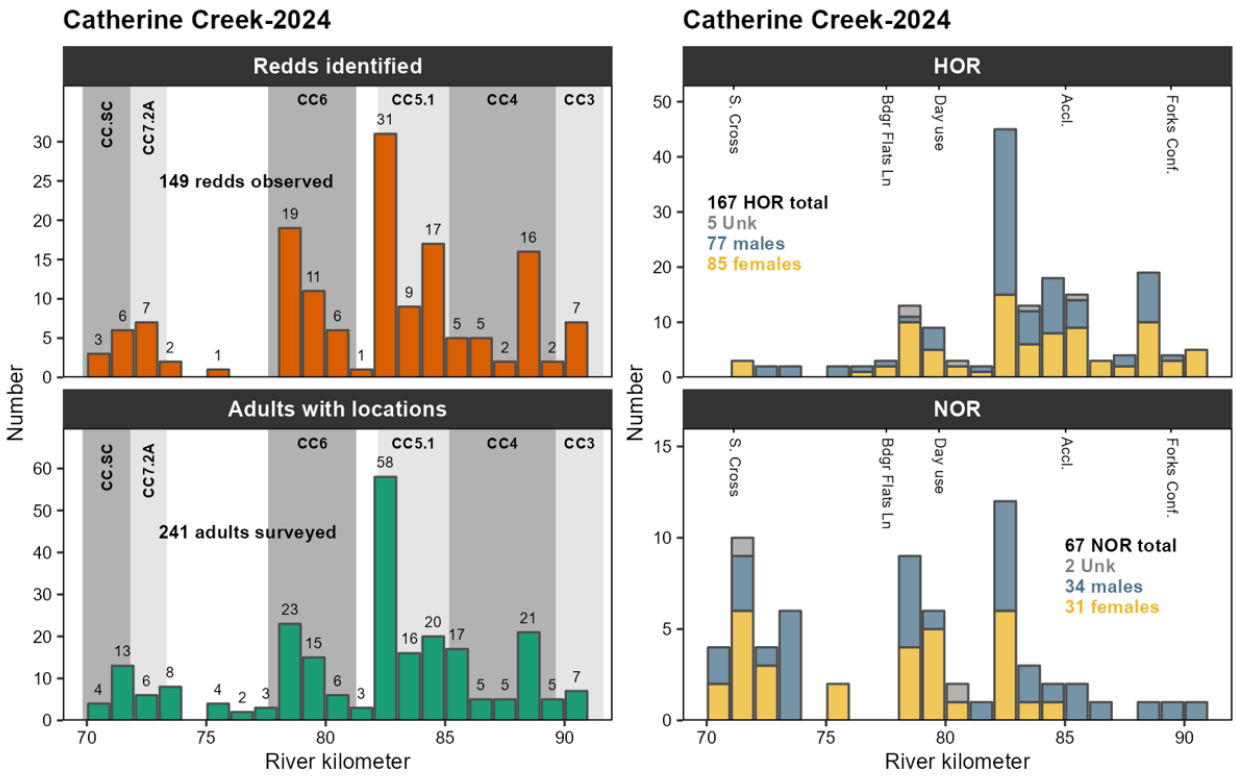

Figure 20: Left panels: Distribution of redds (top) and surveyed adults (bottom) across Catherine Creek in 2024. Right panels: Distribution of surveyed adults separated by hatchery-origin (HOR; top) and natural-origin (NOR; bottom) and color-coded by sex, with blue, yellow, and grey indicating males, females, and unknown sex, respectively. The reach-level labels on the left panel refer to spawning ground survey reaches. The labels on the right panels refer to landmarks: S. Cross = the CTUIR Southern Cross property; Bdgr Flats Ln = where Badger Flats lane crosses over the river; Day use = Catherine Creek State Park – day use area; Accl. = Catherine Creek Hatchery Acclimation Facility; Forks Conf. = The confluence of the North Fork and South Fork Catherine Creek, forming the mainstem CC downstream.

Lookingglass Creek

A total of 83 redds were identified in LKG in 2024; however, a substantial amount of spawning occurs from the confluence with the Grande Ronde River to the weir and only 43 redds were upstream of the LKG adult trap/weir. The offspring of adults that spawned downstream of the weir are unlikely to be captured at the screw trap (located near the weir), and the following results therefore focus on sampling effort upstream of the weir. A total of 47 carcasses were sampled upstream of the weir, and we scanned the PIT-tags of 37 unique adults, 10 of which were later sampled as carcasses. Between sampled carcasses and live-scanned adults, the locations of 74 adults upstream of the weir were determined.

Of the 74 sampled adults, there were 33 females (45%), 34 males (46%), and 7 unknown (9%), whereas of adults sampled at the weir and passed upstream, females and males comprised 57% and 43%, respectively. Most of the 74 adults were hatchery-origin (n = 48; 65%) with only 20 (27%) identified as natural-origin and 6 (8%) with unknown origin, which was similar to the

composition of adults passed upstream of the weir (67% HOR; 33% NOR). The distribution of surveyed adults generally aligned with the distribution of redds (Figure 21).

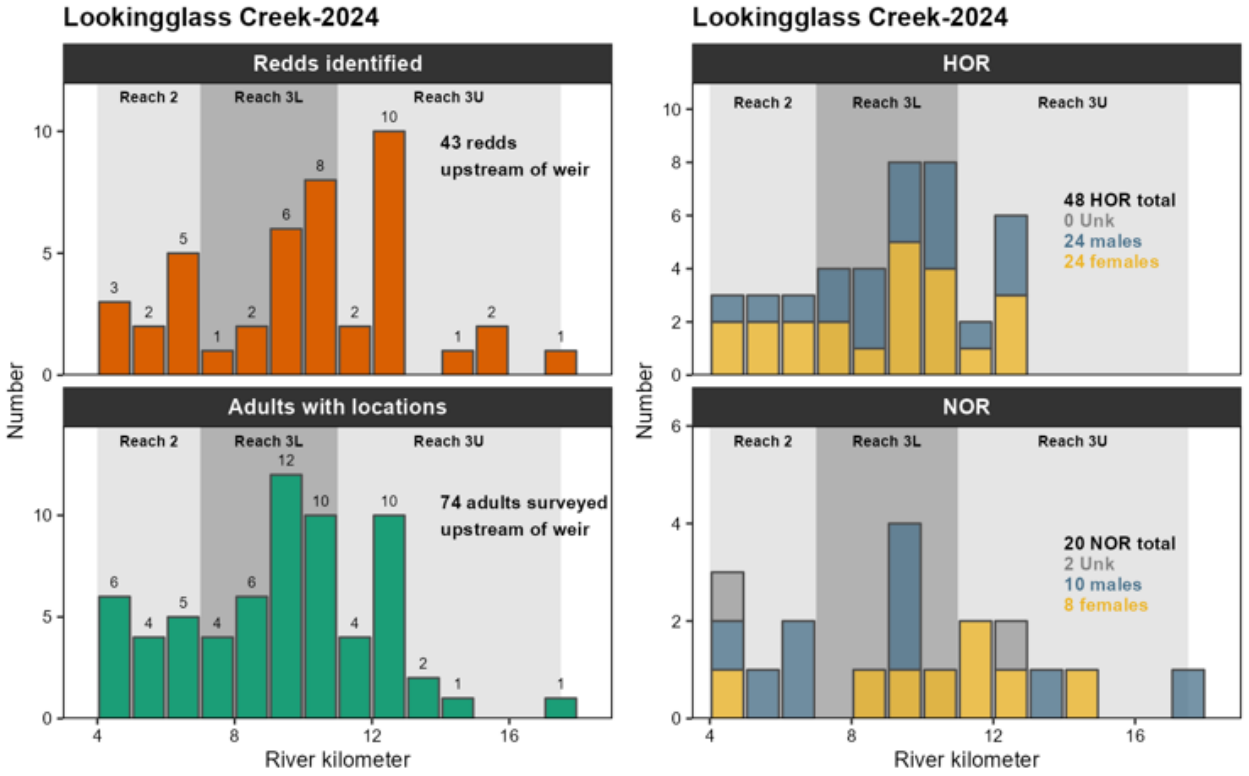

Figure 21: Left panels: Distribution of redds (top) and surveyed adults (bottom) across Lookingglass Creek in 2024. Right panels: Distribution of surveyed adults separated by hatchery-origin (HOR; top) and natural-origin (NOR; bottom) and color-coded by sex, with blue, yellow, and grey indicating males, females, and unknown sex, respectively.

Middle Fork John Day

In 2024, 143 redds were identified in the MFJD watershed. Redds spanned nearly 50 km of the mainstem and there were three redds in Clear Creek. A total of 102 carcasses were sampled, 43 (42%) of which were sampled during supplemental surveys. The distribution of carcasses generally mirrored that of redds, except for the Oxbow Conservation Area (OCA; rkms 91-97) where otter predation and scavenging was particularly high, as has been documented in other years. Spawning activity in the OCA was high with 23 redds observed, but only 8 carcasses were sampled and most were located at the downstream end of the Oxbow reach (Figure 22). There was an even number of male and female carcasses surveyed (n = 43 each) and the sex of 16 carcasses could not be determined due to scavenging and/or degradation. As with the other subbasins, the genetically-determined sex of each adult will be used in analyses rather than visual determination.

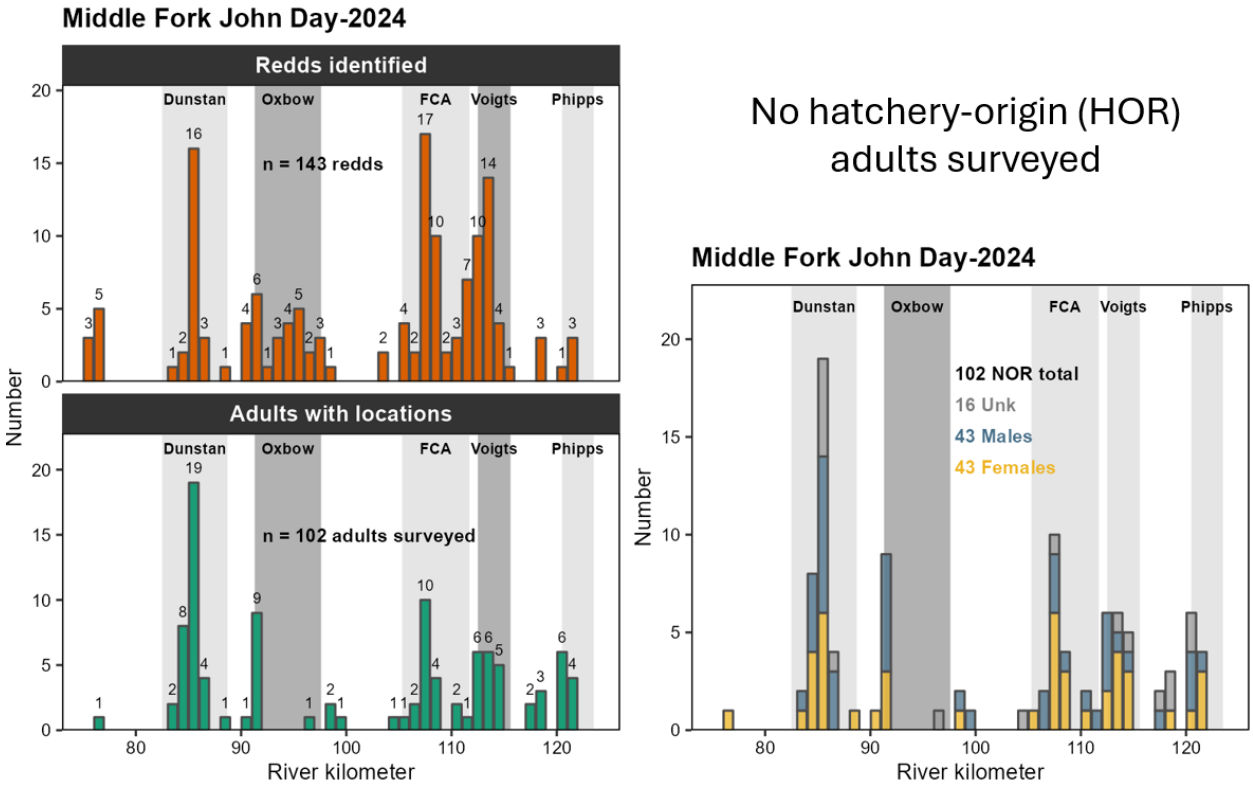

Figure 22: Left panels: Distribution of redds (top) and surveyed adults (bottom) across the Middle Fork John Day River in 2024. Right panel: Distribution of surveyed adults color-coded by sex, with blue, yellow, and grey indicating males, females, and unknown sex, respectively. No adults were identified as hatchery-origin (HOR); the origin of 21 adults could not be determined (i.e., scavenged or too degraded to identify presence of adipose fin), although HOR adults in MFJD are rare.

Lessons learned and discussion

There were several lessons learned from the 2024 adult sampling effort. Carcass retention and recovery rate varied considerably across the three subbasins as well as spatially within each subbasin; 50 rkm distribution in the MFJD vs. 20 rkm distribution in CC and 12 rkms in LKG. Carcass recovery was relatively high in CC, but considerably lower in both MJFD and LKG. Through these surveys, we gained a better understanding of the relative importance of increased efforts (i.e., supplemental surveys), as well as where, when, and how increased effort could be applied among and within these subbasins to increase the efficacy of supplemental surveys in determining adult locations. We also provide considerations for other research/management personnel in determining the applicability of this approach in other areas with anadromous salmonids, and what watershed-level contexts should be taken into consideration.

Carcass recovery was overall high in CC, with 195 carcasses surveyed for 143 redds observed. At first glance, this may appear that standard SGSs alone may be sufficient to obtain adequate sample sizes of adult spawning locations; however, supplemental surveys contributed 94 (48 carcasses and 46 live-scanned adults) of the 241 unique adult locations (39%) and even greater proportional contributions in some sections of CC. For example, supplemental surveys accounted for 74% (58

of 78) of adult locations between rkms 70-80 and 57% (4 of 7) in the South Fork CC, but just 21% (32 of 156) between rkms 80-90. One potential reason for the disproportionate influence of supplemental surveys is that spawn timing is spatially structured, with peak spawning occurring earliest around rkm 90, and latest in the lowest portions of the spawning extent (e.g., rkms 70-75; near Southern Cross). At the time of the last standard SGS (9/10/24), there were still live post-spawn adults downstream of rkm 75 that were found as carcasses or live scanned during supplemental surveys on 9/11 and 9/12. Obtaining adult locations distributed throughout the spawning extent, rather than focusing on just the total number, is critical to evaluate spatial patterns of reproductive success and reach-specific productivity. With this in mind, supplemental survey effort could potentially be reduced between rkms 80-90 (CC State Park day use to Forks) in future years, but surveys targeting rkms 70-80 (i.e., Southern Cross to CC State Park day use area) and South Fork CC should be prioritized. Similarly, supplemental surveys targeting the earliest (i.e., upstream) and latest (i.e., downstream) periods of spawning may be most effective to fill gaps before and after standard SGSs.

Relying on carcasses alone to obtain individual adult spawning locations is not feasible for LKG without considerable additional effort (e.g., daily surveys across the entire spawning extent). Because of poor carcass retention in LKG, we modified survey plans to include scanning the PIT-tags of moribund post-spawn adults when appropriate. Only 10 of the 37 individual adults we successfully scanned were later found as carcasses, demonstrating that carcass recovery alone would have been insufficient and that scanning post-spawn adults was an effective approach to obtain individual spawning locations. Implementing this modified approach earlier likely would have resulted in a higher sample size of adult locations, particularly towards the upstream end of the spawning extent where spawning was earliest.

Unlike CC and LKG, there is no adult collection weir on the MFJD, meaning that we cannot PIT-tag adults and passively scan tags to obtain locations. Across the MFJD watershed, carcass recovery was especially low within the Oxbow Conservation Area (rkms 91-97), which is consistent with prior years (2020, 2021, 2023) due to apparent concentrations of otter predation and scavenging. Even with daily surveys through the Oxbow, live fish on redds observed one day are gone the next with no signs of carcasses to collect genetic samples from. These observations, along those made during surveys in Lookingglass Creek, demonstrate the importance and value-added nature of PIT tagging adults at collection weirs. It is our belief that adults PIT-tagged before they reach the spawning grounds provides a significant proportion of useful data through relatively little additional effort at the weir and partially alleviates the need for, and extent of supplemental survey efforts.

Obtaining robust maternal spawning location data has proven to be a critical aspect of understanding juvenile dispersal patterns as well as maternal egg-to-parr relative reproductive success (Figure 19; Kaylor et. al. 2025). During our efforts to evaluate juvenile dispersal and spatial patterns of relative reproductive success in the MFJD, we expected a lower percentage of offspring to be successfully paired to maternal parent and associated spawning locations due to

seemingly small number of sample females relative to the number of redds. In 2020, 162 redds were observed and 141 carcasses were sampled (~35% of the estimated spawning population) in the MFJD, 67 of which were successfully genotyped females with known spawning locations. Without the considerable extra effort put into supplemental surveys, we would not have been able to obtain a representative sample of the spawning adults, and the data produced from subsequent juvenile capture and genotyping would not have been reliable. As a result, ~39% of offspring sampled in 2021 were assigned to a female parent surveyed in 2020. We expect a lower proportion of juveniles to be successfully assigned to female parents in MFJD, and therefore will need to sample and genotype more individuals to achieve similar numbers of offspring-parent assignments as CC and LKG.

To surmise, before embarking on such an evaluation, careful consideration on whether a sufficient and representative sample of the spawning population can be achieved given the specific watershed context (e.g. weir present, hatchery supplementation, SGS access) and what level of supplemental surveys may be needed to achieve this. In turn, the number of sampled adults relative to observed redds provides insight into the proportion of juveniles expected to be genetically assigned a sampled female parent, and thus, the total number of juveniles required to achieve a target sample size of offspring-maternal parent pairs

Next steps

Screw trap sampling for offspring from the BY 2023 adults began in fall 2024 and will continue through late spring 2025 (June/July). Tissue samples will then be sent to Hagerman Genetics Laboratory for genotyping and PBT assignments to BY 2023 parents, prioritizing female parent assignments. Similarly, offspring from BY 2024 adults will be sampled as outmigrants in fall 2025 and spring 2026, samples will be genotyped, and PBT will be conducted to assign parent-offspring pairs.

References

Kaylor, M. J., L. R. Ciepiela, M. Feden, J. T. Lemanski, C. Justice, B. A. Staton, J. B. Armstrong, S. Kelly, S. R. Narum, I. A. Tattam, and S. M. White. 2025. Watershed-scale dispersal patterns of juvenile Chinook Salmon (Oncorhynchus tshawytscha) revealed through genetic parentage analysis. *Movement Ecology* 13(1):6.

Koch, I. J., T. R. Seamons, P. F. Galbreath, H. M. Nuetzel, A. P. Matala, K. I. Warheit, D. E. Fast, M. V. Johnston, C. R. Strom, S. R. Narum, and W. J. Bosch. 2022. Effects of Supplementation in Upper Yakima River Chinook Salmon. *Transactions of the American Fisheries Society* 151(3):373–388.

Nuetzel, H. M., P. F. Galbreath, B. A. Staton, C. A. Crump, L. M. Naylor, and G. E. Shippentower. 2023. Improved productivity of naturalized spring Chinook salmon following reintroduction from a hatchery stock in Lookingglass Creek, Oregon. *Canadian Journal of Fisheries and Aquatic Sciences* 80(2):375–392.

2.3 Juvenile Chinook Salmon dispersal study

The manuscript associated with this study was published in *Movement Ecology* in February, 2025 and is open access. We provide the reference, DOI, and abstract below.

Kaylor, M. J., L. R. Ciepiela, M. Feden, J. T. Lemanski, C. Justice, B. A. Staton, J. B. Armstrong, S. Kelly, S. R. Narum, I. A. Tattam, and S. M. White. 2025. Watershed-scale dispersal patterns of juvenile Chinook Salmon (Oncorhynchus tshawytscha) revealed through genetic parentage analysis. Movement Ecology 13(1):6. https://doi.org/10.1186/s40462-024-00524-3

Abstract

Background: For many aquatic taxa, juvenile dispersal from spawning locations to rearing habitats is a critical process influencing individual fitness and population dynamics. However, our understanding of dispersal patterns in naturally spawning fish populations remains largely unknown due to the logistical challenges of tagging and tracking movement at early life stages.

Methods: We quantified dispersal patterns of a spring-run Chinook Salmon (*Oncorhynchus tshawytscha*) population in NE Oregon, USA using genetic parentage-based tagging to trace juveniles captured from summer rearing habitats back to their maternal parent and associated spawning location (i.e., juvenile origin). We evaluated overall dispersal patterns, longitudinal trends across the watershed, and relationships between dispersal and biophysical factors, including thermal conditions, network-scale abundance estimates, and juvenile size-at-capture.

Results: Overall dispersal of the 1326 juveniles (*n* sampled = 3388) assigned to a maternal parent (*n* = 64) was downstream-biased, but we estimated that 32% dispersed upstream and 29% moved into adjacent tributaries after initial mainstem dispersal. Dispersal distances were high relative to those found in other studies, with 25% of parr dispersing more than 0.9 km upstream (max = 10.6 km) and 25% dispersing more than 3.7 km downstream (max = 28.6 km). Analysis of dispersal patterns and potential drivers indicated that (1) dispersal distances, directional bias, and variability showed clear longitudinal trends from downstream to upstream origin locations, (2) temperature was a dominant driver of dispersal, with individuals originating from warmer sections of the mainstem typically moving to cooler mainstem sections or tributaries, and (3) dispersal distance was associated with larger size-at-capture for individuals that dispersed downstream, but not upstream.

Conclusions: The widespread dispersal patterns exhibited in this population, including moving considerable distances upstream, downstream, and into tributaries, suggests that dispersal in naturally spawning fish populations may be more extensive and variable than currently recognized. We found that heterogeneity in biophysical conditions shaped within-population variability and riverscape dispersal patterns with important implications for subsequent fish habitat use, distribution, and size. This study provides an approach to evaluate patterns and drivers of dispersal

in naturally spawning populations and inform conservation and restoration planning through better alignment with juvenile fish ecology.

3. Biological responses to restoration and habitat change

3.1 Meadow Creek riparian vegetation and historical outmigrant trap analyses

Background

This objective is funded by the U.S. Forest Service's (USFS) Pacific Northwest Research Station and provides in-kind support to this contract. Meadow Creek is a tributary of the upper Grande Ronde River with much of Meadow Creek's watershed managed by the USFS. Additionally, Starkey Experimental Forest and Range – a USFS operated research station – covers about 7.5 miles of the mainstem of Meadow Creek within the upper watershed. Meadow Creek is slated for a watershed-scale restoration project focusing on restoring ecosystem processes and improving habitat for native biota. The planned restoration actions largely focus on floodplain reset or Stage-0 approaches. Extensive RM&E effort is planned by a collaborative group involving CRITFC, USFS, CTUIR, and ODFW to evaluate the response of aquatic biota to restoration efforts. In addition to planned data collection efforts, an abundance of historical data exists for Meadow Creek with respect to prior restoration actions and their impacts to aquatic habitat and biota. However, much of that data remains unanalyzed and could provide valuable information to guide the forthcoming restoration and RM&E designs.

For this contract year, we focused on two main data sources. The first was riparian vegetation change between 2009 and 2020 using LiDAR data and the second being historical outmigrant trap data. Our progress towards analyzing these data is summarized below.

Riparian vegetation change

LiDAR was collected across the Chinook rearing extent of the upper Grande Ronde River and Catherine Creek in 2009 and 2020. We leveraged this existing data to examine the effects of riparian vegetation plantings and large wood placement to riparian vegetation height within the Starkey Experimental Forest and Range. Approximately 7.2 km of Meadow Creek within Starkey was treated with both restoration actions from 2013-2014.

We assessed the change to vegetation height by generating a series of transects across the floodplain of Meadow Creek within Starkey. Transects occurred every 25m along the stream center line, with transect length varying as a function of floodplain valley width perpendicular to the stream. We then extracted LiDAR data (highest hit minus bare earth DEMs) along each transect line for each year and computed summary statistics for each transect.

Our preliminary results indicate a mean increase in vegetation height of 1.62m across all transects with only 3.5% of transects experiencing no change or negative change and 72% of transects

experiencing an increase of 1m or more. Furthermore, we observed a longitudinal pattern of growth, whereby the lower reaches of Starkey grew more quickly than the middle or upper reaches during the 11 years between the LiDAR flights.

Further analysis will be conducted on the Meadow Creek riparian vegetation data in 2025. We plan to expand the analysis domain to include reaches outside of Starkey such as the CTUIR property at McCoy Meadows, Dark Canyon Creek, and McCoy Creek. Additionally, we are working with USFS employees to expand the scope of analyses within Starkey to include additional remote sensing data that will provide information on riparian vegetation cover type changes over time and to leverage existing on-the-ground measurements of riparian vegetation growth collected between 2014 and 2021.

The outmigrant *O. mykiss* data analysis is summarized below in manuscript form.

Historical Meadow Creek Outmigrant Trap Data from 1987-1999 Trap Years

Introduction

Pacific salmon (*Oncorhynchus sp.*) have been the focus of billions of dollars of restoration funding over the past 50 years due to observed declines across species and populations throughout their range (Gresh et al. 2000; White et al. 2021; Jaeger and Scheuerell 2023). While Pacific salmon require a variety of complimentary habitats to complete their life cycles (Flitcroft et al. 2019), many studies examine restoration responses at the reach-level spatial scale, thereby not capturing the full scope of even the freshwater-period of their life cycle (Fausch et al. 2002). Reach-scale increases in density or abundance of a salmonid species may indicate improved habitat conditions within that specific reach (Wall et al. 2016). However, population-level changes cannot be adequately assessed at the reach scale without extensive and highly expensive monitoring programs (Bouwes et al. 2016). One approach to overcome this problem is to monitor a population at a transition in its life history, such as smolt outmigration, where estimates of total outmigrants could be used as an indicator of population-level changes over time from the upstream basin (Carlson et al. 1998).

In anadromous Pacific salmon, outmigrating juvenile fish (i.e., smolts) within a tributary or watershed are an indicator of fish population health or robustness over time. Since Pacific salmon undergo smoltification, (e.g. a series of physiological and physical changes to their bodies allowing them to transition from freshwater to saltwater survival strategies, Nichols et al. 2008) outmigrating smolts are a particularly useful lifestage to monitor because they integrate the reproductive effort of prior years (e.g., number of effective spawners) with offspring survival across multiple lifestages (e.g., egg-to-fry, fry-to-parr). Both of these vital rates are influenced by the quality and quantity of habitat available in a watershed (Carlson et al. 1998). Smolt trap monitoring programs are often established to enumerate the number of juveniles produced within natal streams and sub-watersheds, with the goal of understanding how outmigrants numbers vary

over time in relation to reproductive effort and habitat influences such as streamflow, stream restoration, or barrier removal (Beechie et al. 1994; Carlson et al. 1998; Roni et al. 2010).

Declines in salmon populations and the quality of freshwater habitats are well documented within the Columbia River basin, and current runs of natural-origin Columbia River salmon species are estimated at 2% of their pre-western settlement size (Gresh et al. 2000). Widespread declines in deep pool frequency were observed throughout the Columbia River watershed from the 1940's to the 1990's (McIntosh et al. 2000), which serves as an indicator of broader losses in habitat complexity. For example, within the upper Grande Ronde watershed, large pool habitat decreased by around 65% (McIntosh 1992). Our study focuses on the Meadow Creek watershed – a major tributary of the upper Grande Ronde – where splash damming, intensive grazing, and industrial timber harvest contributed to declines in pool frequency and habitat degredation (McIntosh 1992; White et al. 2017).

The Meadow Creek smolt trapping project was initiated by the U.S. Forest Service (USFS) in 1987 as a response to planned restoration actions along Meadow Creek within the Starkey Experimental Forest and Range (hereafter SEF; Boehne 1996). Outmigrant trapping began three years prior to restoration implementation to characterize the "before" period. An extensive large wood placement project was conducted along 3.7km of Meadow Creek in 1990. The goal of the large wood (LWD) restoration project was to improve the habitat of Meadow Creek by increasing pool area and frequency (Miller 1997; McIntosh et al. 2000), thus enhancing juvenile salmonid growth, survival, and ultimately outmigration rates. Steelhead/rainbow trout (*Oncorhynchus mykiss*) are the dominate salmonid within the Meadow Creek watershed and the only Pacific salmon species to currently spawn in the watershed.

We analyzed outmigrant *O. mykiss* numbers from the Meadow Creek watershed from 1987-1999. A partial analysis of this data (1987-1992) was completed in the 1990's using slightly different methods (Boehne 1996; Miller 1997). However, the full data set was never analyzed, and the previous analyses are incompatible with outmigration estimates that are currently made for other areas of the Grande Ronde watershed. A resumption of outmigrant trapping is occurring in 2025, along with a watershed-scale floodplain reset project using Stage-0 methods (Powers et al. 2019) which is scheduled to begin in 2027. Our goal with this analysis is to provide insight into how past restoration actions influenced outmigrant *O. mykiss* numbers along with providing baseline data for the more intensive and expansive floodplain restoration project planned across the Meadow Creek watershed.

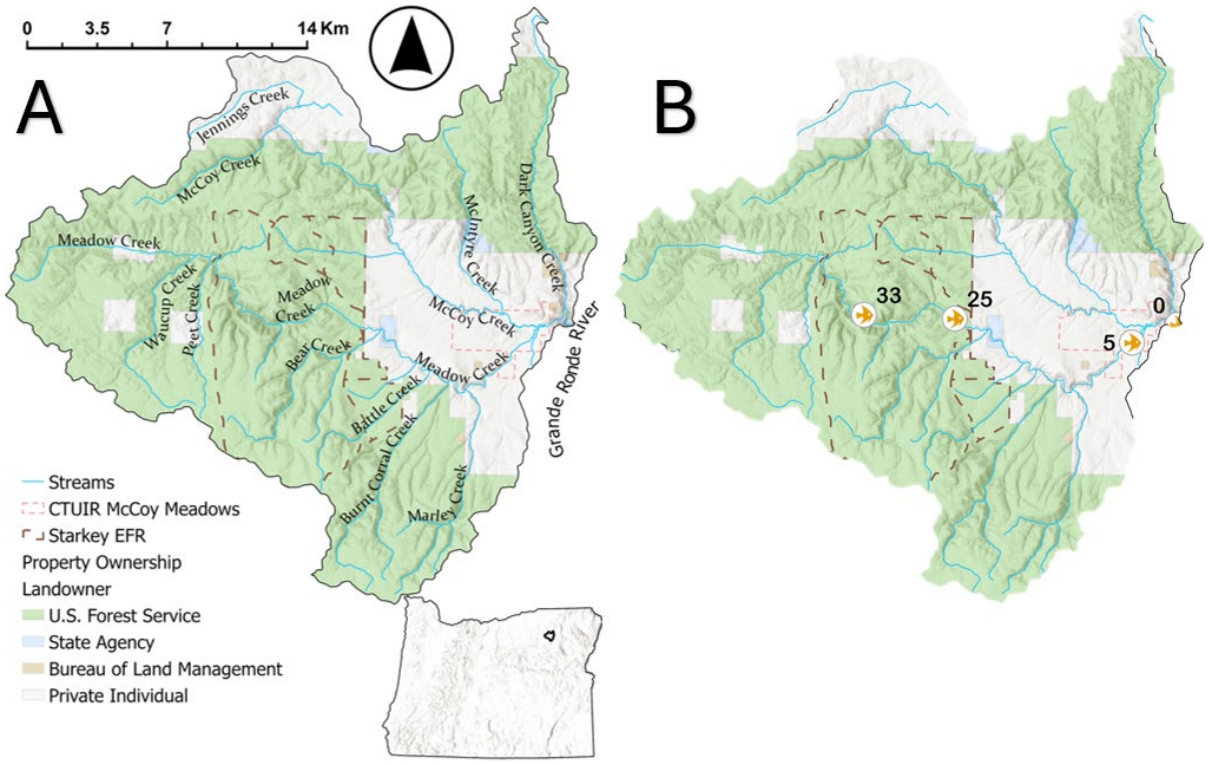

Figure 23: (A) The Meadow Creek watershed with major streams, landownership, and the Starkey Experiment Forest and Range illustrated. (B) The location of smolt traps in river KM (e.g. 33 = trap at river KM33) used in this study within the Meadow Creek watershed.

Study Area & Methods

Meadow Creek is a 313 km² watershed located in the Blue Mountains of Union County, OR. It is a major tributary to the upper Grande Ronde River, which itself is a tributary to the Snake and ultimately Columbia Rivers. Its uplands are dominated by alternating mixed conifer forest and grasslands with basaltic bedrock (Averett et al. 2019). Most of the watershed is public land with 73% being USFS managed including the SEF (Figure 23A). Mean annual discharge is 1.0 m^3/s within the SEF above the confluence with Bear Creek and 3.65 m^3/s below Dark Canyon Creek near the confluence with the Grande Ronde River. Typical base flows are 0.03 and 0.11 m^3/s, respectively (Oregon Water Resources Department, Gage Summary; Gauge #'s 13318060 & 13318210). The watershed consists of alternating confined and alluvial valley segments with meadows occurring in lowlands, especially at the McCoy and Meadow Creek confluence, and in headwater locations (i.e., Waucup and Meadow Creek confluence, Figure 1A).

Outmigrant smolt trapping was conducted by the USFS in the Meadow Creek watershed from 1987-1999. Traps were numbered based on their nearest river kilometer along Meadow Creek (i.e., KM3 for a trap near river kilometer 3). Traps were located at the mouth of Meadow Creek near its confluence with the Grande Ronde River (Trap KM0, hereafter KM0), on Meadow Creek just

upstream of the confluence with McCoy Creek (Trap KM5, hereafter KM5), within SEF near the splash dam (Trap KM25, hereafter KM25), and upstream of Bear and Ray Creeks (Trap KM33, hereafter KM33, all on Figure 23B). Thus, trap numbers moved progressively upstream, with larger numbers representing traps with smaller basin areas. Several trap types were used over the years. Early traps consisted of a floating Humphrey's inclined-plane trap with battery operated screens (McLemore et al. 1989). These traps had a 0.9-meter-wide screen that captured fish. Later in the study, several rotary screw traps with 2-meter diameter drums were used at KM0 and KM5 (Miller 1997).

Smolt traps were operated on a yearly basis as conditions allowed. Typically, this meant installation in mid-February after river ice subsided and snow melt allowed site access. Traps were run until lack of water prevented their operation, which typically occurred in mid-May or early June (Table 10). Thus, the trapping period for a year began on the first day the traps were operated and ended on the last day that the lowest trap was operated (Table 10, KM0 or KM5 depending on year)

Table 10: Trap metadata for traps operated for multiple years during the study period

Year	First Day	Last Day	# of Traps	Days Trapping
1987	4/26/1987	11/17/1987	3	58
1988	3/16/1988	4/30/1988	3	46
1989	3/21/1989	6/4/1989	3	76
1990	3/15/1990	6/13/1990	3	91
1991	2/23/1991	6/3/1991	3	101
1992	2/26/1992	11/23/1992	3	132
1993	3/15/1993	11/22/1993	4	135
1994	3/6/1994	10/29/1994	4	100
1995	3/8/1995	5/30/1995	2	84
1996	3/6/1996	4/8/1996	2	34
1997	3/12/1997	6/9/1997	2	90
1998	3/7/1998	6/28/1998	2	108
1999	3/16/1999	6/6/1999	1	75

Traps were operated 7 days a week as conditions allowed. Occasionally, days were missed due to ice, high flows, low flows, or trap damage. From 1987-1990 traps were operated overnight from dusk to dawn. After detecting outmigrating salmonids during daytime trapping, the lower traps (e.g., KM0 and KM5) were operated 24 hours a day from 1991 onwards.

Traps were checked each morning and salmonids present were anesthetized using MS-222. Fish were then counted, measured to the nearest mm, and weighed to the nearest 0.1g. A subset of trapped salmonid outmigrants were used to estimate trap efficiency and total outmigration numbers.

Trapping efficiency was calculated with mark-recapture methods using a Bailey's estimator (Bailey 1951). Fish captured at a trap were marked with one of seven unique partial fin clips, with each day in the week having a unique mark for each trap currently deployed. Marked fish were placed 0.8 km upstream from the trap with release site chosen to have ample cover and pool habitats. Thus, each time-period contained records for total salmonids encountered, marked, and recaptured.

Trap efficiency ($\hat{e}^i$) for the current analysis was calculated as:

$$\hat{e}^i = \frac{r^i}{m^i}$$

where r^i is the number of recaptures, m^i is the number of marks at a trap during period *i*. Outmigrant estimates ($\widehat{N}$) were produced using a Bailey's estimator calculated as:

$$\widehat{N} = \frac{c^i(m^i + 1)}{r^i + 1}$$

where $\widehat{N}$ is the total number of outmigrants estimated, c^i the total number of outmigrants caught in the trap (regardless of their mark status), m^i is the number of marks, and r^i is the number of recaptures at a trap during a given period *i.* A bootstrapped confidence interval was produced for each estimate by drawing 10,000 bootstrap samples with replacement of r^i from a binomial distribution with a probability parameter of r^i/c^i (Steinhorst et al. 2004). Data were analyzed in the statistical program R using the *recapr* package to produce outmigrant estimates and confidence intervals (Tyers 2021; R Core Team 2023).

The raw trapping data was processed and combined so that each trapping period contained a minimum of 10 recaptures due to low mark and recapture rates at weekly timescales. In some cases, two to four weeks needed to be combined to ensure that 10 recaptures were met for a trap. This methodology follows current Oregon Department of Fish and Wildlife (ODFW) methodology for population estimates from trapping date within the Grande Ronde (Gibson et al. 2022).

We estimated the total outmigrant production for each subreach for the years 1991-1999. The upper trap's outmigrant estimate was used as its estimated contribution to total watershed production. We estimated production from between the upper and middle traps by subtracting the upstream most trap's estimate from the middle trap's estimate. We then took the middle trap's estimate and subtracted it from the lower trap's, to estimate the contribution of the lower trap to total outmigrant production from the watershed. Finally, we calculated the percentage contribution that each trap had to total watershed production. From 1991-1992 we had three subreaches, while for 1993-1999 we had 2 subreaches.

Results

Species Encountered & Trapping Efficiencies

A total of 53,122 fish were encountered over 1,130 days of trapping (Figure S1). Approximately half of all fish encountered in the traps were *Oncorhynchus mykiss.* Under 50 Chinook salmon (*Oncorhynchus tshawytscha*) were detected during the study. Other species detected included redside shiner (*Richardsonius balteatus*), bridgelip sucker (*Catostomus columbianus*), Northern pikeminnow (*Ptychocheilus oregonensis*), chiselmouth (*Acrocheilus alutaceus*), and longnose dace (*Rhinichthys cataractae*). A total of 3680 fish were recaptured, of which 85% were *O. mykiss*. Therefore, trap efficiency and outmigrant population estimates were only produced for *O. mykiss*.

Trapping efficiency was poor early in the study and slowly improved over time (Figure 24). As a result, the estimates for outmigrant *O. mykiss* numbers are not reliable during the 1987-1989 period prior to the LWD restoration within the SEF. During this period, mean trap efficiency across all traps was below 7%, with KM25 and KM33 being consistently below 5%. From 1990 to 1999 trapping efficiency generally improved with mean trap efficiency ranging from 9% to 16%. The lowest efficiencies in this time period occurred in 1997 with an efficiency of 6% with only 77 total recaptured fish across all traps for the year. Peak efficiency of 16% occurred in 1999 with 186 fish recaptured out of a total of 1,118 marked.

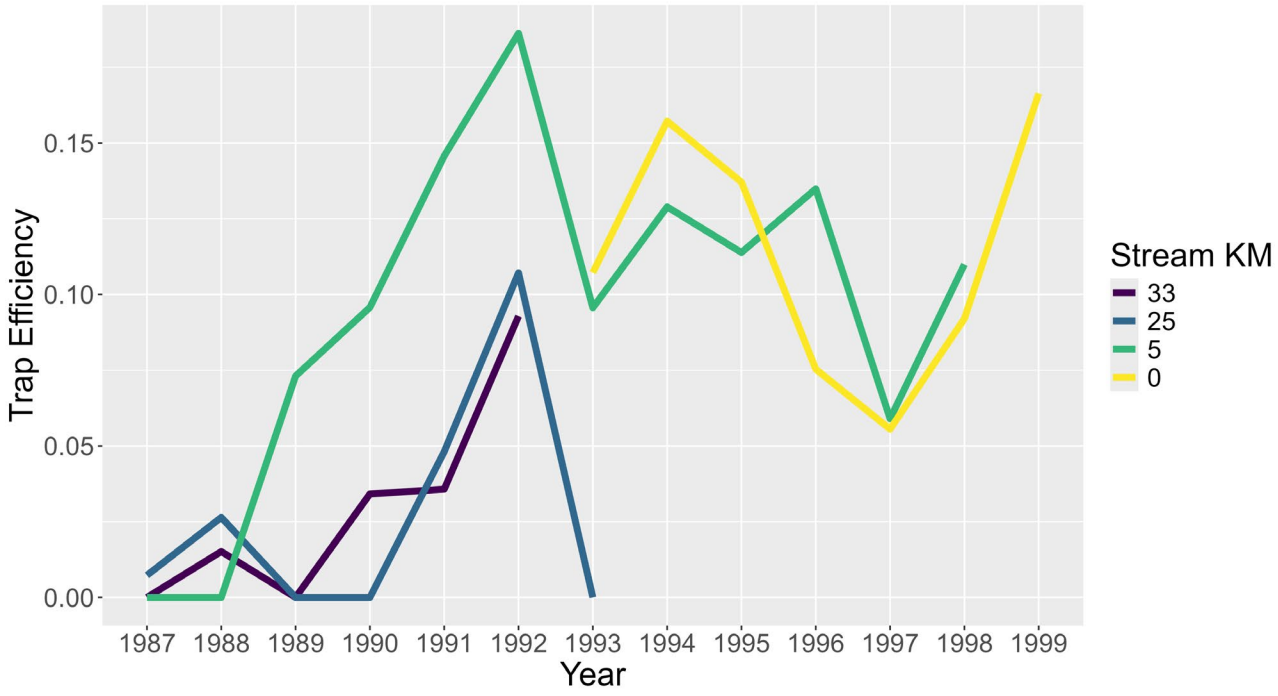

Figure 24: Trapping efficiencies of *O. mykiss* by each trap over time.

Yearly Outmigrant Estimates

No *O. mykiss* outmigrant estimates were produced for years where a trap's efficiency was less than 5%. As such, no estimates were produced for 1987 or 1988 for any traps. KM25 could not have estimates made in 1990, 1991 or 1993, while KM33 could not have estimates made in 1990 or 1991. All other years' estimates are provided in Figure 25.

The highest *O. mykiss* outmigration years occurred in 1990 and 1998 with over 28,000 fish estimated to be leaving the Meadow Creek watershed (Figure 25; KM0). Outmigrant estimates neared or exceeded 15,000 fish in 1995 and 1997. The lowest estimated number of outmigrants were in 1993 and 1996 with under 3,000 fish exiting the watershed above McCoy Meadows (Figure 26, KM5), and less than 7,500 fish estimated exiting the Meadow Creek watershed as a whole (Figure 26, KM0).

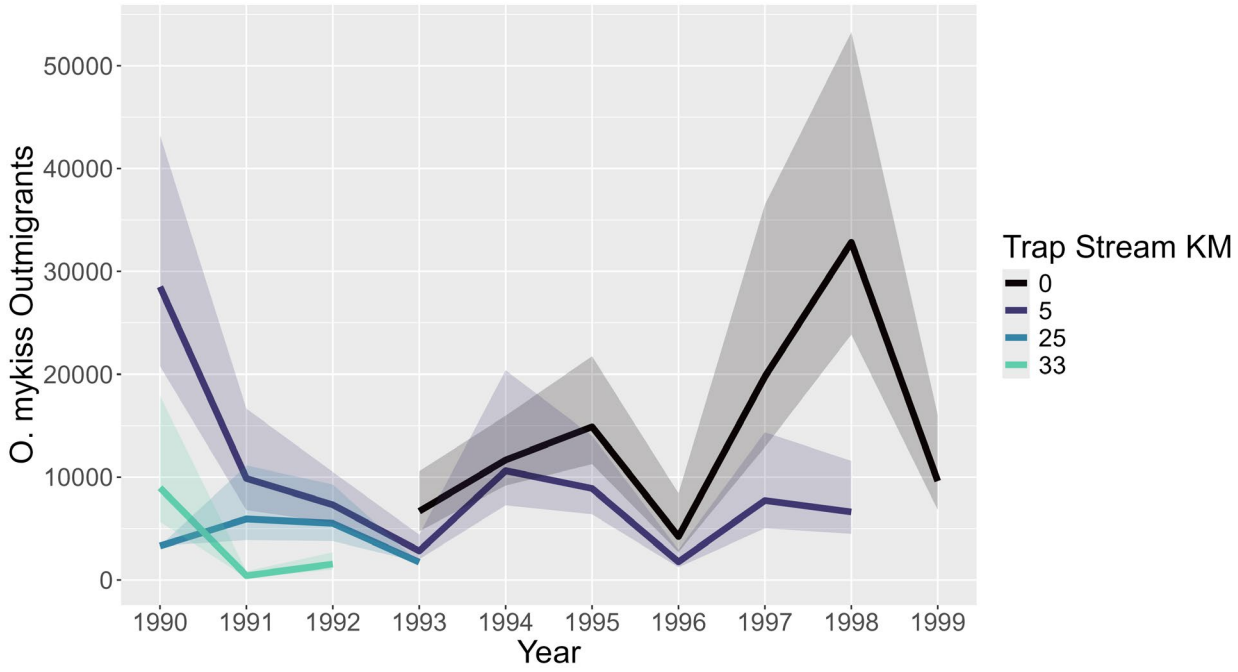

Figure 25: Yearly outmigrant estimates for O. mykiss at the four Meadow Creek trap locations. Shaded areas represent the bootstrapped 95% confidence interval for the outmigrant estimate.

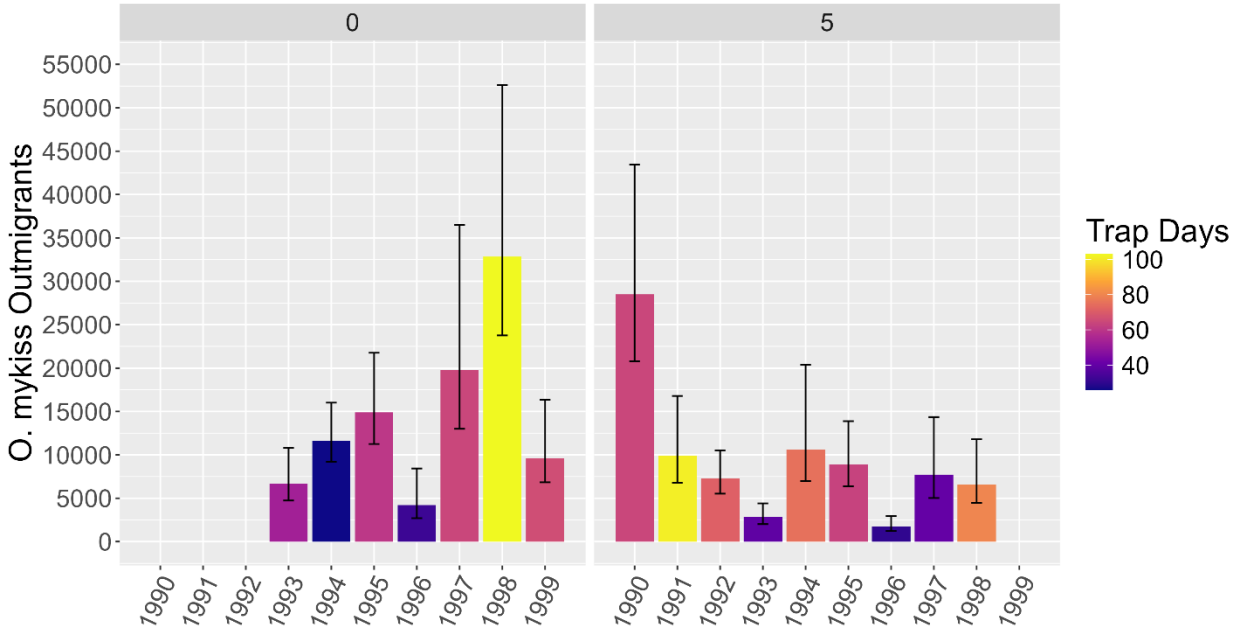

Figure 26: Outmigrant *O. mykiss* estimates with bootstrapped 95% confidence intervals displayed for traps at KM0 on the left and KM5 on the right. The number of days each trap was operated is displayed in the color gradient of each bar.

Reach-based Outmigrant Production within Meadow Creek

We utilized the sequential nature of the traps within the Meadow Creek watershed to attribute outmigrant production to specific zones of the Meadow Creek watershed. From 1991-1992, we could use traps at KM33, 25, and 5 to partition productivity by subreaches from the mainstem of Meadow Creek above McCoy Meadows (see Figure 23B). From 1993-1999, traps at KM5 and KM0 could be used to estimate the proportion of outmigrant productivity from the mainstem of Meadow Creek above McCoy Meadows (KM5, Figure 23B) or from other areas of the watershed (KM0 see Figure 23B).

For 1991 and 1992, we observed relatively constant proportional contributions of outmigrants among subreaches. The watershed upstream of the upper trap at the top end of the SEF (KM33, Figure 23B) contributed 4% and 21% of the total outmigrants in 1991 and 1992, respectively, while the watershed between the middle and upper traps largely consisting of the SEF (KM25, Figure 23B) contributed 56% and 54% of outmigrants, respectively. Meanwhile the lower mainstem of Meadow Creek watershed between the lower trap and the middle trap (including the name tributaries of Bear, Burnt Coral, Battle, and Marley Creeks; KM5, Figure 23B) contributed 40% and 25% of outmigrants across 1991 and 1992 (Table 11).

From 1993 until 1999, we observed large variations in the percentage of fish that could be attributed to the mainstem of Meadow Creek above McCoy Meadows. Among these years, we

estimated that 20-91% of outmigrants came from above KM5, with a mean of 49%. The highest estimated proportion of outmigrants coming from above KM5 occurred in 1994 with 91%, while the lowest occurred in 1998 at 20%. The largest estimated number of outmigrants and greatest proportion of outmigrants from the mainstem of Meadow Creek above KM5 occurred in 1994 and 1995, with 10,622 (91%) and 8,894 (61%) outmigrants, respectively (Table 11).

Table 11: Reach-based O. mykiss outmigrant estimates for 1991 and 1998. Raw outmigrant estimates and proportional contributions to the total number of outmigrants observed at the lower trap are displayed

Year	KM5	KM25	KM33 / Upper Prod.	SEF Production	Lower Production	Upper	SEF	Lower
1991	9876	5936	420	5516	3939	0.04	0.56	0.40
1992	7311	5510	1540	3970	1801	0.21	0.54	0.25

Year	KM0	KM5	Rest of Basin	KM5	Rest of Basin
1993	6678	2821	3857	0.42	0.58
1994	11664	10622	1041	0.91	0.09
1995	14900	8894	6006	0.60	0.40
1996	4216	1751	2464	0.42	0.58
1997	19768	7733	12035	0.39	0.61
1998	32825	6609	26216	0.20	0.80

Discussion

Our study investigated interannual variation in the number of outmigrating *O. mykiss* from the Meadow Creek watershed following a LWD restoration project. Our goal was to better understand outmigrant dynamics and the production of outmigrants from various reaches in the watershed. Interannual variation in outmigrant *O. mykiss* was large, with the largest year in 1998 having 7.8 times more outmigrants estimated than the smallest year in 1996. We determined that the Meadow Creek mainstem above McCoy Meadows was the most consistent producer *O. mykiss* within the watershed. While a mean of 49% of outmigrants came from the mainstem of Meadow Creek above KM5 during the six years KM0 and KM5 were run concurrently, the standard deviation of the outmigrant estimate at KM5 was over 2.5 times smaller than that of the rest of the basin below KM5. This may indicate that the mainstem of the Meadow Creek watershed above KM5 represents the "core" habitat for *O. mykiss* within the basin, with other areas below KM5 such as McCoy and Dark Canyon Creeks being utilized when habitat conditions allow or adult reproductive effort saturates the core habitat with juveniles.

Unfortunately, we could not adequately compare outmigrant fish numbers from the pre-restoration period of 1987-1990 with the post-restoration period of 1991-1999. This was due to poor trap efficiency during the early part of the study when ice, lack of streamflow, and the establishment

of trapping procedures combined to reduce the efficiency of traps at KM5, KM25, and KM33 (Boehne 1996; Miller 1997). As such, we could not produce accurate or informative estimates of outmigrant *O. mykiss* numbers during the pre-restoration period.

Two other published estimates of *O. mykiss* outmigrant numbers are available for the Grande Ronde River basin from this time period. Previous work within Meadow Creek on this same data by Miller 1997 provided similar estimates for *O. mykiss* outmigrant numbers with a few key differences. First, they attempted to separate *O. mykiss* smolts from migrant parr based on appearance at the time of trapping and therefore made two separate estimates (e.g., one for smolts and one for parr) for each time period analyzed. Second, they grouped their observations for mark-recapture analysis at the weekly time scale, whereas we grouped our observations at variable time scales, reflecting the intervals needed to achieve at least 10 recaptures. This meant that our time periods were often longer with more marks and recaptures included in each estimate of trap efficiency and ultimately outmigrant numbers than Miller 1997.

ODFW also creates annual estimates of outmigrant *O. mykiss* from the upper Grande Ronde above Fly Creek and Catherine Creek above Union, OR. These estimates provide a much better benchmark for our Meadow Creek estimates because we followed the same data grouping protocol as ODFW, ensuring that each time period contained at least 10 recaptures for trap efficiency and outmigrant estimates. ODFW estimates exist for these locations for 1997-2023, providing three years of overlap with our data. For the upper Grande Ronde, ODFW estimated *O. mykiss* outmigrant numbers of 15104 ± 3184 (estimate ± 95% confidence interval) in 1997, 10133 ± 1612 in 1998, and 6108 ± 3184 in 1999 (Gibson et al. 2022). Therefore, Meadow Creek's estimated *O. mykiss* outmigrant numbers were 1.3, 3.2, and 1.6 times larger than the upper Grande Ronde from 1997-1999. ODFW estimated that Catherine Creek had *O. mykiss* outmigrant numbers of 25229 ± 4744 in 1997, 20742 ± 2076 in 1998, and 19628 ± 3549 in 1999. Our *O. mykiss* outmigrant estimates for Meadow Creek were 1.3 times larger in 1997 and 1998 than Catherine Creek's estimate. Catherine Creek's estimate was 2.2 times larger than Meadow Creek's in 1999.

Production of *O. mykiss* within the mainstem of Meadow Creek (e.g., above KM5) seemed to drop off over the course of our study, potentially suggesting the LWD restoration effects were waning over time. From 1994-1998 outmigrant *O. mykiss* estimates for KM5 decreased steadily in its percentage contribution to the total watershed outmigration from a high of 91% down to just 20%. Soon after the LWD restoration was implemented, an approximately 20-year return interval flood occurred in the spring of 1991 that displaced much of the wood added to Meadow Creek (Miller 1997). While this flooding may have originally generated additional habitat in the form of scour pools, it's possible the effect of the restoration degraded quickly over time due to the LWD no longer creating complex jams. This loss of complex wood jams could have reduced the quality of both over-summer and over-winter habitat (Roni et al. 2010; Wall et al. 2016), thereby leading to fewer fish surviving to outmigrate from Meadow Creek.

References

Averett, J. P., M. J. Wisdom, and B. A. Endress. 2019. Livestock Riparian Guidelines May Not Promote Woody Species Recovery Where Wild Ungulate Populations Are High. Rangeland Ecology & Management 72(1):145–149.

Bailey, N. T. J. 1951. On Estimating the Size of Mobile Populations from Recapture Data. Biometrika 38(3/4):293.

Beechie, T., E. Beamer, and L. Wasserman. 1994. Estimating Coho Salmon Rearing Habitat and Smolt Production Losses in a Large River Basin, and Implications for Habitat Restoration. North American Journal of Fisheries Management 14(4):797–811.

Boehne, P. 1996. Outmigration of Wild Summer Steelhead (Oncorhynchus mykiss) Juveniles in Meadow Creek, Oregon an Upriver Tributary of the Columbia Basin. Humboldt State University.

Bouwes, N., N. Weber, C. E. Jordan, W. C. Saunders, I. A. Tattam, C. Volk, J. M. Wheaton, and M. M. Pollock. 2016. Ecosystem experiment reveals benefits of natural and simulated beaver dams to a threatened population of steelhead (Oncorhynchus mykiss). Scientific Reports 6(1):28581.

Carlson, S. R., L. G. C. Jr, and C. O. Swanton. 1998. A Simple Stratified Design for Mark–Recapture Estimation of Salmon Smolt Abundance. Alsaka Fishery Research Bulletin 5(2):88–102.

Fausch, K. D., C. E. Torgersen, C. V. Baxter, and H. W. Li. 2002. Landscapes to Riverscapes: Bridging the Gap between Research and Conservation of Stream Fishes. BioScience 52(6):483.

Flitcroft, R. L., I. Arismendi, and M. V. Santelmann. 2019. A Review of Habitat Connectivity Research for Pacific Salmon in Marine, Estuary, and Freshwater Environments. JAWRA Journal of the American Water Resources Association 55(2):430–441.

Gibson, P. P., F. J. Drascic, D. R. Haynes, G. A. McMichael, J. A. Ofiara, M. A. Raines, and C. R. Warnock. 2022. Investigations into the Life History of Naturally Produced Spring Chinook Salmon and Summer Steelhead in the Grande Ronde River Subbasin - Annual Report 2022. Oregon Department of Fish and Wildlife, BPA Project # 1992-026-04.

Gresh, T., J. Lichatowich, and P. Schoonmaker. 2000. An Estimation of Historic and Current Levels of Salmon Production in the Northeast Pacific Ecosystem: Evidence of a Nutrient Deficit in the Freshwater Systems of the Pacific Northwest. Fisheries 25(1):15–21.

Jaeger, W. K., and M. D. Scheuerell. 2023. Return(s) on investment: Restoration spending in the Columbia River Basin and increased abundance of salmon and steelhead. PLOS ONE 18(7):e0289246.

McIntosh, B. A. 1992. Historical changes in anadromous fish habitat in the Upper Grande Ronde River, Oregon, 1941-1990. Oregon State University, Corvallis, OR.

McIntosh, B. A., J. R. Sedell, R. F. Thurow, S. E. Clarke, and G. L. Chandler. 2000. HISTORICAL CHANGES IN POOL HABITATS IN THE COLUMBIA RIVER BASIN. Ecological Applications 10(5).

McLemore, C. E., F. H. Everest, W. R. Humphreys, and M. F. Solazzi. 1989. A floating trap for sampling downstream migrant fishes. Page PNW-RN-490. U.S. Department of Agriculture, Forest Service, Pacific Northwest Research Station, PNW-RN-490, Portland, OR.

Miller, A. C. 1997. Response of juvenile steelhead trout to an instream habitat rehabilitation project in Meadow Creek, Oregon. Oregon State University.

Nichols, K. M., A. F. Edo, P. A. Wheeler, and G. H. Thorgaard. 2008. The Genetic Basis of Smoltification-Related Traits in Oncorhynchus mykiss. Genetics 179(3):1559–1575.

Powers, P. D., M. Helstab, and S. L. Niezgoda. 2019. A process-based approach to restoring depositional river valleys to Stage 0, an anastomosing channel network. River Research and Applications 35(1):3–13.

R Core Team. 2023. R: A language and environment for statistical computing. R Foundation for Statistical Computing, Vienna, Austria.

Roni, P., G. Pess, T. Beechie, and S. Morley. 2010. Estimating Changes in Coho Salmon and Steelhead Abundance from Watershed Restoration: How Much Restoration is Needed to Measurably Increase Smolt Production? North American Journal of Fisheries Management 30(6):1469–1484.

Steinhorst, K., Y. Wu, B. Dennis, and P. Kline. 2004. Confidence intervals for fish out-migration estimates using stratified trap efficiency methods. Journal of Agricultural, Biological, and Environmental Statistics 9(3):284–299.

Tyers, M. 2021. recapr: Two Event Mark-Recapture Experiment.

Wall, C. E., N. Bouwes, J. M. Wheaton, W. C. Saunders, and S. N. Bennett. 2016. Net rate of energy intake predicts reach-level steelhead (Oncorhynchus mykiss) densities in diverse basins from a large monitoring program. Canadian Journal of Fisheries and Aquatic Sciences 73(7):1081–1091.

White, S. M., S. Brandy, C. Justice, K. A. Morinaga, L. Naylor, J. Ruzycki, E. R. Sedell, J. Steele, A. Towne, J. G. Webster, and I. Wilson. 2021. Progress Towards a Comprehensive Approach for Habitat Restoration in the Columbia Basin: Case Study in the Grande Ronde River. Fisheries 46(5):229–243.

White, S. M., C. Justice, D. A. Kelsey, D. A. McCullough, and T. Smith. 2017. Legacies of stream channel modification revealed using General Land Office surveys,with implications for water temperature and aquatic life. Elementa: Science of the Anthropocene 5:3.

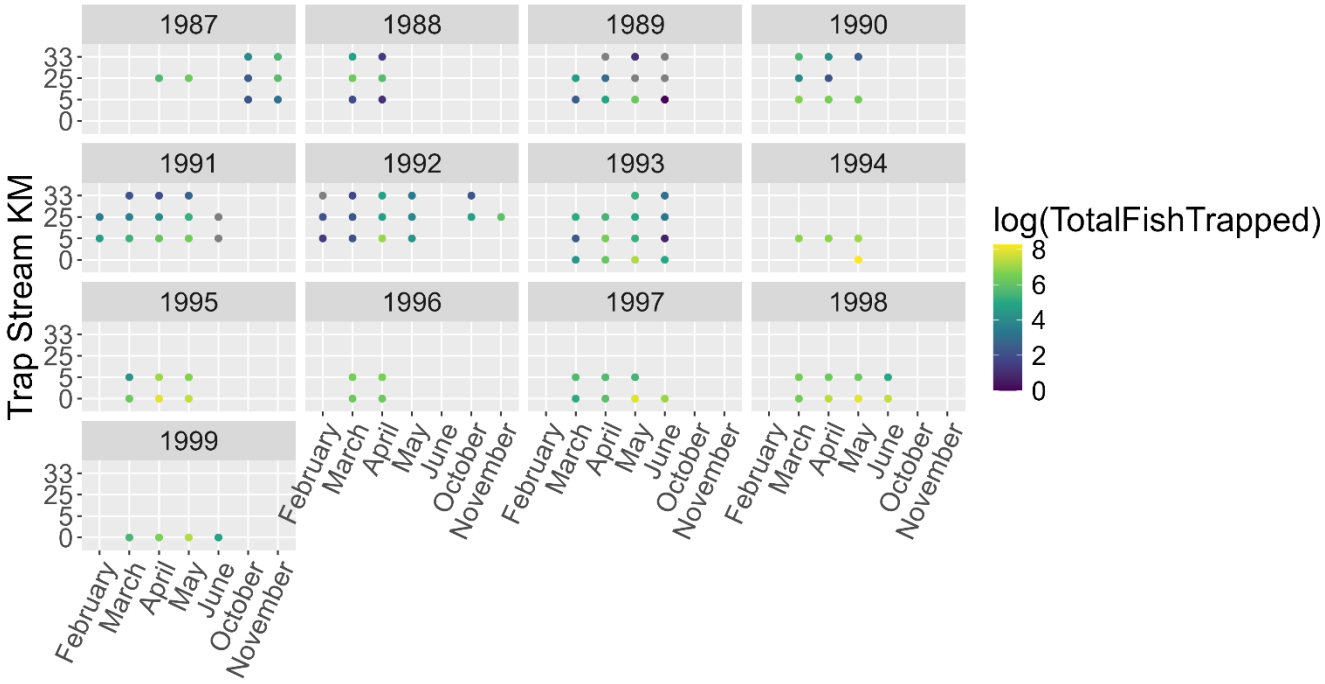

Figure S1: Monthly log transformed trapping data for O. mykiss caught in each trap across all the months and years in which they were operated.

3.2 Meadow Creek response to watershed-scale restoration – pilot year

Background

Extensive floodplain restoration is planned for Meadow Creek, a tributary of the upper Grande Ronde River. Multiple stream reaches within mainstem Meadow Creek and its tributaries will be treated with restoration actions intended to target impaired ecological processes and restore floodplain connectivity, for a total of approximately 32.3 kilometers (valley length, not stream channel length) and 914 acres. Meadow Creek Watershed collaborators, comprised of CRITFC, USDA, ODFW and CTUIR staff, have undergone an iterative process to develop a study design to guide restoration monitoring and evaluate fish response to restoration efforts, especially ESA-listed salmonids (see the Meadow Creek Aquatic Biota Study Design and Sampling Methods for more detail). Evaluation efforts are broadly focused on 1) assessing how *O. mykiss* productivity responds to valley reset restoration, 2) the broader fish community response to restoration as well

as potential interactions with salmonids as the result of shifting patterns in distribution, and 3) how food webs respond to restoration.

To address the first question, salmonid response metrics including *O. mykiss* growth rates (spring-to-fall), abundance and biomass (spring and fall), survival via PIT-tag detections, and prey consumption and composition will be evaluated. In addition, genetic samples will be collected from a subset of captured salmonids (primarily *O.* mykiss) to evaluate effective adult population size and number of spawners, which will complement *O. mykiss* spawning ground surveys. Fish community response will be evaluated by comparing fish assemblage composition, size composition, and spatial patterns in distribution pre and post restoration. The final question regarding the response of the Meadow Creek watershed food web to restoration will be evaluated through benthic macroinvertebrate sampling to quantify biomass and community composition pre and post restoration.

Restoration reaches represent locations of planned valley reset restoration projects (see Figure 27), and range from the headwaters (Reach 2) to the McCoy-Meadows floodplain (Reach 5), as well as Bear Creek (Bear), a tributary to Meadow Creek which may provide thermal refuge to cold water species. Restoration reaches were divided into subreaches based on differences in land ownership, spatial arrangement (e.g., above or below a tributary confluence or road crossing), and restoration implementation/monitoring design (e.g., treatment/control). Subreaches were further divided into sites, with each site classified as either core or supplemental depending on the intensity of data collection slated within each site.

Core sites are the locations within which the most intensive data collection will occur - PIT tagging, fish counts of all species, salmonid abundance estimation, salmonid diet collection, and benthic macroinvertebrate sampling. The number and length of core sites were selected with the goal of sampling a large enough fraction of total habitat (i.e., $1/3^{rd}$) within each restoration subreach to ensure sufficient fish sample sizes for estimation of *O. mykiss* productivity. Additionally, we sought to distribute our sampling effort along the length of each subreach to ensure that longitudinal variability in aquatic biota (i.e., differences between upstream and downstream sites) were accounted for and that sampling effort was spatially replicated (i.e., 2 core site replicates per subreach). Specifically, we divided the total valley polygon within each subreach into 6 sites of equal valley length and then used systematic random sampling to select 2 core sites within each subreach. We selected the first core site within each subreach by randomly selecting (without replacement) a number between 1 and 6. The subsequent core site was then selected by adding 3 to the first number selected, corresponding to a sample spacing of 50% of the valley length within each subreach. We subtracted 6 from any selected core site numbers that exceeded 6, ensuring that the systematic sample looped back to the beginning and included only the 6 sites within each subreach.

Supplemental sites are sampling locations distributed within each restoration subreach and between core sites (Figure 27). The general purpose of supplemental sites is to target *O. mykiss*

and provide additional opportunities to tag, measure, and weigh newly captured fish to increase sample sizes and bolster our ability to estimate fish vital rates within a subreach in the event that low densities/low capture efficiency (or an interaction of the two) are encountered in core sites. For the pilot year, the minimum sample objective for *O. mykiss* within core sites was a total of 100 individuals. Additionally, these sites will provide opportunities for recapturing previously tagged *O. mykiss* for evaluating growth and increase sample size for survival estimation. In cases where sufficient numbers of PIT-tagged *O. mykiss* are present (>10), these sites can also be used to conduct mark-recapture estimates for informing a single-pass calibration model.

Table 12. Summary of length, area, and number of sample sites (i.e., core sites) within each subreach.

Reach	Subreach	Valley area (acres)	Valley length (m)	Stream length (m)	Core sites (i.e., replicates)	Mean site valley length (m)	Mean site stream length (m)
2	2A	36.4	2033	2434	2	339	406
2	2B	46.4	3402	3676	2	567	613
2	2C	72.6	3075	3883			
4	4A	38.2	2307	2502			
4	4B	56.7	2652	2958	2	442	493
4	4C	58.0	2348	2525	2	391	421
4	4D	38.8	1471	1709	2	245	285
4	4E	42.1	1370	1738	2	228	290
5	5A	51.6	1534	1737	2	256	289
5	5B	72.2	1006	1096	2	168	183
5	5C	91.3	1316	2011	2	219	335
5	5D	129.7	1149	1655	2	191	276
5	5E	108.6	1027	1988			
6	6A	29.3	3082	3151			
6	6B	6.9	1108	1163			
6	6C	5.3	434	444			
6	6D	11.9	1586	1680			
6	6E	18.7	1372	1404			
	Min	5.3	434	444	2	168	183
	Max	129.7	3402	3883	2	567	613
	Mean	50.8	1793	2097	2	305	359
	Sum	914.6	32270	37752	20	3047	3590

Collaborators opted to use the 2024 field season as a pilot year, allowing for preliminary aquatic biota data to be collected and analyzed to inform the finalized study design, as well as allowing for the evaluation of the feasibility of proposed field sampling methods given staffing levels, field logistics (number and spatial distribution of sites, access to sites, etc.), and relatively low salmonid densities throughout the Meadow Creek watershed. Meadow Creek has relatively low densities of *O. mykiss* and observations of juvenile Chinook are extremely infrequent, which may inhibit the

use of some metrics (i.e. growth and survival) to assess salmonid response to restoration as the result of inadequate sample sizes at the subreach and reach scale. Spring, summer and fall 2024 sampling efforts were focused on *O. mykiss* sampling, including PIT tagging and collecting diet and genetic samples, with a dual goal of collecting pre-treatment data while also informing future RM&E efforts by evaluating *O. mykiss* density, distribution and recapture rates across the three primary restoration reaches as well as Bear Creek .

Methods

During spring and fall, all core sites were sampled with equal-effort, single-pass electrofishing. Length and weight data were collected for all salmonids captured, and all *O. mykiss* 65 mm or greater in length were PIT tagged. Diet and genetic samples were collected from a subset of *O. mykiss* in core sites, with a target of 10 diet and genetic samples per subreach (i.e. 5 per core). Diet and genetic samples were collected in supplemental sites when targets were not reached in core sites due to low *O. mykiss* densities. Count data was collected for all non-salmonid species to characterize the fish community assemblage and provide data on pre-restoration longitudinal patterns in species distributions. Supplemental sites were sampled using a range of effort levels, including a single, equal-effort pass of the entire site (most frequent), equal-effort sampling of a subsection of the site, and finally, selective sampling targeting only *O. mykiss* habitat. All *O. mykiss* captured in supplemental sites were measured for length and weight and PIT tagged (size allowing). Non-salmonid species were not enumerated in supplemental sites.

Benthic macroinvertebrate samples were collected at each core site during summer base flow conditions in mid-August. Prior to sampling, each core site was divided into 11 equidistant transects across the river channel. Beginning at the farthest downstream transect, the first sample location was randomly selected as the right, center or left of the transect (25%, 50% and 75% of the wetted width, respectively). Samples were collected using a D-frame kick net with 500 µm mesh, in which substrate within the quadrat (0.3 x 0.3 m, ~ 1 ft^2) was thoroughly brushed prior to vigorously kicking the substrate to a depth of 10 cm for 30 seconds. In instances where transects fell within slow water habitats such as pools and glides, kick nets were dragged repeatedly through the kicked area to ensure that all organisms were collected. The process was completed at each transect, resulting in a composite sample which was then transferred into one or more sample jars and preserved in 95% ethanol. Following the completion of benthic macroinvertebrate sampling along with spring and fall *O. mykiss* diet sample collection, samples were delivered to a professional taxonomic lab (Aquatic Biology Associates, Inc, Corvallis, OR) for processing and taxonomic analysis.

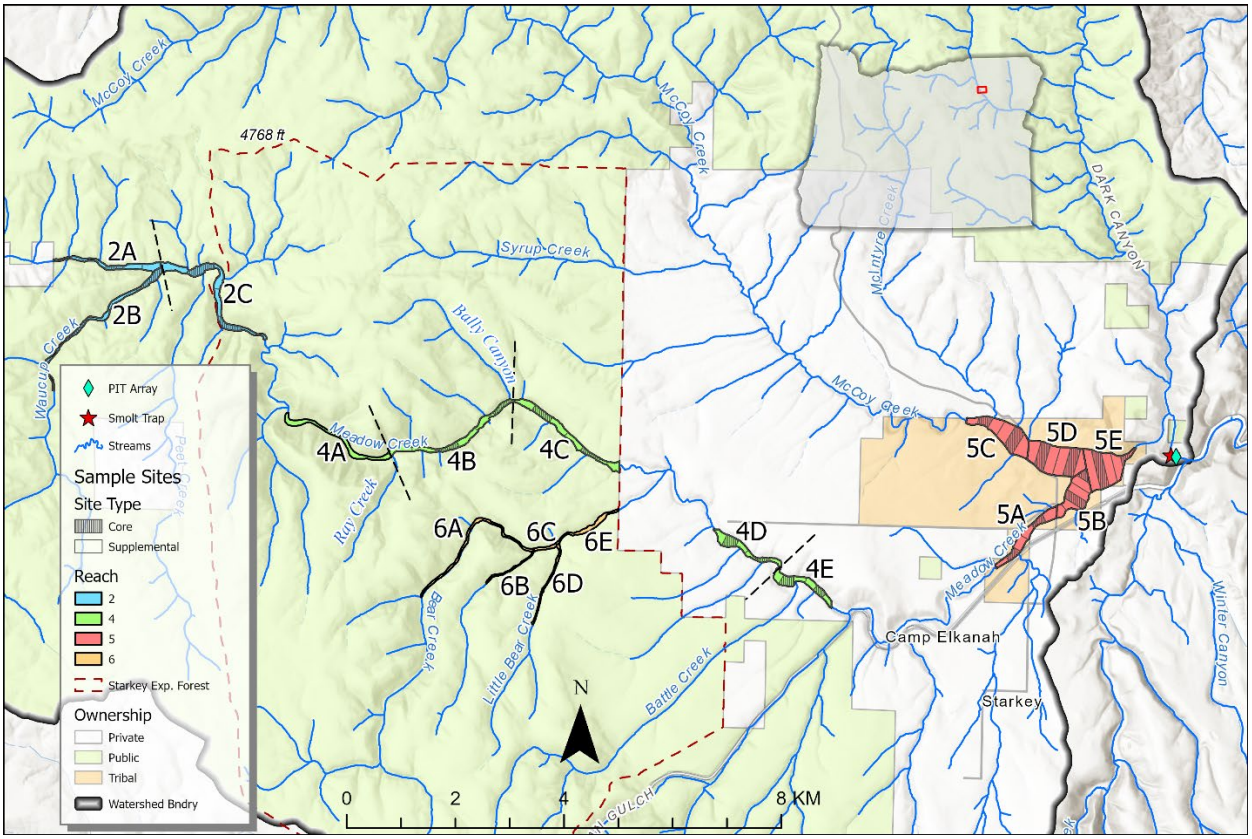

Figure 27. Study area map showing restoration reaches (2-6), subreaches (e.g., 2A-2C), and sample sites (core and supplemental).

Abundance estimates were not derived from preliminary *O. mykiss* data, as doing so relies on planned efforts to develop a single-pass abundance model by conducting paired single pass and mark-recapture at a subset of sampled sites (see Meadow Creek Aquatic Biota Study Design and Sampling Methods for additional details). Instead, preliminary count data is used as a representation of relative densities, particularly regarding the feasibility of using initial study plan thresholds for minimum sample sizes of PIT tagged individuals at the subreach scale.

Growth data was calculated as growth increment (grams/day and mm/day) as well as mass-standardized growth rate (MSGR; Ostrovsky 1995) to standardize for fish size, as growth potential is linked with body size. MSGR scales growth to the specific growth rate of a 1 g fish:

$$\text{MSGR (\%/day)} = \frac{W_2^b - W_1^b}{b\,x\,t} \times 100$$

where W_1 and W_2 are the mean fish weight during the first and second sampling events, t is the number of days between sample events, and b is a general allometric mass exponent for salmonid fishes as an allometric mass exponent has not been developed for *O. mykiss (*Iwama and Tautz 1981).

Results

Catch per unit Effort

No mark-recapture efforts were made during the 2024 pilot season given the already ambitious objective of sampling all core sites and the thermal constraints presented by the Meadow Creek watershed, wherein stream temperatures regularly exceeded sample permit maximums (18° C) by mid-morning, particularly during spring sampling in the Meadow-McCoy area (restoration reach 5). As such, we evaluated relative density across reaches and between sample events using catch per unit effort (CPUE) as well as raw count data. CPUE for salmonids (primarily *O. mykiss* with a small number of captured spring Chinook) varied widely between restoration reaches, season (spring vs fall), site type (core vs supplemental) and between organization field crews (Figure 29). CPUE across sample crews was higher during the fall for most reaches, likely due to increased capture efficiency with decreased flow levels (Figure 29). Unfortunately, shock time was not recorded for early spring sample efforts, somewhat truncating the data available to assess the relationship between flow and CPUE. The data that is available, however, indicates that, as expected, sampling during higher flows likely influenced CPUE values for sites sampled during early June through decreased capture efficiencies (Figure 28).

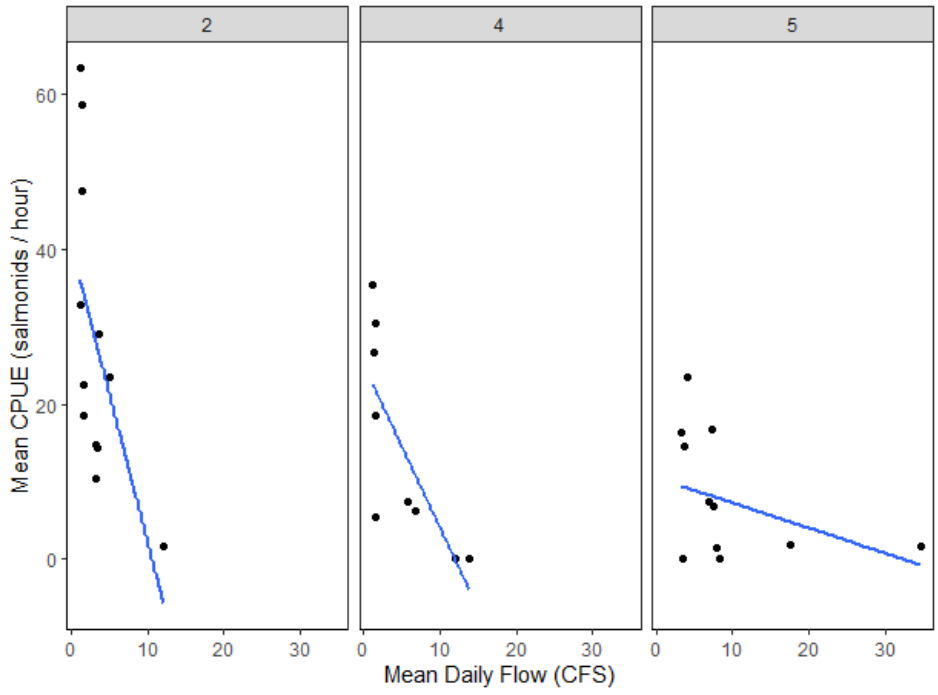

Figure 28. Mean catch per unit effort (salmonids/hour) by mean daily flow (cubic feet per second) for each restoration reach, with spring and fall sample events combined. Daily flow data from the flow gauge above

the confluence with Bear Creek used for Reach 2 and Reach 4, and daily flow data for Reach 5 from the flow gauge below the confluence of Dark Canyon.

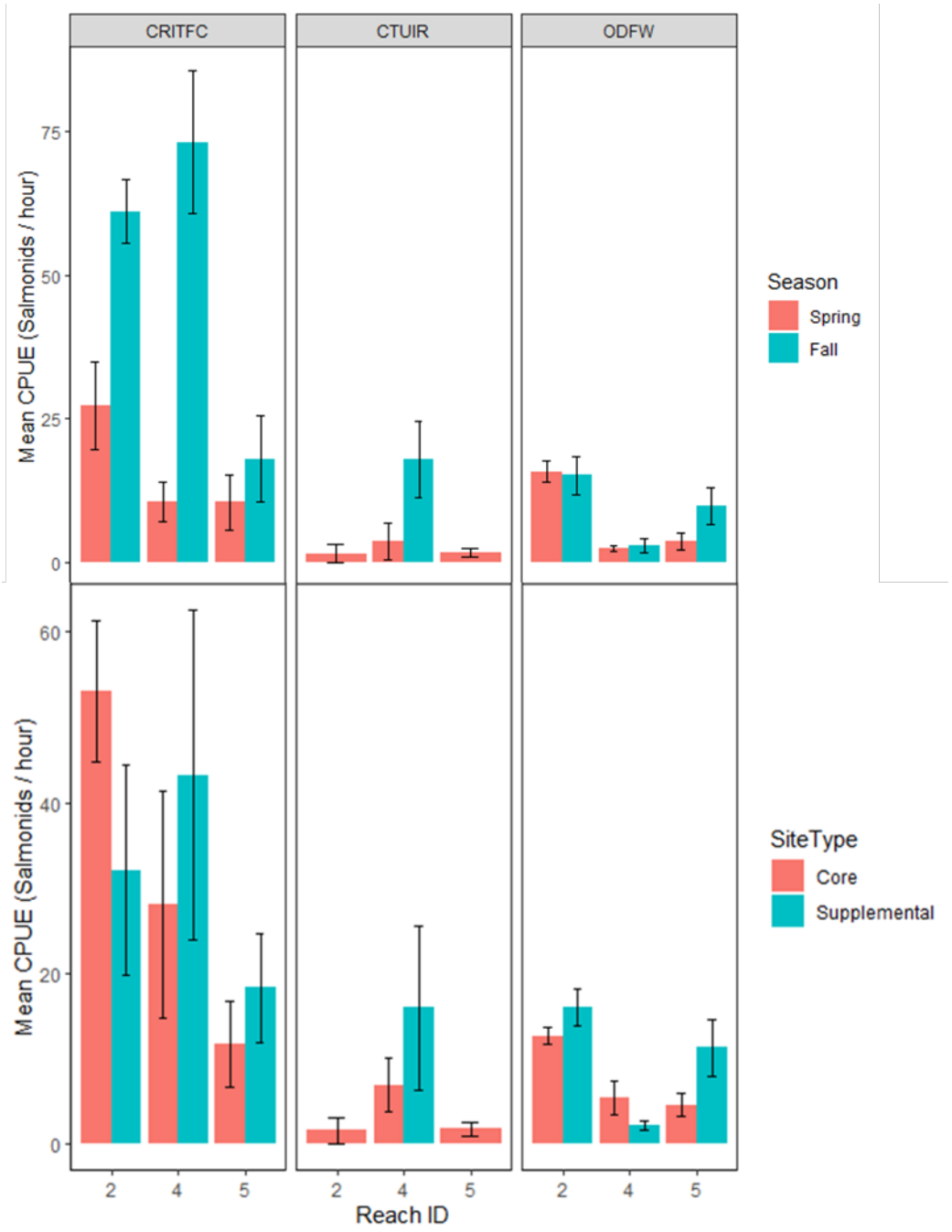

Figure 29. Top: Mean catch per unit effort (salmonids/hour) (± SE) by reach, season (spring or fall), and organization. Bottom: Mean catch per unit effort (salmonids/hour) by reach, site type (core or supplemental) and organization.

Effort- Shock time

Similar to CPUE, effort (measured by electrofishing time in seconds) varied widely across sample events during the 2024 pilot season. Some of this variation in effort can be attributed to differences between site length (ranged from 100 to 750 m), particularly for core sites which were sampled as an equal-effort pass (Figure 30). Supplemental sites did not indicate as strong a relationship between site length and effort, likely due to incongruent interpretations of the sampling protocol for supplemental sites between crews. As a result, some supplemental sites were sampled as equal-effort passes (similar to core sites but with the notable exception of only netting salmonids) and others were sampled only partially or using spot-shocking methods targeting only the best *O. mykiss* habitat.

Restoration reach also explained some variation in effort, indicated by a longitudinal pattern in shock time, with the highest efforts occurring in reach 2 and decreasing efforts through reach 4 and reach 5 (Figure 31). Reach 2 had both the longest site lengths as well as the highest fish capture numbers, particularly for core sites in Waucup Creek. Conversely, reach 5 had some of the shortest site lengths as well as the lowest fish capture numbers (Table 12). Variation in effort is also partially explained by organization, with some crews expending roughly equal effort across site types and reaches and others showing increased effort in core sites as compared to supplemental sites (Figure 32). As mentioned previously, effort was not recorded for the first approximately two weeks of spring sampling efforts, which decreases our ability to fully evaluate the sources of variation in effort for pilot season sampling efforts.

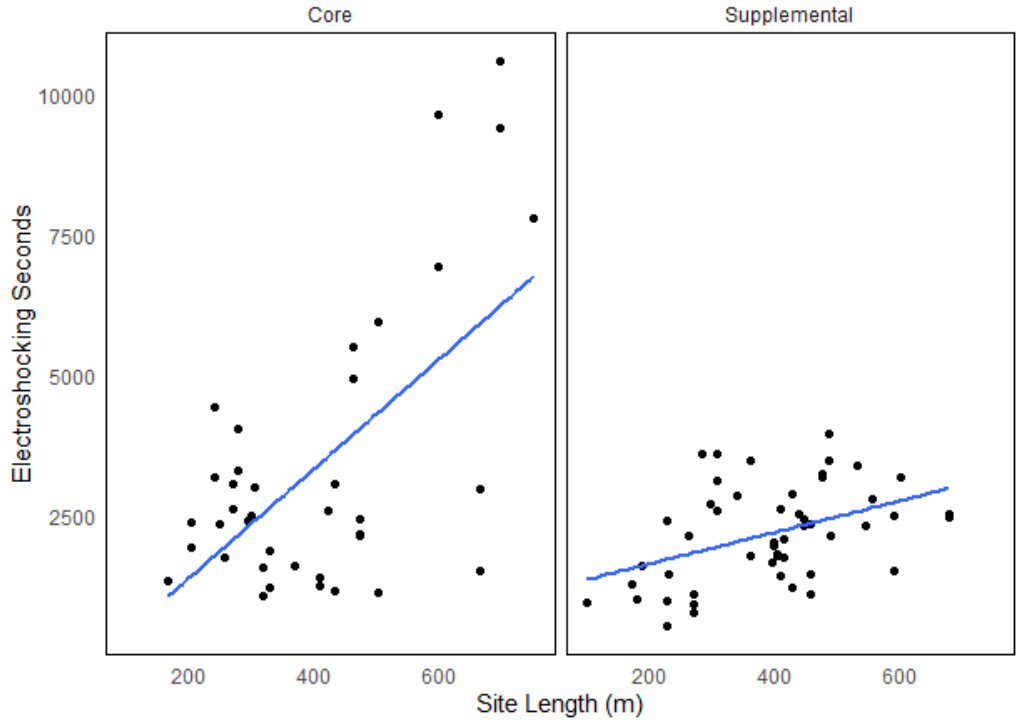

Figure 30. Electroshocking seconds by site length for core and supplemental sites.

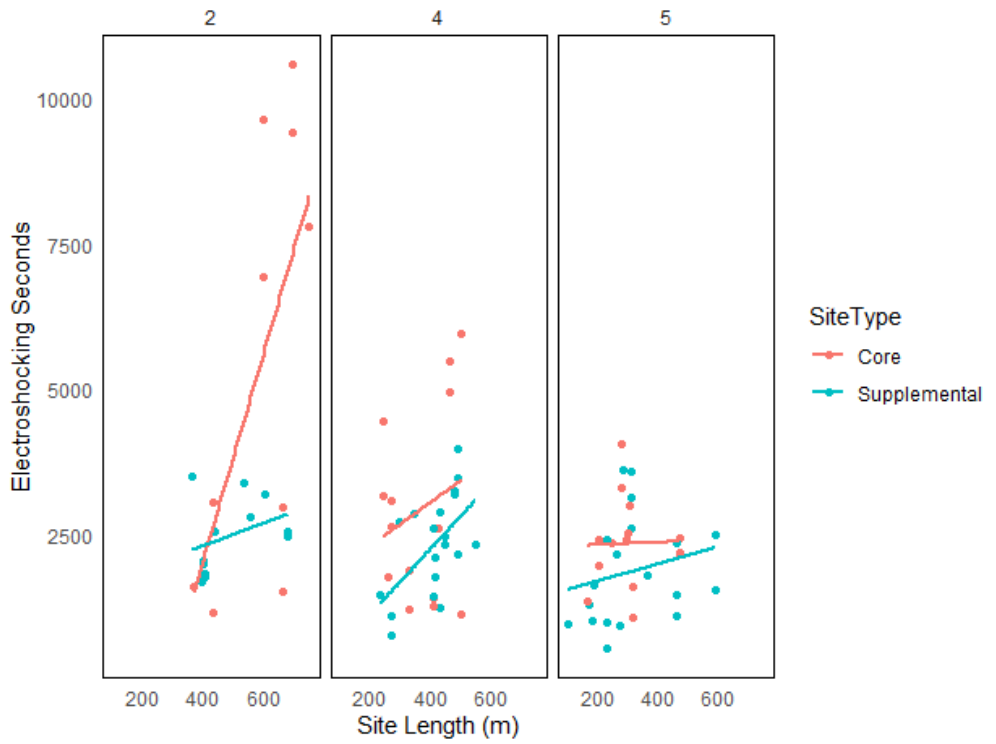

Figure 31. Electroshocking seconds by site length in each of the restoration reaches. Red lines and points indicate core sites, while blue lines and points indicate supplemental sites.

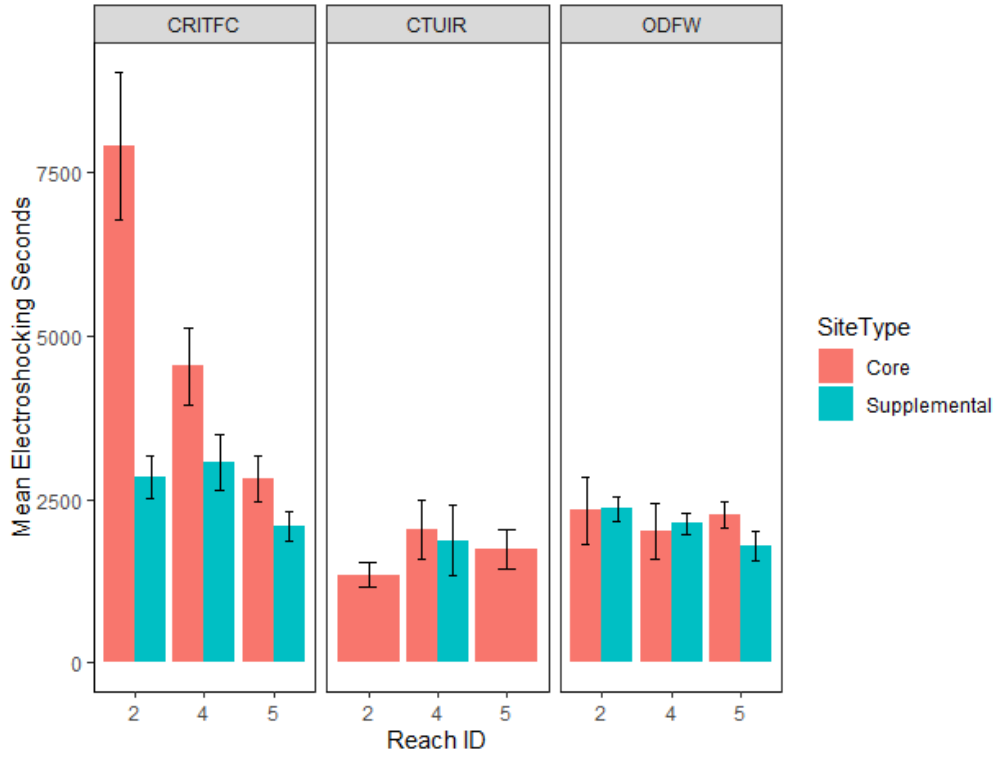

Figure 32. Mean electroshocking seconds by reach, organization, and site type.

O. mykiss Count Data

During spring sampling, substantially higher numbers of *O. mykiss* were captured in reach 2 than in reaches 4 and 5 combined (Table 13; Figure 33). Although capture counts for Bear Creek do not appear particularly high, the Bear Creek reach was short and exhibited high densities compared to other sample sites when reach length was accounted for. Tally counts represent individuals captured that were below the size threshold for PIT tagging in *O. mykiss* (65 mm, i.e. young of the year), and these data are unlikely to be reflective of relative densities of age 0 individuals given both the size-selective bias of electrofishing as a sample method as well as incongruent approaches taken by field crews wherein some crews did not attempt to enumerate age 0 fish in order to prioritize fish health.

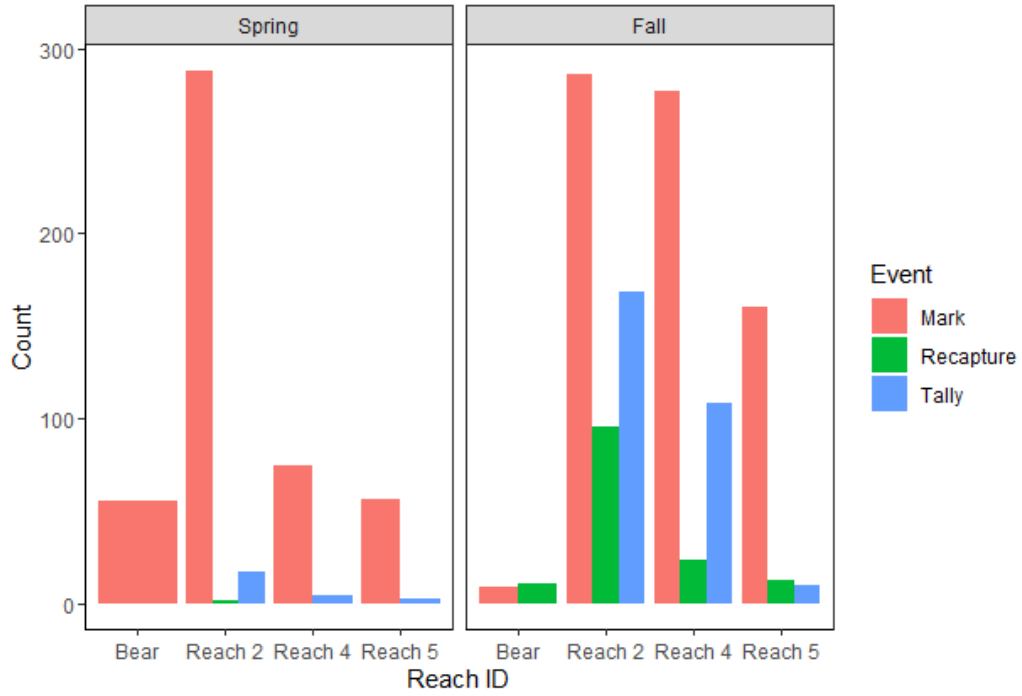

Figure 33. *O. mykiss* counts by sample event and event type (mark, recapture, or tally).

Fall sampling showed similar longitudinal patterns in fish counts, with higher numbers of fish captured in the headwaters and decreasing capture numbers observed with distance downstream. More fish were captured across all reaches during fall sampling relative to spring sampling. The frequency of recaptured individuals followed the same pattern, as would be expected based on the proportion of marked fish across the sample reaches during spring sampling. Tallied age 0 fish counts increased substantially during fall sampling as individuals achieved larger body sizes over the summer and became more susceptible to capture via electrofishing. Interestingly, the number of both marked and recaptured fish in the Bear Creek reach was much lower during fall than in spring, indicating that habitat conditions in Bear Creek likely declined over the summer months.

Table 13. Wild Summer Steelhead and Wild Summer Chinook capture numbers by event type (mark, recapture, or tally) for each Subreach sampled each season (spring and fall).

Subreach ID	Season	SRR Verbose	Mark	Recapture	Tally
2A	Spring	Wild Summer Steelhead	28	1	NA
2A	Fall	Wild Summer Steelhead	45	9	1
2B	Spring	Wild Summer Steelhead	164	NA	NA
2B	Fall	Wild Summer Steelhead	128	64	57
2C	Spring	Wild Summer Steelhead	93	NA	8
2C	Fall	Wild Spring Chinook	1	0	NA
2C	Fall	Wild Summer Steelhead	113	22	110
4B	Spring	Wild Summer Steelhead	39	NA	3
4B	Fall	Wild Summer Steelhead	229	21	106
4C	Spring	Wild Summer Steelhead	8	NA	NA
4C	Fall	Wild Summer Steelhead	9	0	2
4D	Spring	Wild Summer Steelhead	25	NA	1
4D	Fall	Wild Summer Steelhead	30	2	NA
4E	Spring	Wild Summer Steelhead	2	NA	NA
4E	Fall	Wild Summer Steelhead	9	0	NA
5A	Spring	Wild Summer Steelhead	13	NA	NA
5A	Fall	Wild Spring Chinook	1	0	NA
5A	Fall	Wild Summer Steelhead	97	2	NA
5B	Spring	Wild Summer Steelhead	5	NA	NA
5B	Fall	Wild Summer Steelhead	28	0	NA
5C	Spring	Wild Spring Chinook	1	NA	1
5C	Spring	Wild Summer Steelhead	9	NA	9
5D	Spring	Wild Summer Steelhead	4	NA	2
5D	Fall	Wild Summer Steelhead	2	0	2
5E	Spring	Wild Spring Chinook	2	NA	NA
5E	Spring	Wild Summer Steelhead	28	NA	NA
5E	Fall	Wild Summer Steelhead	33	10	8
Bear	Spring	Wild Summer Steelhead	55	NA	NA
Bear	Fall	Wild Summer Steelhead	9	11	NA

Non-salmonid Count Data

Non-salmonid fish counts exhibited similar seasonal patterns, likely due to increased capture efficiencies at lower flow levels, with higher numbers observed during fall sampling for all species except for Sculpin spp. in reach 2 (Figure 34). Several species displayed longitudinal patterns in distribution, with warm water species like Northern Pikeminnow decreasing in relative density with increasing distance upstream, and Sucker spp. and Sculpin spp. showing the opposite pattern. Distribution patterns in dace are likely obscured by the combination of Longnose Dace and Speckled Dace into one count, as Longnose Dace prefer fast-flowing, cold water and primarily inhabit riffles, whereas Speckled Dace have more encompassing habitat preferences in terms of both stream temperature and habitat type.

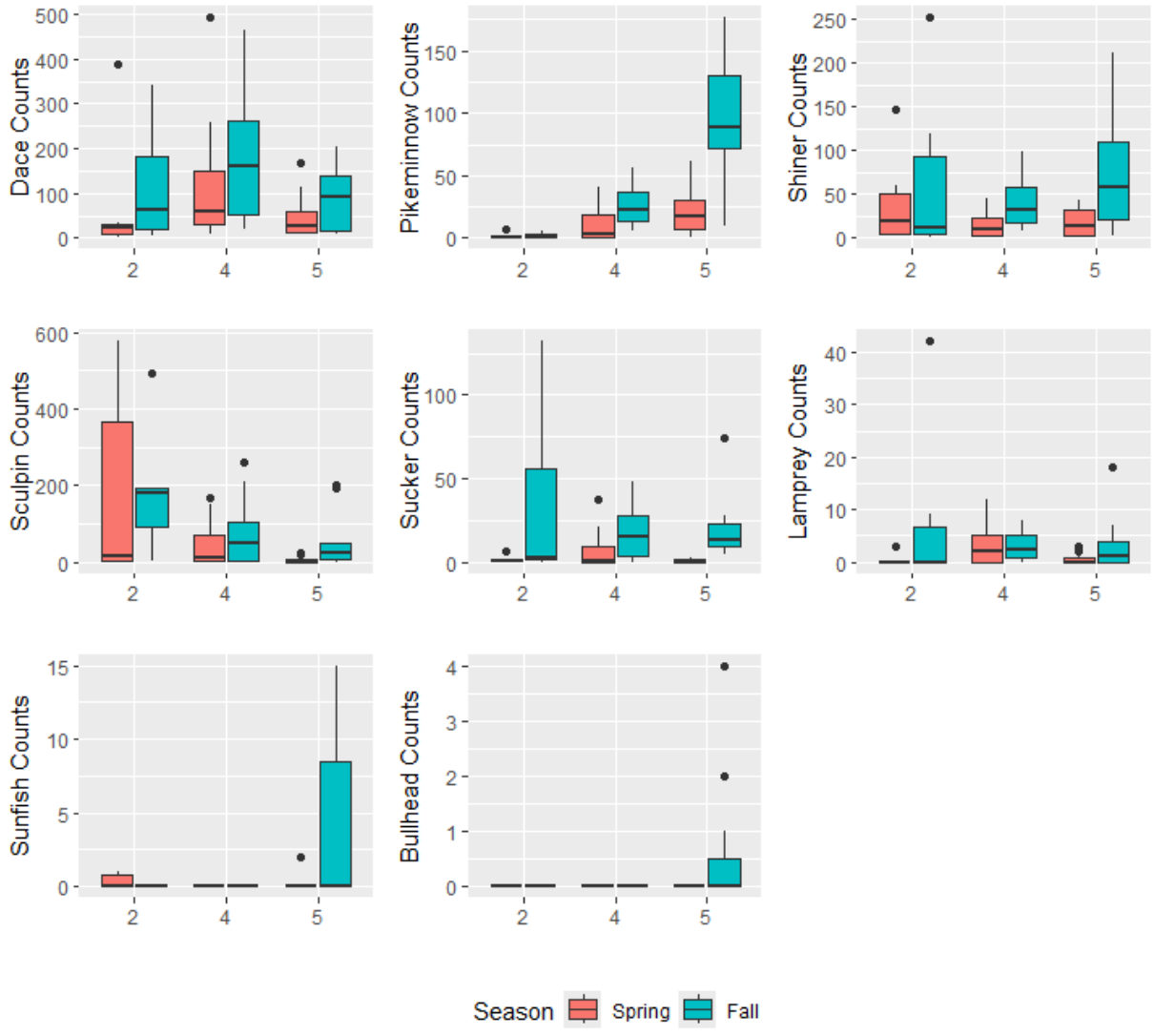

Figure 34. Non-salmonid count data by season for each restoration reach.

Sunfish spp. (Bluegill and Pumpkinseed) were predominantly captured in reach 5, with the majority found in McCoy Creek and only two observed upstream of reach 5; one in Waucup Creek and one in Meadow Creek below the confluence with Waucup (Figure 35). Bullhead sp. were captured only during the fall and only in McCoy Creek, likely due to the large, stagnant pools that provide ideal habitat for ictalurids. Both Sunfish and Bullhead are introduced species to the region, and are presumed to have originated in Indian Lake, a reservoir near the headwaters of McCoy Creek that is stocked with a variety of game fish species. The ODFW district office requires that captured Sunfish spp. and Bullhead sp. be permanently removed; as such, all captured non-native species were euthanized.

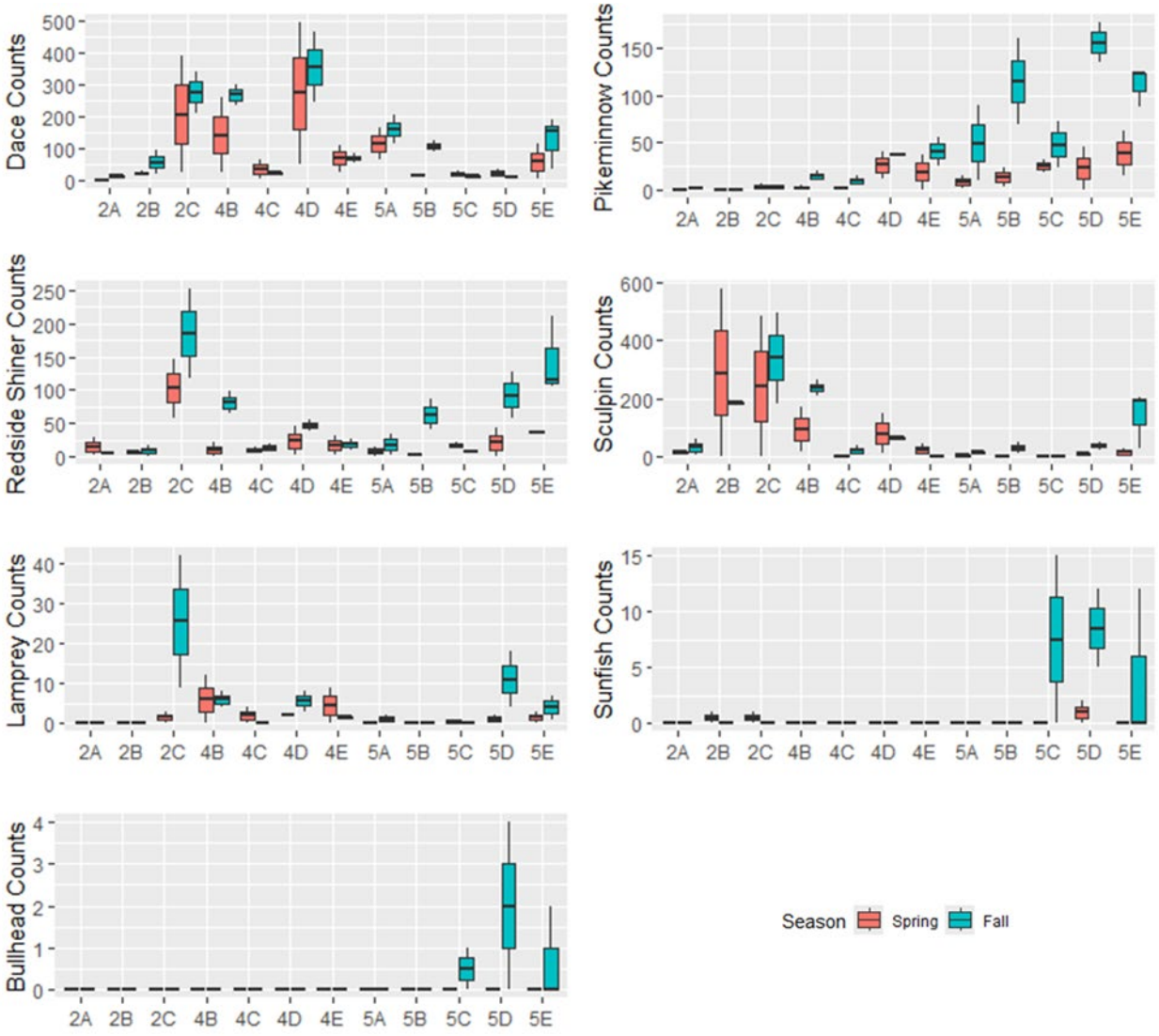

Figure 35. Non-salmonid fish counts by subreach and season.

Recapture rates

Given the high level of spatial variation in tagging numbers across the restoration reaches, recaptures rates (i.e., tagged in spring and recaptured in fall) varied considerably both across and within reaches. Recapture rates ranged from 0 to 0.54 among the 12 subreaches and lower Bear Creek reach (LWB), with the lowest recaptures/lack of recaptures observed in subreaches with the lowest spring PIT tag numbers (Table 14). Relatively high recapture rates were observed in all subreaches in which greater than 25 *O. mykiss* were PIT tagged, indicating that low recapture rates are likely due to spatial density patterns as well as the timing of spring sampling efforts at some sites occurring during high flow levels that likely decreased capture efficiency, resulting in lower numbers of tagged fish at these sites.

Table 14. Recapture rates of O. mykiss by subreach during the 2024 pilot field season.

Subreach	Spring Mark #	Fall Recapture #	Recapture Rate
2A	28	9	0.3214
2B	164	64	0.3902
2C	93	22	0.2366
4B	39	21	0.5385
4C	8	0	0.0000
4D	25	2	0.0800
4E	2	0	0.0000
5A	12	2	0.1538
5B	5	0	0.0000
5C	9	0	0.0000
5D	4	0	0.0000
5E	28	10	0.3571
Bear	55	11	0.2000

Size structure

Captured *O. mykiss* ranged in length from 29 mm to 324 mm (fork length), representing age 0 fish (< 79 mm), age 1 fish (80-129 mm), age 2 fish (130-199 mm), and age 3 fish (> 200 mm) (Figure 36; Crump 2022). These age-length relationships were derived from *O. mykiss* data collected in Lookingglass Creek, as no age-length relationships have been developed for Meadow Creek at this time. Given the contrasting thermal regime experienced by salmonid fish in Lookingglass Creek, these age-length estimates only provide a rough estimate of the age structure of captured *O. mykiss* in the Meadow Creek watershed. Substantially higher numbers of age 0 fish were captured during

fall sampling, likely due to increased body size resulting in higher capture probability. Even after excluding *O. mykiss* in the age 0 category, fall counts were substantially higher, with a total of 441 fish >79 mm captured in spring (496 total) and 700 fish >79 mm captured in fall (1,159 total).

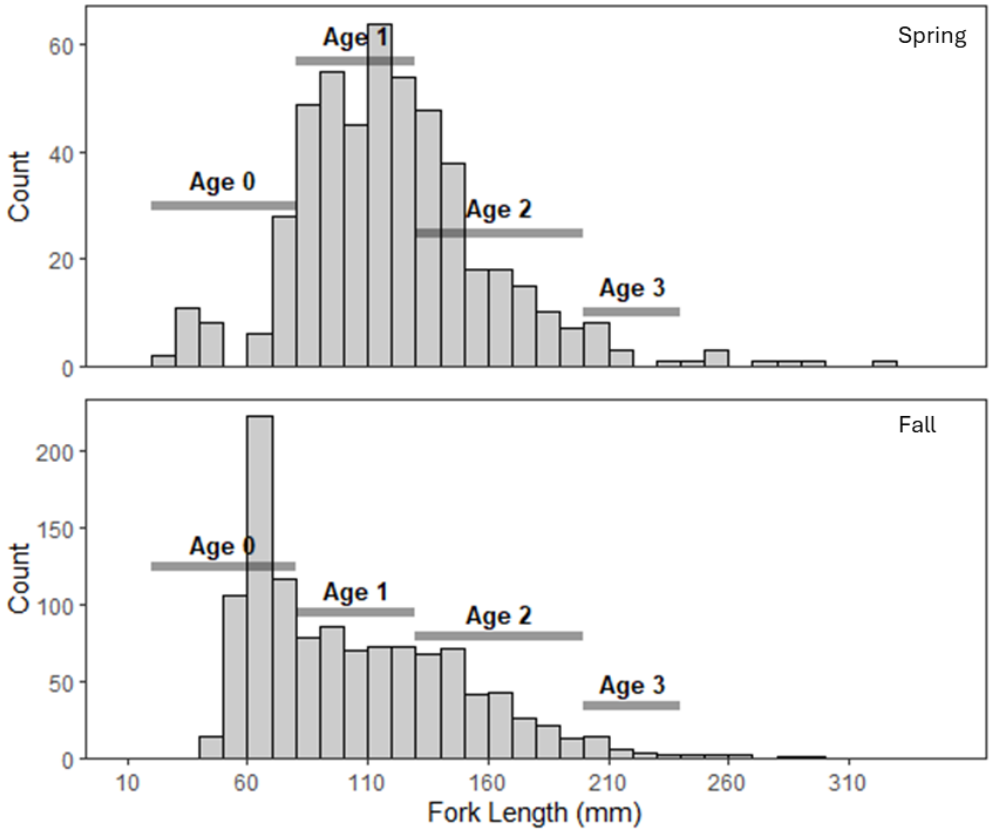

Figure 36. Length frequency of O. *mykiss* captured during spring (top) and fall (bottom) sampling. Age-length categories used were derived from Lookingglass Creek *O. mykiss* age-length data as this relationship has not been determined for Meadow Creek. Age 0 fish are classified as those < 79 mm, age 1 fish as 80-129 mm, age 2 as130-199, and age 3 as those over 200 mm (Crump 2022).

Growth rates/Condition Factor

ANOVA indicated significant differences in growth rate (MSGR) between reaches (p <0.001) (Figure 37). Mean MSGR ranged from 0.24 %/day in Bear Creek to 1.56 %/day in reach 4 (overall mean = 1.11 ± 0.11 %/day; mean ± standard deviation). Growth rates in Bear Creek were significantly lower than all three reaches, while of the restoration reaches, only reach 2 and reach 4 exhibited significantly different growth rates ($p = 0.008$). Two-way ANOVA for condition factor indicated significant differences between reaches ($p < 0.001$) and seasons ($p < 0.001$) as well as a significant interaction between reach and season ($p < 0.001$) (Figure 38). Spring body condition ranged from 0.47 to 1.55, with both the minimum and maximum observed values occurring in reach 2. Fall condition values ranged from 0.43 to 1.841, with both the lowest and highest values in reach 4. The occurrence of overall minima and maxima within the same reach during spring and fall sampling (reach 2 for the spring and reach 4 for the fall), indicates high levels of variability in habitat suitability within reaches.

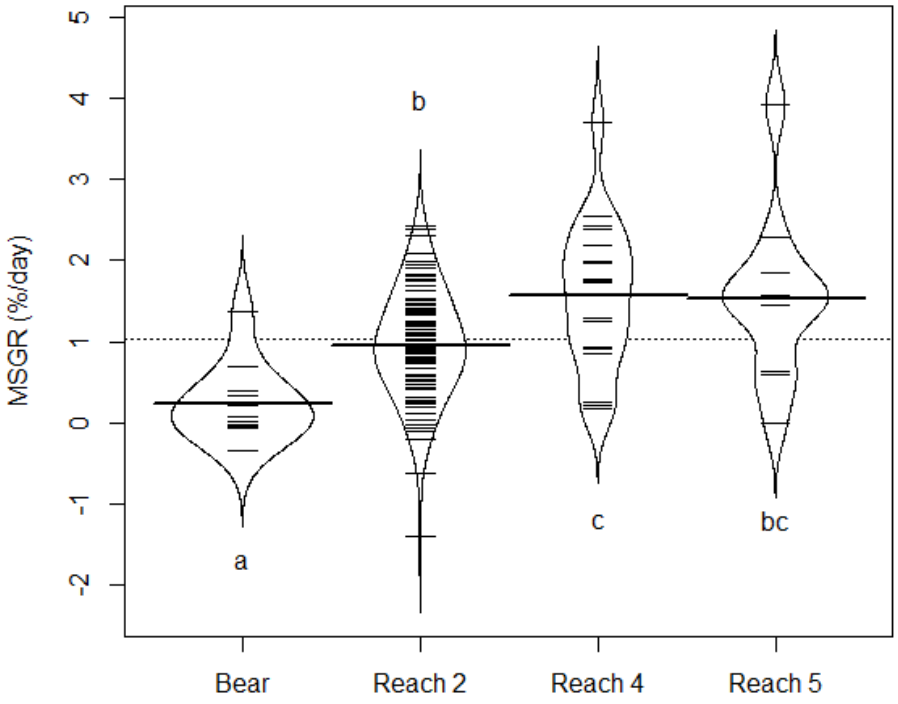

Figure 37. MSGR (%/day) of *O. mykiss* from each reach. The dashed line indicates the overall mean. Letters indicate significant differences in MSGR between reaches.

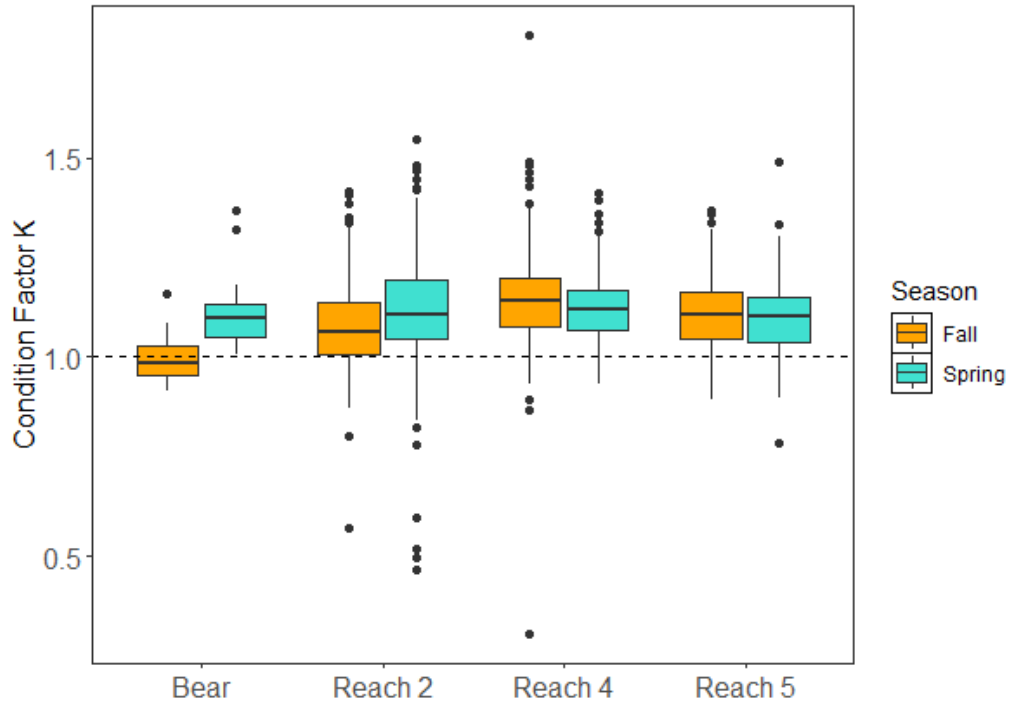

Figure 38. Condition factor of *O. mykiss* by reach in spring and fall sample events. The dashed line at K = 1 indicates a "normal" fish in good condition.

Movement

Only 11 out of 141 recaptured O. mykiss were recaptured in a different site than the initial spring mark site. This preliminary data appears to indicate high site fidelity from spring to fall, which corresponds with general trends in decreased movement during periods of decreased flow. However, mark numbers were much lower in reaches 4 and 5, as well as some core sites in reach 2 during spring sampling, which may have somewhat hindered our ability to detect movement within and among reaches. Of the tagged individuals that were recaptured in a different location, three had moved to different streams, with two individuals moving from Meadow Creek to Waucup Creek and another moving from Meadow Creek to McCoy Creek. This may indicate the use of thermal refugia during the overlap of maximum stream temperatures and minimum flow levels. Additional caveats to consider are the lack of PIT arrays at any locations other than the mouth of Meadow Creek, and the inability to capture upstream or downstream movement between reaches unless fish were recaptured during fall sampling.

Next Steps

Preliminary data from the 2024 pilot season has been used to further refine the Meadow Creek Aquatic Biota Study Design and Sampling Methods in preparation for the next several years of pre-restoration monitoring. Relative density and recapture rate data from the 2024 pilot field season have been used to refine the minimum threshold for PIT tagged *O. mykiss* within core sites (i.e. minimum of tagged *O. mykiss* per subreach) from 100 individuals to 50 individuals. Given the low densities observed, particularly within reach 5, it is recognized that this may not be achievable at all subreaches. The change to a minimum target sample size of 50 was based on an average recapture rate of 30 % (calculated from 2024 pilot data excluding sites with < 25 tagged fish), which would yield a recapture sample size of 15. This sample size was assumed sufficient to estimate average growth rates with a reasonable level of precision, although it may be adjusted based on a power analysis of pilot data from 2024. There is no maximum target sample size for PIT-tagged salmonids except for take requirements specified in fish sampling permits.

Some questions remain, particularly regarding the lower relative densities/CPUE observed during spring sampling relative to fall sampling. To at least some degree, observed relative densities likely resulted from a proportion of sites being sampled at higher flow levels, resulting in variation in capture efficiency between sites sampled in early vs. mid or late June. Additional variation arising from sample methodology can reasonably be attributed to variation in crew sample effort and electrofishing performance. Seasonal variation in relative densities may also be attributable to behavioral patterns, as many studies have found increased long-range movement in *O. mykiss* during springtime linked with stream discharge and followed by sedentary behavior during the summer, fall and winter. It's possible the early June sampling coincided with both increased movement patterns and higher discharge, indicating that efforts should be made to avoid this potential interface to maximize spring sample sizes of PIT tagged fish.

Pre-restoration monitoring will continue in the 2025 field season, including spring and fall fish sampling and summer baseflow benthic macroinvertebrate sampling. Sampling at high flow levels (>10 CFS) will be avoided to increase capture efficiency, and a collaborative sample methodology training will be held at the start of spring 2025 to standardize effort and sample methods across organizations.

References

Effects of Stage 0 restoration on aquatic ecosystem productivity, fish, and biodiversity in the Meadow Creek watershed: Restoration and monitoring study design. Justice, C., Flitcroft, R., Lemanski, J.T., and Naylor, L. 2024.

Crump, C., Naylor, L., Van Sickle, A., Kennedy, J., Mathias, Z. and Shippentower, G. Monitoring and evaluation of supplemented Spring Chinook Salmon and life histories of wild Summer Steelhead in the Grande Ronde Basin 2022 Annual Progress Report [Report]: Annual Report. Portland Oregon: Bonneville Power Administration, 2022.

Iwama, G. K. and Tautz, A. F. 1981. A simple growth model for salmonids in hatcheries. Canadian Journal of Fisheries and Aquatic Sciences 38: 649–656.

Ostrovsky, I. 1995. The parabolic pattern of animal growth: determination of equation parameters and their temperature dependencies. Freshwater Biology, 33, 357-371. https://doi.org/10.1111/j.1365-2427.1995.tb00398.x.

3.3 Evaluation of IGF1 as a tool for assessing growth in juvenile salmonids in Lookingglass Creek

Background

Considerable effort and resources are directed towards the restoration of freshwater habitat for salmonid fish populations, with a focus on increasing juvenile abundance and survival (Roni 2019; Polivka, Mihaljevic, and Dwyer 2020). Assessing the success of restoration activities aimed at improving juvenile rearing habitat requires monitoring to evaluate the abundance, growth, and survival of juvenile salmonids; however, many studies assessing habitat restoration success rely strongly on observations of relative density (i.e., number captured or observed) in restored versus unrestored habitat, which, while useful, often show small or no effects of restoration (Polivka, Mihaljevic, and Dwyer 2020; Roni 2019; Polivka 2020). Measurements of growth can provide a more robust method of evaluating restoration effects, as growth rates are closely linked with habitat conditions and increased growth is also often correlated with increased rearing and emigration survival (Ebersole et al. 2006; Monzyk et al. 2009; Pess et al. 2011).

Growth studies frequently utilize mark-recapture methods which require the tagging and repeated sampling of individuals, necessitating considerable sampling effort. Further, the efficacy of mark-recapture may be limited by population size and density, habitat volume and/or complexity, and

movement patterns (Duguid et al. 2018; Bond et al. 2014). Single-capture sampling methods allow for effective habitat-growth comparisons, particularly in contexts where recapture rates may be low due to dispersal patterns, poor capture efficiency, or other factors. One metric for assessing growth without the recapture of individuals is the concentration of insulin-like growth factor 1 (IGF1), which has been validated as an index of relative growth rate in juvenile salmonid fishes (Duguid et al. 2018; Beckman 2011; Bond et al. 2014). Plasma IGF1 concentration has been found to be strongly correlated with growth rate, and highly responsive to shifts in habitat suitability, with IGF1 concentration responding to changes in environmental conditions within as little as 4 days (Gabillard et al. 2006; Caldarone et al. 2016; Duguid et al. 2018). IGF1 has predominately been utilized in coastal regions as it provides an effective means for comparing growth of individuals of similar size and age classes occupying marine, estuarine, and freshwater habitats, particularly in habitat types characterized by low recapture rates.

Measuring IGF1 to evaluate juvenile salmonid growth in freshwater habitats pre- and post-restoration appears promising, as single-capture methods would eliminate dependence on achieving sufficient numbers of recaptured individuals to effectively evaluate fish response (Bond et al. 2014). Additionally, as IGF1 levels directly stimulate growth and are highly responsive to shifts in habitat conditions, there may be potential to utilize these methods to more finely partition spatio-temporal inflection points in juvenile salmonid growth than is feasible using multiple-capture alternatives. While IGF1 has been well validated as an index of relative recent growth in juvenile salmonids and successfully applied in the field to evaluate recent growth, previous studies have been conducted using lethal sampling methods or have non-lethally sampled individuals with larger body sizes than are typical of juvenile anadromous salmonids occupying inland freshwater habitats (Beckman 2011; Feriss et al. 2014; Bond et al. 2014). Field validation is needed to evaluate the feasibility of non-lethally sampling smaller bodied juvenile salmonids while still collecting a sufficient volume of plasma to assess IGF1 levels.

Tributaries of the upper Grande Ronde River in Northeast Oregon have experienced extensive habitat degradation as the result of the cumulative effects of land use practices in the region (NOAA 2017). This significant decrease in habitat suitability has constricted fish distribution and reduced abundance of native salmonids including spring-run Chinook Salmon (*Oncorhynchus tshawytscha*) and Steelhead (*Oncorhynchus mykiss*). Extensive habitat restoration is planned across the upper Grande Ronde, providing an opportunity for evaluating pre- and post-restoration habitat suitability and growth response of juvenile salmonids. The increased use of large-scale, process-based restoration techniques produces habitat complexity that makes the sampling of juvenile salmonids, particularly methods requiring repeat-sampling, more logistically challenging. As such, monitoring efforts focused on assessing the effectiveness of these restoration projects would benefit from methodology to estimate growth responses using single-sampling approaches.

Project Overview

A paired mark-recapture and insulin-like growth factor (IGF1) pilot study was conducted in 2024 in Lookingglass Creek, a tributary of the Grande Ronde River, to evaluate the feasibility of using IGF1 concentration as a metric of growth in field studies. We are ultimately interested in determining the potential application of IGF1 as a method of assessing juvenile salmonid growth in habitats where traditional mark-recapture methods are not very effective (e.g., complex floodplains, large rivers, and estuaries). Blood draws were performed following two growth stanzas representing summer (mid-July to mid-August) and early fall (mid-August to mid-September) growth to provide a larger range of variation in growth rates with which to evaluate correlations between PIT tag derived growth and IGF1 concentrations.

Preliminary growth data was collected in 2023 to both inform the 2024 pilot study regarding recapture rates and relative densities, as well as providing a total of two years of *O. mykiss* growth data prior to restoration in Lookingglass Creek planned for 2025. Over the last several years, CTUIR has collected pre-restoration data for juvenile spring Chinook (growth, diet, and isotopes) in the downstream treatment and upstream control reach; however, juvenile *O. mykiss* data has previously only been collected at the screw trap located upstream of Lookingglass Fish Hatchery. Providing additional pre-restoration data in the control and treatment reaches allows for evaluation of juvenile *O. mykiss* response to restoration efforts that complement ongoing efforts to evaluate spring-run Chinook response.

Methods

Sample reaches were longitudinally distributed within the pre-restoration control and treatment reaches, with the downstream-most reach extending 100 m above and below the mid-point of the already established CTUIR treatment and control Chinook tagging reaches, respectively. Two additional 200 m reaches in both the control and treatment reaches were spaced at roughly equidistant intervals to maximize spatial coverage within the control and treatment sections, while maintaining a 400 m buffer between reaches within the treatment and control sections (Figure 39).

Initial tagging was conducted during the week of July 15th, 2024, in collaboration with CTUIR biologists and fishery technicians. Recapture sampling for the first growth stanza was conducted the week of August 12th, and the recapture sampling for the second growth stanza was conducted the week of September 15th. For all sample events, fish were captured using a combination of backpack electrofishing and seining, wherein two backpack electrofisher units were used to shock downstream into a seine net while dip netters opportunistically captured fish. Each reach was sampled with one upstream pass followed by a downstream pass to increase the number of *O. mykiss* captured. Captured fish were anesthetized using MS-222 (<0.1 g/L), weighed, measured (fork length) and implanted with a 9- or 12-mm PIT tag for individuals between 65 and 200+ mm in length. In 2023, reaches were sampled for initial tagging the week of August 7th and for recaptures the week of September 18th, using the same sample methods.

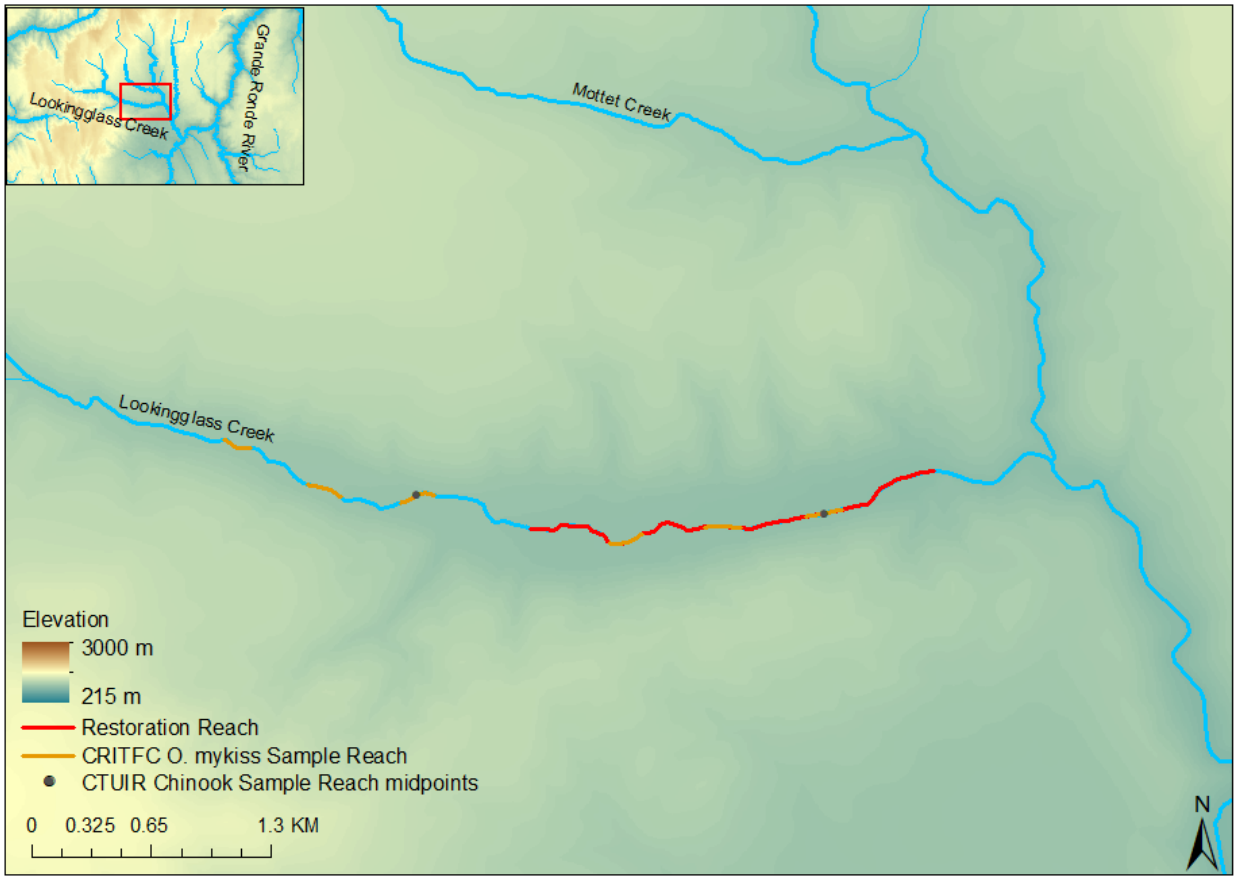

Figure 39.Location of Lookingglass Creek O. mykiss growth study sample reaches for 2023 as well as the planned restoration extent and midpoint locations for CTUIR control and treatment Spring Chinook monitoring reaches.

During the second and third sample events, recaptured individuals were anaesthetized in small groups, and length and mass data was collected prior to collecting blood from the caudal vein using a heparinized 25-gauge syringe, inserted posterior of the anal fin and anterior of the caudal peduncle. Care was taken to avoid excessive pulling pressure on the syringe, which can contribute to hemolysis (bursting of red blood cells) and result in decreased blood plasma concentration. The target volume for each blood sample was 100 µl. In most cases this volume was achieved; however, minimizing fish handling time was a priority and, in any instances where blood flow slowed or stopped short of 100 µl, fish were immediately placed in a recovery bucket and no further efforts to collect blood from said individual were made. Blood was then displaced into blood tubes and placed in a tube rack on wet ice in a cooler. Following the completion of blood draws, blood samples were immediately processed by centrifuging at 8,000 g for five minutes to separate plasma. Care was taken to ensure that no samples sat on wet ice for longer than 45 minutes before being centrifuged to avoid hemolysis; in some cases, samples were centrifuged in two batches to prevent samples sitting on wet ice for excessive amounts of time. Following centrifuging, separated red blood cells were retained to allow for genetic testing of sex in the event that

preliminary analysis indicates a need for the inclusion of sex as a covariate. Red blood cells are currently housed at the University of Idaho and stored in a sub 80 °C freezer.

After centrifuging samples, plasma was then aspirated from blood cell layers and placed in a plasma tube using a micropipette. Plasma tubes were placed on dry ice immediately after this process was completed. Plasma tubes were stored in a freezer box on dry ice for transport from the field site to the CTUIR office in Island City, where they were stored in an ultra-low -20 °C freezer. Following the final sample event, samples were transported on dry ice to the University of Idaho for processing. IGF1 extraction and assay were completed by University of Idaho staff using an IGF1 assay developed for Steelhead kelt blood plasma samples and modified for use with decreased blood plasma volumes to allow for IGF1 sampling in smaller bodied individuals.

Growth was characterized as mass standardized growth rate (MSGR; Ostrovsky 1995) to standardize for fish size, as growth potential is linked with body size. MSGR scales growth to the specific growth rate of a 1 g fish:

$$\text{MSGR (\%/day)} = \frac{W_2^b - W_1^b}{b\ x\ t} \times 100$$

where W_1 and W_2 are the mean fish weight during the first and second sampling events, t is the number of days between sample events, and b is a general allometric mass exponent for salmonid fishes as an allometric mass exponent has not been developed for *O. mykiss (*Iwama and Tautz 1981). Growth was also characterized using metrics based on length (i.e., mm/day-1, SGR), as IGF1 is often more closely correlated with growth in length than growth in mass. Changes in length are directly dependent on IGF1, while changes in mass may reflect growth in organs and/or tissues with varying degrees of dependence on IGF1 (Beckman 2011).

Results

The minimum target number of *O. mykiss* tagged per 200 m reach per sample event for the IGF1 field pilot was 85 individuals, while the number of individuals tagged ranged from 52 to 115 during the initial tagging effort in July and from 64 to 114 during the second tagging effort in August. Additional PIT tags were put out during the September event to increase the number of tagged and later recaptured *O. mykiss* in Lookingglass Creek to quantify growth rates prior to restoration; however, individuals tagged in this event are not included in the IGF1 analysis or growth rates presented in this report. Recapture rates between sampling events ranged from 0.21 to 0.48 among the six reaches, with increased recapture rates between the second and third sample event, which was expected with the greater cumulative number of PIT tagged individuals (Table 16). Fish tagged in 2023 were recaptured across all three 2024 sample events, which suggests relatively high level of site fidelity. These individuals were not excluded from analysis, as in instances in which said fish were recaptured at two subsequent events in 2024, they were selected for blood sampling to increase the number of IGF1 samples collected at each reach and sample event.

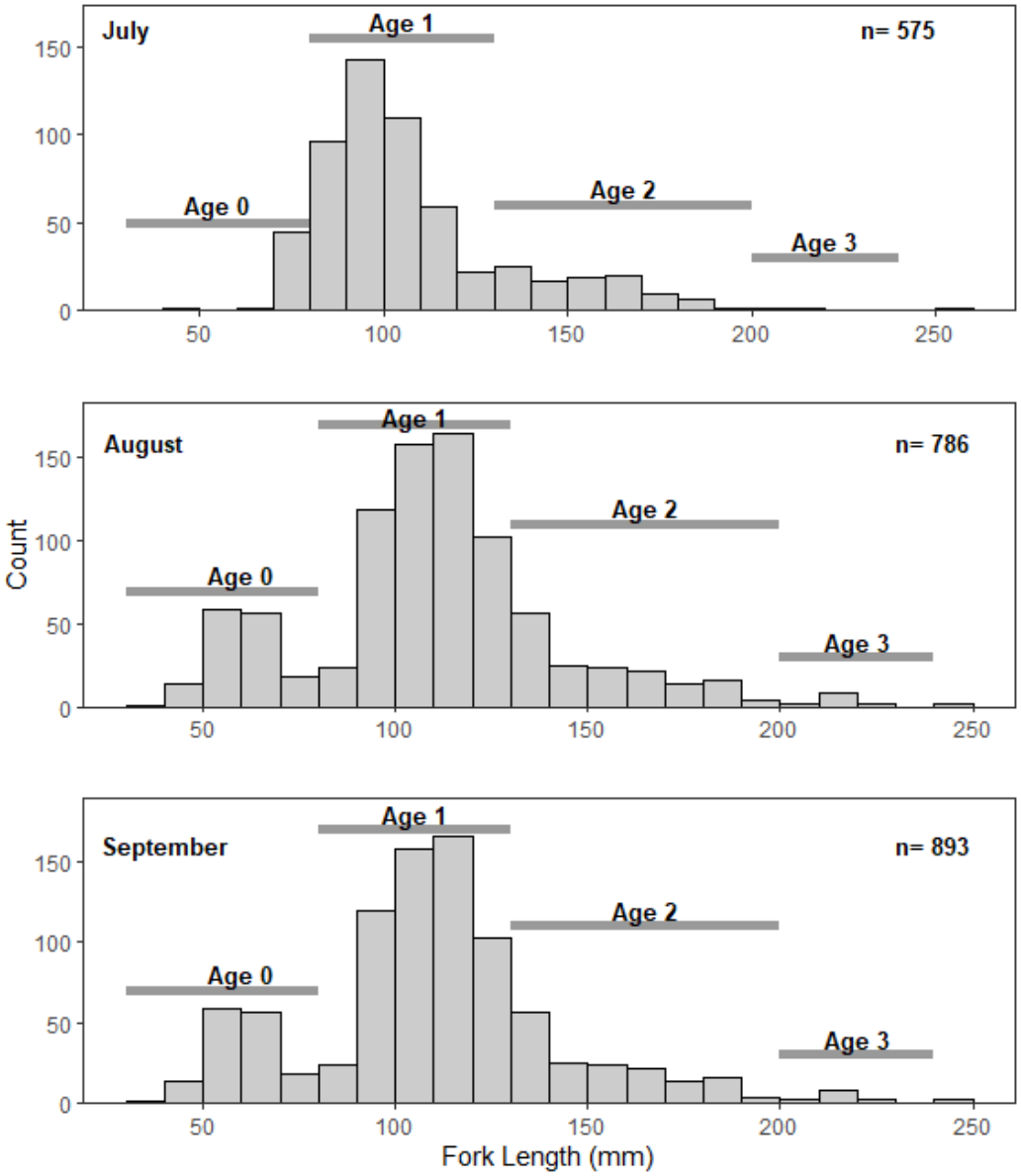

Figure 40. Length frequency of sampled O. mykiss in Lookingglass Creek by age class for July, August and September sample events. Age 0 fish are classified as those < 79 mm, age 1 fish as 80-129 mm, age 2 as130-199, and age 3 as those over 200 mm (Crump 2022).

O. mykiss captured during sample event one (July) ranged in length from 43 mm to 238 mm (fork length), representing age 0 fish (< 79 mm), age 1 fish (80-129 mm), age 2 fish (130-199 mm), and age 3 fish (> 200 mm) (Figure 40; Crump 2022). The size structure of captured *O. mykiss* was comparable across the following sample events, with a minimum of 45 mm and maximum of 260 mm for August sampling and a minimum of 37 mm and maximum of 244 for September sampling. Blood sampled fish ranged in size from 110 mm to 217 mm for growth stanza 1 (July to August), and 106 mm to 227 for growth stanza 2 (August to September), with the majority of individuals sampled across both growth stanzas categorized as age 1 fish based on length and smaller

proportions categorized as age 2 and age 3 fish (Figure 45). A total of 67 recaptured *O. mykiss* fit the criteria (size, captured at first sample event) for blood sampling for the first growth stanza, while 113 recaptured individuals fit the criteria for the second growth stanza. The increase in sample size between growth stanzas can be attributed to both the increase in the proportion of PIT tagged fish in each reach between sample events 2 and 3 as well as growth in tagged individuals throughout the study duration, resulting in higher numbers of fish meeting the minimum size threshold at the final sample event.

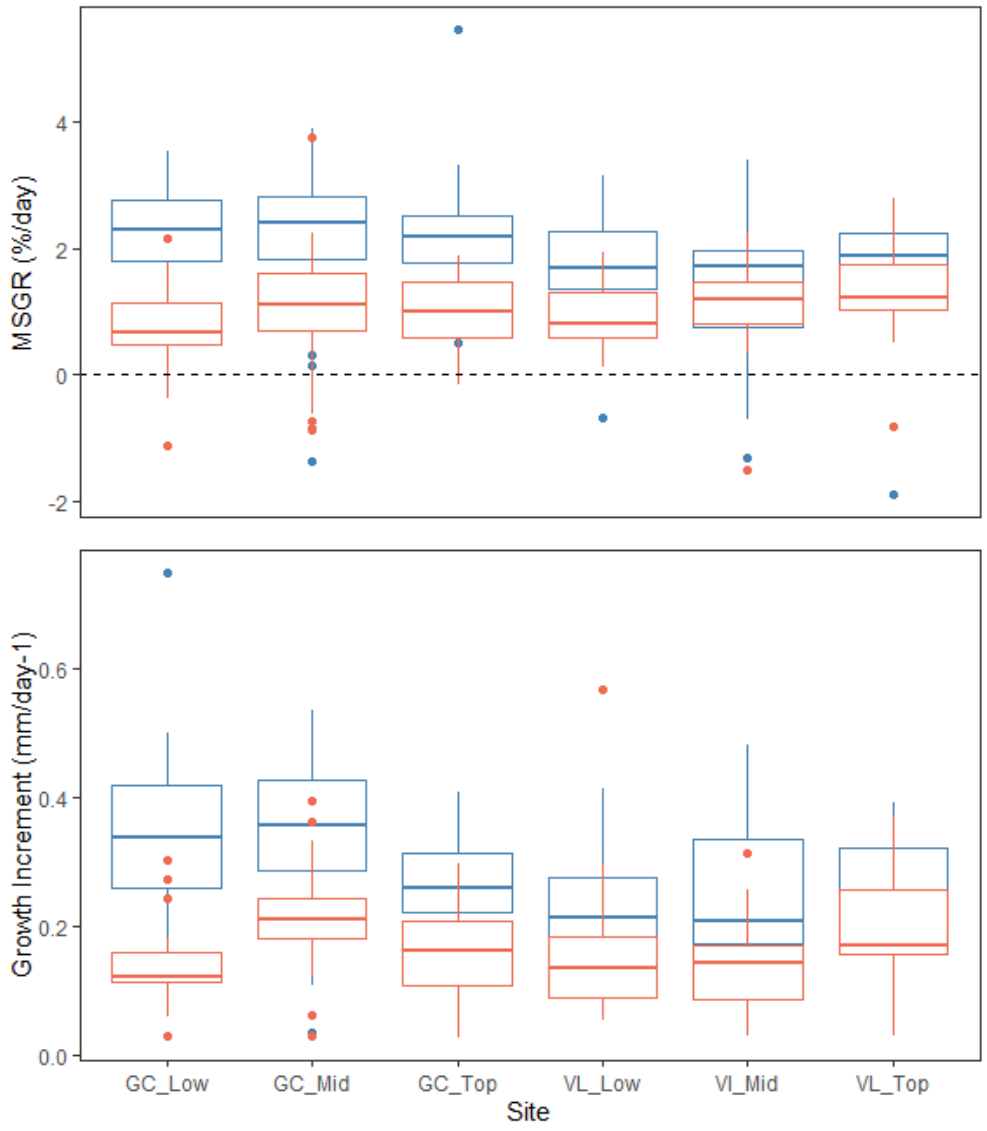

Figure 41. Top plot: Mass standardized growth rate (MSGR) (%/day) for each reach sampled in Lookingglass Creek in 2024. Bottom plot: Growth increment (mm/day -1) for each reach sampled in Lookingglass Creek in 2024. Blue boxplots and points represent the summer growth stanza (July-August) while orange plots and points represent the late summer/fall growth stanza (August-September).

Two-way ANOVA for MSGR of all recaptured *O. mykiss* indicated significant differences between growth stanzas (1: mid-July to mid-August, 2: mid-August to mid-September) ($p < 0.001$) and a significant interaction between reach and growth stanza ($p < 0.005$) but no significant differences between reaches ($p = 0.39$)(Figure 41). Mean MSGR for sample reaches during growth stanza 1 ranged from 1.39 %/day in the mid control reach to 2.19 %/day in the middle treatment reach (overall mean = 1.88± 0.08 %/day; mean ± standard error). Mean MSGR for sample reaches during growth stanza 2 ranged from 0.80 %/day in the lowest treatment reach to 1.22 %/day in the middle treatment reach (overall mean = 0.96± 0.05 %/day; mean ± standard error).

Growth increment in length (mm/day) for all recaptured individuals (excluding those falling outside of the growth stanza) was significantly different between reach ($p < 0.001$) and growth stanza ($p < 0.001$), with a significant interaction between reach and growth stanza ($p < 0.001$) (Figure 41). Mean growth increment for sample reaches during growth stanza 1 ranged from 0.20 mm/day in the lowest control reach to 0.34 mm/day in the middle treatment reach (overall mean = 0.27± 0.01 mm/day; mean ± standard error). Mean growth increment during growth stanza 2 ranged from 0.12 mm/day in the lowest treatment reach to 0.18 mm/day in the middle treatment reach (overall mean = 0.16± 0.006 mm/day; mean ± standard error).

Relationship between IGF1 and Growth Rate

Growth increment and MSGR for blood sampled *O. mykiss* were also evaluated for variation between reaches and growth stanzas (Figure 42). Two-way ANOVA for growth increment (mm/day) showed significant differences between both reach ($p < 0.001$) and growth stanza ($p < 0.001$) but no significant interaction between reach and growth stanza ($p = 0.08$). Growth increment during the first growth stanza exhibited a longitudinal pattern, with the highest growth occurring in the farthest downstream reaches and diminishing growth with increasing distance upstream. Interestingly, the upstream most reach, VL_Top, deviates from the trend with similar growth achieved to the two downstream most reaches. The second growth stanza shows no clear longitudinal trends. It should be noted that preliminary analysis evaluating growth rate as mm/day did not control for the relationship between fish size and growth rate; future analysis will control for variation in growth arising from differences in fish size.

Two-way ANOVA for MSGR in blood sampled fish indicated significant differences between growth stanzas ($p < 0.001$) and a marginally significant effect of the interaction between reach and growth stanza ($p = 0.03$), but no significant difference between reaches ($p = 0.095$). Compared to growth increment, MSGR showed no longitudinal patterns in growth rate during either growth stanza, although VL_Top did exhibit higher growth rates than neighboring control sites. Growth rates achieved during the first growth stanza were higher than those achieved during the second growth stanza.

IGF1 values indicated significant differences between reach ($p < 0.001$) and growth stanza ($p < 0.001$) as well as a significant interaction between reach and growth stanza ($p = 0.003$) (Figure 42). Similar to growth increment and MSGR, IGF1 values from growth stanza 1 largely followed a longitudinal pattern, with decreasing IGF1 levels with increasing distance upstream, but one notable exception. The farthest upstream reach, VL_Top, showed an increase in IGF1 relative to

the two preceding reaches. This may be due to differences in habitat complexity between the three control sites. VL_Top is characterized by relatively higher frequencies of large wood and pools than the other two control sites, which may have compensated for presumed decreases in temperature with increasing river kilometer. IGF1 values decreased between growth stanzas, with higher levels from July to August than from August to September, with the exception of VL_Top, which exhibited marginally higher IGF1 values in the early-fall growth stanza.

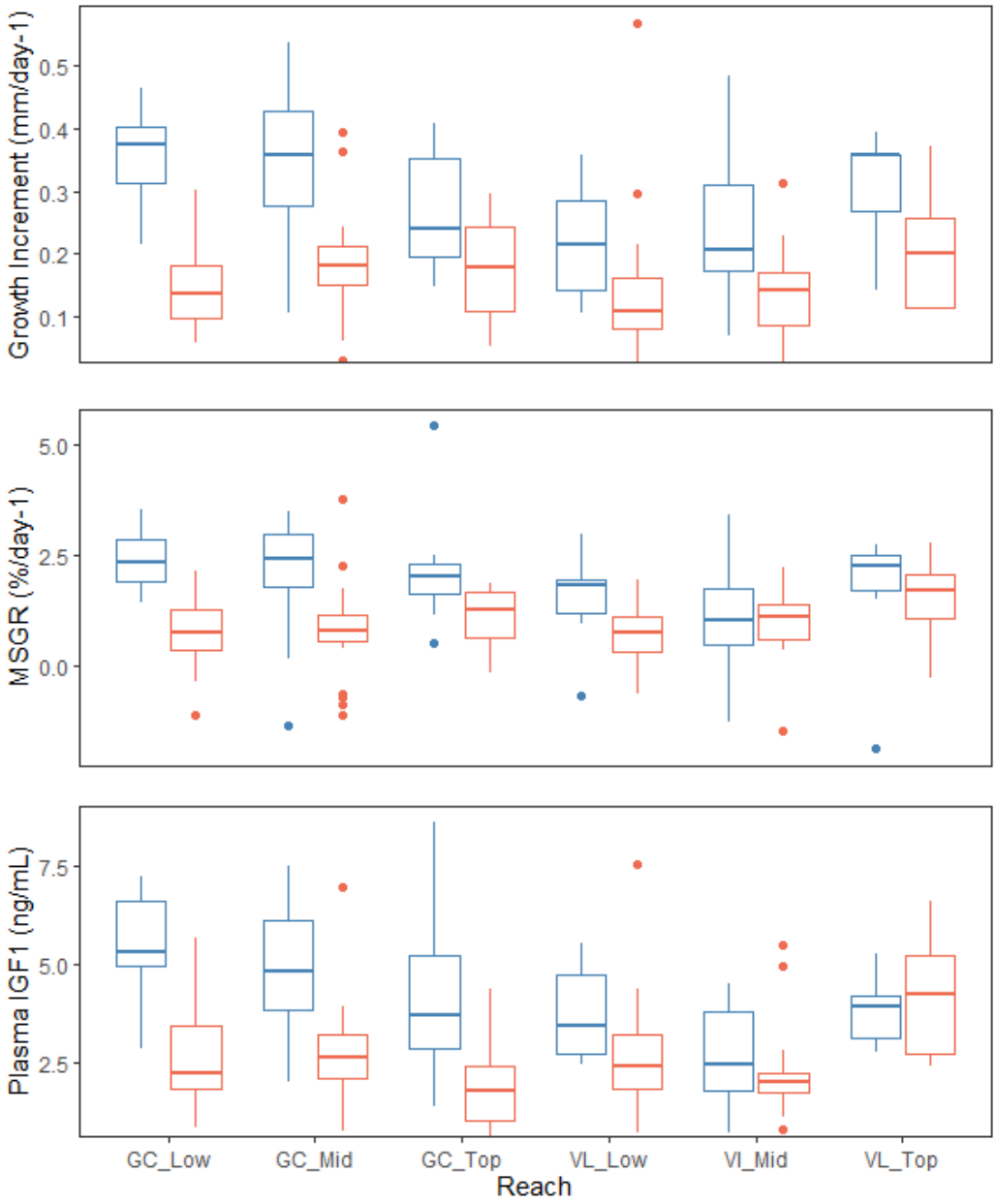

Figure 42. Top: Growth increment (mm/day-1) for blood sampled *O. mykiss* during 2024 sampling by reach and growth stanza. Middle: MSGR (%/day) for blood sampled *O. mykiss* by reach and growth stanza. Bottom: Plasma IGF1 (ng/mL) levels in each reach for each growth stanza. Blue boxplots and points represent the summer growth stanza (July-August) while orange plots and points represent the late summer/fall growth stanza (August-September).

Across all growth metrics examined, higher growth was observed during growth stanza 1 (mid-July to mid-August) than in growth stanza 2 (mid-August to mid-September) (Figure 42; Table 15). This suggests that the timing and duration of the growth stanzas selected for our study design provide sufficient seasonal contrast in growth rates for future data analysis evaluating the relationship between individual growth rates and IGF1 values. Preliminary evaluation of the linear relationship between plasma IGF1 values (ng/mL) and growth increment (mm/day) indicates a significant, positive relationship ($r^2 = 0.39$, < 0.001; Figure 43). The relationship between plasma IGF1 values and MSGR shows a weaker but still significant relationship ($r^2 = 0.30$, < 0.001; Figure 44). Growth stanza 1 shows a stronger relationship between IGF1 and growth for both MSGR and growth increment than growth stanza 2, indicating that seasonal influences such as shifts in photoperiod may potentially reduce concordance between IGF1 and growth rate during this interval (Figure 44).

Next Steps

Blood plasma IGF1 assays were completed in April 2025, and exploratory data analysis is currently ongoing. The relationship between individual growth rates and IGF1 values will be evaluated using a mixed effects model, with specific growth rate as the response variable, IGF1 concentration, season (summer growth stanza vs early fall growth stanza) and initial length as fixed effect covariates, and sample site as a random effect. Previous studies have suggested that basal IGF1 levels differ with fish size, however, other studies have found no relationship between IGF1 levels and length/size (Shimizu et al. 2009; Beckman et al. 2011). If necessary, potential size effects will be addressed by adjusting the measured value of IGF1 for differences in size based basal IGF1 values (Shimizu et al. 2009):

$$IGF_{Sadj} = IGF_{obs} - 4 + 0.07(Length)$$

where IGF_{Sadj} represents the corrected IGF1 value for size-related basal IGF1, IGF_{obs} represents the values measured in the study, and length (mm) is measured fork length. Full analysis is anticipated to be completed by the next report.

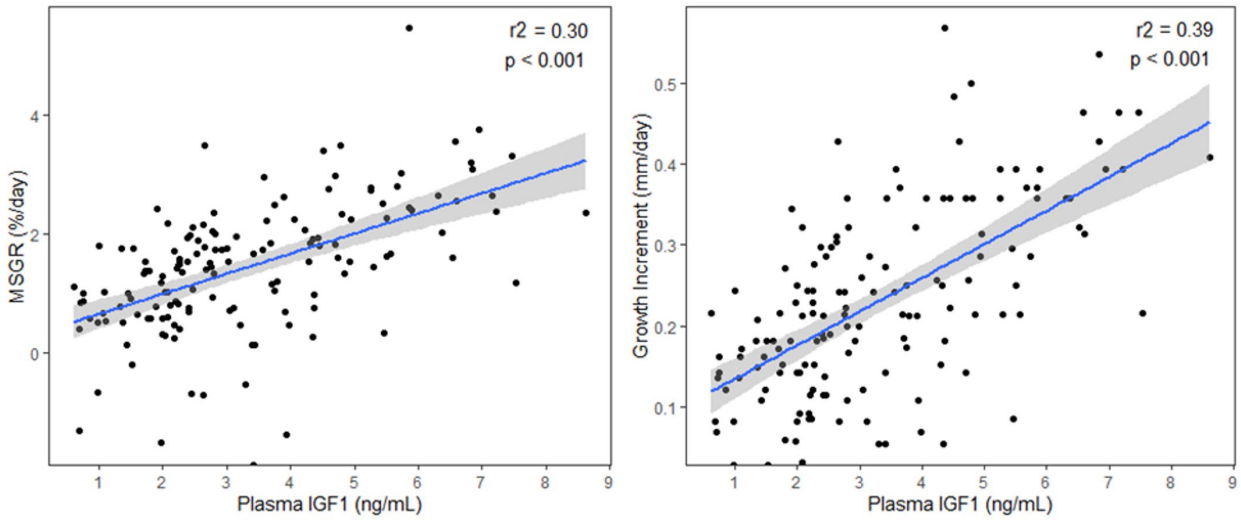

Figure 43. Left: The linear relationship between plasma IGF1 (ng/ml) and mass-standardized growth rate (%/day). This includes IGF1 values from both growth stanzas. Right: The linear relationship between plasma IGF1 and growth increment in length (mm/day).

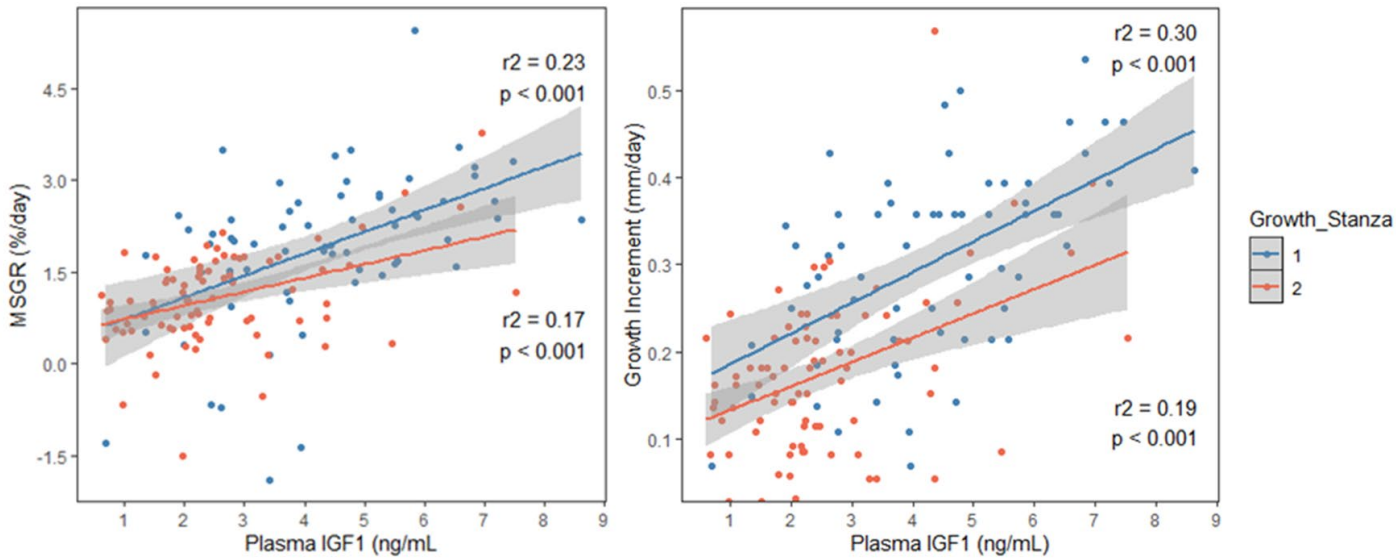

Figure 44. Left: The linear relationship between plasma IGF1 (ng/mL) and MSGR (%/day) for each of growth stanzas. Right: The linear relationship between plasma IGF1 (ng/mL) and growth increment in length (mm/day).

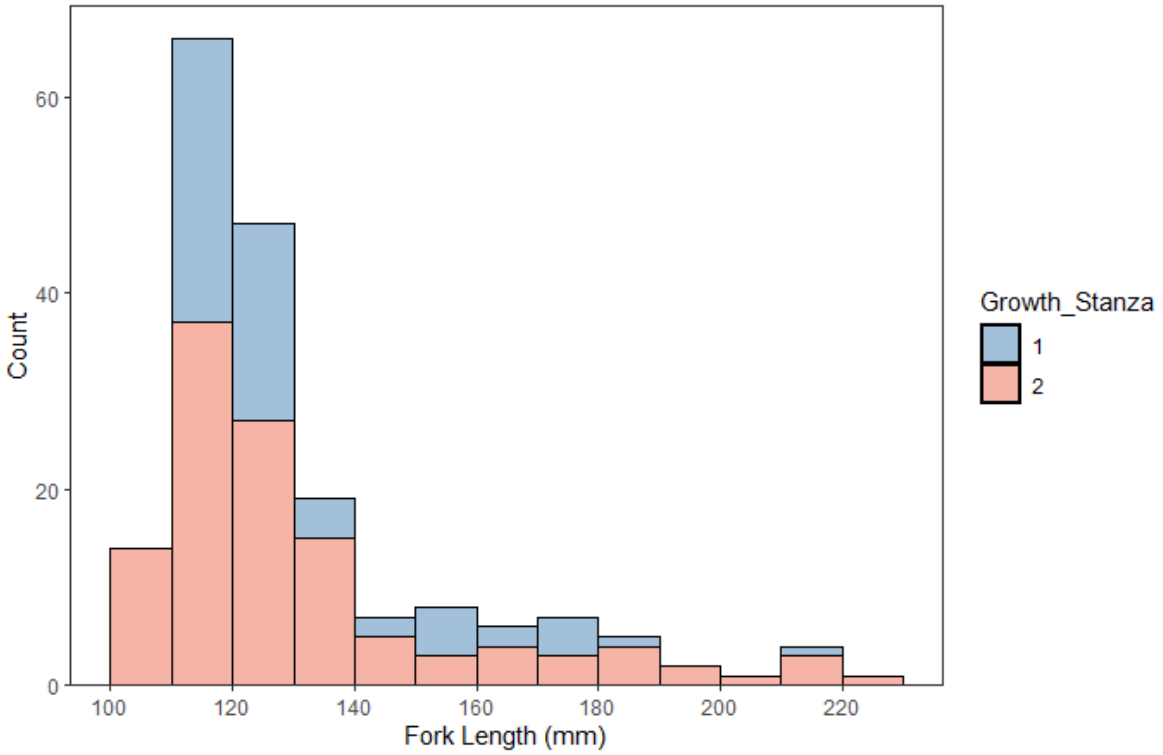

Figure 45. Length frequency of blood sampled fish during 2024 sampling in growth stanza 1 (mid-July to mid-August) and growth stanza 2 (mid-August to mid-September).

Table 15. Mean mass standardized growth rate (MSGR), mean standardized growth rate (mm) and minimum and maximum fork length (at time of blood draw, not initial length) for blood sampled O. mykiss during growth stanza 1 and growth stanza 2.

Reach	Growth Stanza	n	Mean MSGR	SE	Mean mm/day	SE	Min FL	Max FL
VL Low	1	9	1.53	0.34	0.20	0.02	112	170
VL Mid	1	9	1.03	0.49	0.24	0.03	112	159
VL Top	1	7	1.64	0.61	0.23	0.02	112	184
GC Low	1	9	2.07	0.39	0.33	0.04	110	176
GC Mid	1	24	2.16	0.24	0.34	0.02	110	217
GC Top	1	10	2.16	0.41	0.25	0.02	114	159
VL Low	2	18	0.71	0.16	0.14	0.02	108	227
VL Mid	2	19	0.96	0.78	0.13	0.01	108	217
VL Top	2	9	1.56	0.32	0.18	0.02	107	137
GC Low	2	20	0.75	0.17	0.12	0.02	110	204
GC Mid	2	25	0.74	0.21	0.18	0.01	108	213
GC Top	2	28	1.12	0.12	0.16	0.01	106	166

Table 16. Mark and recapture count and recapture rates by reach and sample event. Sample event 1=July, sample event 2=August, and sample event 3 = September. No recapture rates are provided for event 1 as these recaptures are from 2023 tagging efforts and are therefore not informative regarding 2024 efforts. Recapture rates calculated for event 3 combine mark counts from event 1 and event 2. For these preliminary results, recaptured fish from 2023 tagging efforts were not separated out from fish tagged in 2024. As such, these recapture rates are only estimates.

Reach	Event	Mark	Recapture	Recapture Rate
VL Low	1	112	*10*	*NA*
VL Mid	1	52	*2*	*NA*
VL Top	1	91	*4*	*NA*
GC Low	1	67	*3*	*NA*
GC Mid	1	115	*5*	*NA*
GC Top	1	107	*4*	*NA*
VL Low	2	93	34	0.30
VL Mid	2	86	25	0.48
VL Top	2	86	20	0.22
GC Low	2	73	24	0.36
GC Mid	2	64	69	0.37
GC Top	2	114	35	0.33
VL Low	3	40	43	0.21
VL Mid	3	51	48	0.35
VL Top	3	69	43	0.24
GC Low	3	58	49	0.35
GC Mid	3	64	69	0.30
GC Top	3	39	101	0.46

References

Beckman, B.R., 2011. Perspectives on concordant and discordant relations between insulin-like growth factor 1 (IGF1) and growth in fishes. General and Comparative Endocrinology, Profiles in Comparative Endocrinology: Glen Van Der Kraak 170, 233–252. https://doi.org/10.1016/j.ygcen.2010.08.009.

Bond, M. H., B. R. Beckman, L. Rohrbach, and T. P. Quinn. 2014. Differential growth in estuarine and freshwater habitats indicated by plasma IGF1 concentrations and otolith chemistry in Dolly Varden *salvelinus malma*. Journal of Fish Biology 85(5):1429–1445.

Caldarone, E. M., S. A. MacLean, and B. R. Beckman. 2016. Evaluation of nucleic acids and plasma IGF1 for estimating short-term responses of postsmolt Atlantic Salmon (Salmo salar) to food availability. U.S. National Marine Fisheries Service Fishery Bulletin 114:288–301.

Crump, C., Naylor, L., Van Sickle, A., Kennedy, J., Mathias, Z. and Shippentower, G. Monitoring and evaluation of supplemented Spring Chinook Salmon and life histories of wild Summer Steelhead in the Grande Ronde Basin 2022 Annual Progress Report [Report]: Annual Report. Portland Oregon: Bonneville Power Administration, 2022.

Iwama, G. K. and Tautz, A. F. 1981. A simple growth model for salmonids in hatcheries. Canadian Journal of Fisheries and Aquatic Sciences 38: 649–656.

Ostrovsky, I. 1995. The parabolic pattern of animal growth: determination of equation parameters and their temperature dependencies. Freshwater Biology, 33, 357-371. https://doi.org/10.1111/j.1365-2427.1995.tb00398.x.

Pess, G.R., Kiffney P.M., Liermann M.C., Bennett T.R., Anderson J.H., and Quinn T.P. 2011. The influences of body size, habitat quality, and competition on the movement and survival of juvenile coho salmon during the early stages of stream recolonization. Trans. Am. Fish. Soc. 140(4): 883–897.

Polivka, K.M. 2010. Population ecology and effectiveness monitoring of small-scale instream habitat restoration structures in the Entiat River. In Upper Columbia Regional Technical Team 2010 Analysis Workshop Synthesis Report. Edited by M.B. Ward, J. Morgan, and C. Baldwin. Prepared for the Upper Columbia Salmon Recovery Board by the Upper Columbia Regional Technical Team and Terraqua, Inc., Wenatchee, Wash., UCSRB.

Polivka, C. M., J. R. Mihaljevic, and G. Dwyer. 2020. Use of a mechanistic growth model in evaluating post-restoration habitat quality for juvenile salmonids. PLOS ONE 15(6).

Roni, P. 2019. Does river restoration increase fish abundance and survival or concentrate fish? the effects of project scale, location, and fish life history. Fisheries 44(1):7–19.

Shimizu, M., K. A. Cooper, W. W. Dickhoff, and B. R. Beckman. 2009. Postprandial changes in plasma growth hormone, insulin, insulin-like growth factor (IGF)-I, and IGF-binding proteins in coho salmon fasted for varying periods. American Journal of Physiology-Regulatory, Integrative and Comparative Physiology 297(2).

3.4 LCM Phase I: Development of spring Chinook statistical estimation Life Cycle Model

We have finalized development of the statistical life cycle model for Grande Ronde spring Chinook Salmon and have completed a manuscript documenting it, to be submitted to the journal *Ecological Modelling* in the very near term. The abstract is included below. The draft manuscript text/figures are included in Appendix C, and complete mathematical details are in Appendix D (which will accompany the manuscript upon submission as a supplement).

Abstract

Pacific salmon face different mortality sources throughout life, requiring monitoring and modeling at various life stages to understand the relative influences of regulating processes. For example, density dependence may be important for freshwater juveniles, whereas ocean conditions may drive later-life outcomes; in addition, delayed effects further complicate these phenomena. State-space models offer a flexible and robus approach to analyze these complexities when faced with uncertain data. We constructed a state-space model for Grande Ronde Basin (NE Oregon, USA) spring Chinook salmon (*Oncorhynchus tshawytscha*) that tracks the abundance of ~30 cohorts from 4 populations, modeling variability in freshwater juvenile growth and survival using density-dependent relationships and stochastic process noise that acknowledges synchronous dynamics. Model substructures include rearing origin setting (i.e., natural vs. hatchery), juvenile life history type, and adult age-of-return to account for heterogeneity at these scales. The model was fitted to empirical information collected by a variety of monitoring projects and included an index of freshwater habitat capacity to scale density-dependent processes. We found evidence of early-life density-dependent survival and growth, with subsequent over-wintering and out-migration survival mediated by early-life growth rates. Rearing capacity and growth rates showed positive, though uncertain, relationships with the habitat index. Life stage-specific covariances were overwhelmingly positive, indicating among-population synchronous dynamics throughout life. Post-hoc analyses showed juvenile life history is important for increasing productivity and that increasing habitat availability would reduce density dependence. Model posteriors reflect current understanding of life cycle dynamics for these populations which can parameterize simulations of future population status.

Next Steps

LCM Phase II – management scenarios

Restoration scenarios to impose on the statistical estimation life cycle model output are in development but have not been finalized. Several planning meetings have occurred, including a well-attended workshop devoted to brainstorming with partners in the basin and a loose plan has been developed. Briefly, we plan to assess combinations of restoration and other management actions (e.g., changes to supplementation) of various intensities. In-basin management scenarios will be crossed with additional scenarios that involve out-of-basin factors, such as changes to the hydrosystem or ocean mortality. More details will be forthcoming in the 2025 annual report.

LCM Phase III – simulation of outcomes

With the finalization of the LCM Phase I estimation model, we have now started constructing a simulation model that accepts output from the estimation model to simulate the populations into the future. We plan to make significant progress and have results available for the 2025 report.

4. RM&E coordination and adaptive management

4.1 Adaptive management

In 2024, our group provided continued contributions towards adaptive management through several forums that bring together restoration practitioners and individuals focused on RM&E efforts. We continue to work closely with colleagues at the Grande Ronde Model Watershed (GRMW) and other basin partners to evaluate progress toward and refine an Adaptive Management Plan for the Grande Ronde basin. An initial version of the Adaptive Management Plan was presented in White et al. (2021) – a collaborative publication assessing progress to date in habitat and salmon restoration in the Grande Ronde basin – and we have continued refining this plan through 2024 (Figure 46).

In 2024, we participated in the Grande Ronde State of the Science meeting hosted by GRMW, which provides a forum to present and discuss restoration progress, RM&E findings, and emerging uncertainties/questions pertinent to management efforts in the basin. Some important highlights from the workshop included 1) a modeling exercise and discussion focused on how restoration to reconnect floodplains may impact riparian evapotranspiration and baseflow discharge, 2) an overview of collective RM&E studies within the Grande Ronde basin, 3) presentations on the state of Oregon's regulations pertaining to beaver and ODFW's invasive species program, and 4) a discussion of what may be missing from the Atlas scoring criteria to rank restoration priorities, which highlighted the need for greater emphasis on future conditions under climate change, including alter flow regimes and expansion of invasive species ranges.

CRITFC is a partner in the Grande Ronde Atlas process and provides basin-scale analysis of restoration effects and habitat/aquatic biota conditions, which feed into restoration management decisions (e.g., Figure 47). While we have not been directly involved in the Wallowa Atlas process to date, we have provided monitoring data (e.g., LiDAR, water temperature [thermal imagery and in-stream temperature measurements], snorkel and habitat surveys) to basin partners that are used in the Grande Ronde and Wallowa Atlas process. Additionally in 2024, we initiated a process to compile spatial information and other metadata for all stream restoration projects conducted in the upper Grande Ronde and Catherine Creek watersheds (e.g., where were projects implemented, what was done, and when were projects completed?). This information will be used to analyze how habitat conditions (e.g., channel morphology and riparian vegetation from LiDAR, thermal heterogeneity from thermal imagery) have changed in response to restoration activities.

We have continued working with partners in the John Day River basin (CTWSOR, ODFW) including contributing to RM&E efforts associated with the Middle Fork John Day Intensively Monitored Watershed (MFIMW) working group. We regularly attend and contribute towards the monthly MFIMW meetings as well as the broader Joint John Day Basin Partnership/MFIMW Meeting, an annual meeting to present and discuss research findings among practitioners and individuals focused on RM&E efforts.

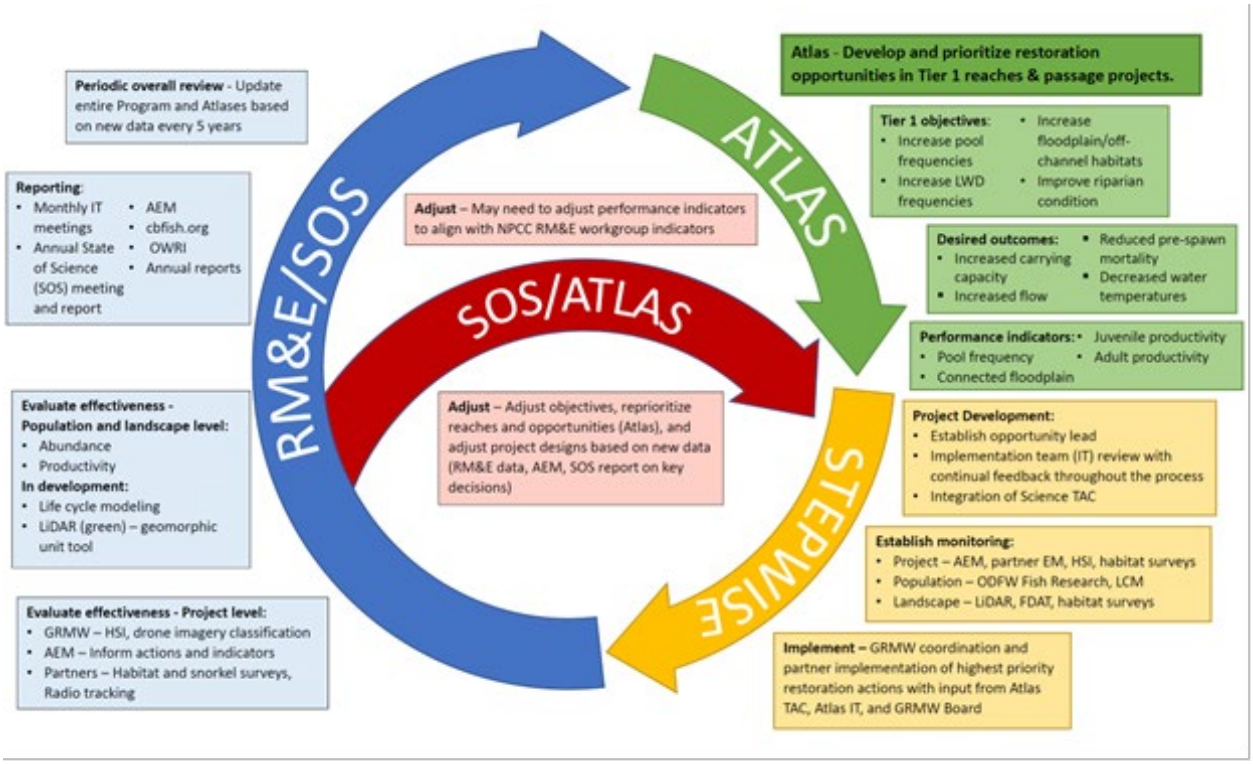

Figure 46. The adaptive management framework established by GRMW and Grande Ronde basin partners.

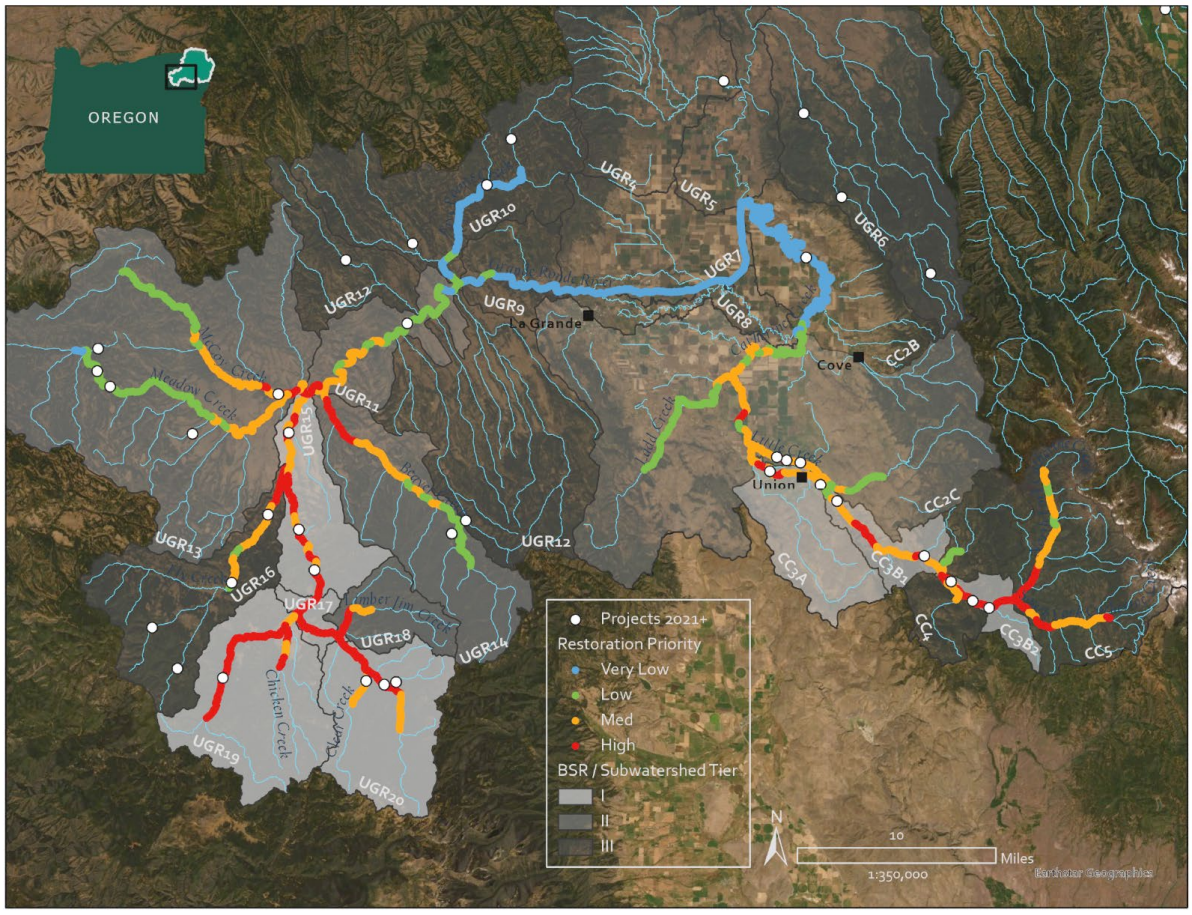

Figure 47. Restoration projects planned in the upper Grande Ronde River and Catherine Creek in 2021 and later, in relation to Atlas Tier I-III biological significant reaches (BSRs) and the restoration prioritization from Justice et al. 2017 developed in BPA project 2009-004-00. Most projects outside of the high and medium priority areas are either passage improvements or small, headwater stream meadow restoration projects by the USFS.

4.2 RM&E coordination and assistance

Coordination with other entities involved in fish habitat restoration and associated RM&E across the Columbia River basin is a critical component of this project. Close coordination and communication are essential to ensure that data being collected across various watersheds are similar enough that they can be used to draw inferences about the broader Columbia River basin (e.g., Is the habitat adequate for salmonid survival to specific stages?; Are key limiting factors for habitat quality improving with time and as an aggregate or site-specific expression of restoration actions taken?). Coordination among agencies also helps to reduce duplication of effort and allows pooling of resources and knowledge to answer broader and more impactful research questions. A list of key partner projects that are closely related to this project are listed in Table 17.

Meadow Creek collaborative RM&E

In 2022, the USDA Forest Service spearheaded a multi-agency project to implement and monitor a watershed-scale process-based restoration effort in Meadow Creek, a tributary to the upper Grande Ronde River. As a key partner in this collaborative restoration project, we continue to participate in regular meetings with staff from the USFS, CTUIR, ODFW, BOR, and BPA to collectively determine RM&E approaches to assess key metrics relevant to restoration objectives that are appropriate for a project of this scale. We have also continued to contribute to the formal development of a comprehensive restoration plan including assembling available data and content describing the current status of physical characteristics, biota and land use history across the watershed. In 2024, we conducted a pilot field season in collaboration with CTUIR and ODFW. We conducted electrofishing surveys in June and September to PIT-tag salmonids, collect diet and genetic samples from salmonids, characterize the relative abundance of the broader fish community, and quantify salmonid growth between seasons. We then used data and lessons learned from this pilot effort to formalize a sampling protocol for future years to rigorously evaluate fish and ecosystem response to watershed-scale restoration using a BACI design. In 2025, we plan to sample fish across the watershed in June and September and sample benthic macroinvertebrates in August.

OSU study on juvenile Chinook dispersal in Catherine Creek

In 2024, we worked closely with partners from OSU, CTUIR, NOAA and ODFW to develop sampling plans for a master's student (OSU) project evaluating juvenile Chinook Salmon dispersal in Catherine Creek, including how restoration, location within the watershed and adult origin may influence juvenile salmon dispersal patterns, distribution, and habitat use. In July and August 2024, we assisted in sampling nearly 5000 juvenile Chinook Salmon across Catherine Creek and collecting tissue samples for genotyping and genetic-assignments to post-spawn adults sampled from spawning locations in 2023. We continue to contribute towards data analysis and interpretation of dispersal results from this project.

Middle Fork John Day RM&E

We are working closely with ODFW and CTWSOR to evaluate Chinook Salmon fry dispersal and floodplain habitat use using genetic parentage-based tagging (PBT). We developed a study design with CTWSOR and ODFW to expand the use of PBT to evaluate female reproductive success (out-migrating smolts/female) as a function of spawning location. We sampled tissue from adult salmon from spawning locations in 2023 and 2024, we began sampling offspring from 2023 spawners as out-migrants captured at a downstream screw trap in fall 2024, and we plan to collect offspring from 2024 spawners from fall 2025-spring 2026. and we plan to collect out-migrating parr and smolts in fall 2024 and spring 2025. Results from this study will provide data to evaluate spatial patterns of female reproductive success to identify habitat characteristics and areas within the watershed where female reproductive output are higher or lower, providing critical information to guide conservation and restoration efforts. Over multiple years, these data may provide an

approach to evaluate how inter-annual variation in biophysical conditions may alter longitudinal patterns of reproductive success, and potential changes in reproductive success pre- and post-restoration. Lastly, in 2024 we led the third year of a collaborative effort to characterize juvenile salmonid abundance and distribution across the MFJD. Between CRITFC, ODFW, and CTWSOR, we snorkeled 46 mainstem reaches (10.6 km) and 110 tributary reaches (8.1 km) across 18 tributaries. This data will be used to evaluate factors shaping inter-annual variability in juvenile salmonid distributions, assess trends in distribution over time, and evaluate broad, population-level responses to cumulative restoration implementation.

Grande Ronde Life Cycle Model

The development of the state-space life cycle model for Grande Ronde spring Chinook Salmon has been a highly collaborative process between CRITFC, NOAA, and ODFW. Staff from each organization have contributed to the development following their individual strengths. NOAA staff developed an early version of the state-space model and have been instrumental in providing advice and feedback on changes to the model structure. ODFW staff, being most intimately familiar with the biological monitoring programs in the basin, have been primarily in charge of decisions around how to treat the various data sources and for compiling and maintaining the data sets into a format usable by the state-space model. CRITFC staff have led the model development and have compiled estimates of weighted usable rearing habitat that will serve a key role in all phases of this work. All parties have been consulted prior to making major developmental changes to the model and will be invited to serve as co-authors on manuscripts that are produced as result of this collaboration (such as Appendix C).

Instruction in the Use of Version Control Systems

One of our staff has been invited to provide instructional presentations and demonstrations of how to use Version Control Systems, specifically GitHub, for the Pacific Northwest Aquatic Monitoring Partnership (PNAMP) as part of planned seminar series on modeling, analysis, and working with PIT-tag data. Current plans are for two presentations in late-winter/early-spring 2025, one “lecture” focused on the importance of version control in data analysis and the key functionalities of GitHub, and another live demonstration of how to actually use GitHub. Both presentations will be recorded and made available through the PNAMP website and will be attended and viewed by data analysis practitioners throughout the region.

Table 17: List of key partners and projects related to the proposed work in the Grande Ronde (GR) basin and beyond.

Organization	Related project(s)	Relationship to proposed project
Bonneville Power Administration	Project Action Effectiveness Monitoring (AEM) Programmatic (BPA 2016-001-00)	Findings from the BPA AEM project will be useful in developing and evaluating CRITFC's models of aggregate restoration impacts on limiting factors
Bureau of Indian Affairs	Climate Change Threats to Salmonid Food Webs (BIA A19AV00480); Resilient Aquatic Food Webs for Tribal Communities (BIA A19AP00024)	Provided funding for development and analysis of benthic macroinvertebrate metrics related to salmonid food webs; funded expansion of benthic macroinvertebrate sampling to tribal partners in the Columbia basin
Confederated Tribes of the Umatilla Indian Reservation	Grand Ronde Watershed Restoration (BPA 1996-083-00); Grande Ronde Supplementation M&E (BPA 2007-083-00); Biomonitoring of Fish Habitat Enhancement (BPA 2009-014-00)	GR Atlas Partner; implements habitat projects that CRITFC's surveys of habitat and biological monitoring characterize; has adopted CRITFC M&E methodologies (e.g., snorkel surveys, benthic macroinvertebrate collections); leads weir sampling of adult Chinook which produces data used in our life cycle model; Chinook Salmon supplementation program will be assessed using a life cycle model
Confederated Tribes of the Warm Springs Reservation of Oregon	John Day Habitat Enhancement Implementation Strategy (BPA 2007-397-00)	Key partner with CRITFC and ODFW in evaluating juvenile salmonid dispersal, habitat use, and distribution within the Middle Fork John Day River. Implements habitat restoration projects in the John Day basin and collects RM&E data used by CRITFC.
Grande Ronde Model Watershed Foundation	Grande Ronde Model Watershed (BPA 1992-026-01)	Leads coordination of adaptive management framework (Atlas) in GR basin; uses CRITFC's limiting factors assessments to guide restoration prioritization; documents restoration activities in basin that CRITFC will use for modeling restoration impacts on limiting factors; co-funded collection of topobathymetric LiDAR in 2020
National Oceanic and Atmospheric Administration	Various	Key partner with CRITFC and ODFW in developing the life cycle model; co-funding CRITFC's research on emergence phenology, floodplain use, and early life history of Chinook Salmon; co-funded a public outreach film with GRMW, CRITFC, and USFS on restoration in the GR basin
Nez Perce Tribe	Protect & Restore NE OR & SE WA Watershed Habitat (BPA 2007-393-00)	GR Atlas associate; utilized GIS products developed by CRITFC for restoration planning in the Wallowa basin; CRITFC collected topobathymetric LiDAR in Wallowa basin in 2020 that will be used for limiting factors assessment; provided water temperature data used in recent analysis of Chinook pre-spawn survival

Organization	Related project(s)	Relationship to proposed project
Oregon Department of Fish and Wildlife	Grande Ronde Fish Habitat Improvement (BPA 1984-025-00); Grande Ronde Salmonid Life Cycle Monitoring (BPA 1992-026-04); John Day Basin Escapement and Productivity of Spring Chinook and Steelhead (BPA project 1998-016-00)	GR Atlas partner; implements habitat projects that CRITFC's surveys of habitat and biological monitoring characterize; has adopted CRITFC M&E methodologies (e.g., snorkel surveys, benthic macroinvertebrate collections); collects population level fish data (e.g., spawner abundance) used in life cycle model; key partner with CRITFC and NOAA in developing the Grande Ronde life cycle model. Key partner with CRITFC and CTWSOR on several projects evaluating juvenile salmonid dispersal, habitat use, and distribution within the Middle Fork John Day River.
Oregon State University	Long-term ecological effects of passive restoration in the Middle Fork John Day (OWEB 218-6041); CTUIR John Day Watershed Restoration (BPA 2007-397-00); ODFW John Day Habitat Enhancement (BPA 1984-021-00); Co-sponsored a post-doc (Matt Kaylor) to conduct research on juvenile salmon ecology; Juvenile Chinook dispersal patterns in Catherine Creek led by M.S. student Kayla Kelly and advisor Dr. Seth White.	OSU & UO Initiated study of long-term effects of cattle grazing management on river channel, riparian, and floodplain conditions in Middle Fork John Day; CRITFC contributed benthic macroinvertebrate sampling and analysis; Research led by post-doc Matt Kaylor directly addressed key objectives of this project relating to juvenile salmon ecology and prioritization of river restoration and management actions; CRITFC is collaborating closely with Kayla Kelly and Seth White on data collection and analysis related to juvenile Chinook dispersal in Catherine Creek.
University of Oregon	Long-term ecological effects of passive restoration in the Middle Fork John Day (OWEB 218-6041); CTUIR John Day Watershed Restoration (BPA 2007-397-00); ODFW John Day Habitat Enhancement (BPA 1984-021-00)	OSU & UO Initiated study of long-term effects of cattle grazing management on river channel, riparian, and floodplain conditions in Middle Fork John Day; CRITFC contributed benthic macroinvertebrate sampling and analysis
Trout Unlimited	Various	Implements stream and floodplain restoration projects in the Grande Ronde basin (e.g., Sheep Creek, Indian Creek, Wallowa River) that CRITFC's surveys of habitat and biological monitoring characterize
U.S. Bureau of Reclamation	Various	Implements and conducts RM&E on various restoration projects in GR basin, implements habitat projects that CRITFC's surveys of habitat and biological monitoring characterize
U.S. Forest Service	Various	GR Atlas partner; conducts M&E (Level II surveys) and implements habitat projects that CRITFC's surveys of habitat and biological monitoring opportunistically characterize
Union Soil and Water Conservation District	Various	GR Atlas partner; implements habitat projects that CRITFC's surveys of habitat and biological monitoring opportunistically characterize

4.3 Development and refinement of RM&E methodology

Snorkel Survey Protocol Updates

Snorkel surveys are widely implemented to characterize the relative abundance and distribution of fish populations because they can be conducted without capturing fish and are less time consuming than traditional capture approaches (e.g., electrofishing, seining). However, the proportion of fish present within a channel unit or stream reach that are observed (e.g., detection) is not known and varies as a function of habitat conditions (e.g., lower detection rates with high amounts of wood). We previously developed a snorkel detection model to relate habitat characteristics (e.g., depth, channel unit type, large wood density, visibility) to estimates of detection (Staton et al. 2022). The model was informed by paired snorkel surveys and mark-recapture abundance estimates conducted in 2012 and 2015. However, we realized that the model was poorly suited to estimate snorkel detection probability in very deep (e.g., pools > 0.5 m average depth) or complex channel units (e.g., > 0.2 pieces of large wood per m^2) – conditions that are increasingly common in restored habitats – because these values exceed covariate ranges in the initial dataset used to develop the model.

In response to this shortcoming, CRITFC and ODFW collected additional paired snorkel count and mark-recapture data in 2023 (57 individual channel units), targeting deeper and more complex habitats that are within the known rearing area for Chinook Salmon. We are in the process of updating the detection model by integrating 2023 data, including assessing which covariates significantly affect detection and warrant inclusion in the model and re-estimating covariate relationships and coefficients.

This detection model is widely used by our group and our partners CTUIR, CTWSOR, and ODFW. Updating the model and improving detection estimates will result in more reliable abundance estimates across these RM&E programs.

IGF1 Sampling Methods

The increased use of large-scale process-based restoration techniques like those utilized in floodplain restoration projects produce complex habitat where traditional sampling techniques for juvenile salmonid growth estimation may lack efficacy. The addition of numerous channels and abundant cover habitat in the post-restoration environment can make it difficult to achieve the desired number of recaptures for accurate growth estimation in a repeat-sampling protocol. As such, monitoring efforts focused on assessing the effectiveness of these restoration projects would benefit from methodology to estimate growth responses using single-sampling approaches. Single-capture sampling methods can be applied to evaluate habitat-growth comparisons and may be particularly effective in contexts where recapture rates may be lowered due to low capture efficiency, dispersal patterns or other factors. One metric for assessing growth without the recapture of individuals is the concentration of insulin-like growth factor 1 (IGF1), which has been validated as an index of relative growth rate in juvenile salmonid fishes (Duguid et al. 2018;

Beckman 2011; Bond et al. 2014). Plasma IGF1 concentration strongly correlates with growth rate and is highly responsive to shifts in habitat suitability as IGF1 concentration responds to changes in environmental conditions affecting growth within 4 days (Gabillard et al. 2006; Caldarone et al. 2016; Duguid et al. 2018). However, the use of IGF1 has largely been limited to either lethal sampling or to non-lethal sampling of larger individuals (i.e., smolts) than the size range of juvenile salmonids typically encountered in NE Oregon.

Prior to conducting a field pilot to evaluate the feasibility of using IGF1 to assess growth of smaller bodied juvenile salmonids, a hatchery study was conducted at the OHRC in 2023 using juvenile Steelhead/Rainbow trout to assess mortality across a range of body sizes (fork lengths ranging from 80 – 140 mm) and determine a minimum size threshold for non-lethal sampling. This study was followed up by an additional study in winter 2024 conducted at the Hagerman Fish Culture Experiment Station (HFCES) in Hagerman, Idaho to further refine the non-lethal blood draw methodology and provide additional size-based mortality data (fork lengths ranging from 94-183 mm).

The HFCES study provided data indicating a lack of significant differences in growth and hematocrit levels between blood sampled and control fish, including no evidence of a greater impact of blood sampling on smaller fish. Very few fish were available in the lower size ranges (90-99 mm, 100-110 mm) due to enhanced growth rates under hatchery conditions, and only four total mortalities occurred during the study, providing insufficient data to draw conclusions regarding the minimum body size for non-lethal blood sampling. Future effort needs to be made to establish a minimum size threshold for non-lethal sampling in juvenile salmonids. HFCES results appear to support the 10% maximum percentage blood volume proposed by Lawrence et al. (2020), however, more robust empirical data is needed to fully evaluate the non-lethal usage of IGF1 in field studies of juvenile salmonids.

We successfully utilized the refined sample methodology determined by hatchery studies to conduct a field pilot study in summer 2024 to evaluate the use of IGF1 as an index of recent growth in juvenile *O. mykiss* in the field. The objectives of the field pilot study were to (*i*) evaluate the validity of using plasma IGF1 values as an index of growth in juvenile *O. mykiss* in the field by assessing the relationship between individual growth rates and IGF1 concentrations and (ii) assess shifts in IGF1 values during the seasonal temperature shift from mid-summer to early fall. Preliminary analysis from the field pilot can be found in Section 3.3.

Spatial Relative Reproductive Success

Relative Reproductive Success (RRS) studies are an important tool to evaluate anadromous salmon population trends and the efficacy of hatchery supplementation actions. We plan to extend the utility of RRS and Parentage-Based Tagging (PBT) as tools to evaluate female spring-run Chinook Salmon reproductive success as a function of where they spawn within watersheds. While this approach has not been implemented to our knowledge, we believe it has the potential to be a powerful tool that could be widely implemented with relatively little additional effort and cost in

watersheds where RM&E programs currently include adult spawning ground surveys and rotary screw traps to capture out-migrating juveniles. However, testing and refinement are needed prior to broader implementation. We are implementing a spatial RRS study across three subbasins and two brood years to refine sampling approaches, determine lessons learned, and identify methodological considerations that we can document and share to provide a road map for others interested in implementing this approach.

This approach could be particularly powerful because the key metric – the relative number of offspring produced by individual female spawners – integrates numerous processes (e.g., growth, survival) across multiple life stages, providing a cumulative metric to assess productivity across freshwater life stages. As such, spatial RSS could be used to assess habitat-productivity relationships and limiting factors across multiple life stages, evaluate response to restoration and other management actions (e.g., hatchery supplementation), and inform population responses to climate change and disturbances (e.g., drought, fire).

Water temperature and approaches to assess thermal heterogeneity

Altered thermal regimes in rivers including higher peak water temperatures, reduced thermal heterogeneity (including both cold-water refugia during summer and warm-water refugia during winter), and an extended duration of stressful temperatures are critical limiting factors for salmonids and other aquatic biota in the Grande Ronde River and broader Columbia River basin. These alterations to thermal regimes are likely to be exacerbated by climate change in the future. Therefore, it's critical to understand the degree to which management actions such as river restoration can improve temperature conditions for fish and climate change resiliency more broadly.

We collaborated with two partners in the Grande Ronde basin including the Grande Ronde Model Watershed (GRMW) and Union Soil and Water Conservation District (USWCD) to collect airborne thermal imagery data across 570 kilometers of stream in the upper Grande Ronde and Wallow River basins (see chapter 1.4 and Appendix B for more details). These data will be used in-part to evaluate how thermal heterogeneity (e.g., quantity of cold-water refugia) at the watershed scale and at restoration project sites has changed since a previous thermal imagery acquisition in 2010. Additionally, we are evaluating the use of two emerging technologies to better map and quantify thermal heterogeneity in riverscapes including 1) thermal imagery mapping using unmanned aircraft systems (UAS) and 2) mobile temperature and depth (TAD) devices that mount to real-time kinematic (RTK) positioning systems to efficiently collect temperature, depth, and precise location information at discrete locations within the water column (Frye et al. 2025). Our progress to date on the use of UAS thermal imaging technology is described in section 1.3 of this report, with additional data collection and analysis forthcoming in 2025. We plan to use the mobile temperature and depth (TAD) devices during 2025 and 2026 to assess thermal refugia use by radio-tagged adult Chinook Salmon.

References

Beckman, B.R., 2011. Perspectives on concordant and discordant relations between insulin-like growth factor 1 (IGF1) and growth in fishes. General and Comparative Endocrinology, Profiles in Comparative Endocrinology: Glen Van Der Kraak 170, 233–252. https://doi.org/10.1016/j.ygcen.2010.08.009.

Bond, M. H., B. R. Beckman, L. Rohrbach, and T. P. Quinn. 2014. Differential growth in estuarine and freshwater habitats indicated by plasma IGF1 concentrations and otolith chemistry in Dolly Varden salvelinus malma. Journal of Fish Biology 85(5):1429–1445.

Caldarone, E. M., S. A. MacLean, and B. R. Beckman. 2016. Evaluation of nucleic acids and plasma IGF1 for estimating short-term responses of postsmolt Atlantic Salmon (Salmo salar) to food availability. U.S. National Marine Fisheries Service Fishery Bulletin 114:288–301.

Duguid, W. D., T. W. Iwanicki, M. L. Journey, A. L. Noel, B. R. Beckman, and F. Juanes. 2018. Assessing indices of growth for field studies of Juvenile Salmon: An experiment and synthesis. Marine and Coastal Fisheries 10(2):204–223.

Frye, J., A. W. Tranmer, A. Bertagnoli, A. Hurst, C. Ubing, J. Sholtes, and D. Tonina. 2025. Morphology-Induced Thermal Refuge in a Gravel-Bed River. Hydrological Processes 39(4):e70107.

Gabillard, J.-C., B. B. Kamangar, and N. Montserrat. 2006. Coordinated regulation of the GH/IGF system genes during refeeding in Rainbow Trout (Oncorhynchus mykiss). Journal of Endocrinology 191:15–24.

Justice, C., S. M. White, D. A. McCullough, D. S. Graves, and M. R. Blanchard. 2017. Can stream and riparian restoration offset climate change impacts to salmon populations? Journal of Environmental Management 188:212–227.

Staton, B. A., C. Justice, S. White, E. R. Sedell, L. A. Burns, and M. J. Kaylor. 2022. Accounting for uncertainty when estimating drivers of imperfect detection: An integrated approach illustrated with snorkel surveys for riverine fishes. Fisheries Research 249:106209.

White, S. M., S. Brandy, C. Justice, K. A. Morinaga, L. Naylor, J. Ruzycki, E. R. Sedell, J. Steele, A. Towne, J. G. Webster, and I. Wilson. 2021. Progress Towards a Comprehensive Approach for Habitat Restoration in the Columbia Basin: Case Study in the Grande Ronde River. Fisheries:fsh.10562.

Wolf Water Resources. 2022. Upper Grande Ronde River, Union County, OR Sediment Budget Study. Page 35. Wolf Water Resources, Portland, OR.

DISSEMINATION OF PROJECT FINDINGS

Presentations and workshops

Justice, C., M. Kaylor, A. Ringelman, B. Staton, M. Wolf, and D. Graves. November 19, 2024. Spatiotemporal patterns of stream temperature and associated vulnerability of Chinook Salmon in the Grande Ronde River basin. Grande Ronde State of the Science Meeting. La Grande, Oregon.

Lemanski, J.T. (co-presenter), L. Naylor, and A. Ringelman (co-presenter). November 19, 2024. Research Monitoring and Evaluation in the Grande Ronde Basin. Grande Ronde State of the Science Meeting, La Grande, Oregon.

Staton, B., P. Gibson, C. Justice, M. Kaylor, M. Liermann, A. Ringelman, T. Sedell, R. Sharma, and S. White. February 5, 2024. State-space life cycle models and application to Grande Ronde Basin Spring Chinook salmon. Invited Seminar for the Monday Morning Meeting, Oregon State University Department of Fisheries and Wildlife, Corvallis, OR.

Staton, B.A., H. Hershey. September 14, 2024. Introductory Bayesian Inference with JAGS for Fish Biologists. AFS National Meeting, Honolulu, HI.

Staton, B.A., H. Hershey. September 15, 2024. Intermediate Bayesian Inference with JAGS for Fish Biologists. AFS National Meeting, Honolulu, HI.

Staton, B.A., M. Lierman, P. Gibson, C. Justice, M. Kaylor, R. Sharma, S. White. Sep. 19, 2024. State-space models for integrated analysis of Pacific salmon time series data. AFS National Meeting, Honolulu, HI.

White, S., C. Justice (presenter), L. Burns, and B. Staton. March 21, 2024. Setting targets for habitat conditions. Presentation to the Grande Ronde Atlas Implementation Team. La Grande, OR.

Wolf, J.M., C. Justice, and R.L. Flitcroft. February 28, 2025. Synthesizing three decades of Steelhead focused restoration and research in Oregon's Blue Mountains. Bend, OR

Publications (Published Papers, Draft Manuscripts and Technical Reports)

Feddern, M. L., R. Shaftel, E. R. Schoen, C. J. Cunningham, B. M. Connors, B. A. Staton, A. Von Finster, Z. Liller, V. R. Von Biela, and K. G. Howard. 2024. Body size and early marine conditions drive changes in Chinook salmon productivity across northern latitude ecosystems. Global Change Biology 30(10):e17508.

Justice, C., M. Kaylor, A. Ringelman, and B. Staton. May 2024. Evaluating salmonid and stream ecosystem response to conservation measures and environmental stressors in the Columbia

River basin. Page 130. Columbia River Inter-Tribal Fish Commission, BPA Project # 2009-004-00, Portland, OR.

Kaylor, M., L. Ciepiela, M. Feden, J.T. Lemanski, C. Justice, J. Armstrong, B. Staton, S. Kelly, S. Narum, I. Tattam, and S. White. 2025. Watershed-scale dispersal patterns of juvenile Chinook Salmon revealed through genetic parentage analysis. *Movement Ecology,* 13:6.

Middle Fork IMW Working Group. 2024. Middle Fork John Day River Intensively Monitored Watershed - 2024 Summary Report. John Day, Oregon.

Ouellet, V., A. H. Fullerton, M. Kaylor, S. Naman, R. Bellmore, J. Rosenfeld, G. Rossi, S. White, S. Rhoades, D. A. Beauchamp, M. Liermann, P. Kiffney, and B. Sanderson. 2025. Food for fish: Challenges and opportunities for quantifying foodscapes in river networks. *WIREs Water* 12(1):e1752.

Rossi, G. J., J. R. Bellmore, J. B. Armstrong, C. Jeffres, S. M. Naman, S. M. Carlson, T. E. Grantham, M. J. Kaylor, S. White, J. Katz, and M. E. Power. 2024. Foodscapes for salmon and other mobile consumers in river networks. *BioScience* 74(9):586–600.

Staton, B., M. Liermann, P. Gibson, C. Justice, M. Kaylor, R. Sharma, and S. White. A state-space model to quantify density dependence, demographic heterogeneity, and spatial synchrony in Grand Ronde Basin Chinook salmon populations. Draft manuscript will be submitted in 2025. Presented in Appendix C.

Appendix A Data Storage and Access

Data collected under this project is currently managed in different ways depending on the data type. General spatial data such as monitoring sites, stream layers, land ownership, and various other datasets that are used for analyses but are not deliverable end products are stored in a geodatabase at CRITFC and managed for internal use by CRITFC GIS specialists and project managers. Physical habitat data collected by CRITFC using the CHaMP protocol from 2011 to 2017 is now managed by the StreamNet Program and is available to the public at https://www.streamnet.org/home/data-maps/champ/. Habitat data collected using CRITFC's Tributary Habitat Assessment protocol including drone imagery is stored on CRITFC servers and is available upon request. Fish abundance data was recently uploaded to StreamNet's Data Store for use in expanding the Fish Density Analysis Tool (FDAT) developed by Dan Isaak and his team at the Rocky Mountain Research Station. These data are available for download at https://app.streamnet.org/datastore_search_classic.cfm?id=844. Water temperature data collected by CRITFC is stored on CRITFC's CDMS and is available for download upon request.

The code for the Grande Ronde spring Chinook state-space life cycle model and the data it fits to are stored in two separate GitHub repositories. We chose to organize it this way to enable tracking data-related changes separately from model-related changes, and this has proven to be quite useful. Further, all collaborators have access to the most current main and development versions and GitHub includes a useful issue tracker where needed changes can be discussed; these aspects have greatly facilitated collaboration. Both repositories are private currently (only collaborators have access), however, we plan to make both completely public as supplements to the manuscript that presents this work.

Appendix B NV5 Thermal Imagery Acquisition Summary Report

Survey: Aug 16-19, 2024
Report (revised): April 27, 2025

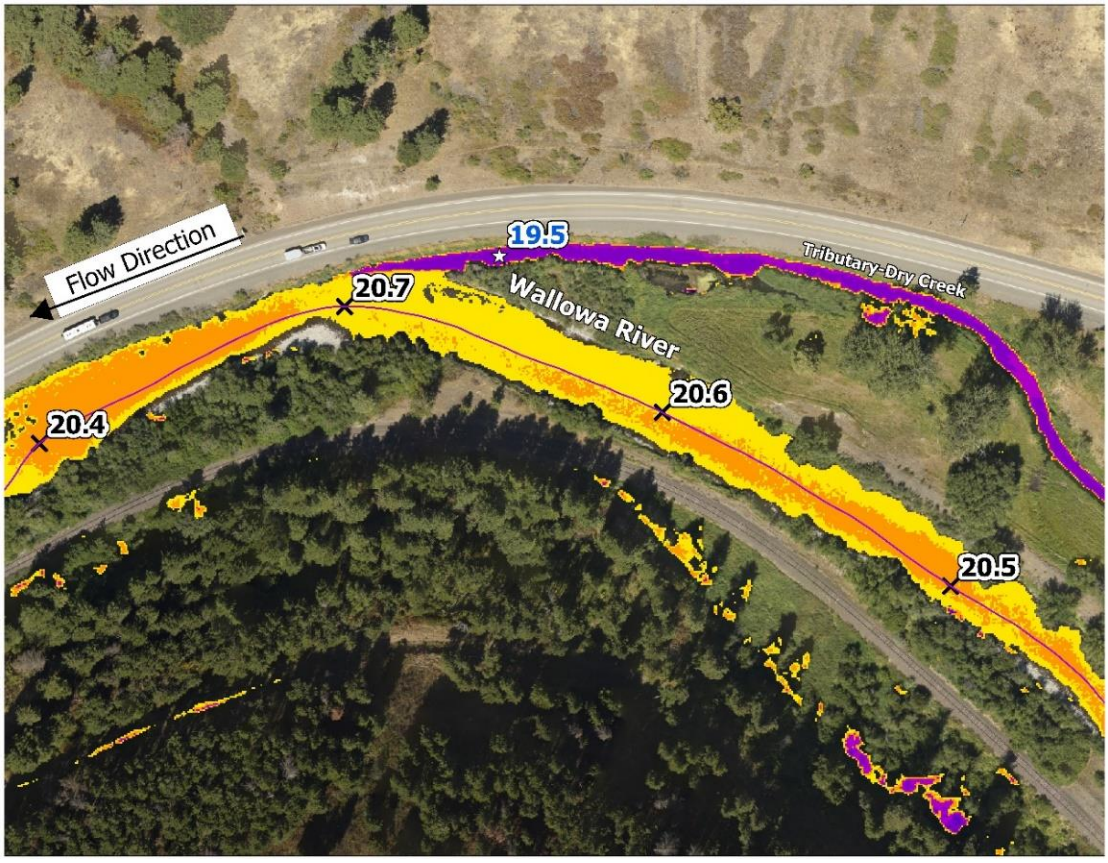

Grande Ronde River, Oregon

Airborne Thermal Infrared and True Color Imagery

2024 Technical Report

Casey Justice
Columbia River Inter-Tribal Fish Commission (CRITFC)
700 NE Multnomah St, Suite 1200.
Portland, OR, 97232
Ph: 503-593-7456
jusc@critfc.org

NV5
1100 NE Circle Blvd., Ste. 126
Corvallis, OR, 97330
PH: +1-541-752-1204

TABLE OF CONTENTS

Cover Photo: Thermal infrared imagery overlayed on true color imagery, both of which were co-acquired on August 18, 2024. An example of the Dry Creek Tributary's inflow of cold water (19.5 °C) relative to Wallowa River (20.6 °C).

Thermal infrared and true color imagery was processed, analyzed, and reported by:
Mousa Diabat, Ph.D. - Hydrologist, Thermographer Level III
Chris Miwa, MS - Certified Photogrammetrist

List of Figures

List of Tables

INTRODUCTION

The Columbia River Inter-Tribal Fish Commission (CRITFC) contracted NV5 to co-acquire airborne thermal infrared (TIR) and true color imagery data during the summer of 2024 for the Grande Ronde River area of interest (AOI) in northeastern Oregon. The survey was conducted between August 16 and August 19, 2024, covering a total length of 570 kilometers (km) of the Grande Ronde Lower Tributaries, Upper Grande Ronde River, Lostine River, Catherine Creek, and Minam River (Figure 1). Prior to the data collection campaign, NV5 field crew deployed data loggers at 28 sites throughout the survey area to record water temperature throughout the data acquisition time frame and later used the records to calibrate the TIR imagery.

This report accompanies the delivered imagery and support files, and documents the contract specifications, data acquisition procedures, processing methods, and analysis of the final datasets. TIR acquisition dates and times are shown in Table 1, deliverable projection information is shown in Table 2, a complete list of contracted deliverables provided to CRITFC is shown in Table 3, and the project extent is shown in Figure 1.

Table 1: TIR acquisition dates and stream reaches collected on the Grande Ronde River

Basin	Tributary	Section covered (km)	Date	Time of day (PDT)
Grand Ronde	State Ditch	0 - 7.4	16-Aug-24	14:40 - 14:50
	Grande Ronde River	0 - 48.9	16-Aug-24	14:40 - 15:22
	Dark Canyon Creek	0 - 1.4	16-Aug-24	15:22 - 15:26
	Spring Creek	0 - 23.2	17-Aug-24	13:57 - 14:10
	Chicken Creek	0 - 10.5	17-Aug-24	15:09 - 15:13
	West Chicken Creek	0 - 3	17-Aug-24	15:14 - 15:20
	Clear Creek	0 - 1.9	17-Aug-24	15:20 - 15:32
	Limber Jim Creek	0 - 6	17-Aug-24	15:32 - 15:40
	Five Points Creek	0 - 16.4	17-Aug-24	12:57 - 13:21
	Rock Creek	0 - 7.9	17-Aug-24	13:25 - 13:48
	Beaver Creek	0 - 10.1	17-Aug-24	14:16 - 14:21
	Grande Ronde River	47.9 - 88.1	17-Aug-24	14:30 - 15:24
	Fly Creek	0 - 13.4	17-Aug-24	14:40 - 14:51
	Sheep Creek	1.8 - 23.2	18-Aug-24	17:06 - 17:15
	Sheep Creek	0 - 23.2	19-Aug-24	14:46 - 14:56
	Grande Ronde River	0 - 49.5	19-Aug-24	13:30 - 14:11
	Meadow Creek	0 - 34.4	19-Aug-24	14:16 - 15:16
	McCoy Creek	0 - 6.8	19-Aug-24	14:17 - 14:23
	Waucup Creek	0 - 4.2	19-Aug-24	15:20 - 15:23
Lookingglass Creek	Little Lookingglass	0 - 2.4	18-Aug-24	14:43 - 14:57
	Lookingglass	0 - 16.78	18-Aug-24	14:36 - 14:46
Indian Creek	Indian	0 - 13.75	17-Aug-24	16:24 - 16:33
	Little Indian	0 - 0.56	17-Aug-24	15:40 - 15:55
Catherine Creek	Little Catherine Creek	0 - 3	16-Aug-24	14:08 - 14:20
	NF Catherine Creek	0 - 40.9	16-Aug-24	13:17 - 13:57
	SF Catherine Creek	0 10.1	16-Aug-24	13:49 - 13:53
	Milk Creek	0 - 3.3	16-Aug-24	14:00 - 14:07
	Little Creek	0 - 14.4	16-Aug-24	14:19 - 14:31
Minam River	Little Minam	0 - 5.56	18-Aug-24	15:52 - 15:56
	Minam River	0 - 14.5	18-Aug-24	14:56 - 16:33
Bear River	Bear River	0 - 21.5	18-Aug-24	13:31 - 13:38
Wallowa River	Wallowa	0 - 43.28	18-Aug-24	12:03 - 14:02
	Hurricane	0 - 4.09	18-Aug-24	12:15 - 12:23
	Lostine	0 - 27.23	18-Aug-24	12:54 - 13:16

Deliverable Products

Table 2: Deliverable product coordinate reference system information

Projection	Horizontal Datum	Vertical Datum	Units
UTM Zone 11 North	NAD83(2011)	NAVD88(GEOID12B)	Meters, Celsius

Table 3: Products delivered to CRITFC for the Grande Ronde River site

Product Type	File Type	Product Details
Rasters	**Thermal infrared Imagery** 0.5m GeoTIFF (*.tif) **3-Band (RGB) Digital Imagery** 20 cm GeoTIFF (*.tif) 20 cm GeoTIFF (*.tif) 20 cm MrSID (*.sid)	**Thermal infrared Imagery <u>(cell values = Celsius x 10)</u>** • Calibrated, rectified images • Calibrated, rectified imagery mosaics **3-Band (RGB) Digital Imagery** • Orthorectified Frames • Tiled Imagery Mosaics • AOI Imagery Mosaic
Vectors	Shapefiles (*.shp)	• Stream centerlines • Temperature accuracy assessments • TIR image center points and sensor exterior orientation (EO) • Longitudinal temperature profile (LTP) • Significant thermal features (STF) • RGB Mosaic Tile Index • RGB Orthorectified Frames Index
Supplemental	MS Excel Format (*.xlsx) Layer Files (*.lyr)	• "xlsx" folder contains longitudinal temperature profiles (LTP) and significant thermal features (STF) in MS Excel format (*.xlsx) • "Color ramps" folder contains customized layer files (*.lyrx) for visualization in ArcGIS Pro
Metadata	Extensible Markup Language (*.xml)	• FGDC (CSDGM) compliant Metadata
Reports	Adobe Acrobat (*.pdf)	• Technical Data Report

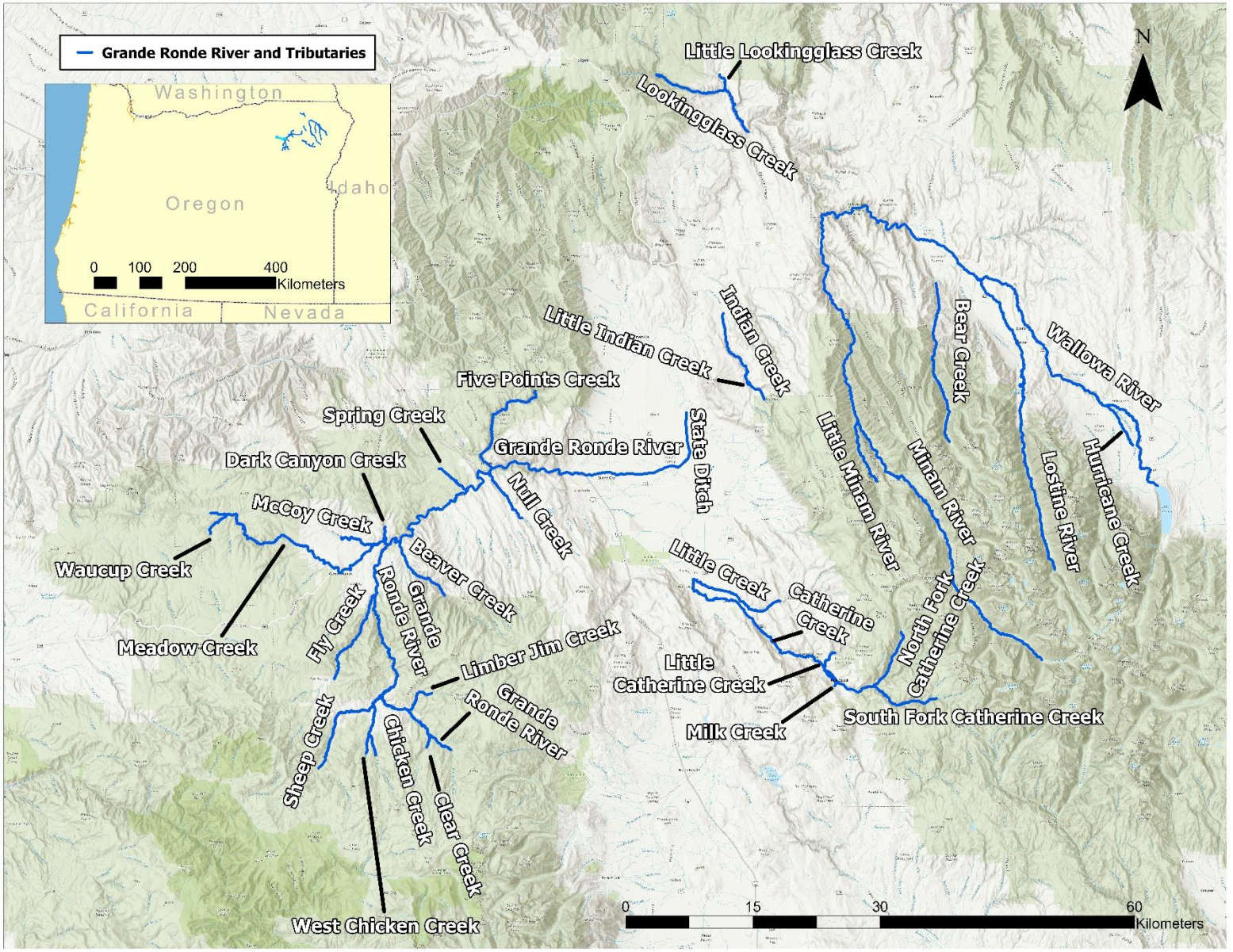

Figure 1: Map of the Grande Ronde, OR thermal infrared survey area

Thermal Infrared Imagery Acquisition Planning and Execution

Data Acquisition

In preparation for data collection, NV5's team reviewed the project area and developed a specialized flight plan to ensure complete coverage of the Grande Ronde River study area. The Grande Ronde River project data was successfully acquired between August 16 and 19, 2024, in four aircraft flown no earlier than 12:00 PM and no later than 17:00 PM PDT (Table 1). This time window is optimal for maximizing the thermal contrast between the river water and surrounding banks. Flight windows targeted clear skies for high solar loading of the riverbanks and the highest air temperatures possible for the season. Weather stations near the area of interest were monitored to meet these conditions. Airborne data for each mission went through daily post-flight quality control processes to determine potential re-flies as needed. Weather stations near the area of interest were monitored to meet these conditions.

The helicopter flight path targeted the river where the active channel occupies the center of the frame. Multiple flight lines were needed along sections where the channel was wider than the image frame (Figure 2) or significant side channels were identified. The flight plan was designed to achieve a ground sampling distance (GSD) of less than or equal to 0.5 meters (m) at an altitude of 500 meters above ground level (AGL).

Thermal Infrared Sensor: FLIR SC6000

Thermal infrared images were collected using a FLIR SC6000 LWIR sensor (8 – 9.2 μm) mounted to a Bell 206 Long Ranger helicopter. The sensor was installed in an enclosed fiberglass capsule mounted at the bottom of the helicopter with a designated opening for the down-facing lens (Figure 3). The FLIR SC6000 sensor uses a focal plane array of detectors to sample incoming radiation based on the technology of Quantum Well Infrared Photodetector (QWIP). The sensor's array records the change of state of electrons in a crystal structure reacting to incident photons. This technology is faster and more sensitive than polymer thermal detectors. A cooling mechanism is required for this sensor to stabilize its internal temperature and minimize thermal drift during acquisition. To achieve uniformity across the detector array, a factory scheme is generated to reduce non-uniformity across the image frame. Differences in temperature (typically <0.5 °C) might be observed near the edge of the image frame. Flight planning ensures sufficient image overlap so that frame edges can be excluded from the river channel in the TIR image mosaics. The resulting thermal infrared image frames were recorded directly from the sensor to an on-board computer as raw photon counts which were then converted to radiant temperatures. Sensor and acquisition specifications for the Grande Ronde River TIR study are listed in Table 4.

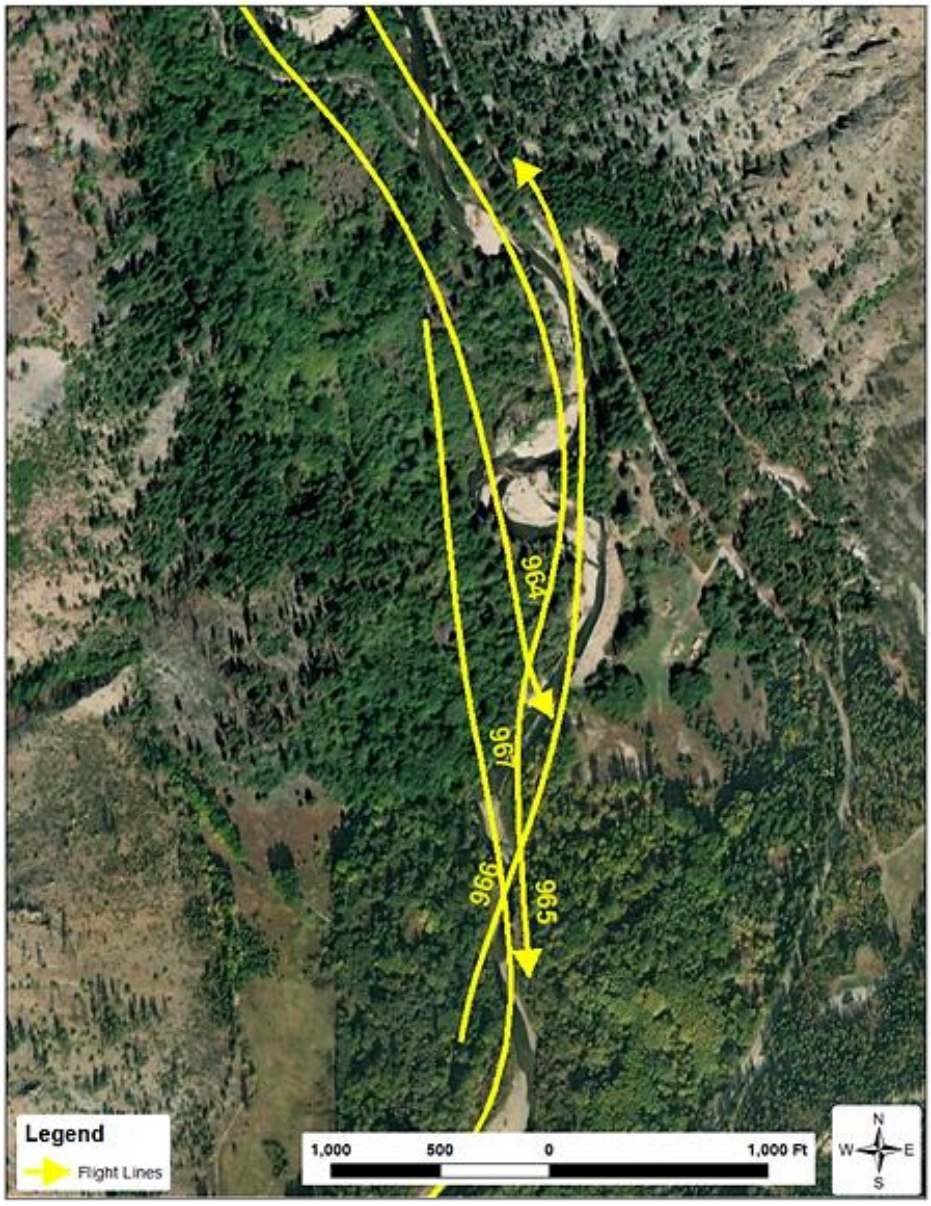

Figure 2: Example of flight lines collected for TIR and True Color Imagery

The positional coordinates of the aircraft (latitude, longitude, and altitude) and the orientation (pitch, yaw, and roll) were recorded continuously throughout the data collection mission. Aircraft position was measured twice per second (2 Hz) by an onboard differential global navigation satellite system (GNSS), while aircraft attitude was measured 200 times per second (200 Hz) by an onboard inertial measurement unit (IMU). Airborne global positioning system (GPS) data were post-processed into a smoothed best estimate of trajectory (SBET) using Applanix PP-RTX data for corrections. To ensure sufficient image overlap and ground sampling distance (GSD), TIR images were acquired at 1 image per second (1 Hz), flight speed was 50 knots on average, and flying altitude targeted 500 meters above ground level (AGL). Images were indexed by GPS time (event time) and paired with the SBET to resolve the exterior orientation (EO) of the sensor for each image event.

Table 4: Summary of TIR sensor and acquisition specifications

Parameter	FLIR System SC6000 (LWIR)
Wavelength:	8 – 9.2 μm
Noise Equivalent Temperature Differences (NETD):	0.035 °C
Pixel Array:	640 (H) x 512 (V)
Encoding Level:	14 bit
Horizontal Field-of-View:	35.5°
Sensor Focal Length	25 mm
Acquisition Dates:	August 16-19, 2024
Planned Flying Height Above Ground Level (AGL):	≤500 meters
Image Ground Footprint Width:	≤320 meters
TIR Ground Sampling Distance (GSD)	≤ 0.50 meter

Figure 3: An example of the sensor package setup used for the project

True Color Sensor: PhaseOne iXM-RS150F

Aerial imagery was acquired using a PhaseOne iXM-RS150F digital camera (Table 5). The PhaseOne is a medium format aerial mapping camera which collects imagery in three spectral bands (Red, Green, and Blue).

Table 5: Camera manufacturer's specifications for the PhaseOne iXM-RS150F

Parameter	PhaseOne iXU-RS150F Specification
Focal Length	50 mm
Spectral Bands	Red, Green, Blue
Pixel Size	3.76 µm
Image Size	14,204 x 10,652 pixels
Frame Rate	GPS triggered
FOV	56° x 43.6°
Date Format	8-bit TIFF

True color imagery for the Grande Ronde study area was co-acquired with the TIR data with at least 60% along track overlap between frames. The acquisition flight parameters were designed to yield a native pixel resolution of ≤ 20 cm. Orthophoto specifications particular to the Grande Ronde River project are in Table 6.

Table 6: Project-specific orthophoto specifications

Parameter	Digital Orthophotography Specification
Ground Sampling Distance (GSD)	≤ 20 cm
Along Track Overlap	≥60%
Cross Track Overlap	NA
Height Above Ground Level (AGL)	<500 m
GPS PDOP	≤3.0
GPS Satellite Constellation	≥6

Ground Control

To calibrate thermal infrared imagery to absolute temperatures, stream water temperature and atmospheric data are required.

In-Stream Water Temperature Sensors

Water temperature data loggers were deployed at 28 sites throughout the survey area by NV5's field crew (Figure 4) to radiometrically calibrate the thermal signature in the imagery. The data loggers recorded water temperature at five-minute intervals. The loggers used for this project were HOBO Water Temperature Pro V2 ONSET U22-001[1]. In a number of cases, the same data logger site was used to calibrate more than one TIR mosaic as a result of repeated acquisition of the same section or overlapping mosaics. The field crew also may have retrieved a handful of logger post collection and redeployed them at new sites due to the limited number of loggers that were available.

NV5 field crew adhered to the following list of guidelines for deploying data loggers:

1) In well mixed, flowing water sections of the river or stream and not in pools or riffles sections.
2) Avoid deploying the sensor in shallow waters where it can be exposed to direct sunlight. Sensors under direct sun light heat up and skew the recorded temperature.
3) In a water column deeper than 0.5 meters and shallower than 2 meters to allow for fully submerged data loggers and to avoid a stratified water column.
4) Within the channel's thalweg to measure a larger bulk of flowing water in the stream.
5) In a water body with a surface sufficiently exposed to the sky so that the monitored area is not obstructed from view of the TIR sensor during acquisition.
6) Away from the bank where riparian vegetation may block the view from the aircraft.
7) In stream reaches free from above-water surface features such as boulders and riparian and aquatic vegetation to allow for uniform water temperatures across the stream or the water body.
8) Perform acute temperature measurements at the time of deployment and retrieval using a handheld calibrated thermistor.
9) Perform test temperature measurements at the beginning and at the end of the season following the manufacturer's standards.

Atmospheric Parameters

Radiometric calibration of the TIR imagery requires atmospheric data collected by local weather stations. Records of atmospheric parameters, namely air temperature and relative humidity, were extracted from the closest weather stations for the time frame of the flight.

[1] https://www.onsetcomp.com/products/data-loggers/u22-001

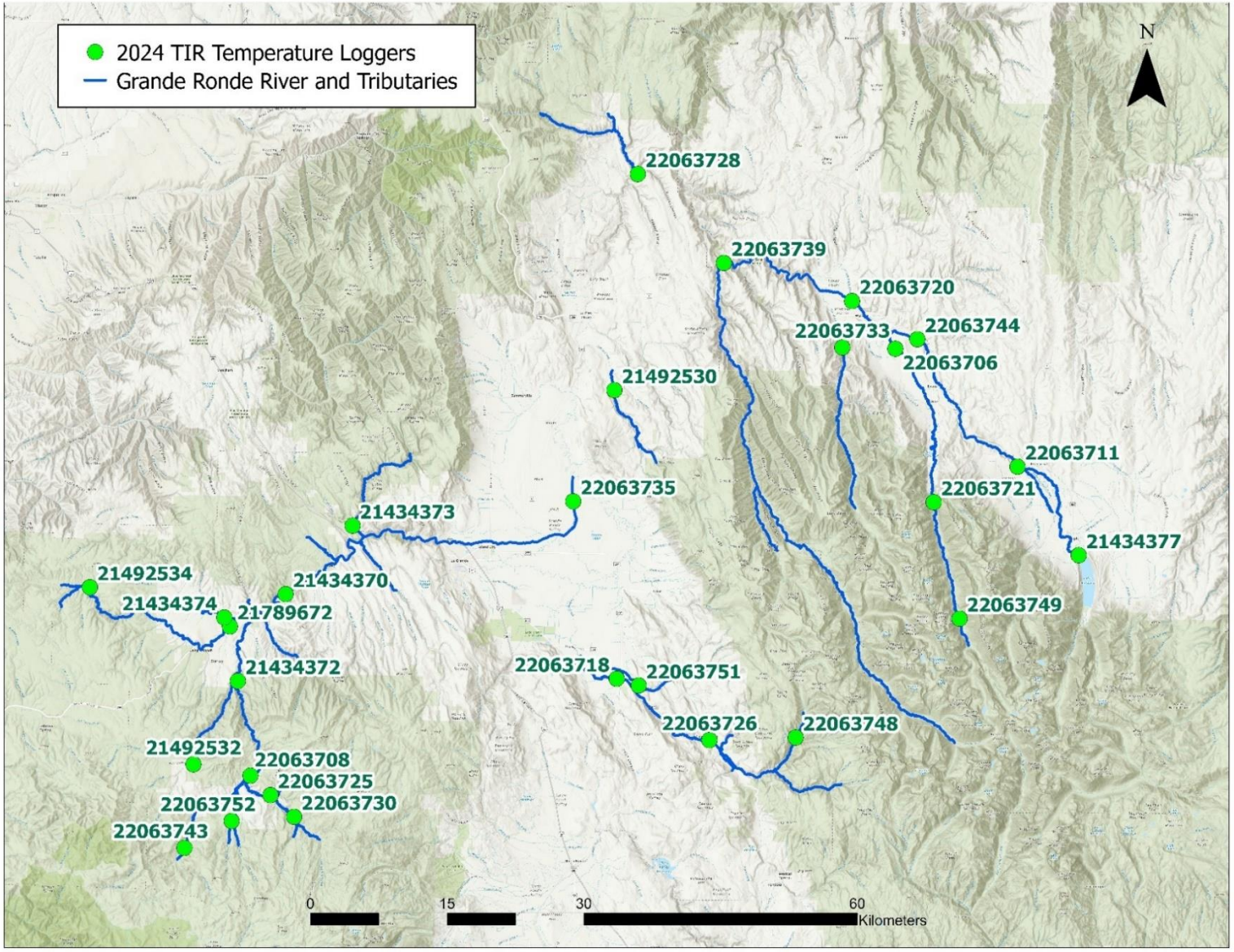

Figure 4: Map of survey area and location of water temperature data loggers

Thermal Infrared Data Processing

Thermal Infrared Imagery Calibration

The process of TIR calibration connects the TIR signature recorded by the FLIR sensor and the kinetic temperature of the targeted object (in case of river surveys, this is the in-stream water temperature data). Response curves of the TIR radiation and temperature were measured in a laboratory environment as part of the periodic maintenance procedure stated by the sensor's manufacturer. In the laboratory environment, the sensor records thermal infrared radiation emitted by a black body as digital numbers which were used to generate the response curves. All objects have physical parameters of emitting, reflecting, and transmitting radiation with varying values as the following equation shows:

$$emissivity + reflectivity + transmisivity = 1$$

In theory, a black body has an emissivity (e) value of 1.0, and reflectivity (r) and transmissivity (t) values of 0.0. However, the TIR calibration is based on the recorded temperature of water which has an emissivity value of 0.98,[2] a reflectivity value of 0.02, and a transmissivity value of 0.0. The water surface reflects thermal radiation from the atmosphere, while the water column is opaque and does not transmit radiation in the longwave thermal spectrum.

The longwave radiation that is emitted from the target's surface (water, rocks, vegetation) is attenuated through the atmospheric column reaching the sensor's lens. Therefore, the relative humidity, distance, and ambient air temperature (obtained from weather station data) are input parameters to FLIR's imagery software to complete the calibration process. Imagery from flight lines that did not cover data loggers were calibrated based on overlapping imagery from adjacent flight lines, a technique that is referred to as "line-to-line calibration". Minor deviations from the initial calibration might be needed to achieve the best possible temperature continuity throughout the mosaic.

TIR Mosaic Generation

Initially, a boresight calibration flight was processed to calculate the misalignment angles between the sensor and IMU system; this step allows for direct georeferencing of imagery without aerial triangulation. For each production flight, a series of corrections were applied to the aircraft trajectory and orientation using Applanix PP-RTX processing methodologies. Image timestamps were linked to the corrected trajectory to resolve the exterior orientation (EO) parameters of the sensor for each image event. The resulting EO, sensor interior orientation (IO), and calibrated TIR images were input into Inpho's OrthoMaster software to orthorectify images using the best publicly available digital elevation model (DEM). Finally, the TIR ortho images were mosaicked without applying color balancing and only

[2] Baldridge, A. M., S.J. Hook, C.I. Grove and G. Rivera, 2009. The ASTER Spectral Library Version 2.0. Remote Sensing of Environment, vol 113, pp. 711-715.

minimal seam line feathering to preserve the original temperature values of the TIR imagery as best as possible. The processing steps and software are detailed in Table 7.

Table 7: Processing step for TIR mosaic generation

Orthophoto Processing Step	Software Used
Calculate camera misalignment angles from a system boresight flight conducted close to survey area.	Applanix CalQC v9.1
Resolve kinematic corrections for aircraft position data using kinematic aircraft GPS and PPRTX data. Develop a smoothed best estimate of trajectory (SBET) file that blends post-processed aircraft position with sensor head position and attitude recorded throughout the survey.	Applanix POSPac MMS v9.1
Calculate exterior orientation (EO) for each image event by linking the event time stamps with the SBET.	Applanix POSPac MMS v9.1
Convert raw (*.seq) TIR data into thermally calibrated TIFF images.	FLIR Examine IR v4.3
Import DEM and generate individual orthophoto images.	Inpho OrthoMaster v14.1
Mosaic orthorectified imagery, generating seams between individual photos.	OrthoVista v14.1

Temperature and Color Ramps

The final TIR mosaic contains pixel values of degrees Celsius multiplied by 10, stored in a 16-bit unsigned integer raster format. Temperature values occupy a relatively narrow range of the full 16-bit histogram; thus, visual representation of the imagery is enhanced by the application of a customized color ramp. Color ramps also highlight different features relevant to the analysis, such as spatial variability of stream temperatures and inflows (Figure 5). The color ramps for the TIR mosaics were developed to maximize contrast for most surface water features and are tailored to each tributary or mosaic. A TIR specialist at NV5 customized unique color ramps to improve visual presentation of the TIR mosaic and exported the color ramps as ESRI layer files (*.lyrx).

Accuracy Assessment Methodology

The radiometric accuracy of the final TIR mosaic was assessed by comparing sampled pixels of the mosaic (of water features) at the data logger locations against the temperature recorded by the respective logger. The goal was to reach a mean absolute error (MAE) of ≤1.0 °C temperature difference between the mosaic and logger-recorded values at the time of acquiring the TIR imagery. The threshold of MAE ≤1.0 °C accounts for factory reported errors of the water temperature data logger (≤0.2 °C) and the FLIR sensor (≤0.035 °C).

True Color Imagery Processing

As with the TIR data, the collected true-color photographs went through multiple processing steps to create final orthophoto products. Initially, images were geometrically corrected for lens distortion using camera calibration parameters and output as 8-bit TIFF images. The SBET from TIR airborne GNSS post-processing was then paired with image timestamps to resolve EO parameters of the camera for each image event and allow for direct georeferencing of the imagery. Direct georeferencing forgoes the need for an aerial triangulation block adjustment, instead relying on the high precision of the onboard GPS/IMU instruments and camera to IMU rotational offset angles calculated from a boresight flight conducted prior to data acquisition.

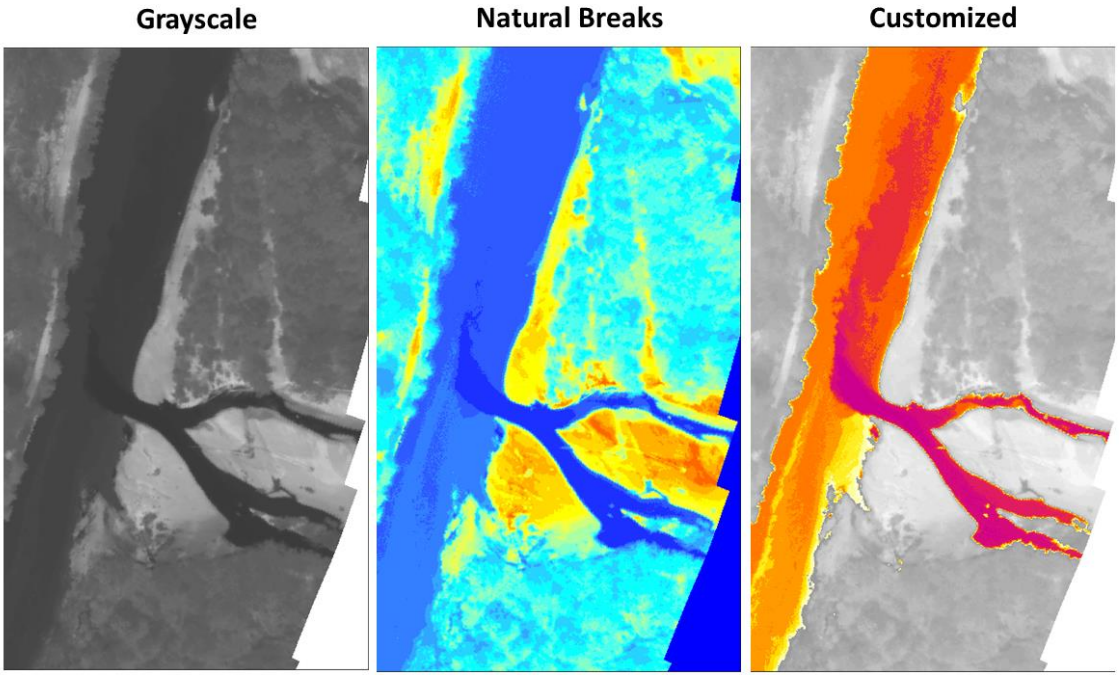

Figure 5: Examples of different color ramps applied to the same TIR image

Images were orthorectified using the best publicly available bare-earth model to remove displacement effects from topographic relief inherent in the imagery. The surface model used may have come from multiple data sources and pixel resolutions to cover the entire AOI; it may also represent different ground conditions than those of the Grande Ronde TIR and RGB data collection. Therefore, the orthorectification process may result in small spatial offsets in the imagery in areas where there have been temporal changes to the ground surface or the resolution of the model is not high enough to support that of the imagery. In the final processing step, all images were mosaicked together using blockwide global color balancing and automated seamline generation. The processing workflow for orthophotos is summarized in Table 8.

Table 8: Orthophoto processing workflow

Orthophoto Processing Step	Software Used
Resolve kinematic corrections for aircraft position data using kinematic aircraft GPS and static ground GPS data. Develop a smoothed best estimate of trajectory (SBET) file that blends post-processed aircraft position with sensor head position and attitude recorded throughout the survey.	POSPac MMS v.9.1
Generate camera exterior orientations (EO) by linking image events with the SBET file, resulting orientations are in Omega, Phi, and Kappa representing the image coordinate system.	POSPac MMS v.9.1
Convert raw imagery data into geometrically corrected TIFF images.	iX Capture v3.4
Apply EO to photos and perform aerial triangulation using automatically generated tie points and ground control data.	Inpho Match AT v14.1
Import DEM and orthorectify image frames	Inpho OrthoMaster v14.1
Mosaic orthorectified imagery, blending automated and manually drawn seams between photos and applying global color balancing to the project.	Inpho OrthoVista/Seameditor v14.1

Interpretation and Feature Extraction

To begin interpretation of thermal infrared data, a trained analyst reviewed the final mosaics to obtain a detailed understanding of the temperature distribution across the survey area. An emphasis was put on identifying the thermal signature of water bodies and streams. This was also the first step in identifying the thermal signature and location of potential inflow sources of cold/hot water.

A stream centerline was digitized using the TIR mosaics including stream names (*at a scale of 1:5,000*). This step was performed for the entire contracted river length. As the centerline was digitized, care was taken to avoid non-water features where possible, such as aquatic vegetation, boulders, and overhanging canopy. However, a few non-water features cannot always be avoided, such as bridges. River length was measured cumulatively from the most downstream point in the AOI towards the most upstream point. Therefore, the calculated length represents only the streams within the surveyed AOI and is not relative to the overall river network outside the AOI.

Thermal Infrared Mosaic Sampling and Interpretation

Two analysis techniques were used to interpret TIR data: 1) an interval-based automated sampling of the stream to generate a longitudinal temperature profile (LTP) and 2) a manual point source sampling to identify significant thermal features (STF).

Longitudinal Temperature Profile

The LTP is the result of sampling the TIR mosaic at specified intervals (100 meters) along the previously digitized centerlines of the study area. This profile captures the longitudinal variation in river temperature, reflecting the potential heat exchange between the river's water and a suite of variables such as tributaries, springs, groundwater upwelling, air temperature, solar radiation, shading, or anthropogenic inputs. Using NV5's proprietary algorithm, the sampling results were stored in a geospatial data file format (shapefile) and were plotted against river distance. For each interval, the algorithm extracted the pixel values from the TIR mosaic at 10 points along the centerline within a 5-meter distance from the interval point (Figure 6). The results were summarized in terms of statistical parameters of mean, median, maximum, minimum, and standard deviation. The results were plotted against river distance to visualize temperature trends along the reach. Sampling points with unusually high standard deviation were flagged as potential outliers, often indicating non-water surfaces such as exposed rocks or other features that can distort thermal readings.

Significant Thermal Features

The STFs are the result of sampling the TIR mosaics at pre-defined locations in the study area. Such locations were identified by an analyst as thermal anomalies in the study area that represent potential cold or warm water inflows from springs, hyporheic exchange zones, tributary confluences, or side channels. Identifying these features is a core objective in TIR analysis, as they highlight potential cold-water refugia critical for aquatic species and inform habitat restoration planning.

The STFs are manually identified through expert interpretation of the TIR mosaic, supported by co-acquired RGB imagery. Candidate features are selected based on the presence of thermal plumes and temperature deviations from surrounding river temperatures. A feature is generally considered significant if its thermal signature is at least 0.5 °C warmer/colder than the main channel and occupies at least 25 pixels in the TIR mosaic. STFs appear as localized cooler or warmer areas extending into the mainstem's banks.

The likely source of the thermal anomaly is considered during classification. **Tributary** inflows are typically characterized by a plume-shaped thermal anomaly entering the main channel along one of its banks, downstream of the identified STF. The STFs of **Hyporheic exchange zones** often appear as cold patches near river margins or downstream of gravel bars. STFs of **groundwater** inflow are commonly inferred when temperatures align with regional annual air temperature (approximately 11–15 °C in the Pacific Northwest). Groundwater inflows are commonly colder than the main channel in the summer and warmer in the fall and winter. **Side channels** may also exhibit thermal anomalies due to surface-subsurface interactions.

Once a feature is identified, an automated algorithm extracts pixel values within a 1-meter buffer surrounding the STF. The shortest distance to the river centerline is calculated, bankside is defined (left or right), and the associated river kilometer (river km) is assigned based on the nearest point along that line. The extracted pixel values are summarized using the same statistical parameters used for the LTP analysis: mean, median, minimum, maximum, and standard deviation. These results are stored in a geospatial dataset (ESRI shapefile) and plotted by river distance to facilitate comparison with the LTP data.

Because the 1-meter buffer may not always perfectly align with the actual size of the thermal feature, interpretation of the summary statistics varies. For example, the minimum temperature may best represent a small, focused spring or upwelling, while the median value may better represent the thermal signature of a broader tributary plume. As a general classification rule, STFs with temperatures below 15 °C during the summer may be flagged as “spring” features, indicating potential groundwater influence. Some environmental conditions can introduce uncertainty. Dense vegetation or confined river reaches can obscure the TIR signal, sometimes causing high apparent temperatures due to canopy interference rather than true water surface readings. During the STF identification process, these areas are carefully evaluated to minimize misclassification.

Calculated Statistic Parameters

The statistical parameters below summarize the temperature values of all 10 sample points for the LTP and all pixels inside the buffered area for the STF.

- **Mean and median:** Represent the central tendency of all sampled points or pixels within each feature or interval.
- **Minimum and maximum:** Define the lowest and highest temperature values recorded. For STFs, the **minimum** is often used to highlight cold inflows (e.g., springs), while the **maximum** may be used to identify warm inflows.
- **Standard deviation:** Defines the variability in temperature across all sampled points or pixels. This value is important in identifying sample points that represent non-water features. A low standard deviation indicates homogeneous thermal features among the sample points and a high standard deviation could indicate that the set of sample points includes non-water features (e.g., exposed rocks/boulders) with temperatures significantly different than the water body. The standard deviation is important for identifying and removing invalid sample points.

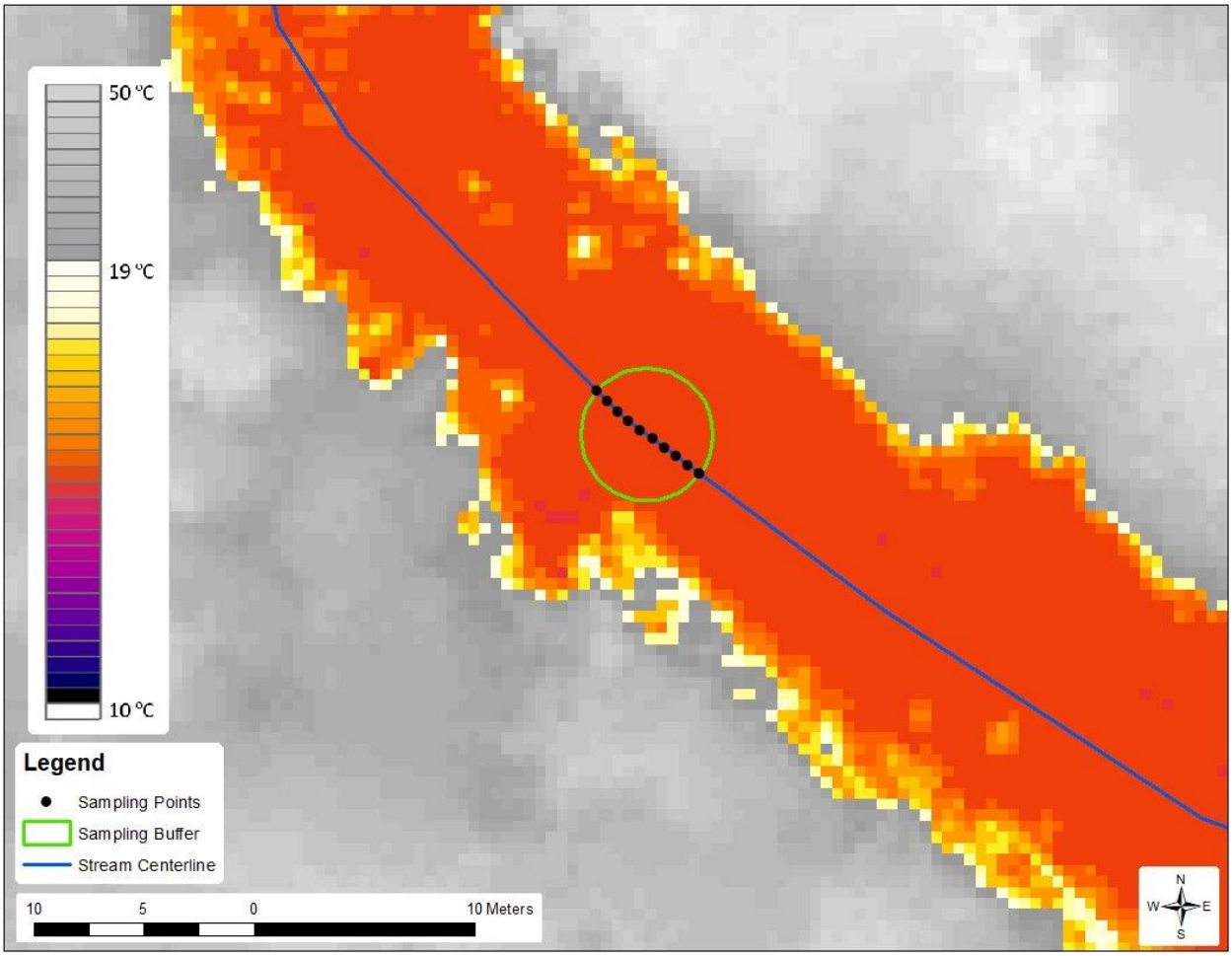

Figure 6: An example set of sample points (n = 10) that are used to generate the LTP along the river centerline within the defined buffer. Water temperature is displayed in units of °C.

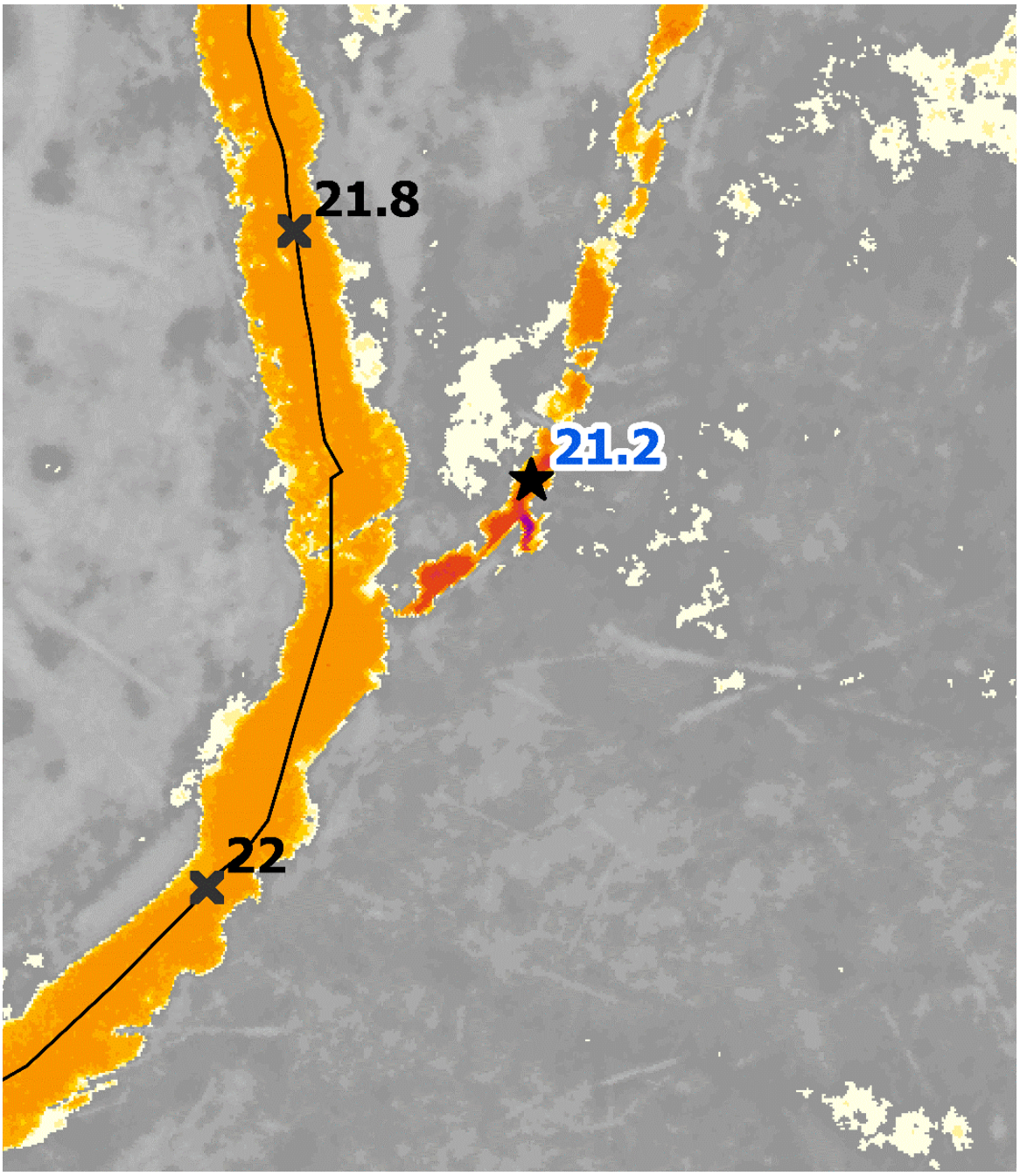

Figure 7: An example of a STF, the map shows a cold water spring or hyporheic inflow to the main channel

Table 9: Summary of the processing steps used in the thermal analysis.

Processing and Analyses Steps	Data File	Description	Software used
Calibrate thermal imagery to absolute temperatures	*<TIMESTAMP >.tif*	Convert raw TIR image digital numbers to radiance temperatures based on the sensor's factory calibration. Adjust radiant temperatures based on the ground control kinetic temperatures.	FLIR ResearchIR v. 4.3
Generate orthorectified thermal imagery	*<TIMESTAMP >.tif*	Use sensor EOs, TIR images and DEM to generate orthophotos.	Inpho v14
Develop color ramp	*<STREAM>_<SECTION>.lyrx*	Develop a color ramp that highlights spatial variability of stream temperatures.	ArcGIS Pro
Digitize stream centerline along main flow path seen in TIR imagery	*Centerline_ <STREAM>.shp*	Digitize and route streamlines based on the final thermal mosaics to best represent the centerline/main flow path.	ArcGIS Pro
Create longitudinal temperature profile	*LTP_<STREAM>.shp*	Using automated NV5 tools, generate a GIS point layer from the stream center line layer at 100-meter intervals. Assign each point a river kilometer measurement and sample the TIR radiant temperature based on an average of 10 sample points located within a 3-meter buffer, upstream and downstream, along the centerline.	ArcGIS Pro NV5 script
Identify and sample significant thermal features sites	*STF_<STREAM>.shp*	Manually digitize and sample significant thermal features. Sampling all pixels inside a 1-meter buffer area radiating from the digitized point.	ArcGIS Pro NV5 script
Plot longitudinal profiles	*LTP_STF_<STREAM>.xlsx*	Plot temperature against river km for the longitudinal profile and the manually identified STFs.	Excel

Thermal Infrared Analysis

The following analysis provides a review of the longitudinal temperature profile gradient of the stream, significant thermal features at the edge of the stream channel and point source and non-point source inflows (e.g., tributaries, side channels, groundwater upwelling, seepage, effluents, springs, and hyporheic flow) in the floodplain. Identification of such features relies on visual inspection by a trained analyst and automated sampling algorithms. While the visual inspection is qualitative, it assists in identifying the span of river water temperature and isolating it from the temperature of the banks. The results of running the automated sampling algorithms are quantitative and are provided in two statistical datasets: the LTP and STF. Both datasets are provided in shapefile and tabular formats. The LTP was generated by plotting the mean stream temperature at a 100-meter interval. Significant thermal features along the river and in the survey area were incorporated with the LTP plot to provide spatial context for interpreting temperature patterns.

Accuracy Assessment Results

TIR imagery was calibrated using in-stream temperature data from the loggers that were distributed along the river channel. The accuracy of the calibrated TIR mosaics were assessed by comparing the water temperatures recorded by the in-stream data loggers to the radiant temperatures derived from the TIR mosaic, summarized in Table 10 and Table 11.

The final mosaic is considered within the specified accuracy requirements when the mean differences between TIR radiant and in-stream kinetic temperatures, also known as the mean absolute error (MAE), is ≤1.0 °C. The accuracy assessment is based on the data recorded by all data loggers within a single river section or mosaic. The Grande Ronde River thermal infrared mosaic was within this accuracy threshold. In a number of cases, the same data logger site was used to calibrate more than one TIR mosaic as a result of repeated acquisition of the same section or overlapping mosaics. The field crew also may have retrieved a handful of logger post collection and redeployed them at new sites due to the limited number of loggers that were available. Therefore, the number of accuracy assessment points can be higher than the number of sites where the loggers were deployed, and a repeated serial number could be observed.

Table 10: Error values between radiant temperatures derived from the TIR mosaic and kinetic water temperature recorded by in-stream data loggers in 2024. This table includes repeated data loggers' serial numbers where TIR mosaics overlapped or if the logger was retrieved and redeployed at a different site. Therefore, this table has a higher number of records than the number of deployment sites.

Stream	Serial Number	Location (River km)	Calibration Temperature (°C)	Time	Median (°C)	Error (°C)
McCoy Creek	21434374	2.69	19.6	8/16 15:29	20.1	-0.5
Grande Ronde River	21434370	41.13	25.1	8/16 15:17	24.3	0.8
State Ditch	22063735	2.85	24.5	8/16 14:40	24.7	-0.2
Little Creek	22063751	9.18	21.7	8/16 14:20	21.7	0.0
McCoy Creek	21434374	2.69	19.6	8/16 15:29	19.6	0.0
Meadow Creek	21789672	4.73	25.0	8/16 16:28	24.6	0.4
Meadow Creek	21492534	30.16	20.6	8/16 15:57	21.0	-0.4
Grande Ronde River	22063730	83.24	17.2	8/17 15:24	17.6	-0.4
Grande Ronde River	22063725	78.68	21.1	8/17 15:37	19.8	1.3
Grande Ronde River	22063708	71.70	23.4	8/17 15:44	22.9	0.5
Fly Creek	21492532	13.44	23.0	8/17 14:48	22.9	0.1
Grande Ronde River	21434372	57.64	21.5	8/17 15:51	23.0	-1.5
Chicken Creek	22063752	6.94	16.5	8/17 15:09	16.5	0.0
Indian Creek	21492530	2.50	22.3	8/17 16:33	22.3	0.0
Five Points Creek	21434373	1.91	21.9	8/17 12:57	21.9	0.0
Bear Creek	22063733	1.10	20.3	8/18 13:38	20.3	0.0
Wallowa River	21434377	69.62	20.7	8/18 12:03	19.8	0.9
Wallowa River	22063744	29.89	17.8	8/18 12:49	19.0	-1.2

Stream	Serial Number	Location (River km)	Calibration Temperature (°C)	Time	Median (°C)	Error (°C)
Wallowa River	22063720	20.15	19.4	8/18 13:46	19.7	-0.3
Minam River	22063739	0.08	24.8	8/18 14:56	23.2	1.6
Wallowa River	22063711	52.11	16.0	8/18 12:27	17.3	-1.3
Lookingglass Creek	22063728	0.22	16.4	8/18 14:46	16.3	0.1
Lostine River	22063749	40.13	13.8	8/18 13:20	13.4	0.4
Lostine River	22063721	24.85	13.2	8/18 13:11	13.2	0.0
Lostine River	22063706	2.05	18.6	8/18 12:56	18.2	0.4
Minam River	22063739	0.08	24.8	8/18 14:56	24.7	0.1
Sheep Creek	22063743	21.36	15.1	8/18 17:06	15.1	0.0
Grande Ronde River	21434370	41.13	25.1	8/16 15:17	25.1	0.0
McCoy Creek	21434374	2.69	19.6	8/16 15:29	19.6	0.0
Meadow Creek	21789672	4.73	25.0	8/16 16:28	24.9	0.1
Meadow Creek	21492534	30.16	20.6	8/16 15:57	20.6	0.0
Sheep Creek	22063743	21.36	15.2	8/19 14:46	15.1	0.1

Table 11: Summary of accuracy assessment values. This table lists the accuracy summary for all TIR mosaics, where more than one logger can be listed per TIR mosaic, and the same logger could have been used to calibrate more than one TIR mosaic.

Mosaic	Number of Loggers Used	Minimum Error (°C)	Maximum Error (°C)	Average Error (°C)
20240816 Grande Ronde	3	-0.5	0.8	0.0
20240816A Catherine Little SF NF Milk	3	-0.4	0.4	0.0
20240816A Little Creek	1	0.0	0.0	0.0
20240816A Meadow McCoy Dark Canyon	1	0.0	0.0	0.0
20240816A Meadow Waucup	2	-0.4	0.4	0.0
20240817 Grande Ronde	5	-1.5	1.3	0.0
20240817A Chicken West Chicken	1	0.0	0.0	0.0
20240817A Indian	1	0.0	0.0	0.0
20240817A Spring Five Points Null	1	0.0	0.0	0.0
20240818 Bear Creek	1	0.0	0.0	0.0
20240818 Wallowa all	5	-1.3	1.6	-0.1
20240818A Lookingglass Little Lookingglass	1	0.1	0.1	0.1
20240818A Lostine	3	0.0	0.4	0.3
20240818A Minam Little Minam	1	0.1	0.1	0.1
20240818A Sheep	1	0.0	0.0	0.0
20240819A Grande Ronde	1	0.0	0.0	0.0
20240819A Meadow McCoy	1	0.0	0.0	0.0
20240819A Meadow Waucup	2	0.0	0.1	0.1
20240819A Sheep	1	0.1	0.1	0.1

Longitudinal Temperature Profiles and Significant Thermal Features

The LTP of a stream is an informative tool to detect stream temperature gradients and the response to water inflow sources. It is common to plot the mean or the median water temperature against river length, though the other calculated statistical information can be used as well. The final LTP data excludes most of the non-water features that were accidentally sampled by the automated algorithm. An easy approach to exclude non-water features is by excluding results of high standard deviation and high minimum/maximum temperatures. However, further refinement might be required by the end user based on local information and familiarity with the survey area. The LTP was generated using the parameters in Table 9, unless specified otherwise for smaller tributaries.

Significant thermal features such as tributaries, side channels, or point sources/sinks were identified based on their unique thermal signature and proximity to the active channel. The STF information assists in explaining the changes to LTP or localized water temperature differences. The STF identification focuses on locating tributaries entering the main channel, hyporheic flow at the river edge, side channels, and agricultural backflow. The majority of identified STFs had temperatures colder than the main channel, mostly leading to a cooling gradient. Warm inflows were also identified along the water's edge, but with fewer occurrences.

The end user should manually inspect the spatial variability of STFs to better understand its thermal influence. Groundwater upwelling appears colder than the main channel in the summer, providing a strong indicator of the interaction between the stream and its floodplain. Tributaries and side channels are usually larger than 1-meter in width, while the hyporheic, spring, and groundwater inflows vary in size. Hyporheic zones are often located on the edges of active channels and downstream of gravel bars as an indication to subsurface flow.

Grande Ronde River Main Channel

A total of 88.1 kilometers of Grande Ronde were flown on August 16, 17, and 19. The August 19 mission included a reflight of the main channel covered during August 16, and thus the latter was not used for the analysis. The final analysis was based on both the August 17 and 19 missions only. Along the main channel of the Grande Ronde River, a total of 69 significant thermal features and 11 tributaries were identified, sampled, and plotted. Figure 8 shows the important data points of the STFs and tributaries.

The thermal survey of Grande Ronde shows an overall gradient of downstream warming for the majority of Grande Ronde's length, which is typical thermal behavior of rivers in the Pacific northwest during the summer. Localized sections of downstream cooling were apparent and can be spatially correlated to several cold-water inflows that were identified in the data (Figure **9**). Tributaries flowing into the main channel of the Grande Ronde River varied between colder and warmer than the main channel and subsequently resulted in a downstream cooling or warming effect, respectively. Of particular note, the data showed a river stretch of rapid cooling and warming between Meadow Creek and Spring Creek which coincided with a series of STF inflows along this section.

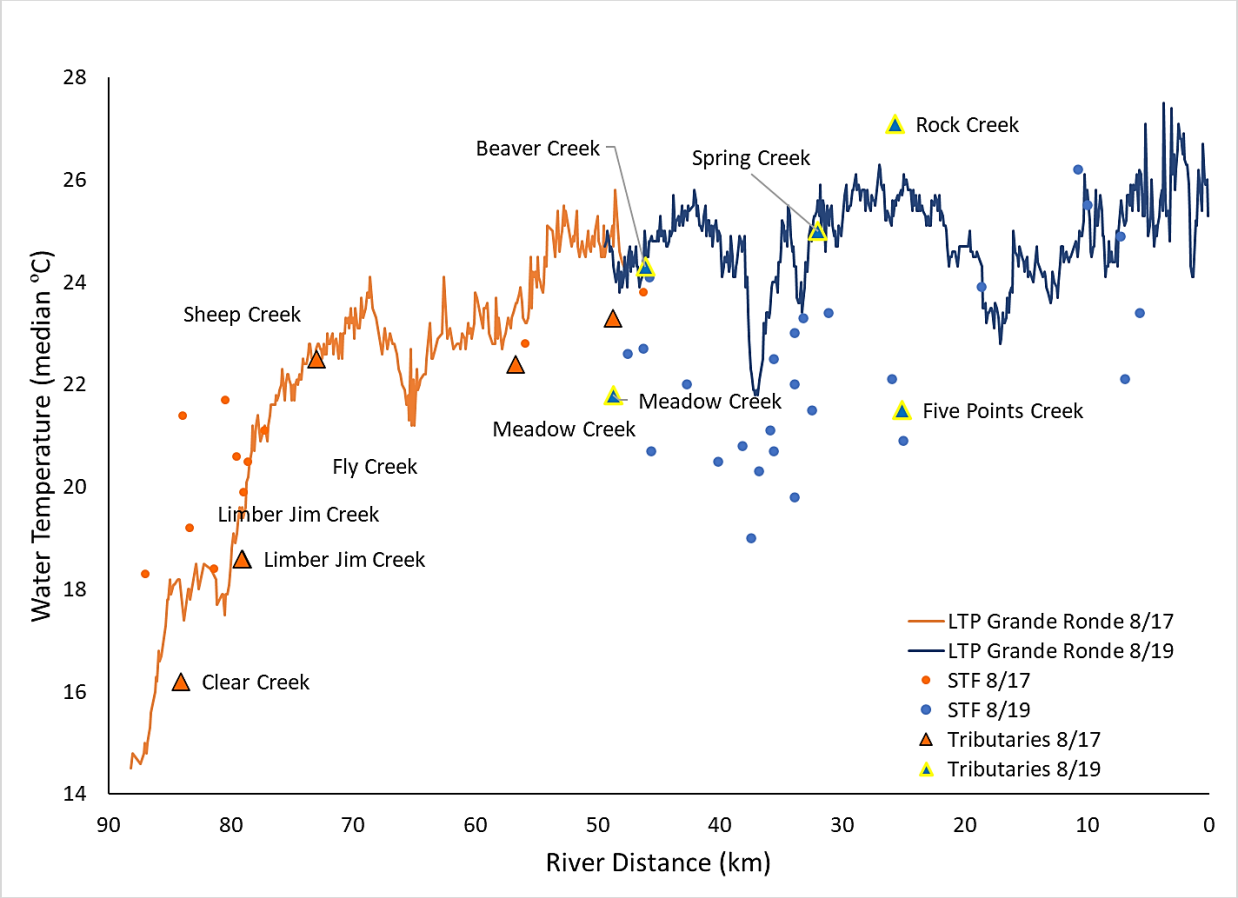

Figure 8: Plot showing LTP, tributaries, and STFs entering the main channel, Grande Ronde. The plot was prepared using the median values of the sampled pixels of the thermal mosaic.

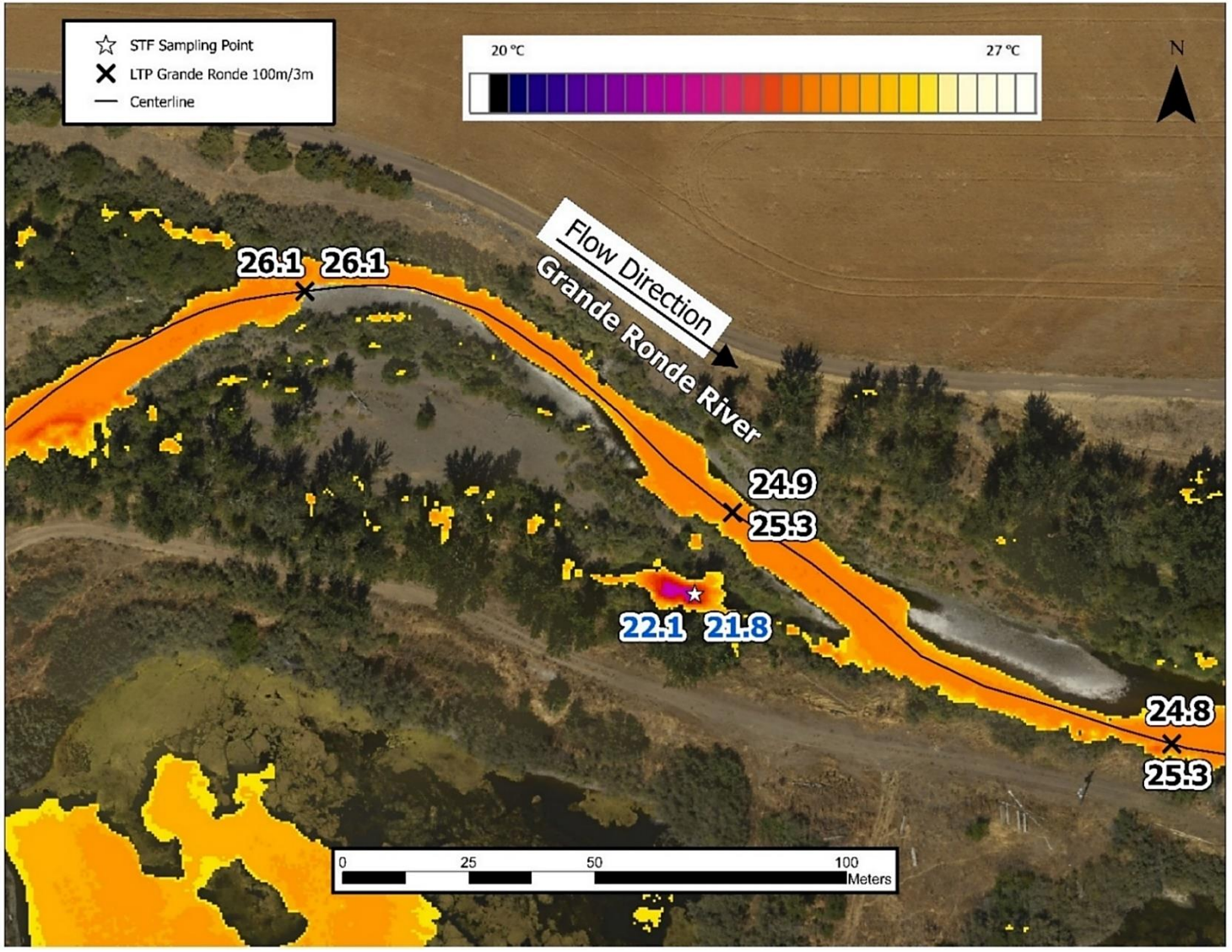

Figure 9: Map of TIR imagery colored by temperature overlayed on RGB imagery showing what looks like a hyporheic zone on the Grande Ronde. The wide bend flowing around a gravel bar is one of the areas where hyporheic zones can form. The labels represent results from two flights, both of which showed that the hyporheic zone is colder than the main channel.

Clear Creek and Limber Jim Creek

Both Clear Creek and Limber Jim Creek were collected on August 17, 2024, covering 1.9 km and 6 km, respectively. The collection occurred during the same time window as the main channel of the Grande Ronde River (into which they flow). Clear Creek contributed colder water than Limber Jim Creek, 16.2 °C vs 19.7 °C, respectively, while the Grande Ronde was at 19.4 °C (Figure 10 and Figure 10). Despite its low discharge relative to the main channel of the Grande Ronde River, Clear Creek contributed to a localized cold-water section just downstream of its confluence. Limber Jim Creek has no impact given that it provided same-temperature discharge to the Grande Ronde River.

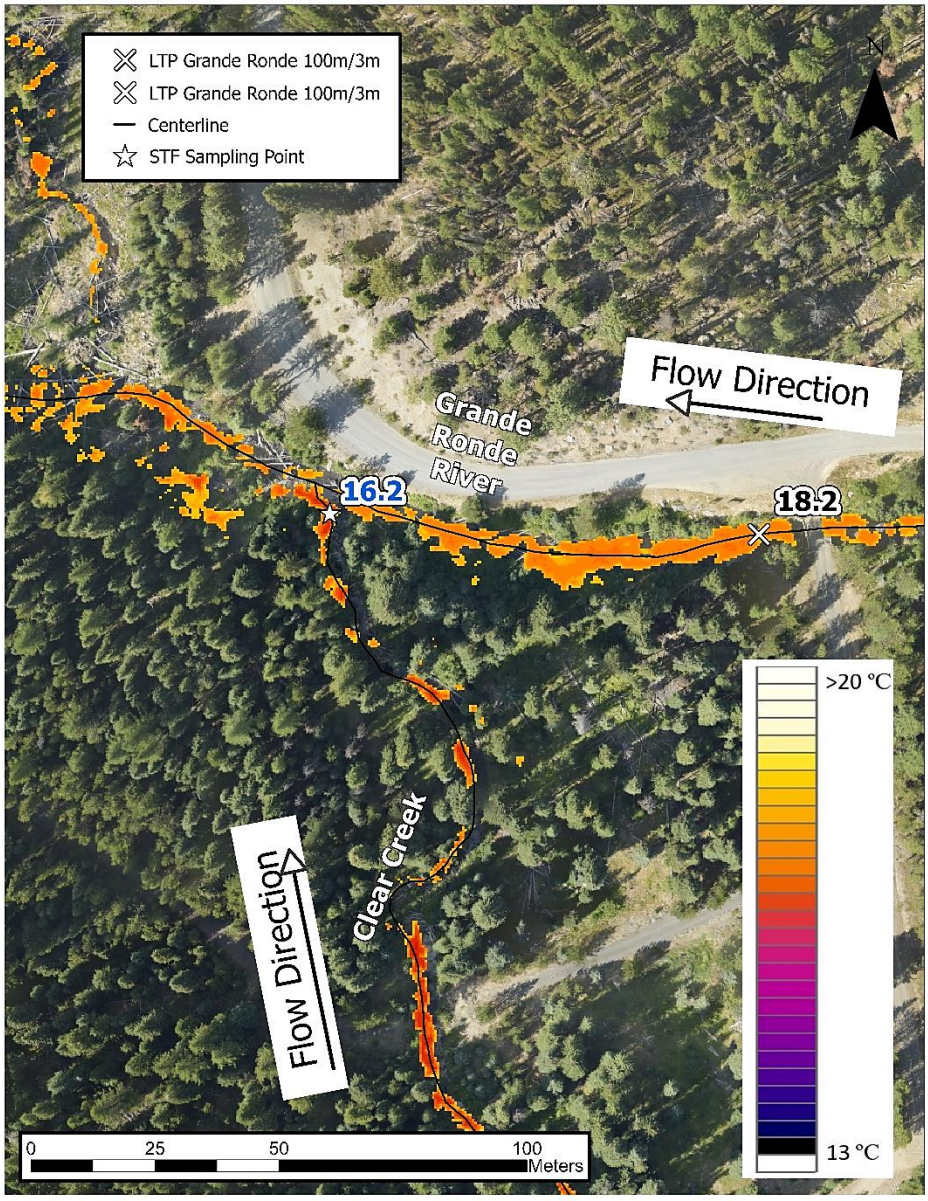

Figure 10: Map of the TIR imagery on the co-acquired RGB imagery, showing Clear Creek flowing into Grande Ronde River at river km 83.9.

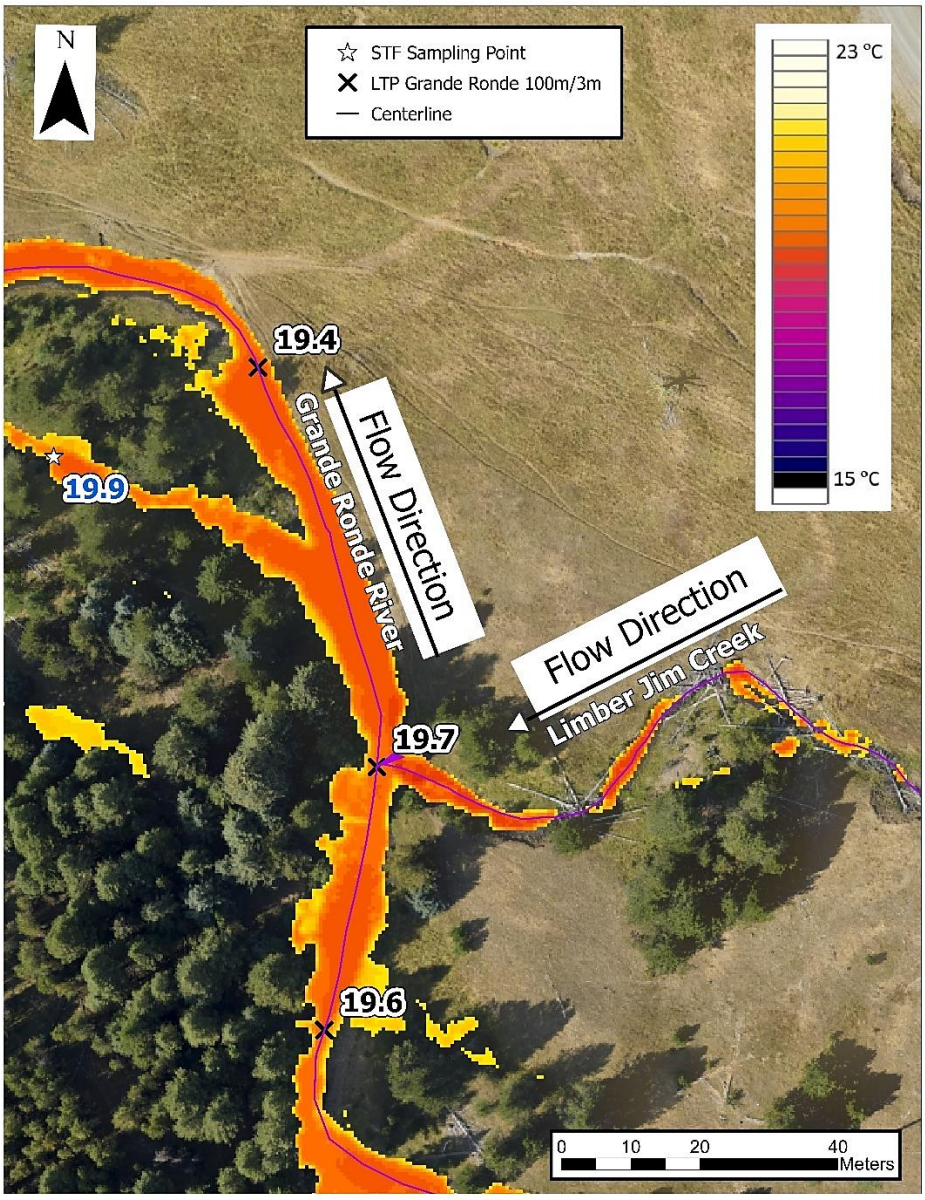

Figure 11: Map of the TIR imagery on the co-acquired RGB imagery, showing Limber Jim Creek flowing into Grande Ronde River at river km 79.

Sheep Creek Basin (Sheep, Chicken, and West Chicken creeks)

A total of 36.7 kilometers of Sheep Creek Basin were flown on August 17, 18, and 19, 2024, covering all three tributaries. The August 17 flight covered Chicken Creek and West Chicken Creek, the August 18 flight covered most of the main channel of Sheep Creek, except the downstream most 1.8 km, and the August 19 flight covered the entire length of Sheep Creek.

West Chicken Creek was the only identifiable inflow to the Chicken Creek, providing it with most of the cold water. However, the latter's temperature rapidly increased from 19 °C to 24 °C in a short distance as the channel meandered through a wide floodplain with minimal riparian canopy and low shading (Figure 12).

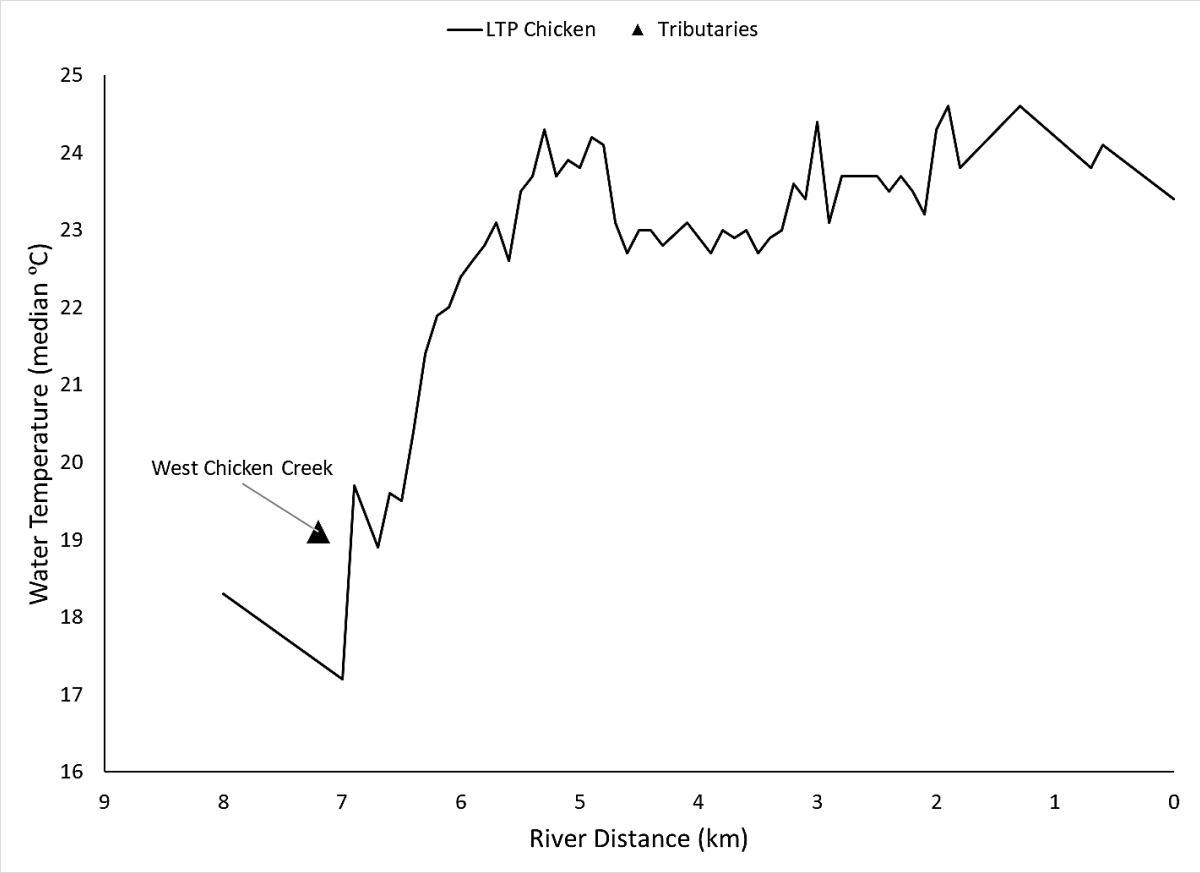

Figure 12: Plot showing the LTP for Chicken Creek. West chicken Creek was the only tributary flowing into Chicken Creek providing it with most of the cold water

Both flights of Sheep Creek (August 18 and 19) showed a similar downstream warming gradient, from 14 °C to 22 °C, and slight variability that could be attributed to minimal air temperature change between both days (Figure 13). Inflow from Chicken Creek appears to be correlated with the downstream cooling gradient, despite the observed thermal signature showing that its discharge was at similar temperatures to Sheep Creek on both dates (Figure 13, and separately in Figure 14 and Figure 15). The TIR mosaics and analysis results for both flights were delivered.

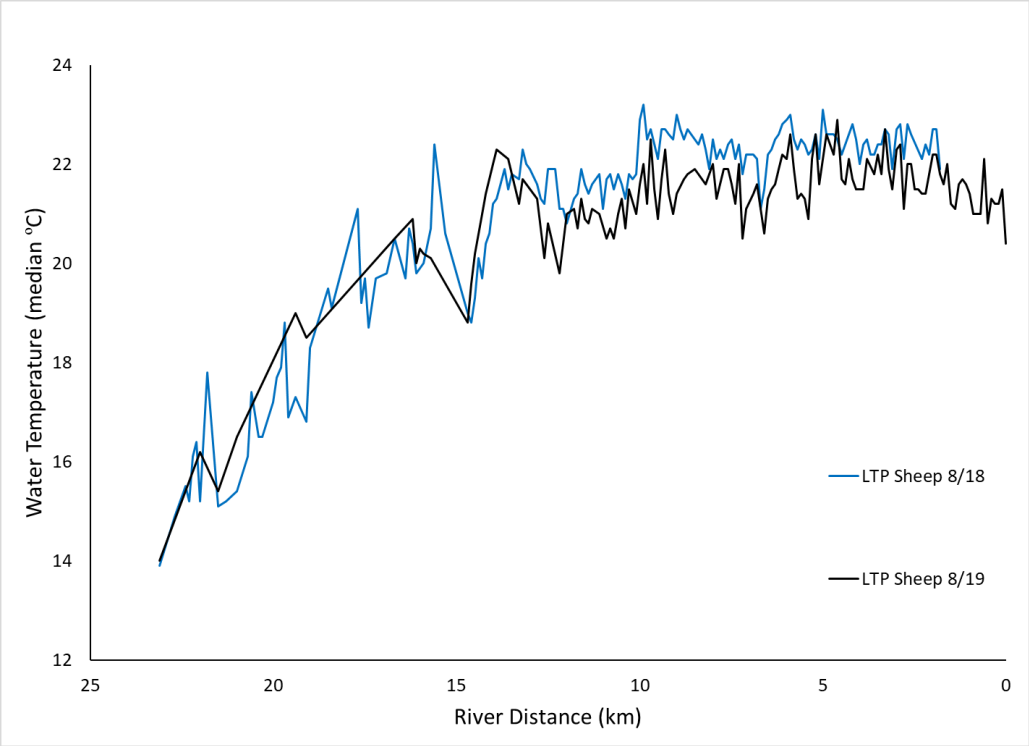

Figure 13: Plot showing the LTP, tributaries, and STFs entering the main channel, Sheep Creek (August 18 and 19)

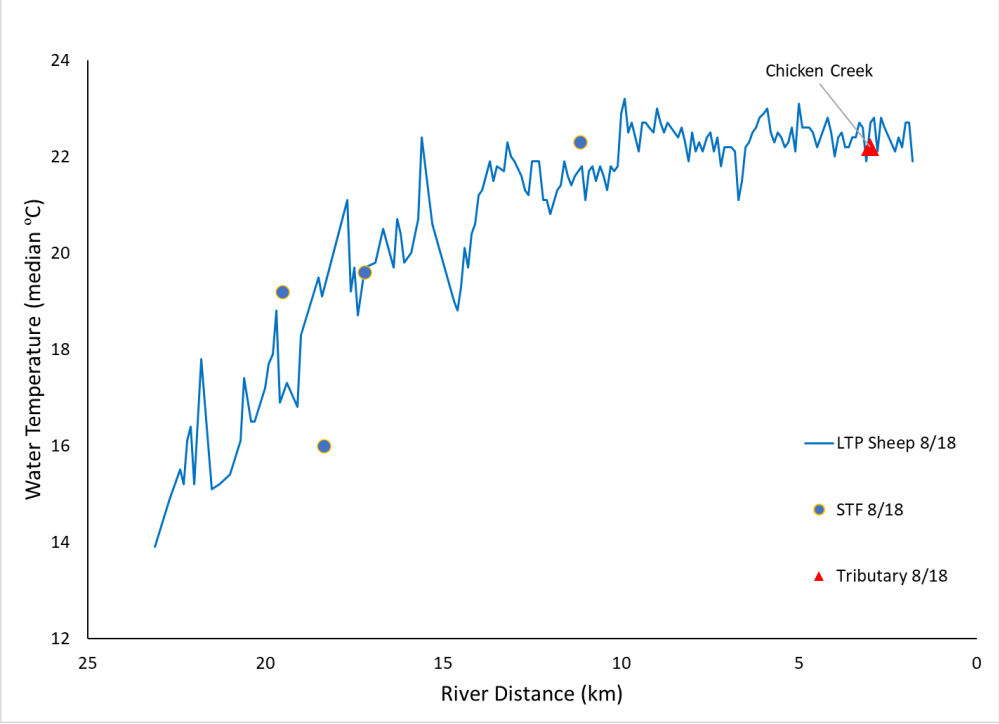

Figure 14: Plot showing the LTP, tributaries, and STFs entering the main channel, Sheep Creek (August 18)

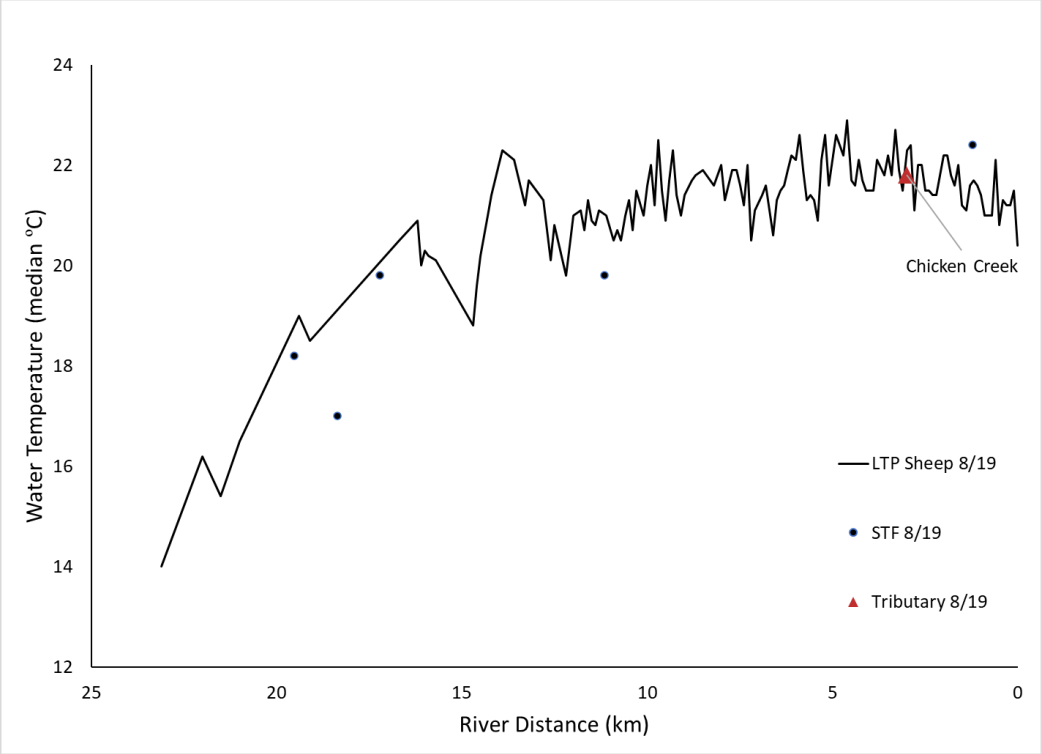

Figure 15: Plot showing the LTP, tributaries, and STFs entering the main channel, Sheep Creek (August 19)

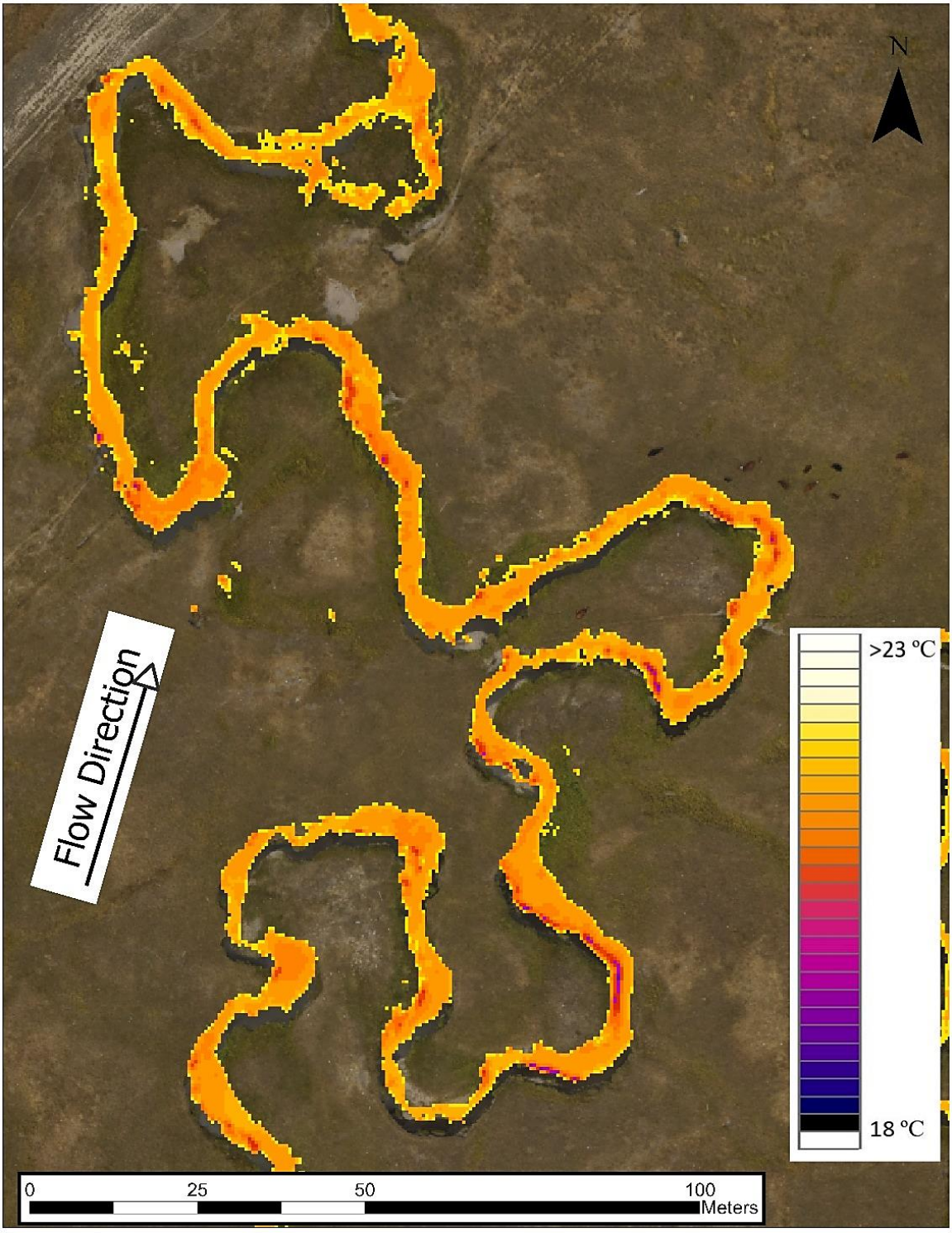

Figure 16: A map showing TIR imagery on true color. This map emphasizes the presence of hyporheic zones along river sections of meandering channels

Fly Creek

A total of 13.7 km of Fly Creek were flown on August 17, 2024, the same time window as the main channel of Grande Ronde. It was not possible to generate a comprehensive LTP plot for Fly Creek due to the heavy vegetation and small active channel, however it provided cold inflow to the Grande Ronde at 22.4 °C where the main channel was 23.6 °C (Figure 17).

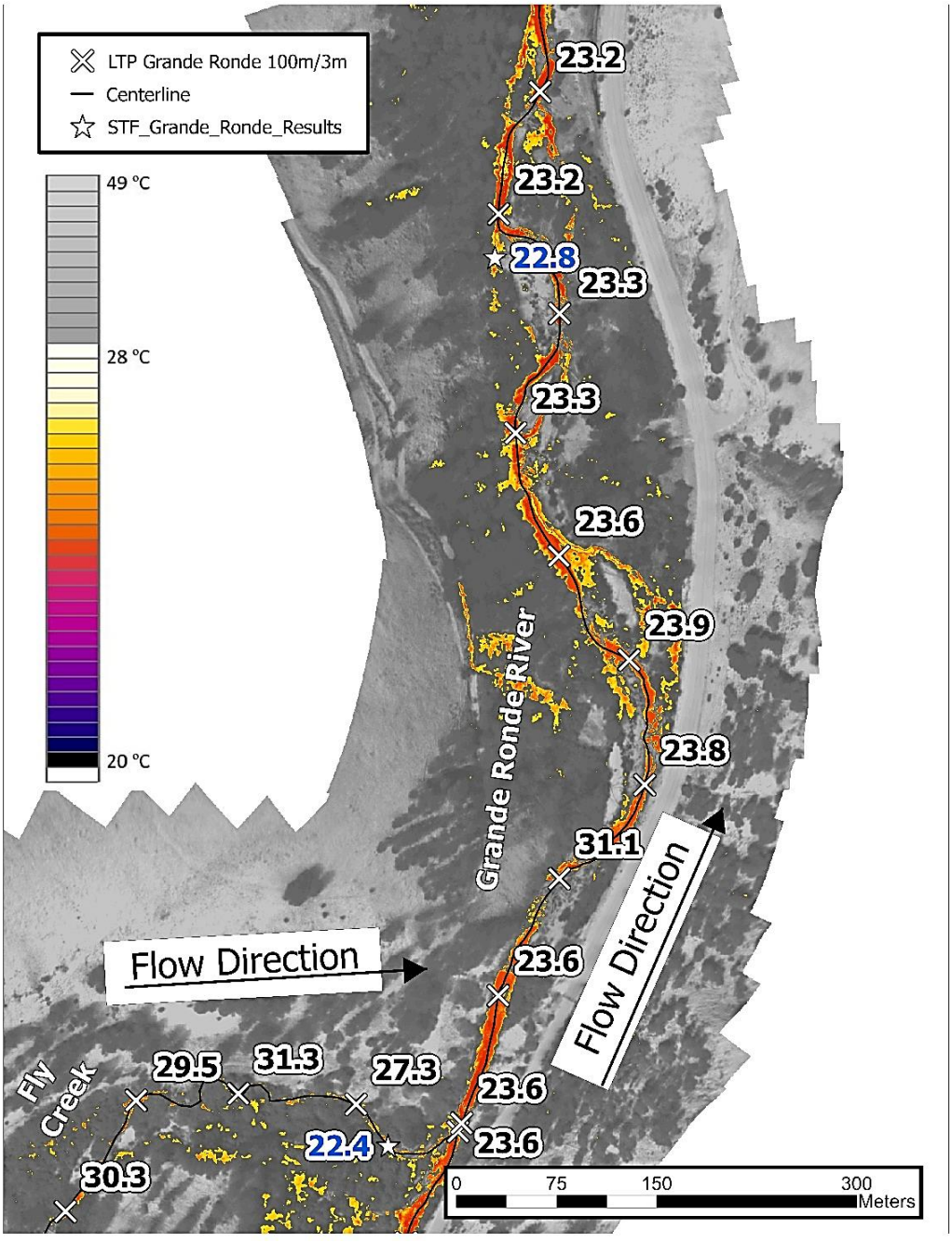

Figure 17: Map showing inflow from Fly Creek to the main channel of Grande Ronde River at 22.4 °C, which is about 1 °C colder

Meadow Creek Basin (Meadow, Wauccup, McCoy, and Dark Canyon creeks)

A total of 46.8 kilometers of Meadow Creek Basin were flown on August 16 and 19, 2024, including Meadow Creek as the main channel with inflows from Wauccup, McCoy, and Dark Canyon Creeks. Over a dozen STFs were identified within the basin varying between hyporheic zones and side channels. The basin is characterized by its meandering channels and wide floodplain allowing for multiple active channels during the summer.

The analysis below focused on data collected on August 16 where the lower section of the river was based on a TIR mosaic that included Dark Canyon Creek (black line in Figure 8). All tributaries in Meadow Creek Basin contributed colder water than the main channel. The majority of the STFs also appeared to have colder thermal signatures across the floodplain. Despite the cold water influences an overall subtle downstream warming was observed along the main channel.

The TIR imagery was processed to generate two mosaics to maintain both the integrity of the thermal imagery and to stay true to the calibration records from water temperature loggers.

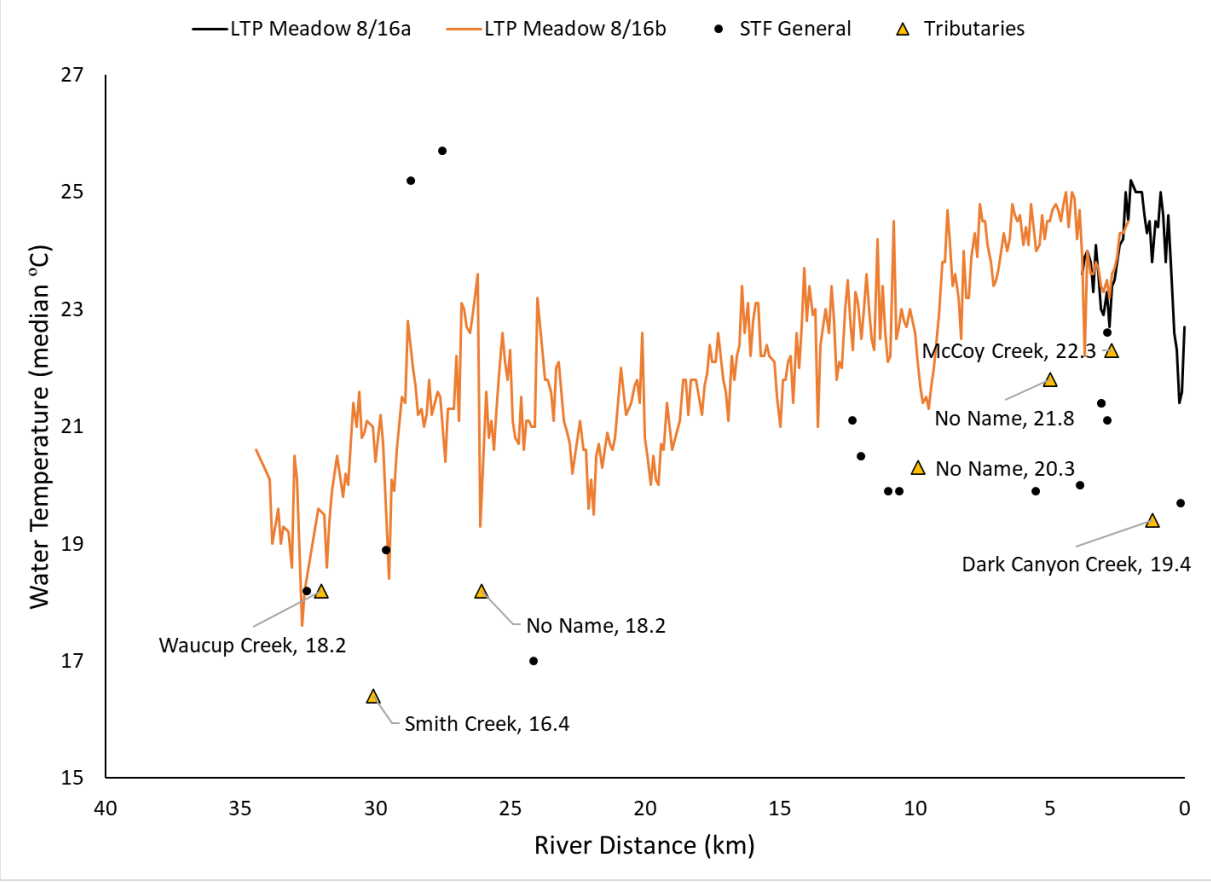

Figure 18: Plot showing the LTP, tributaries, and STFs entering the main channel, Meadow Creek

While it was not possible to generate LTP plots of the tributaries entering Meadow Creek, their thermal imagery can be further investigated by the end user. For example, the TIR data showed that Mccoy Creek's discharge was 1 °C colder than Meadow Creek, at 22.4 °C (Figure 20). Two cold-water sources across the floodplain may be having a cooling influence on McCoy Creek (Figure 19).

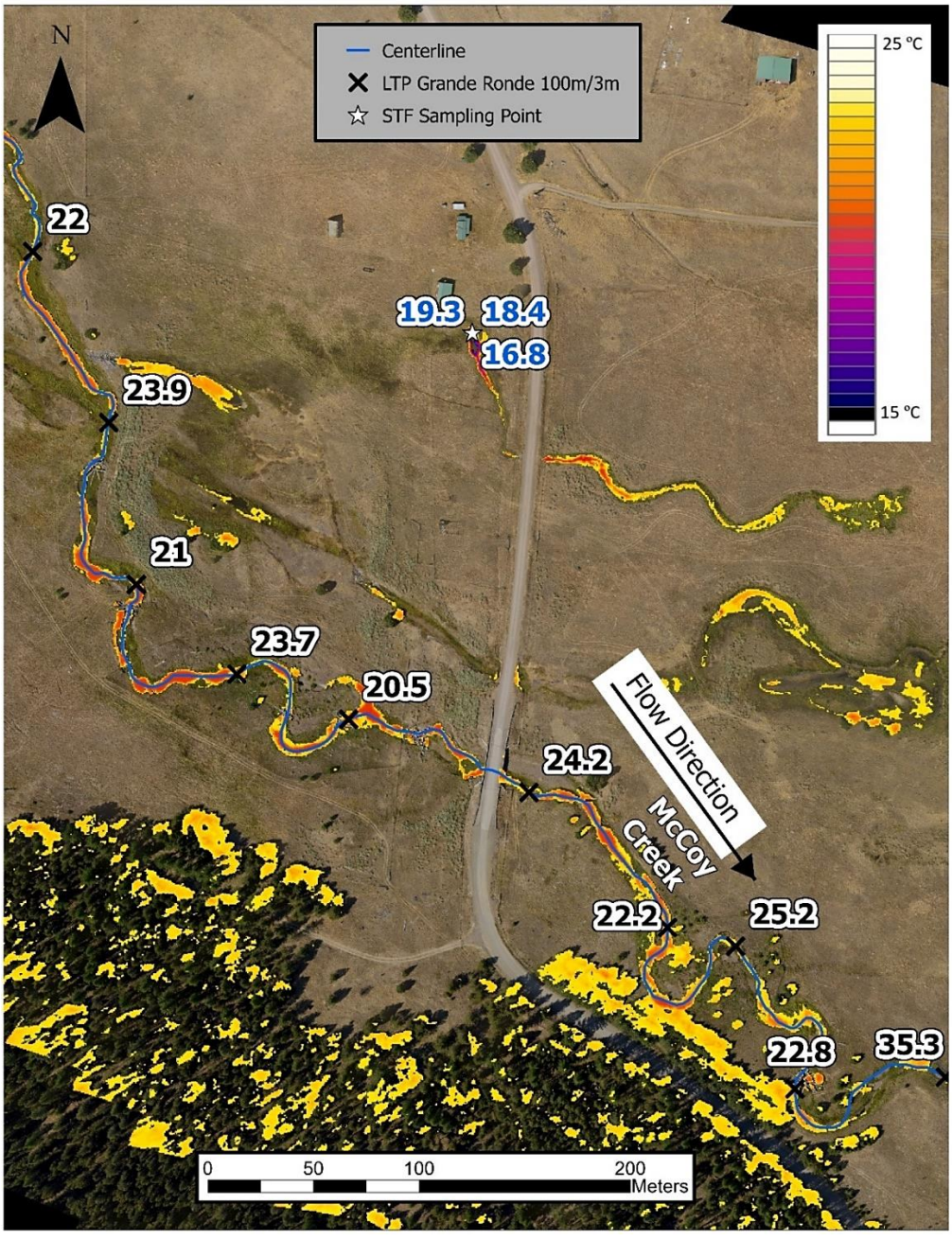

Figure 19: Map showing the thermal signature of the meandering channel across McCoy Creek's floodplain. The map also shows one of the cold-water sources that were identified in this survey.

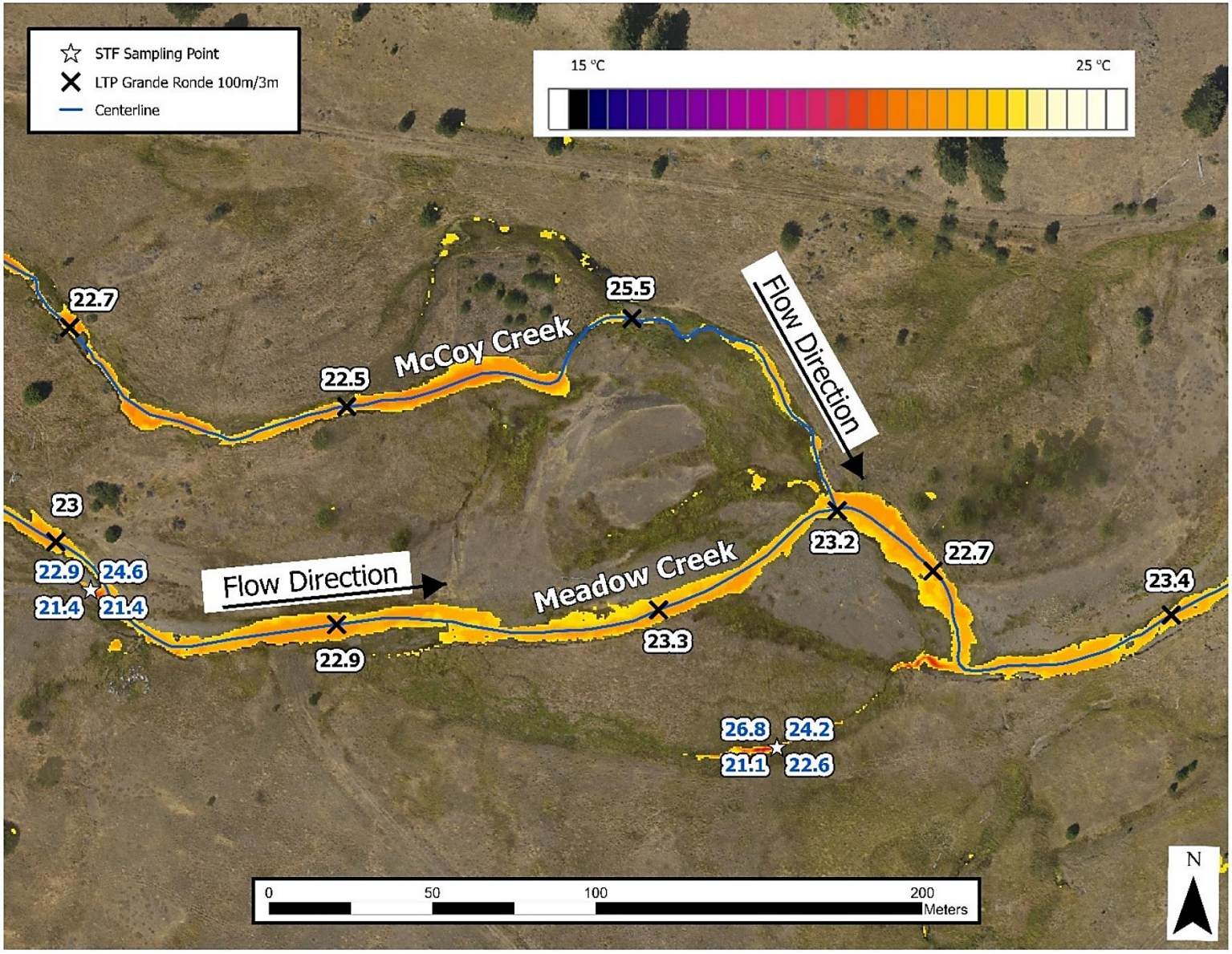

Figure 20: Map of McCoy Creek's confluence with Meadow Creek showing its discharge being 1 °C colder at 22.4 °C

Beaver Creek

A total length of 10.1 km of Beaver Creek was covered on August 17, 2024, from the confluence with Grande Ronde to its headwaters. The TIR data were sampled for LTP at 100-meter intervals and a total of four STFs were identified as hyporheic zones or side channels. The LTP analysis showed downstream warming from nearly 20 °C at the headwaters to 25 °C at the confluence. The STFs varied between colder and warmer than the active channel (Figure 21).

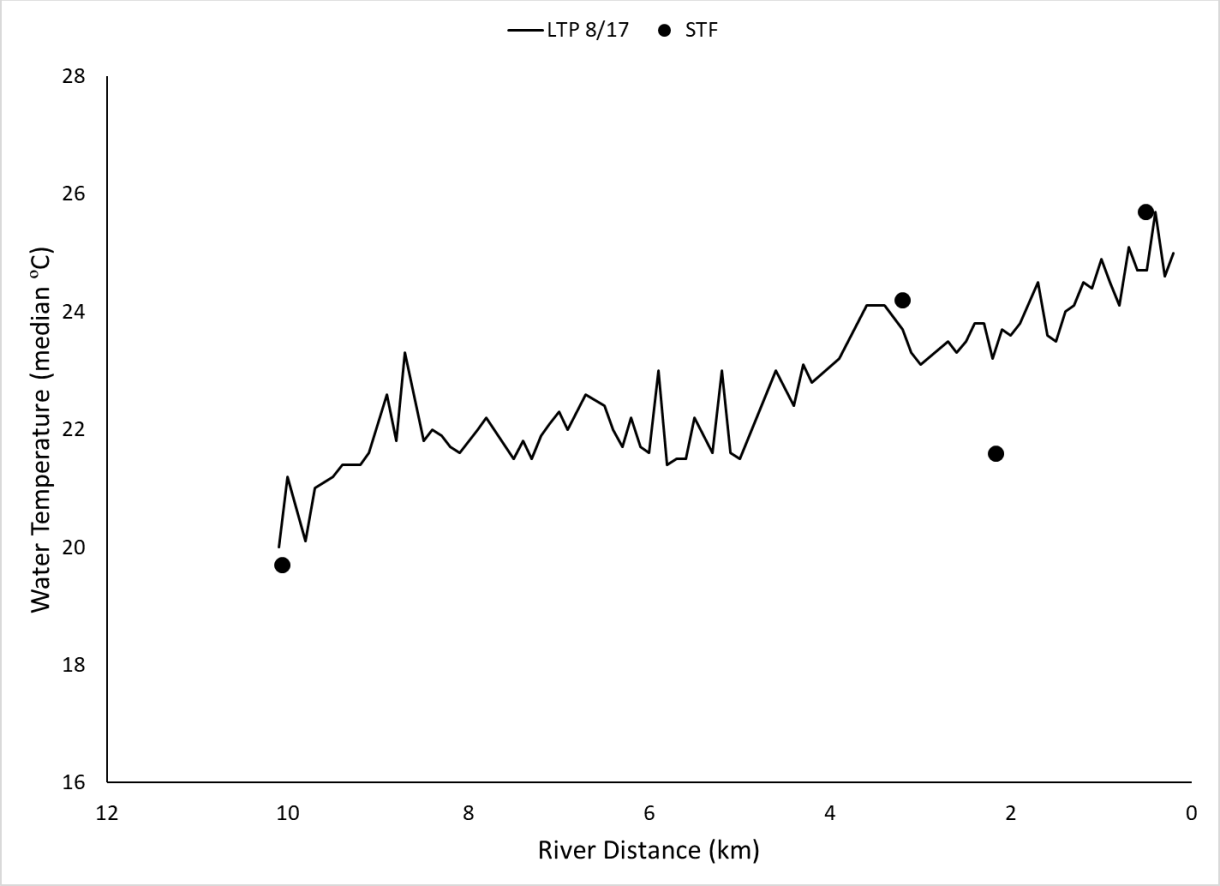

Figure 21: Plot showing the LTP and STFs for Beaver Creek where a downstream warming gradient was present and STFs varied in temperature relative to the active channel.

Spring Creek, Rock Creek, and Five Point Creek

All three tributaries of the Grande Ronde were collected on August 17, 2024, covering a total length of 29.5 km. While it was possible to locate the confluence of the tributaries with the main channel Grande Ronde, it was not possible to sample the entire length of the tributaries or to generate useful LTP plots due to the narrow channel and overhanging vegetation. For example, Five Points Creek contributed cold-water (blue labels) flowing into Grande Ronde (black labels) in Figure 22. Each LTP/STF point was sampled three times from their respective mosaics.

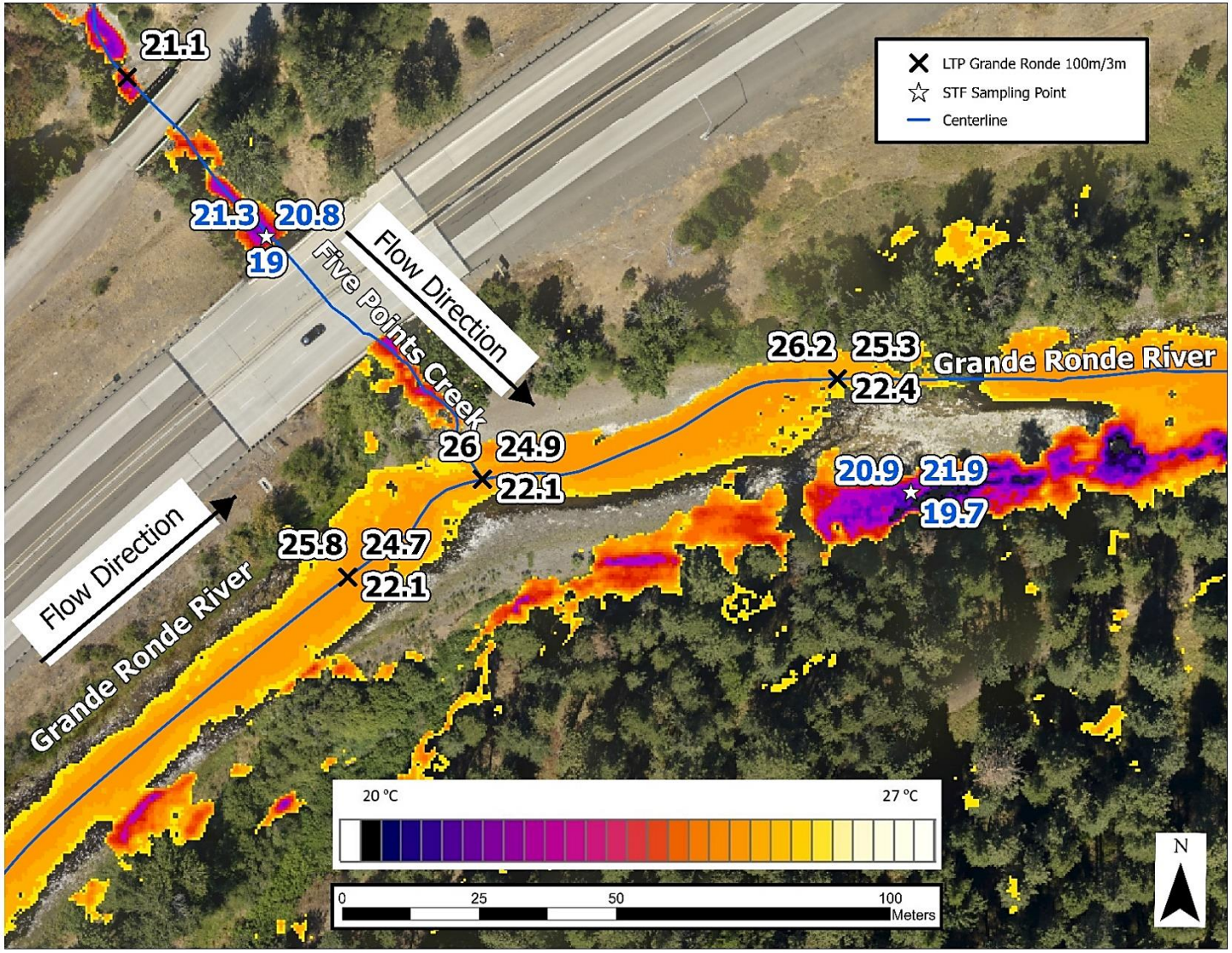

Figure 22: Map of the TIR layer overlayed on top of RGB (co-acquired) showing Five Points Creek flowing into the Grande Ronde River providing it with colder water (blue labels). The map also shows a potential hyporheic zone on the right bank sand bar of Grande Ronde (blue labels).

State Ditch of Grande Ronde

A total length of 7.4 km of a state ditch flowing into the Grande Ronde was covered on August 16, 2024. It was sampled for LTP and showed a temperature range of approximately 24-26 °C(Figure 23). No STFs were identified.

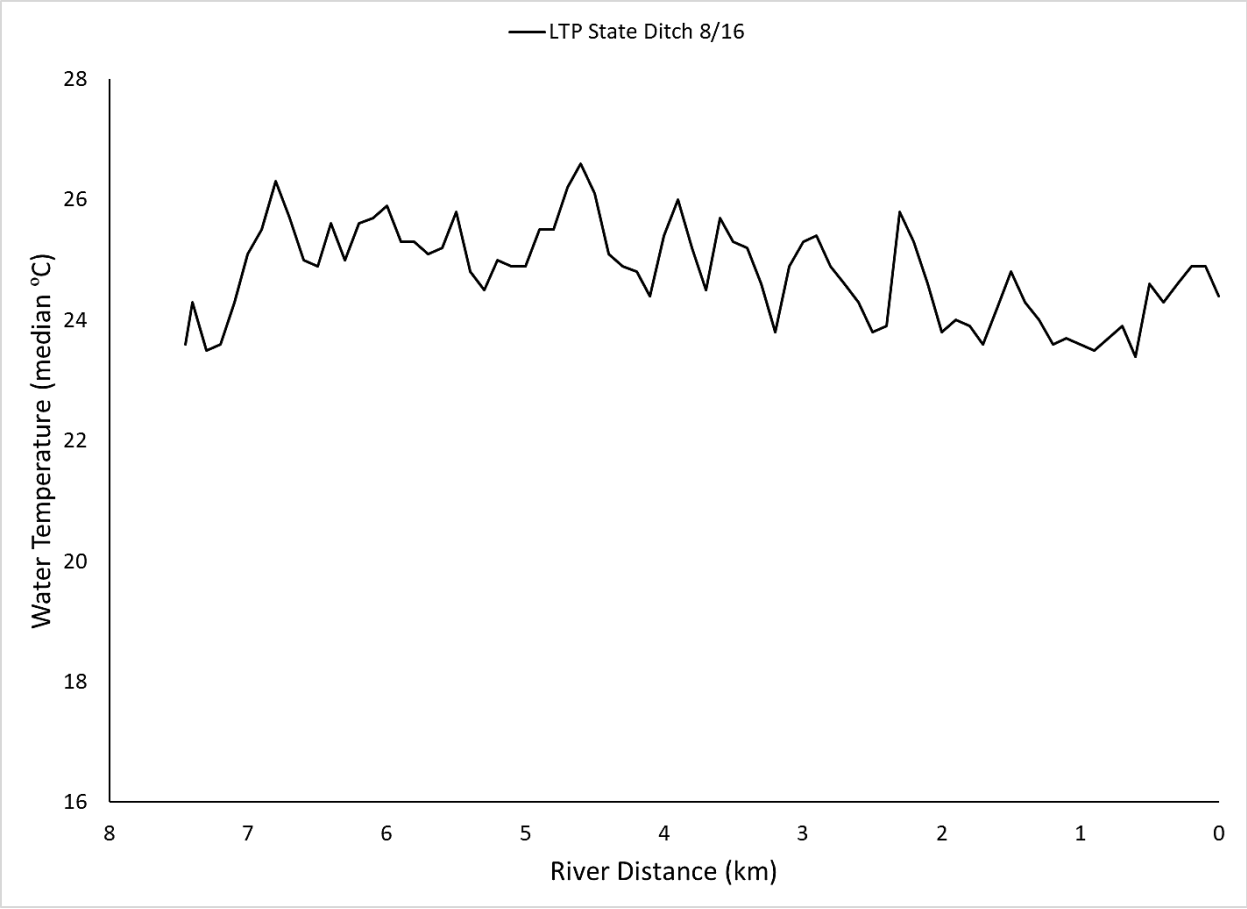

Figure 23: LTP plot profile for State Ditch flowing into the Grande ronde.

Lookingglass and Little Lookingglass

A total of 16.8 km and 2.4 km of Lookingglass and Little Lookingglass creeks, respectively, were flown on August 18, 2024. Their centerlines were digitized and sampled at 100-meter intervals to generate the LTP. Along the main channel, Lookingglass, one STF of a side channel and two tributaries were identified (Summer Creek and Little Lookingglass), sampled, and plotted in Figure 24. One tributary, Mottet Creek, was found to flow into Little Lookingglass Creek. Due to the narrow channel and low discharge of Little Lookingglass, the plot may not be as informative compared to that for the main channel of Lookingglass. The TIR data showed an overall warming gradient along Lookingglass Creek (from 8 °C to 16 °C) which stabilizes towards the last 4-kilometer stretch. An example of Little Lookingglass Creek's confluence with Lookingglass Creek is shown in Figure 25.

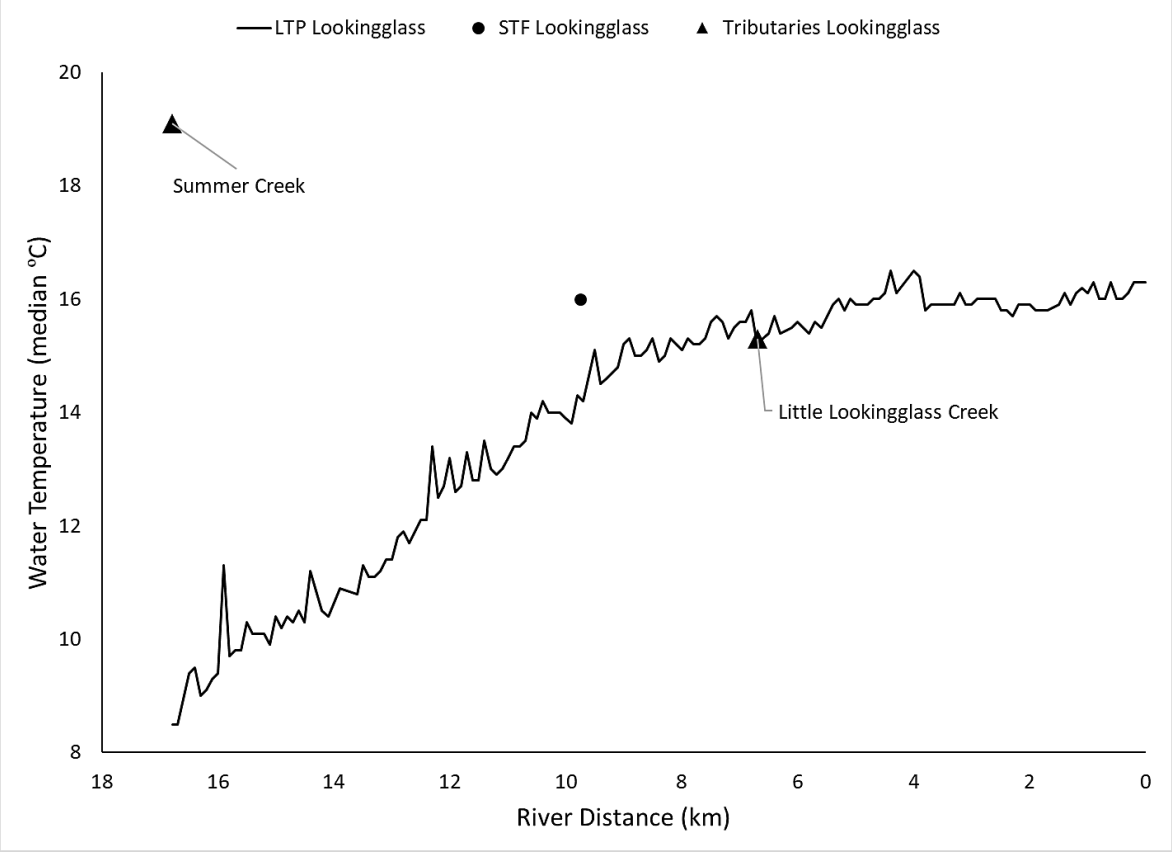

Figure 24: Plot showing the LTP, tributaries, and STFs entering the main channel, Lookingglass Creek. The plot was prepared using the median values of the sampled pixels in the thermal mosaic.

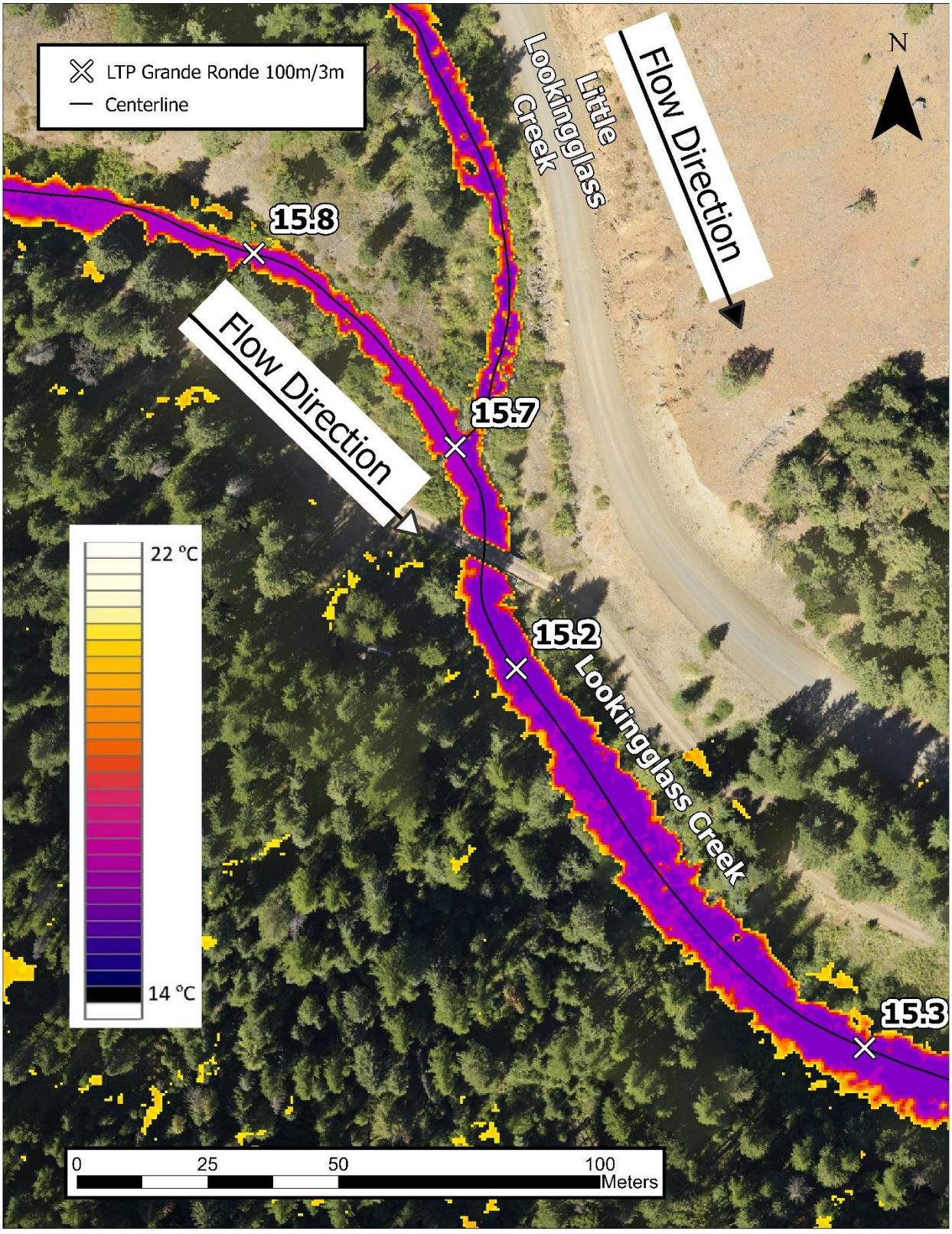

Figure 25: Map of the TIR layer overlayed on top of RGB (co-acquired) showing the confluence of Lookingglass and Little Lookingglass Creek.

Indian and Little Indian

A total of 13.7 km and 0.6 km of Indian and Little Indian Creek, respectively, were flown on August 17, 024, and their centerlines were digitized and sampled at 100-meter intervals to generate the LTP. Along the main channel, Indian, two tributaries were identified, Little Indian and North Fork Indian Creeks; they both were sampled and plotted in Figure 26. Due to the narrow channel and low discharge of Little Indian Creek, the plot may not be as informative compared to that for the main channel of Indian Creek. Therefore, the following analysis focuses on the main channel. The data shows an overall downstream warming gradient, from 17 °C to 24 °C. While North Fork Indian Creek provided cold water to the main channel, Little Indian Creek contributed relatively warm water.

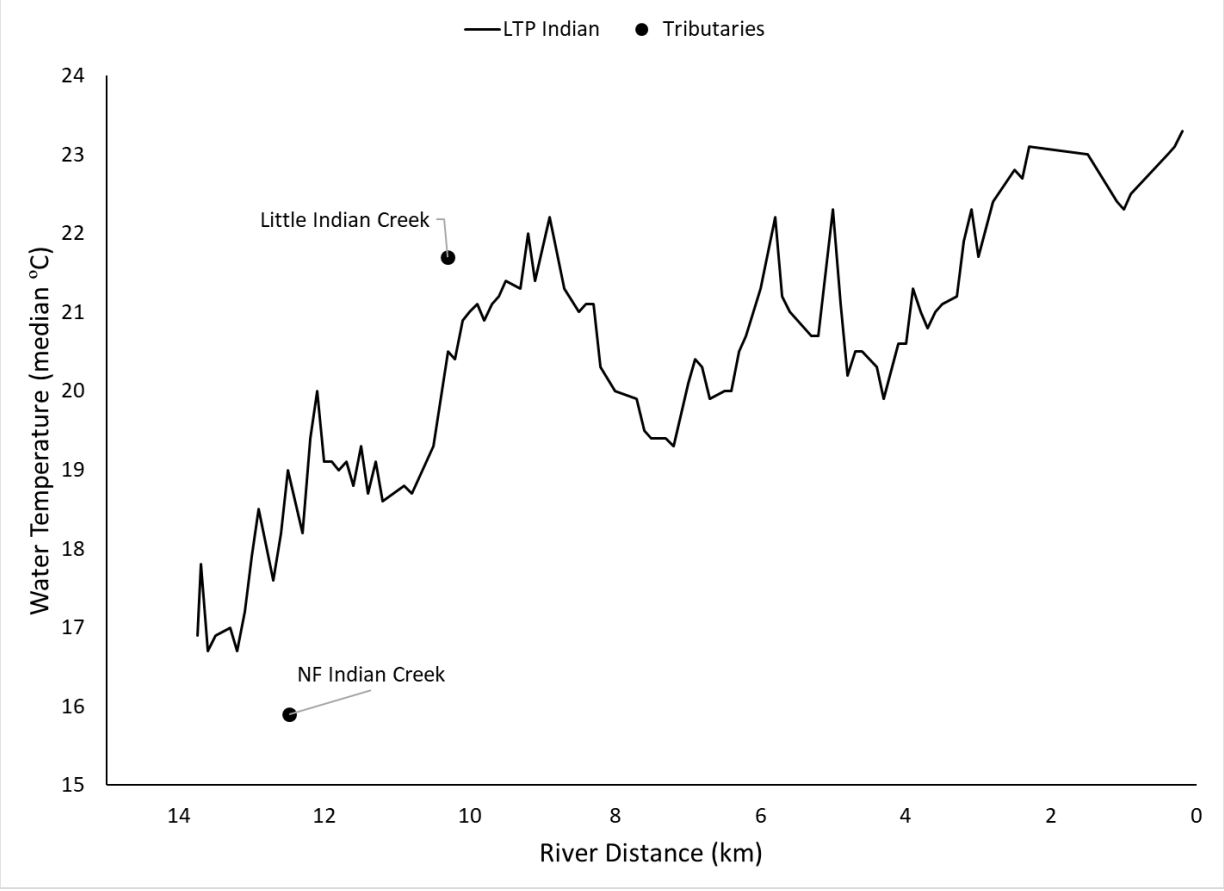

Figure 26: Plot showing the LTP and the tributaries entering the main channel, Indian Creek.

Catherine Creek Basin (Catherine, Little Catherine, Little, North Fork, South Fork, and Mild)

A total of 71.7 km of river in the Catherine Creek basin were flown on August 16, 2024; their centerlines were digitized and sampled at 100-meter intervals to generate the LTP. The main channel of Catherine Creek is formed by the discharge from both of its North Fork and the South Fork. At that point, the water temperature was nearly 14 °C and warms rapidly to 18 °C within the course of 10 km distance. At river km 24 the water temperature increased from 14 °C to 18 °C. Both Milk Creek and Little Catherine discharged cold water and brought the temperature of the main channel down a few degrees. The water in the main channel, Catherine Creek, then resumes its downstream warming gradient for the remaining 20 km (Figure 27).

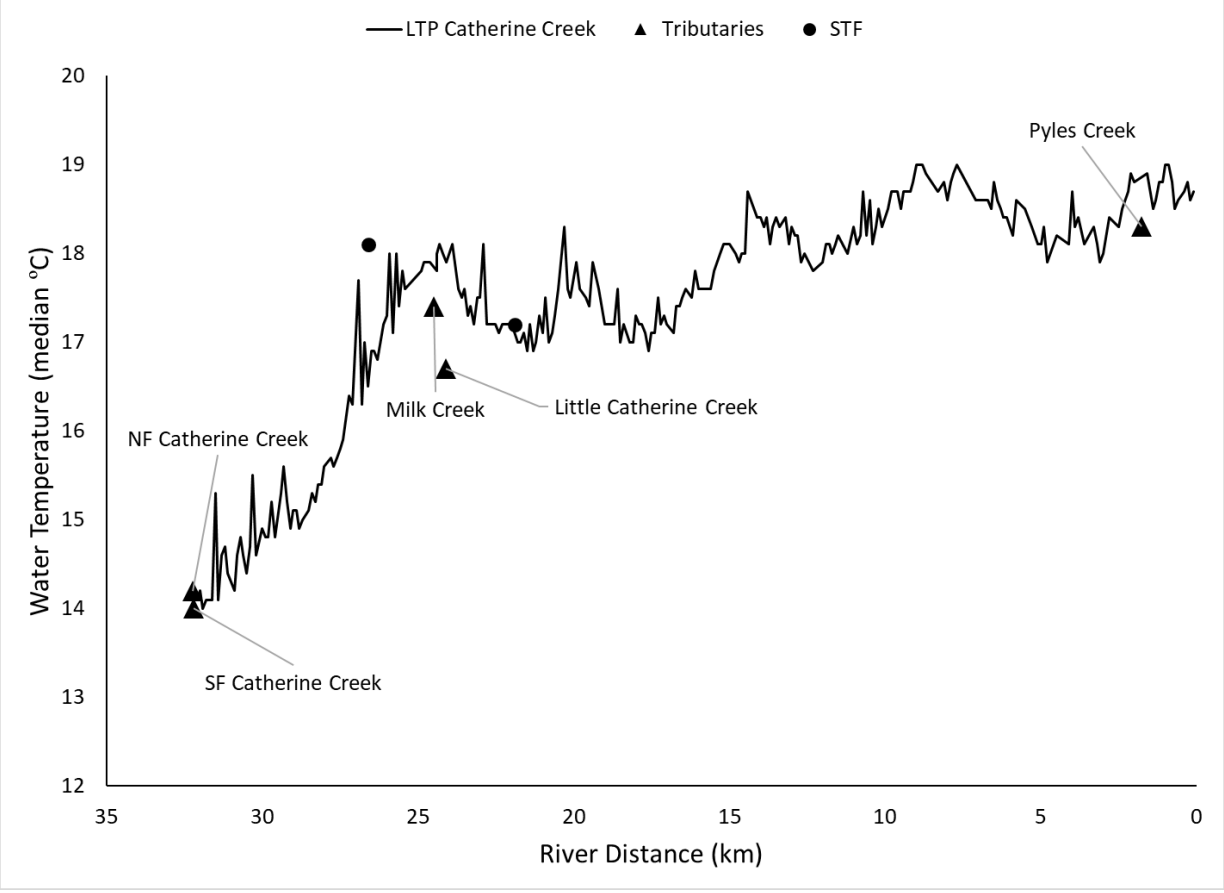

Figure 27: Plot showing the LTP, STFs, and the tributaries entering the main channel, Catherine Creek. Both the North Fork and the South Fork Catherine Creek provide cold-water discharge to the main channel.

Minam River and Little Minam Creek

A total of 74.6 km and 8.9 km of Minam and Little Minam Creeks, respectively, were flown and their centerlines were digitized and sampled at 100-meter intervals to generate the LTP. Along the main channel, Minam, a total of three significant thermal features and over 20 tributaries (including Little Minam) were identified, sampled, and plotted in Figure 28 and Figure 29.

Minam River followed the theme of downstream warming gradient with temperature rising from 14 °C at the headwaters to over 24 °C at the mouth. This occurred despite the presence of several -cold water tributaries along the channel. Most of the side channels also appeared to be colder than the main channel. Some tributaries were colder or had higher discharge than others leading to localized sections of cooling and warming or at least a reduced rate of warming. The data showed that the last 10-kilometer stretch retained stable temperatures.

Despite a short flowing distance of 9 km, Little Minam Creek warmed from 16 °C to 19 °C; however it still contributed relatively cool water to Minam river (Figure 28 through Figure 30).

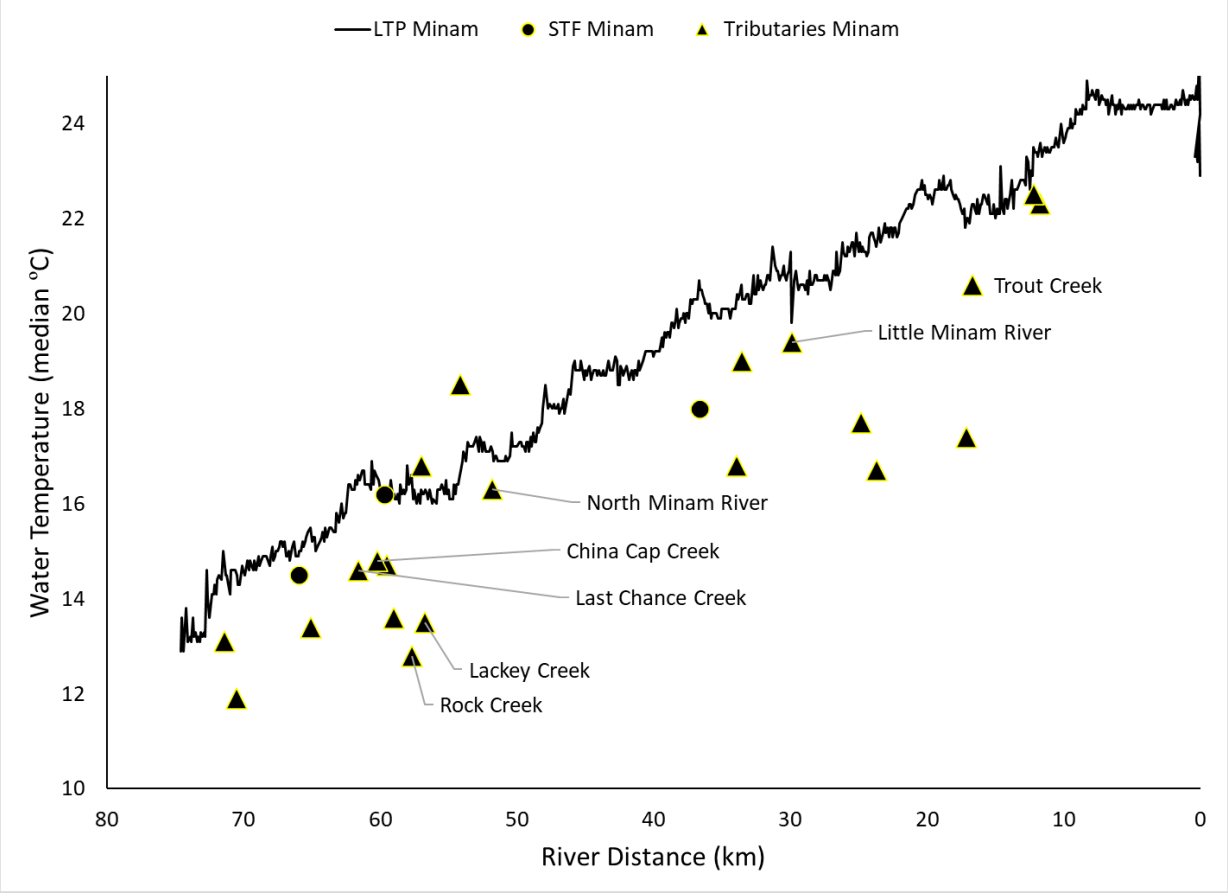

Figure 28: Plot showing the LTP, tributaries, and STFs entering the main channel, Minam River. The plot was prepared using the median values of the sampled pixels of the thermal mosaic.

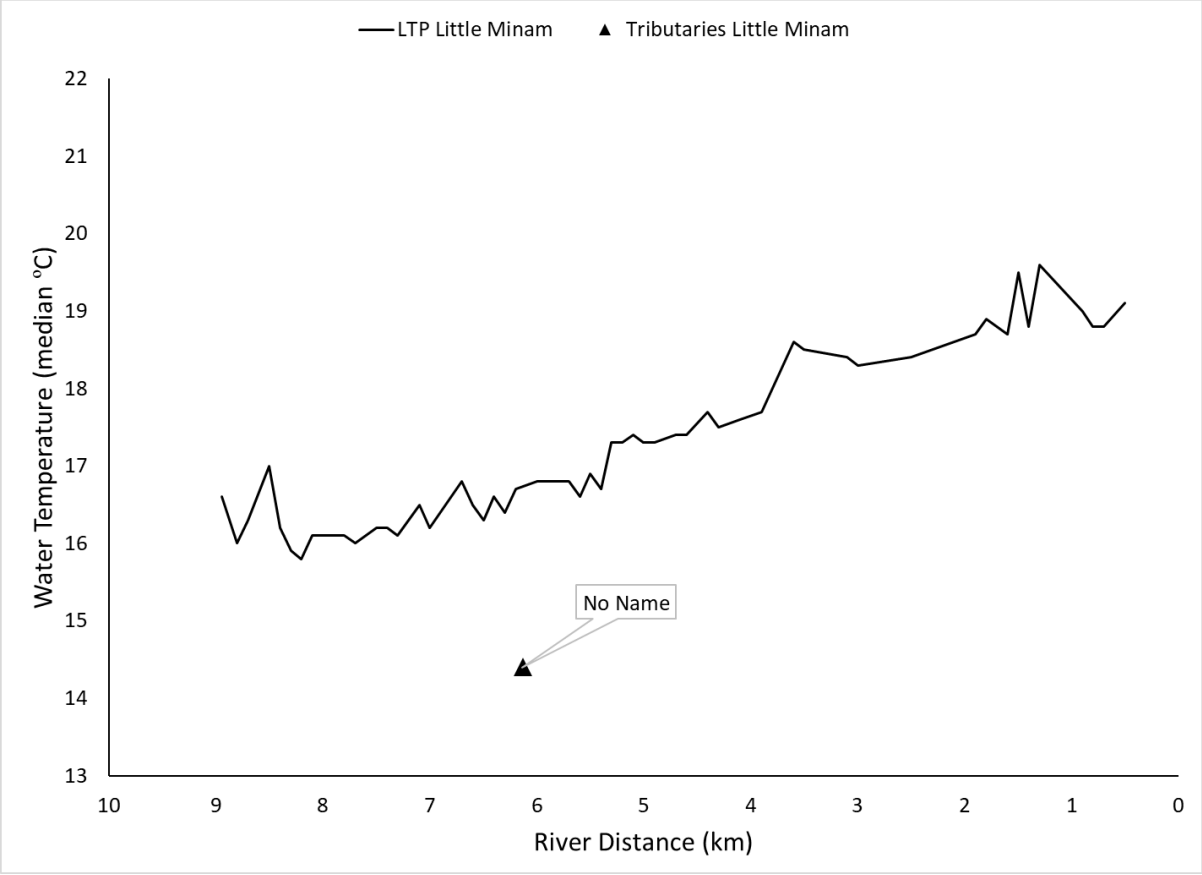

Figure 29: Plot showing the LTP, tributaries, and STFs entering the main channel, Little Minam Creek. The plot was prepared using the median values of the sampled pixels of the thermal mosaic.

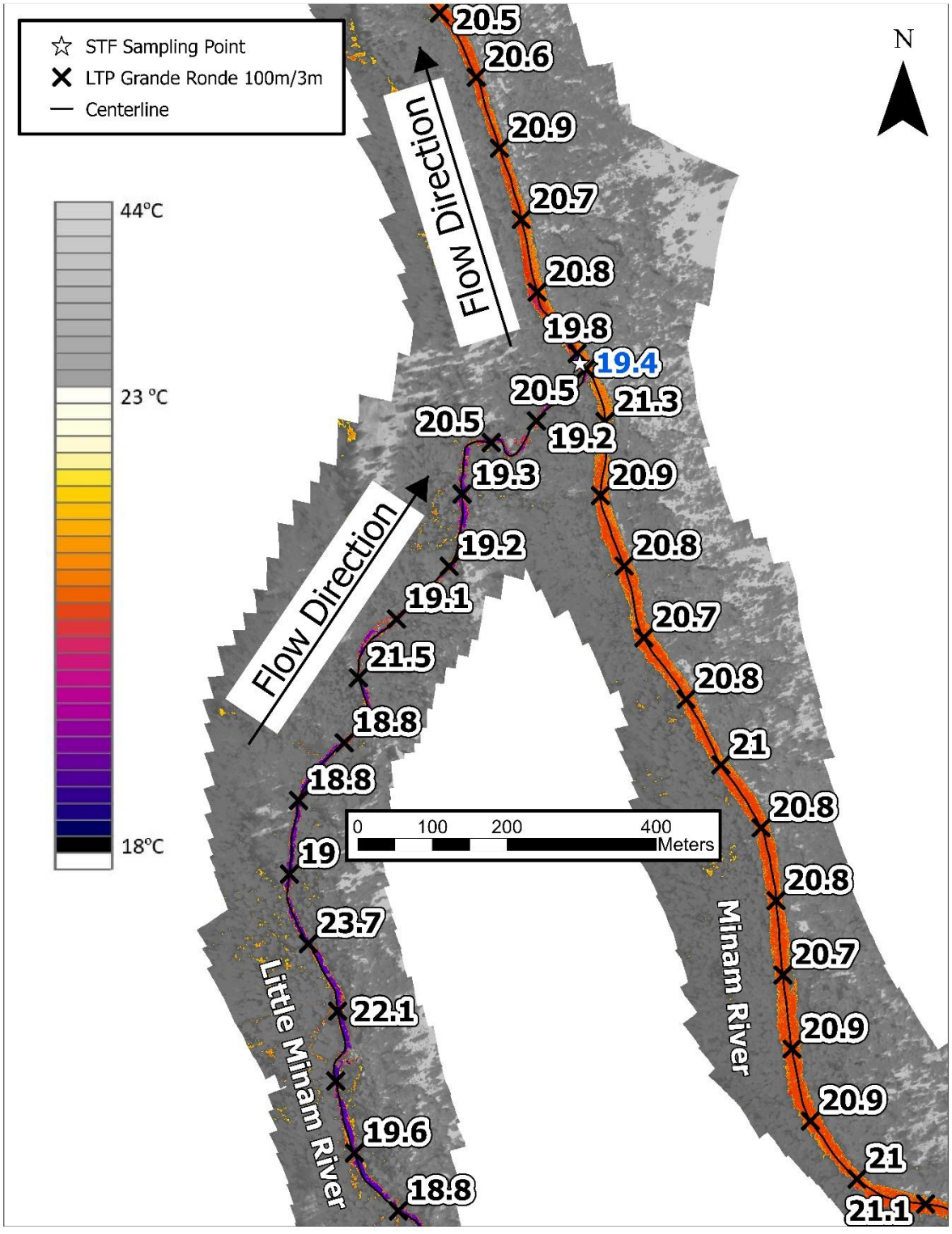

Figure 30: TIR map depicting sampled LTPs showing Little Minam Creek's colder discharge into the main channel Minam River.

Bear Creek

A total of 21.9 km of Bear Creek was flown on August 18, 2024, and the centerlines digitized and sampled at 100-meter intervals to generate the LTP. Four significant thermal features were identified, sampled, and plotted in Figure 31, but there were no identifiable tributaries. The TIR data showed a gradual downstream warming from 12 °C to 21 °C. The headwaters temperatures indicated that of potential groundwater or spring sources at 12 °C.

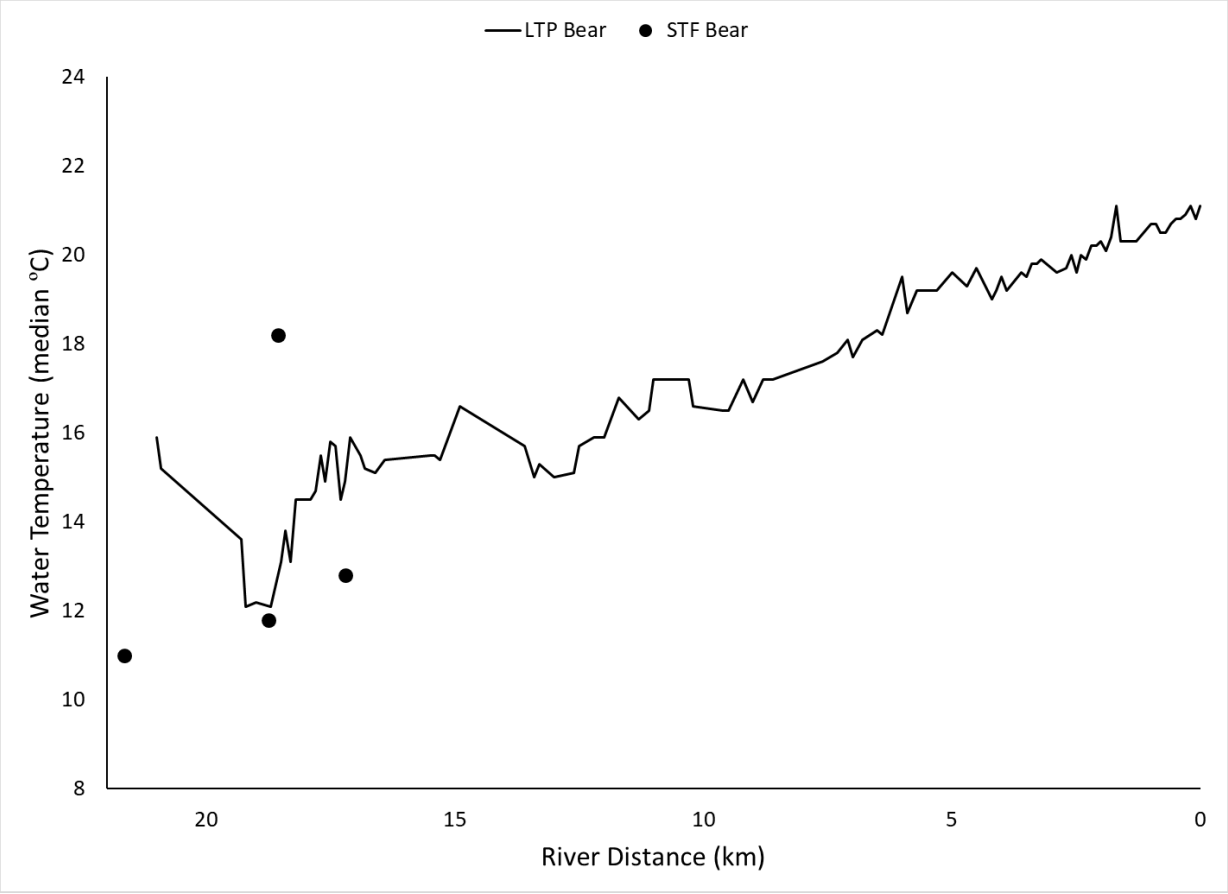

Figure 31: Plot showing the LTP and STFs entering the main channel, Bear Creek. The plot was prepared using the median values of the sampled pixels of the thermal mosaic.

Wallowa River, Hurricane Creek, and Lostine River

A total of 120.1 km was collected on August 18, 2024, covering 69.7 km of Wallowa River, 6.6 km of Hurricane Creek, and 43.8 km of Lostine River. Their centerlines were digitized and sampled at 100-meter intervals to generate the LTP. Along the main channel, Wallowa, a total of four significant thermal features and seven tributaries (including Hurricane) were identified, sampled, and plotted (Figure 32). The same was done for Lostine River where one significant thermal feature and 12 tributaries were identified (Figure 33 and Figure 34). Sampling Hurricane Creek was not successful due to the channel's low flow and dense canopy, nevertheless, it was possible to sample it above the confluence with Wallowa River.

Wallowa River's TIR data showed a steady warming gradient as the water flowed downstream with cold- and warm-water inflows from the identified tributaries. Such tributaries showed localized cooling or warming sections of the main channel, respectively. There were also relatively small unnamed tributaries providing warmer water than the main channel, having minimal impact. The LTP along the uppermost section of the river showed warmer temperatures with higher variability, which can be due to low flows and dense vegetation preventing the sampling algorithm from producing reliable data. However, over the span of the lower 50 km of the river, water temperatures increased from 16 °C to 22 °C.

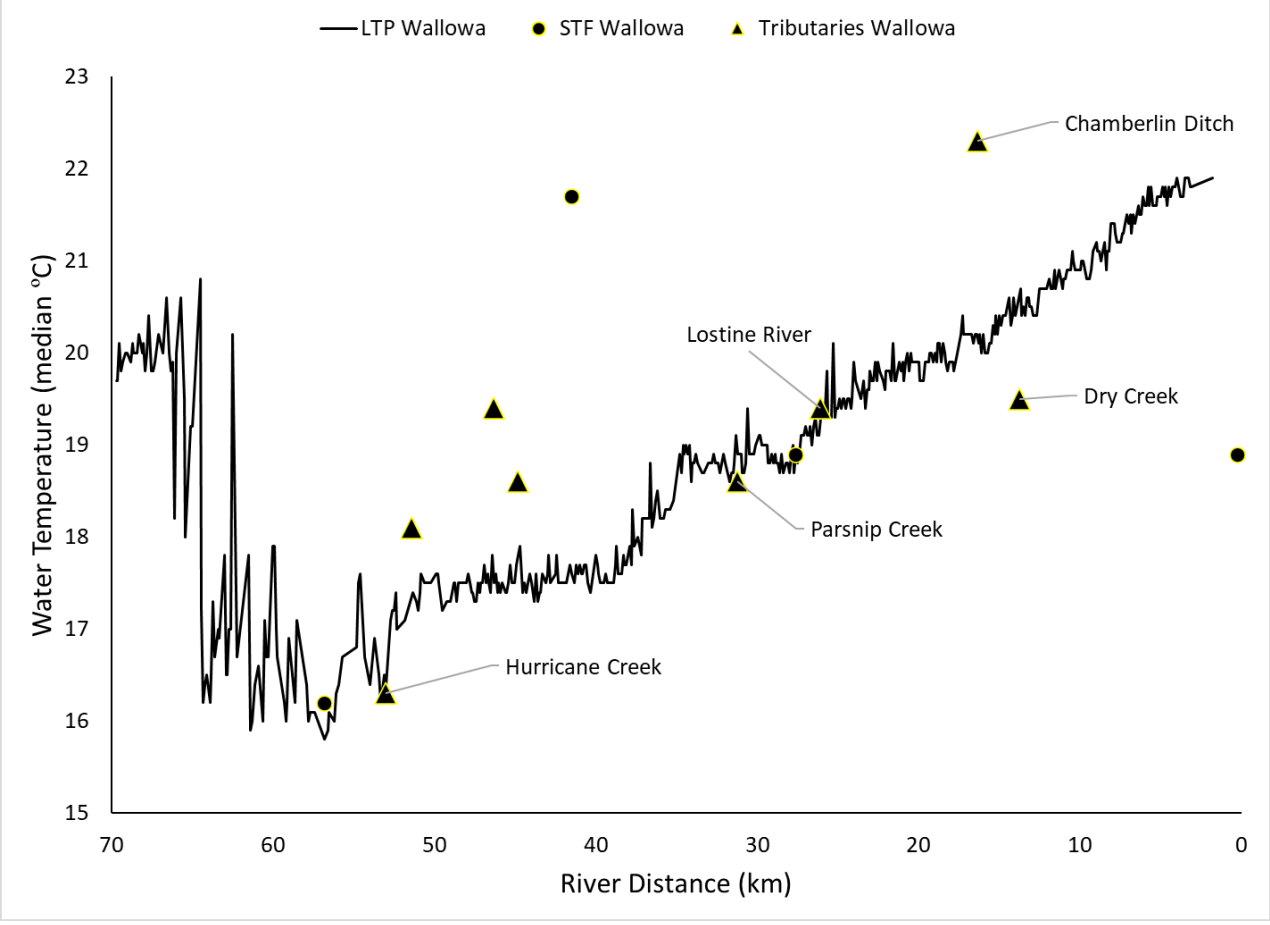

Figure 32: Plot showing the LTP, tributaries, and STFs entering the main channel, Wallowa River. The plot was prepared using the median values of the sampled pixels of the thermal mosaic.

Lostine River was characterized by alternating downstream warming and cooling sections. Its headwaters begin with cold water temperatures indicative of groundwater influence. It then warms from 12 °C to 15 °C before it cools again around km 25 where inflows from Lake Creek, Storm Creek, Silver Creek, and Bitter Creek discharged cold water into the Lostine River (Figure 33). From km 25 to the mouth there was a warming gradient in the LTP reaching just over 18 °C at the mouth.

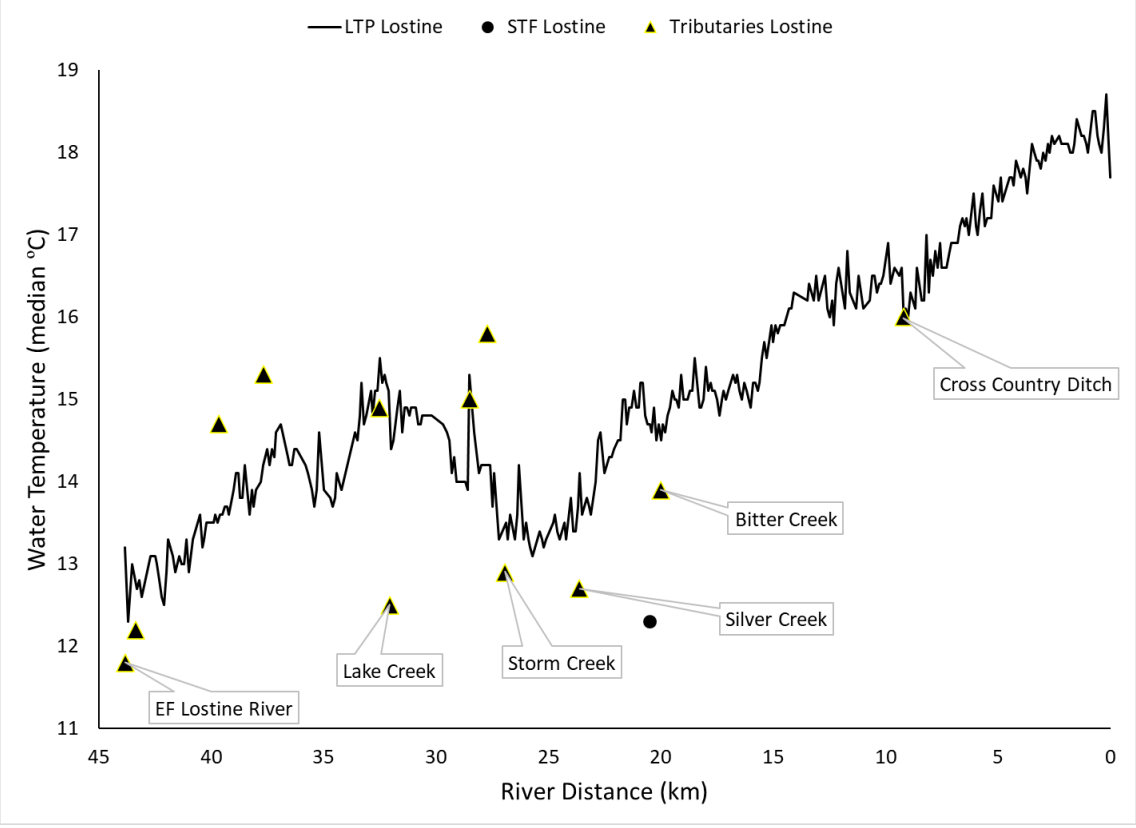

Figure 33: Plot showing the LTP, tributaries, and STFs entering the main channel, Wallowa River. The plot was prepared using the median values of the sampled pixels of the thermal mosaic.

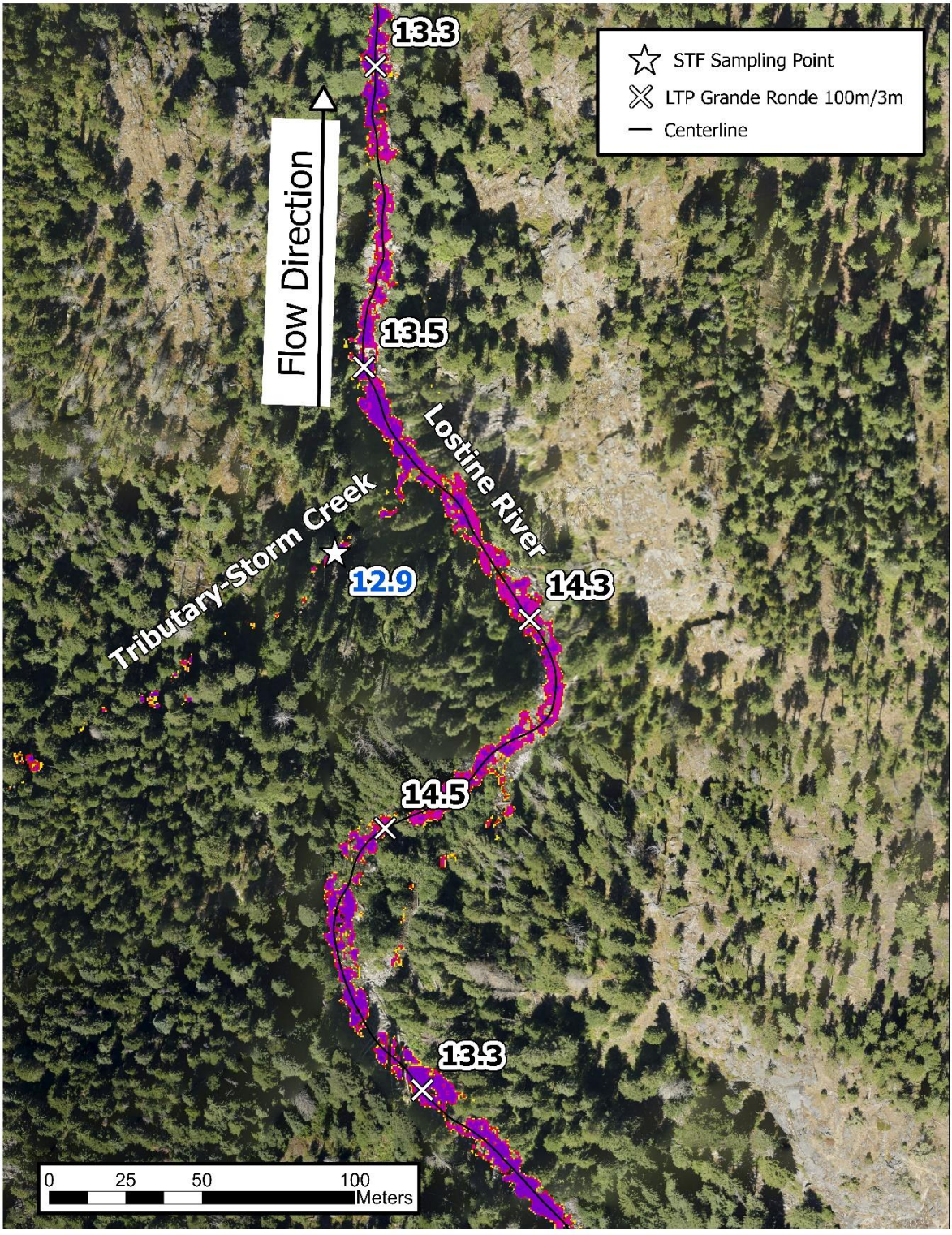

Figure 34: Combined RGB and TIR map depicting sampled LTPs, showing the tributary (Storm Creek) at the 26.94 river km, contributing colder water than the main channel Lostine River.

APPENDIX A - SIGNIFICANT THERMAL FEATURES

The following table details temperature statistics for significant thermal features (STFs) for the named tributaries along the Grande Ronde River project.

Stream Name	Tributary	River (km)[3]	Mean (°C)[4]	Median (°C)[5]	Min (°C)[6]	Max (°C)[7]	Standard Deviation (°C)[8]
Tributary- Pyles Creek	Catherine Creek	1.78	18.3	18.3	18.2	18.4	0.060
Tributary- Little Catherine Creek	Catherine Creek	24.10	16.7	16.7	16.6	16.9	0.073
Tributary- Milk Creek	Catherine Creek	24.50	17.4	17.4	17.1	18.0	0.244
Tributary- SF Catherine Creek	Catherine Creek	32.20	14.0	14.0	14.0	14.0	0.000
Tributary- North Fork Catherine Creek	Catherine Creek	32.24	14.2	14.2	14.1	14.2	0.042
Tributary- West Chicken Creek	Chicken Creek	7.30	19.0	19.1	17.2	20.7	1.054
Tributary- Five Points Creek	Grande Ronde River	25.10	20.8	20.7	20.6	21.1	0.150
Tributary- Five Points Creek	Grande Ronde River	25.10	19.0	19.0	18.9	19.2	0.090
Tributary- Five Points Creek	Grande Ronde River	25.10	21.6	21.5	21.5	21.7	0.064
Tributary- Five Points Creek	Grande Ronde River	25.10	20.8	20.8	20.6	21.2	0.159
Tributary- Five Points Creek	Grande Ronde River	25.10	19.0	19.0	18.9	19.2	0.088
Tributary- Five Points Creek	Grande Ronde River	25.10	21.3	21.3	21.1	21.6	0.161

[3] River distance (km) along the digitized centerline that is closest to the STF location
[4] Mean temperature (ºC) of sampled pixels of the TIR mosaic inside the buffered area of STF sampling point
[5] Median temperature (ºC) of sampled pixels of the TIR mosaic inside the buffered area of STF sampling point
[6] Minimum temperature (ºC) of sampled pixels of the TIR mosaic inside the buffered area of STF sampling point
[7] Maximum temperature (ºC) of sampled pixels of the TIR mosaic inside the buffered area of STF sampling point
[8] Standard deviation temperature (ºC) of sampled pixels of the TIR mosaic inside the buffered area of STF sampling point

Stream Name	Tributary	River (km)[3]	Mean (°C)[4]	Median (°C)[5]	Min (°C)[6]	Max (°C)[7]	Standard Deviation (°C)[8]
Tributary- Rock Creek	Grande Ronde River	25.70	23.7	23.6	23.4	24.2	0.206
Tributary- Rock Creek	Grande Ronde River	25.70	27.7	27.2	26.1	30.3	1.442
Tributary- Rock Creek	Grande Ronde River	25.70	27.2	27.1	26.5	28.0	0.446
Tributary- Spring Creek	Grande Ronde River	32.00	24.3	24.3	23.8	24.9	0.372
Tributary- Spring Creek	Grande Ronde River	32.00	21.6	21.5	20.9	22.4	0.427
Tributary- Spring Creek	Grande Ronde River	32.00	24.9	25.0	24.1	25.6	0.499
Tributary- Waucup Creek	Grande Ronde River	32.00	17.9	17.9	17.8	18.2	0.124
Tributary- Beaver Creek	Grande Ronde River	46.11	22.6	22.5	22.4	22.7	0.101
Tributary- Meadow Creek	Grande Ronde River	48.75	21.3	21.3	21.2	21.3	0.046
Tributary- Meadow Creek	Grande Ronde River	48.75	23.3	23.3	23.2	23.4	0.062
Tributary- Meadow Creek	Grande Ronde River	48.75	21.8	21.8	21.7	21.9	0.061
Tributary- Fly Creek	Grande Ronde River	56.70	22.4	22.4	22.2	23.0	0.198
Tributary- Sheep Creek	Grande Ronde River	73.00	22.5	22.5	22.4	22.5	0.049
Tributary- Limber Jim Creek	Grande Ronde River	79.10	18.7	18.6	18.4	19.1	0.199
Tributary- Clear Creek	Grande Ronde River	84.10	16.3	16.2	15.9	17.2	0.323
Tributary- Little Indian Creek	Indian Creek	10.30	21.9	21.7	21.6	22.4	0.222
Tributary- North Fork Indian Creek	Indian Creek	12.49	16.1	15.9	15.4	17.9	0.716
Tributary- Little Creek	Little Creek	0.01	19.6	19.5	19.3	19.8	0.167

Stream Name	Tributary	River (km)[3]	Mean (°C)[4]	Median (°C)[5]	Min (°C)[6]	Max (°C)[7]	Standard Deviation (°C)[8]
Tributary- Mottet Creek	Little Lookingglass Creek	2.43	14.2	14.1	13.9	15.6	0.457
Tributary- Little Lookingglass Creek	Lookingglass Creek	6.70	15.3	15.3	15.2	15.4	0.058
Tributary- Summer Creek	Lookingglass Creek	16.78	19.3	19.1	18.6	20.0	0.442
Tributary- Cross Country Ditch	Lostine River	9.22	16.0	16.0	15.9	16.1	0.055
Tributary- Bitter Creek	Lostine River	20.01	13.9	13.9	13.7	14.0	0.083
Tributary- Silver Creek	Lostine River	23.64	13.1	12.7	12.6	14.1	0.504
Tributary- Storm Creek	Lostine River	26.94	13.2	12.9	12.4	14.6	0.641
Tributary- Lake Creek	Lostine River	32.07	12.5	12.5	12.4	12.8	0.113
Tributary- EF Lostine River	Lostine River	43.82	11.8	11.8	11.6	12.0	0.121
Tributary- Dark Canyon Creek	Meadow Creek	1.20	20.0	20.0	19.9	20.5	0.164
Tributary- Dark Canyon Creek	Meadow Creek	1.20	19.6	19.4	19.4	20.3	0.286
Tributary- McCoy Creek	Meadow Creek	2.70	22.3	22.3	22.0	22.5	0.146
Tributary- McCoy Creek	Meadow Creek	2.70	26.6	26.6	26.1	27.0	0.282
Tributary- McCoy Creek	Meadow Creek	2.90	25.6	25.6	24.7	26.3	0.527
Tributary- Smith Creek	Meadow Creek	30.06	16.5	16.6	15.2	18.1	1.014
Tributary- Waucup Creek	Meadow Creek	32.00	18.2	18.2	18.1	18.4	0.077
Tributary- Trout Creek	Minam River	16.70	21.0	20.6	20.1	22.3	0.746
Tributary- Little Minam River	Minam River	29.91	19.4	19.4	19.2	19.9	0.213

Stream Name	Tributary	River (km)[3]	Mean (°C)[4]	Median (°C)[5]	Min (°C)[6]	Max (°C)[7]	Standard Deviation (°C)[8]
Tributary- North Minam River	Minam River	51.81	16.3	16.3	16.2	16.4	0.057
Tributary- Lackey Creek	Minam River	56.75	13.5	13.5	13.5	13.6	0.049
Tributary- Rock Creek	Minam River	57.70	13.0	12.8	12.7	14.1	0.388
Tributary- China Cap Creek	Minam River	60.22	14.9	14.8	14.2	16.0	0.521
Tributary- Last Chance Creek	Minam River	61.61	14.6	14.6	14.5	14.7	0.067
Tributary- Chicken Creek	Sheep Creek	3.00	22.3	22.2	22.0	22.6	0.205
Tributary- Chicken Creek	Sheep Creek	3.00	21.8	21.8	21.7	21.9	0.057
Tributary- Pole Creek	South Fork Catherine Creek	9.34	11.6	11.4	11.2	13.0	0.464
Tributary- Sand Pass Creek	South Fork Catherine Creek	10.04	12.1	12.1	11.4	13.1	0.508
Tributary- Dry Creek	Wallowa River	13.74	19.5	19.5	19.4	19.5	0.050
Tributary- Chamberlin Ditch	Wallowa River	16.38	22.3	22.3	21.9	22.6	0.209
Tributary- Lostine River	Wallowa River	26.10	19.4	19.4	19.3	19.4	0.039
Tributary- Parsnip Creek	Wallowa River	31.23	18.6	18.6	18.5	18.6	0.026
Tributary- Cross Country Ditch	Wallowa River	38.78	24.0	24.0	22.7	25.2	0.706
Tributary- Hurricane Creek	Wallowa River	53.00	16.3	16.3	16.2	16.4	0.073

APPENDIX B - SHAPEFILES HEADERS

The following are the header details of the LTP, STF, and Temperature Loggers (Accuracy) shapefiles:

LTP:

Header	Explanation
GNIS_NAME	The river name
Rvr_meas_m	River length (meter) at which temperature was sampled, starting from the downstream end
Rvr_km	River length (km) at which temperature was sampled, starting from the downstream end
Rvr_mile	River length (mile) at which temperature was sampled, starting from the downstream end
Mean	Mean water temperature, a result of 10 sampled points along the centerline within the specified buffer
Median	Median water temperature, a result of 10 sampled points along the centerline within the specified buffer
Min	Minimum water temperature, a result of 10 sampled points along the centerline within the specified buffer
Max	Maximum water temperature, a result of 10 sample points along the centerline within the specified buffer
Std_Dev	Standard deviation water temperature, a result of 10 sampled points along the centerline within the specified buffer

STF:

Header	Explanation
Id	Unused field. It can be used by end user to recategorize points
Notes	Note about the significant thermal feature
Strm_Name	Stream name closest to the location of the significant thermal feature
L_R_Bank	The location of the significant thermal feature, left or right bank, relative to the centerline
M_Off_str	Distance of the significant thermal feature from the closest stream (meter)
Rvr_meas_m	River length (meter) where the significant thermal feature was found, starting from the downstream end
Rvr_km	River length (km) at which temperature was sampled, starting from the downstream end
Rvr_mile	River length (mile) where the significant thermal feature was found, starting from the downstream end
Mean	Mean water temperature at the significant thermal feature, a result of all pixels within the specified buffer
Median	Median water temperature at the significant thermal feature, a result of all pixels within the specified buffer
Min	Minimum water temperature at the significant thermal feature, a result of all pixels within the specified buffer

Max	Maximum water temperature at the significant thermal feature, a result of all pixels within the specified buffer
Std_Dev	Standard deviation of the water temperature at the significant thermal feature, a result of all pixels within the specified buffer

Temperature Loggers (Accuracy):

Header	Explanation
Name	Logger's name provided by client
Tw_C	Water temperature by the logger at the time of acquiring the specific flight line (see below)
Date_Time	Date and time at which the water temperature was recorded and coinciding with the time window of acquiring TIR flightlines that covers the logger's site
Flight_lin	Flightline's serial number covering the logger's site
Strm_Name	Stream name closest to the location of the significant thermal feature
L_R_Bank	The location of the significant thermal feature, left or right bank, relative to the centerline
M_Off_str	Distance of the significant thermal feature from the closest stream (meter)
Rvr_meas_m	River length (meter) where the significant thermal feature was found, starting from the downstream end
Rvr_km	River length (km) at which temperature was sampled, starting from the downstream end
Rvr_mile	River length (mile) where the significant thermal feature was found, starting from the downstream end
Mean	Mean water temperature at the significant thermal feature, a result of all pixels within the specified buffer
Median	Median water temperature at the significant thermal feature, a result of all pixels within the specified buffer
Min	Minimum water temperature at the significant thermal feature, a result of all pixels within the specified buffer
Max	Maximum water temperature at the significant thermal feature, a result of all pixels within the specified buffer
Std_Dev	Standard deviation of the water temperature at the significant thermal feature, a result of all pixels within the specified buffer

Navigating to Data Folders and Files in ESRI ArcCatalog

ArcCatalog is used to navigate data folders and files where data properties/metadata can be found.

To load files into ArcGIS Pro, drag and drop files from ArcCatalog. It is also possible to drag and drop the *.shp/*.tif files using the local operating system navigation platform.

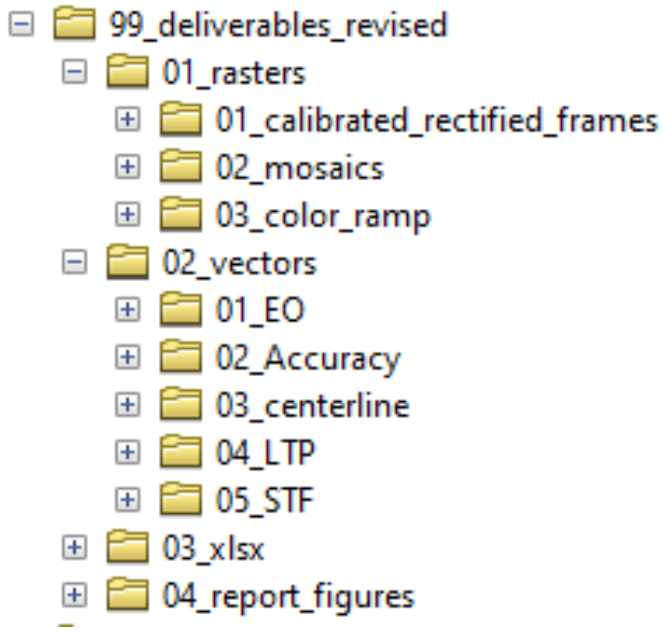

Load Mosaic Rasters

The main raster data used is mosaicked imagery. Individual frames are provided for reference.

Load the mosaic files (*.tif) of interest into ArcPro - the stretched color scheme of the file is automatically shown in grayscale. TIR mosaics are found in the mosaics folder.

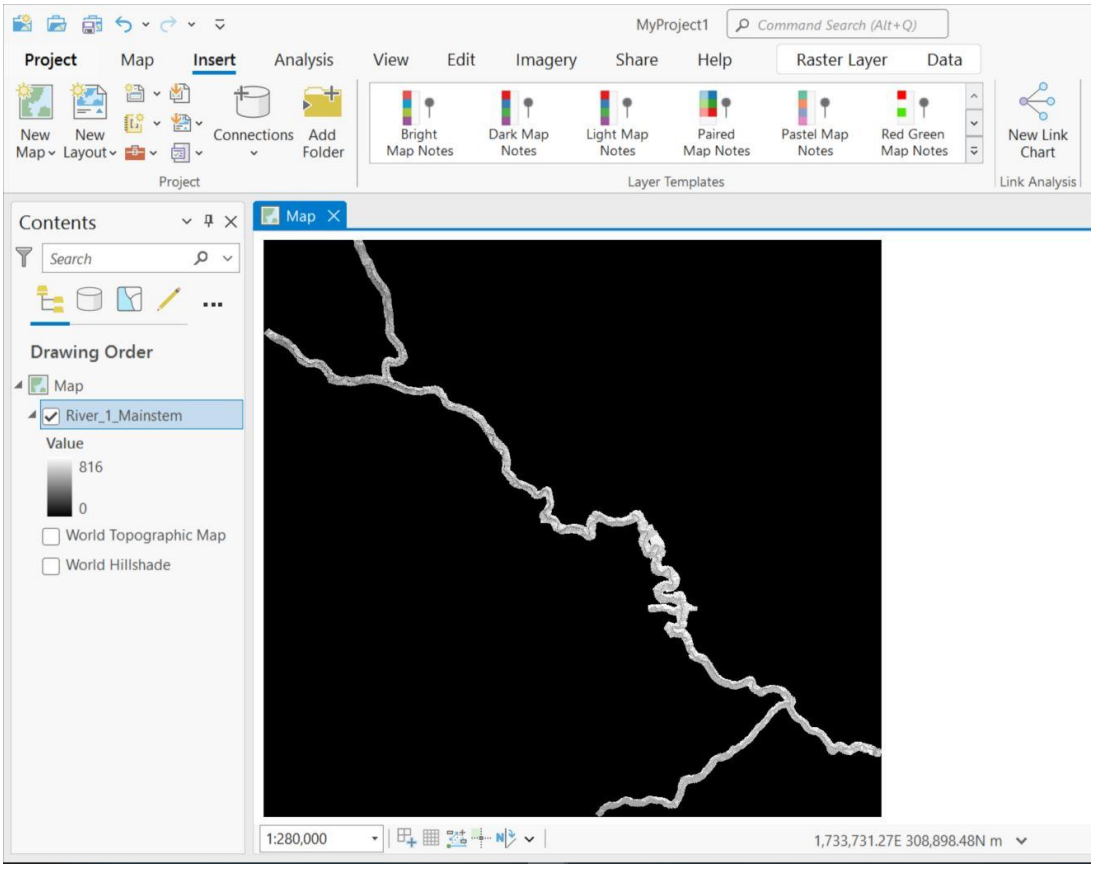

Working with Color Ramps

There are several different ways to bring up the symbology properties to apply the provided, customized color ramp file (*.lyr). From the contents pane, either double click on the color bar under “Value” (see the image above) or right click symbology from the corresponding layer. Another way involves clicking on the mosaic in the contents pane, this will bring up a Raster Layer tab in the ribbon, then Symbology → Classify (below left image). In the symbology dialogue box, click on the three horizontal lines in the upper right corner and “Import from layer file” (bottom right image).

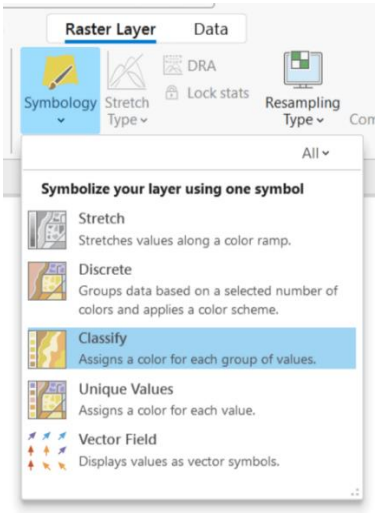

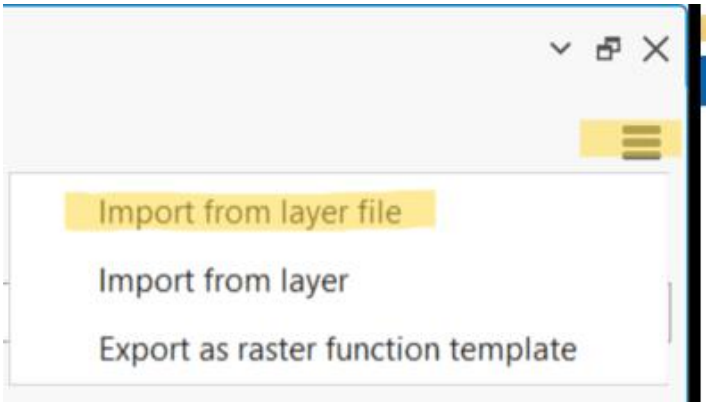

The color ramp layers, in the “color ramps” folder, can be arranged according to the names of tributaries of your project, according to customized temperature ranges, or a combination of both. The goal of customizing the color ramps is to highlight temperature anomalies of interest.

- The numbers in the color ramp file name symbolize the specific temperature range from cold to warm color scheme.
- Temperatures above the upper value visualize raster pixels in the grayscale.
- The first example below includes the temperature unit and the multiplication value: Celsius multiplied by 10.
- The second example highlights pixel values with temperatures 18 °C to 26 °C. The coldest pixel value is 18 °C and the warmest in this temperature range is 26 °C. Any temperature colder than 14 °C will be colored as 14 °C. Pixel values above 26 °C are in grayscale stretched to the warmest pixel value.
- The legend then shows the color ramps in the specified temperature. The values are edited to remove the multiplication. NOTE: This is not done automatically. If any of the values of the mosaic are changed in ArcGIS Pro, the original, imported color ramp will need to be changed or the colors might not accurately reflect the dataset. The name (selected in the first image) can be changed without changing the color ramp.

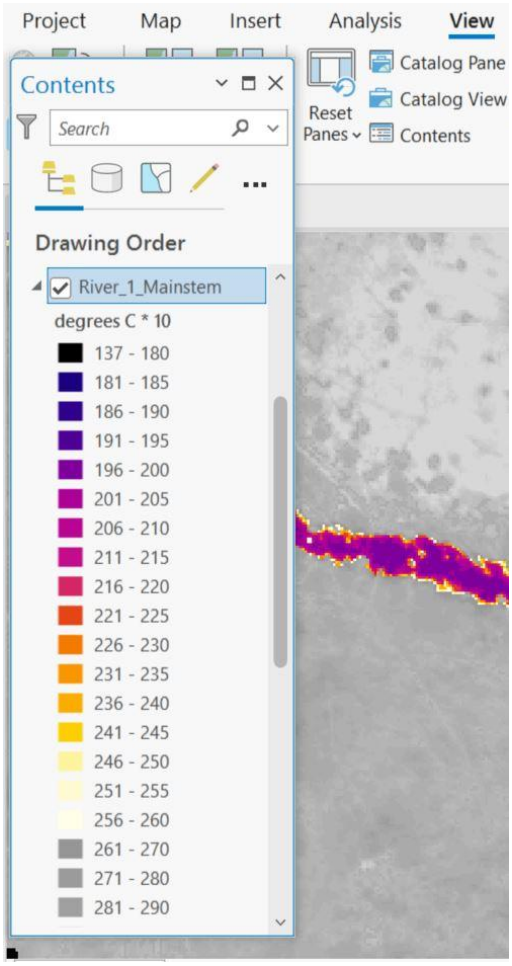

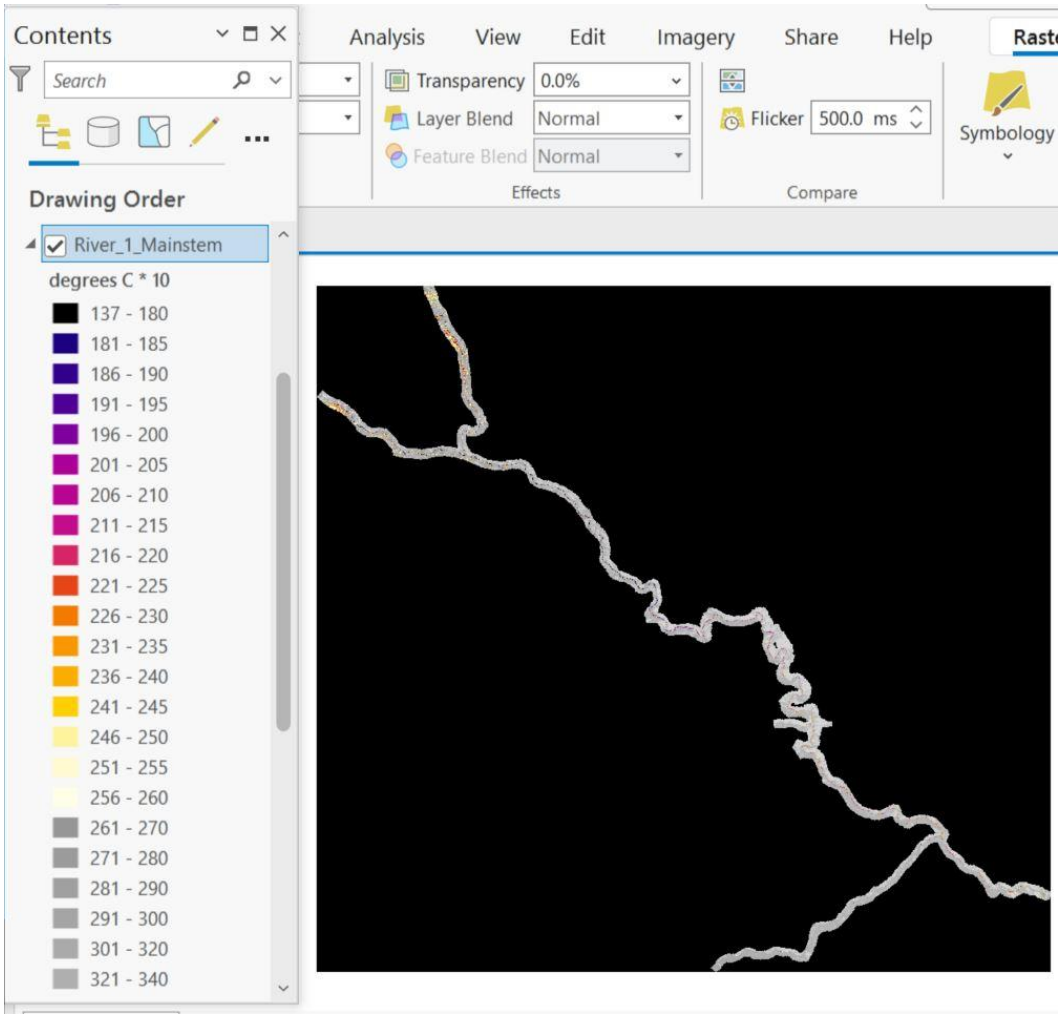

Zoom in and pan to review the mosaic:

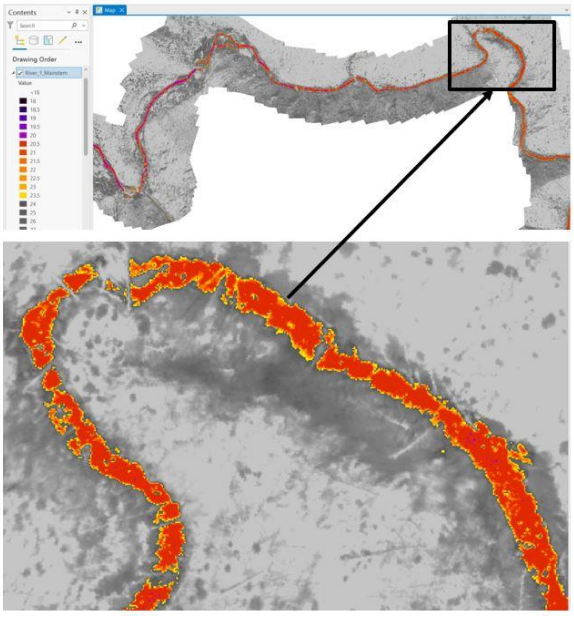

Load Vector Files

The vector files represent analyses of the thermal data in shapefile format:

1- The exterior orientation (EO) file is a point shapefile representing information related to each image frame used in the project.
2- The accuracy assessment point shapefile contains information of the water temperature data loggers that were used to calibrate the thermal infrared imagery. It also includes comparison analysis (accuracy assessment) between the recorded water temperature and the calibrated mosaic pixel values.
3- The centerline file is a polyline shapefile that was manually digitized to follow the river's thalweg based on the thermal mosaic and is used in generating the longitudinal temperature profile and significant thermal feature files.
4- The longitudinal temperature profile (LTP) is a point shapefile of the sampled mosaic at specified intervals.
5- The significant thermal feature (STF) is a point shapefile of the sampled features of interest for the project.

Working with Centerlines, LTP, and STF

Make sure that when you load in the vectors that you set the coordinate system of the map to match the layers so that everything shows up together. Either double click or right click on the map layer.

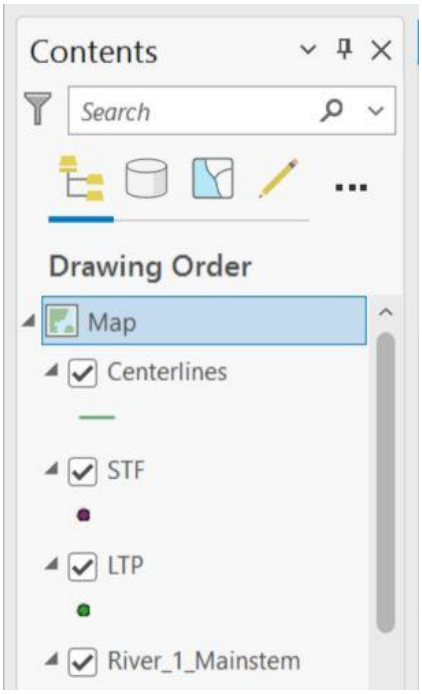

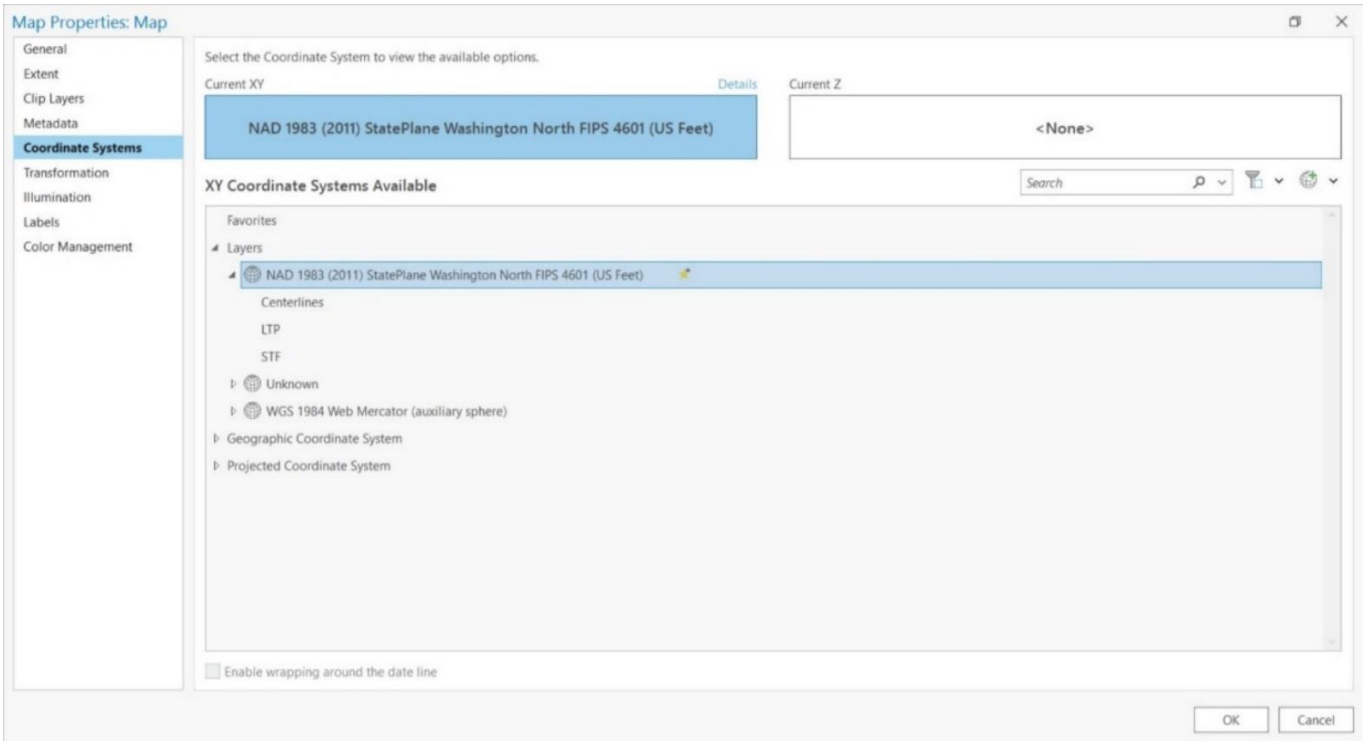

Note that any of the symbols can be adjusted for easier viewing by either double clicking or right clicking on the symbol in the contents pane. The “Gallery” tab provides pre-set shapes to use for the symbol.

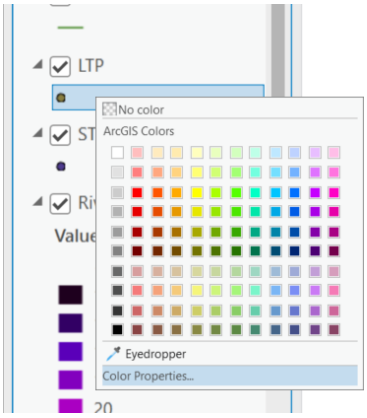

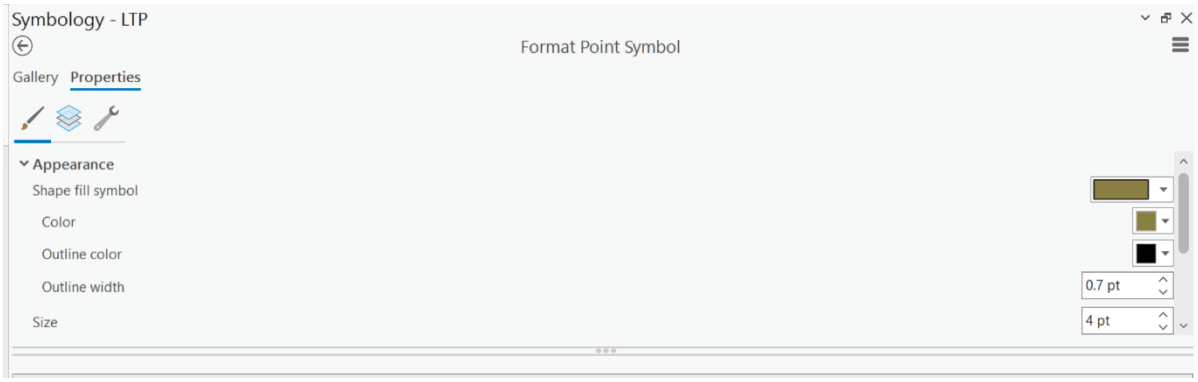

Attribute Tables

Open the attribute table to show feature details. Fields from the attribute tables are explained in the *.xlsx file. Select a feature and zoom in or pan across the TIR mosaic.

Right click on the layer of interest in the contents pane and select “Attribute Table”:

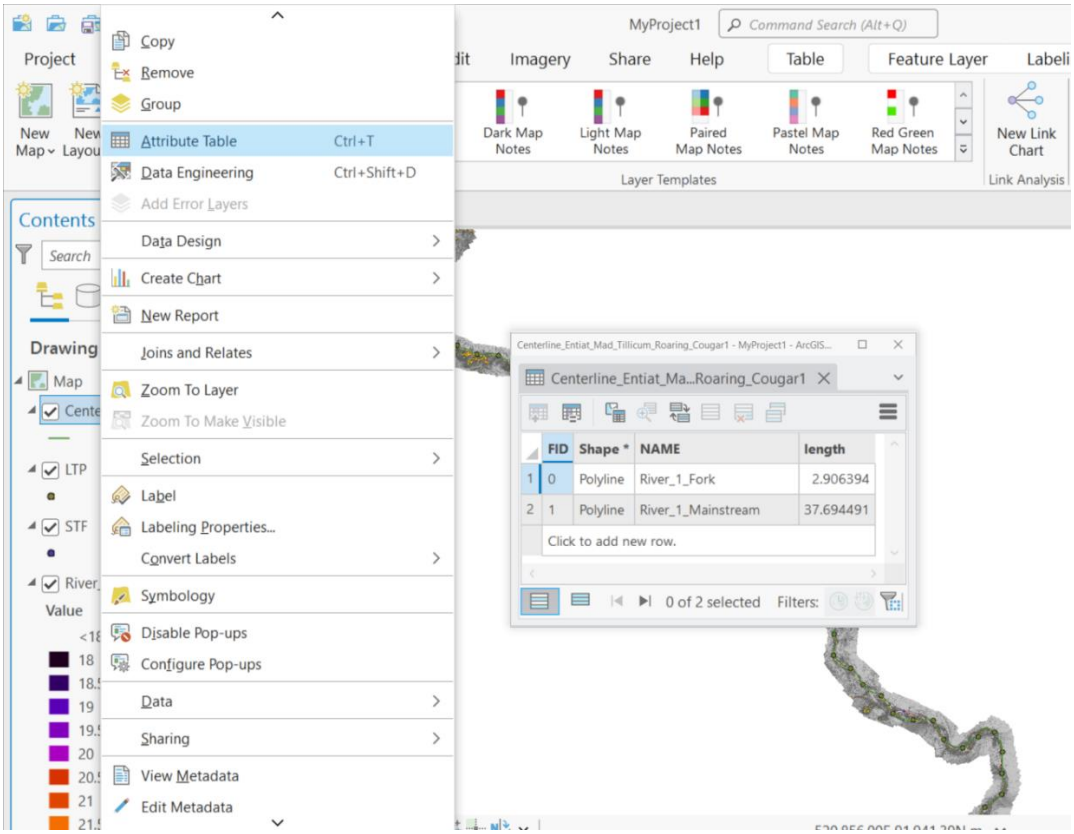

Putting everything together, it should look similar to this:

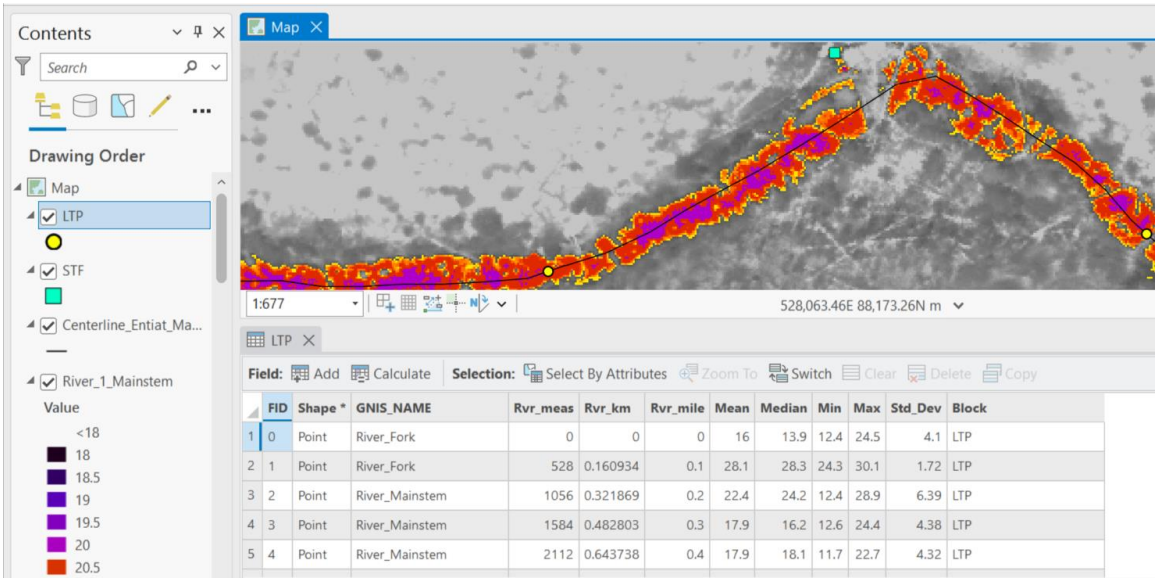

Vector Labels

Show vector labels of each feature for statistics and temperature values:

1. Right click on STF or LTP symbol in contents pane
2. Select “Labeling Properties”
3. Select script language; “VBScript” is used in this example. This should be done before typing in the script or the script will be erased.
4. Type in the correct script. The script used in this example is “Round([Median], 1).” Round means that it is rounding up, median is what it is labeling, and the 1 is number of decimal points. Double clicking a field in the “Fields” box will add that field to the script.
5. Click “Apply.”
6. Select label to see the label appear on the map. This can be done before changing the label properties, but the label will be the default feature.
7. The font, font style, size, background, etc. can be changed under the symbol tab, and the position of the label adjusted under the position tab. The “Appearance” and “Halo” subitems were modified under the symbol tab to produce the example image (at the top of the next page).

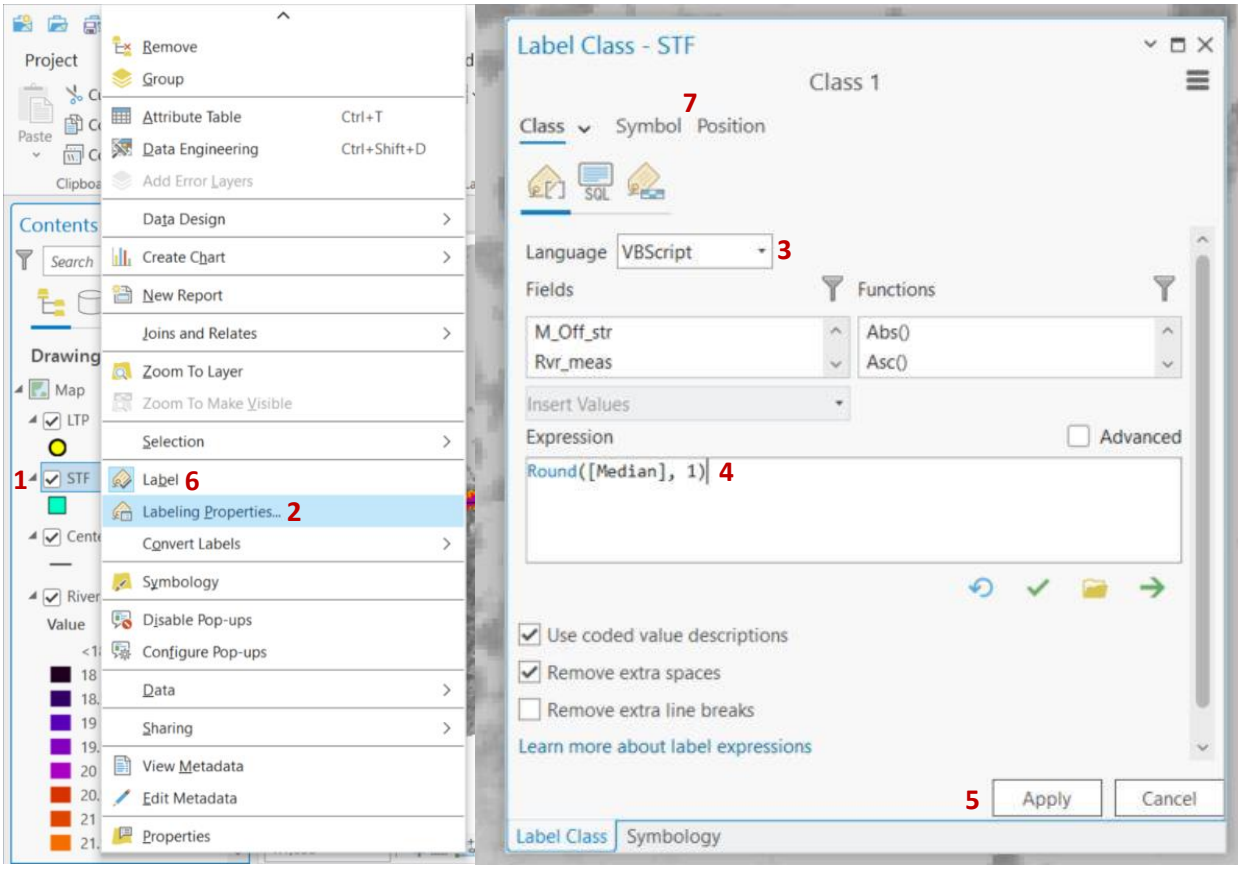

These steps produce an image like this:

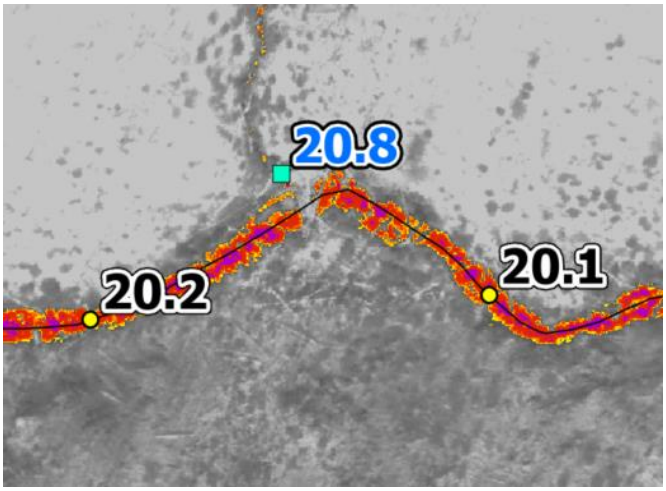

Combined RGB and TIR Imagery:

See “Load Mosaic Rasters” section to see how to load the *.sid layer. Note that the HTML file has *.sid as the file extension but will not load in ArcPro.

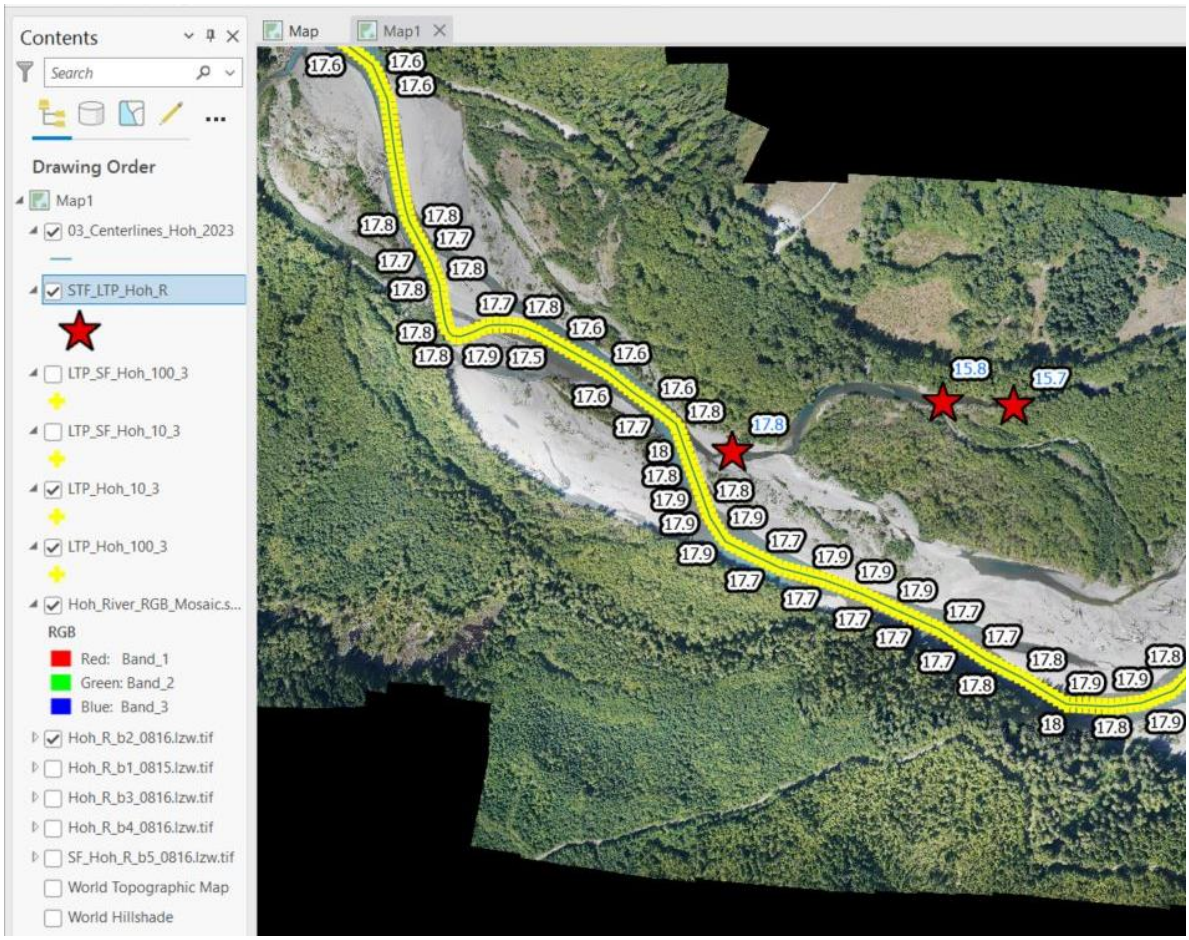

To display the TIR mosaic with a color ramp overlaid onto the 3-band (RGB) imagery:

1. Add a color ramp to the TIR mosaic (see “Working with Color Ramps”)
2. Place the TIR mosaic above the RGB mosaic.
3. In the symbology dialogue box, select all the grey scale values, depicting the riverbanks and trees, using the shift key and select “No color”. Note that selecting the color itself will bring up a color palette for that specific item and will not allow multiple rows to be selected. Click on the line or other columns to select all the grey scale values.

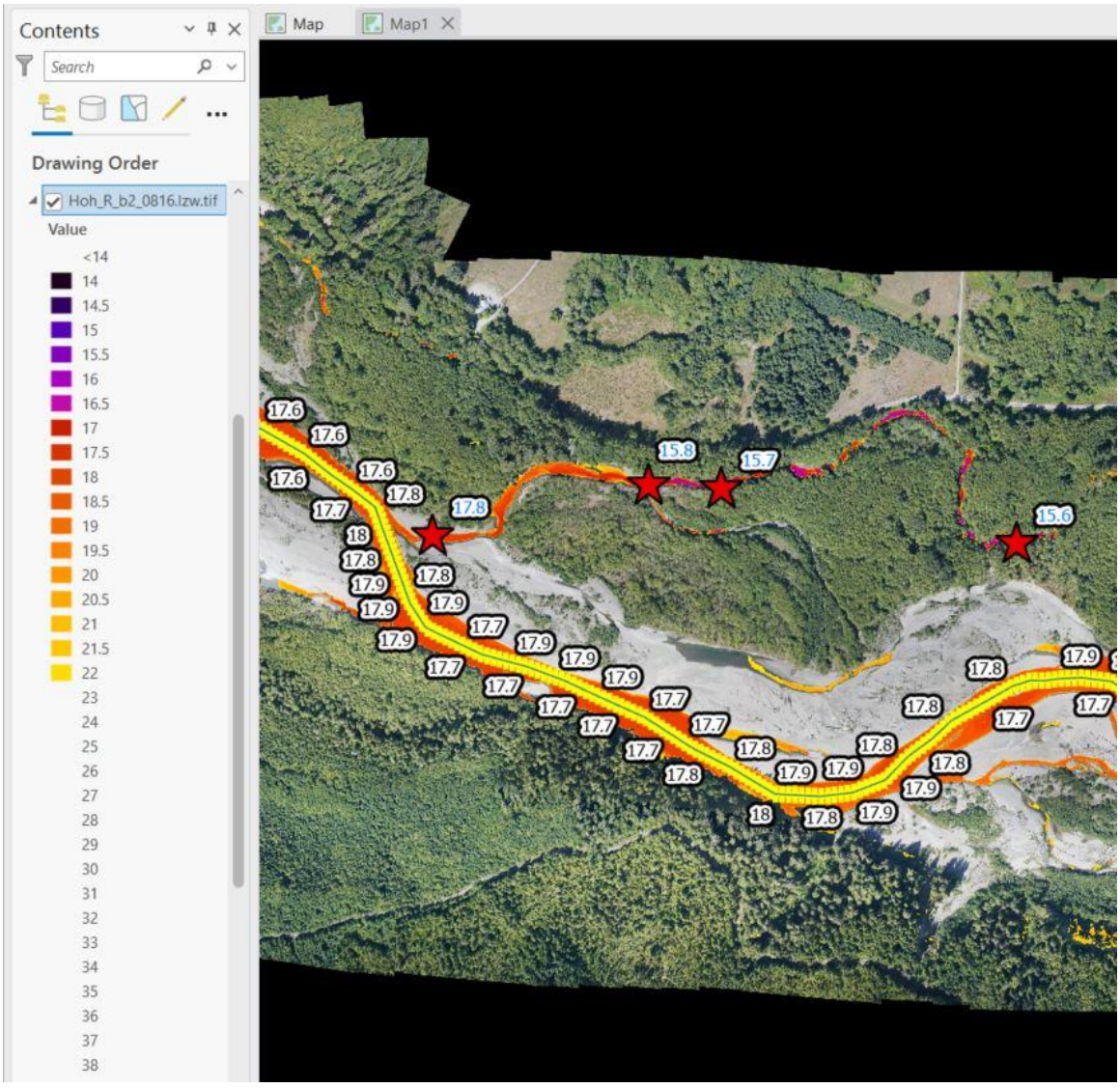

Appendix C Grande Ronde Draft LCM Manuscript

Manuscript Title: A state-space model to quantify density dependence, demographic heterogeneity, and spatial synchrony in Grande Ronde Basin Chinook salmon populations

Manuscript Co-authors: Ben Staton, Polly Gibson, Martin Liermann, Casey Justice, Matt Kaylor, Rishi Sharma, Seth White

Keywords: State-space models, density-dependence, synchronous dynamics, Pacific salmon

Target Journal: *Ecological Modelling*

A state-space model to quantify density dependence, demographic heterogeneity, and spatial synchrony in Grande Ronde Basin Chinook salmon populations

Benjamin A. Staton *
Fisheries Science Department, Columbia River Inter-Tribal Fish Commission
700 NE Multnomah St., Ste. 1200, Portland, Oregon 97232, USA

Polly P. Gibson
East Region Fish Research, Oregon Department of Fish and Wildlife
One University Blvd., Badgley Hall 203, La Grande, Oregon 97850, USA

Martin Liermann
Watershed Program, NOAA Northwest Fisheries Science Center
2725 Montlake Blvd E., Seattle, Washington 98112, USA

Casey Justice
Fisheries Science Department, Columbia River Inter-Tribal Fish Commission
700 NE Multnomah St., Ste. 1200, Portland, Oregon 97232, USA

Matthew J. Kaylor
Fisheries Science Department, Columbia River Inter-Tribal Fish Commission
700 NE Multnomah St., Ste. 1200, Portland, Oregon 97232, USA

Rishi Sharma
FAO Regional Office for Asia and the Pacific
39 Phra Athit Rd., Phra Nakorn, Bangkok 10200, Thailand

Seth M. White
Department of Fisheries, Wildlife, and Conservation Sciences, Oregon State University
104 Nash Hall, Corvallis, Oregon 97331, USA

Keywords: State-space models, Density dependence, Synchronous dynamics, Pacific salmon

*Corresponding Author (bstaton@critfc.org)

Abstract

Pacific salmon face different mortality sources throughout life, requiring monitoring and modeling at various life stages to understand the relative influences of regulating processes. For example, density dependence may be important for freshwater juveniles, whereas ocean conditions may drive later-life outcomes; in addition, delayed effects further complicate these phenomena. State-space models offer a flexible and robust approach to analyze these complexities when faced with uncertain data. We constructed a state-space model for Grande Ronde Basin (NE Oregon, USA) spring Chinook salmon (*Oncorhynchus tshawytscha*) that tracks the abundance of ~30 cohorts from 4 populations, modeling variability in freshwater juvenile growth and survival using density-dependent relationships and stochastic process noise that acknowledges synchronous dynamics. Model substructures include rearing origin setting (i.e., natural vs. hatchery), juvenile life history type, and adult age-of-return to account for heterogeneity at these scales. The model was fitted to empirical information collected by a variety of monitoring projects and included an index of freshwater habitat capacity to scale density-dependent processes. We found evidence of early-life density-dependent survival and growth, with subsequent over-wintering and out-migration survival mediated by early-life growth rates. Rearing capacity and growth rates showed positive, though uncertain, relationships with the habitat index. Life stage-specific covariances were overwhelmingly positive, indicating among-population synchronous dynamics throughout life. Post-hoc analyses showed juvenile life history diversity is important for increasing productivity and that increasing habitat availability would reduce density dependence. Model posteriors reflect current understanding of life cycle dynamics for these populations which can parameterize simulations of future population status.

Highlights

- A state-space model used information from throughout the Chinook salmon life cycle
- Early-life survival and growth were density-dependent for all populations
- Later survival was linked to growth, indicating delayed effects of density dependence
- Many populations displayed synchronous dynamics, indicating shared external drivers
- Output will aid in evaluating potential outcomes of habitat restoration actions

C1 Introduction

Population dynamics models are widely used tools for synthesizing available knowledge and data to inform decision-making in fisheries resource management (Walters and Martell 2004). Although there are a wide variety of types of population dynamics models and frameworks, it is important to draw a distinction between retrospective and prospective modeling. Retrospective models are statistical by nature and seek to estimate unknown parameters from observed data and stated assumptions. They can be used to gain insights about ecological systems (Hilborn and Mangel 1997) and test empirical support for alternative hypothesized processes regulating populations. Conversely, prospective models take parameter estimates and data summaries as inputs to predict population outcomes given a set of circumstances (e.g., management strategy evaluation; Punt et al. 2016, population viability analysis; Reed et al. 2002). The utility and reliability of prospective models are conditioned upon knowledge of population regulating processes. Thus, a key step in prospective modeling is rigorous retrospective analysis grounded in empirical observations.

Anadromous Pacific salmon (*Oncorhynchus* spp.) often have extensive biological monitoring data and there is broad interest in the development of prospective models for guiding recovery plans. Given these species occupy a range of different habitat types as they progress through life stages, analyses are often spatiotemporal models that quantify cohort- and life stage-specific abundance and mortality. Density-dependent factors have been widely observed to influence Pacific salmon populations, particularly growth and survival early in life (Walters et al. 2013; Grossman and Simon 2020) that can affect later-life attributes (e.g., age-at-maturity; Tattam et al. 2015), and it is essential that retrospective analyses disentangle these effects from extrinsic drivers (e.g., environmental noise/forcing, harvest, density-independent factors; Zabel et al. 2006; Cunningham et al. 2018). Understanding the effects and strength of density dependence across life stages is critical for realistic prospective modeling of population dynamics (Rose et al. 2001; Reed et al. 2002). Further, many salmon species exhibit life history diversity (including Chinook salmon *O. tshawytscha*; Bourret et al. 2016), meaning that demographic rates are homogeneous at some life stages and heterogeneous at others as fish diverge into alternative pathways. Similar complexity is common in salmon due to their origin – fish spawned in the wild versus in hatchery conditions often have different demographic rates (e.g., pre-spawn mortality rates or age structure; Bowerman et al. 2021; Chen et al. 2023). Although anadromous species tend to have reasonably predictable migrations that facilitate monitoring abundance and survival at various life stages, data collection is inevitably imperfect: sampling variability, missing years, and inconsistencies of scale are common. Therefore, analyses that account for these life cycle complexities and data imperfections while providing robust retrospective inference are important for parameterizing useful prospective models.

State-space models (SSMs; Newman et al. 2023) have grown in popularity in recent decades

as a means to address challenges in retrospective population modeling. SSMs are time series models that partition noise into process (i.e., environmental) and observational (i.e., measurement) components, making them useful for addressing measurement error bias, expressing relative weights for different data sources, and preventing non-process noise from entering prospective analyses (de Valpine and Hastings 2002; Lindén and Knape 2009; Newman et al. 2023). SSMs are constructed by (*i*) specifying a set of process equations that represent expected population responses to intrinsic (e.g., density affects survival) and extrinsic (e.g., quantity and quality of available habitat) drivers, (*ii*) adding process noise to obtain the "latent" (i.e., true but hidden) state, and (*iii*) assuming that the data values have been observed with error, conditioned on the latent values via statistical likelihood functions (Auger-Méthé et al. 2021). Since SSMs are inherently time series models, they are useful for handling the time lags and linkages involved with modeling stage- and/or age-structured populations. Specific examples include reducing time series bias (Walters 1985; Myers and Barrowman 1995), accounting for delayed effects (Beckerman et al. 2002), and preventing issues associated with overly simplistic treatments of age information (Zabel and Levin 2002). SSMs have been widely applied to salmon populations; however, often only with adult time series due to lack of data on intermediate life stages (Su and Peterman 2012; Fleischman et al. 2013; Staton et al. 2017, 2020, 2021; Connors et al. 2022; Su 2023). SSMs that partition the salmon life cycle into multiple life stages are less common, but when applied, they can provide detailed insights into population dynamics (Rivot et al. 2004; Perry et al. 2020; Jacobs et al. 2023).

Statistical models that include spatiotemporal variability often encounter spatial autocorrelation (González-Megías et al. 2005). Noisy extrinsic population drivers, such as inter-annual fluctuations in environmental conditions, may vary at scales experienced by multiple populations (or population subcomponents) such that temporal variability may be shared (Ranta et al. 1997). Interest in quantifying spatial synchrony in population models has increased in recent years (Bjørnstad et al. 1999; Thorson et al. 2014; Riecke et al. 2019; Staton et al. 2020; Bouchard et al. 2022) because it can provide useful insights for conservation ecology, particularly when partitioned among life stages (Thorson et al. 2014). First, the strength of the portfolio effect (Schindler et al. 2015) is inversely related to synchrony, meaning that estimates of low correlation between populations can indicate which life stages most impact stability at aggregated scales. Second, strongly synchronous population dynamics result in unstable aggregate-scale dynamics and increase the likelihood of simultaneous extirpation of multiple populations (Heino et al. 1997; Isaak et al. 2003). Third, knowledge of which life stages are most synchronous may be useful in predicting those that are likely to be co-affected by a changing climate (Hansen et al. 2020; Bouchard et al. 2022). Finally, a potential statistical advantage of accounting for synchrony may be to increase precision by facilitating information sharing in hierarchical time series models (i.e., reconstructing missing portions of partially overlapping or sparse time series; Staton et al. 2020). However, many retrospective analyses

of salmon data ignore synchrony among populations and/or population components, which is perhaps a missed opportunity to extract useful information from the data.

In this article, we describe a SSM for quantifying population dynamics parameters and synchrony that we applied to Grande Ronde Basin spring Chinook salmon populations. Prompted by substantial declines in abundance, extensive long-term standardized monitoring for these populations initiated in the early 1990s now provides the opportunity to ground detailed population dynamics models with empirical data. The model tracks cohort-specific abundance through various life stages – across cohorts via a production relationship and within cohorts via transition probabilities. The model integrates multiple data sources and fits to them simultaneously in a single joint likelihood to maximize information use and enforce parameter consistency with all available data sets. We structured the model to simultaneously analyze data for four spawning populations, and where relevant, to further stratify life stages by juvenile migratory strategy, rearing origin type, and adult return age. With this structure, the SSM can provide a wealth of retrospective insights into population dynamics and regulating mechanisms, which alone may have direct management implications, in addition to great utility for informing prospective analyses. Thus, our objectives are to (*i*) quantify heterogeneity in demographic rates (e.g., survival) among populations and population subcomponents (e.g., life history types), (*ii*) quantify early-life density dependence for naturally rearing fish and evaluate the evidence for it being at least partially mediated by growth and size-based survival, (*iii*) assess the degree of synchronicity among populations and individual life stages, and (*iv*) demonstrate the utility of the model output for prospective applications using two post-hoc analyses including hypothetical (*a*) increases to available rearing habitat and (*b*) the loss of juvenile life history diversity.

C2 Methods

C2.1 Study Area and Populations

The Grande Ronde River is a large tributary of the Snake River in the Columbia River Basin, flowing approximately 340 km from its headwaters in the Blue Mountains of NE Oregon to its mouth in SE Washington. The Grande Ronde Basin (10,630 km^2) is semi-arid, characterized by hot, dry summers and cool, wet winters with snow comprising most annual precipitation at higher elevations. The focal populations of this study inhabit four Grande Ronde River sub-basins (Figure C1): Catherine Creek (CAT; 1,051 km^2), Upper Grande Ronde River (UGR; 1,896 km^2) upstream of the town of La Grande, Lostine River (LOS; 240 km^2), and Minam River (MIN; 618 km^2).

We selected these four populations for several reasons. First, rigorous and near-identical fish and habitat monitoring data has been consistently collected for several decades, providing a robust data set to model population dynamics. Second, the range in habitat conditions and management

practices among the four sub-basins provide contrast to assess impacts on populations dynamics. Lastly, quantitative understanding of population dynamics will be useful in further planning of recovery actions for the populations spawning in these sub-basins.

Land use activities within UGR, CAT, and LOS including beaver trapping, timber harvest, the use of splash dams, irrigation, grazing, mining, and urbanization have degraded aquatic habitats and reduced the quality and extent of salmonid spawning and rearing habitat (White et al. 2017, 2021), exacerbated by ongoing and future alterations to thermal and hydrologic regimes under climate change (Justice et al. 2017). Much of MIN is within designated wilderness and has experienced less habitat degradation. These in-basin factors, combined with out-of-basin impacts in the mainstem Grande Ronde River, Snake River, Columbia River, estuary, and ocean have contributed to population declines. Snake River spring/summer Chinook salmon were listed as threatened under the Endangered Species Act in 1992 (Ford 2022), prompting efforts to identify limiting factors and implement recovery actions. Extensive restoration efforts have been implemented in CAT, UGR, and LOS, but not in MIN as habitat conditions remain relatively intact. Beginning in the late 1990s, local broodstock has been used to supplement CAT, UGR, and LOS with hatchery-raised smolts, whereas no intentional supplementation has occurred in MIN.

All four populations exhibit similar juvenile and adult life history strategies, but the proportional expression of each strategy varies among populations. Adults enter natal rivers in late spring through early summer and spawn in August–September, after which embryos incubate through the fall and winter, emerge as fry the following spring, and spend a full year rearing in freshwater post-emergence prior to out-migration as smolt. Like many other Snake River spring Chinook salmon populations (Copeland and Venditti 2009; Copeland et al. 2014), Grande Ronde spring Chinook salmon display life history diversity in timing of migration from parr summer rearing habitats (Cooney et al. 2017; Gibson et al. 2024). One group migrates downstream in the fall to rear lower in their natal basin over winter (termed "fall migrants") and the other group remains in upstream habitats to rear over winter (termed "spring migrants"). Smolts of both types out-migrate to the estuary in spring (now age-2) and spend 1–3 years in the ocean before returning to natal rivers to spawn as total age-3 (essentially non-existent for females), age-4 (predominant age-of-return), or age-5 adults (least abundant).

C2.2 Data Sources

The model relies upon a wealth of data sources, most of which have been gathered during routine biological monitoring (Figure C2 – numbered circles denote specific data sources). We use six categories for presentation; categories *i-iv* include data sets assumed to have error and to which we assigned explicit likelihood functions, whereas we used those in categories *v* and *vi* deterministically: (*i*) juvenile and adult abundance, (*ii*) juvenile and adult survival rates, (*iii*) juvenile mean length, (*iv*) adult age/origin composition, (*v*) "auxiliary" information (e.g., hatchery smolt releases, weir

removal numbers, fecundity-at-age), and (*vi*) weighted usable habitat. Although we refer these information sources colloquially as "data" in the sense that the SSM fits to them or requires them to populate calculations, they are often externally derived estimates from empirical monitoring data. For example, juvenile abundance estimates were obtained from rotary screw trap passage counts and expanded for imperfect detection, and many of the survival rate estimates were obtained from open capture-recapture models fitted to PIT-tag detection records. We allowed the SSM to acknowledge that these data sources (estimates) are not perfect representations by using the standard errors from the external estimation models as the (assumed known) standard deviations of observation error. Further details on all data sets and associated field and analytical methods are included as part of the data repository accompanying this article (Gibson 2025).

C2.2.1 Abundance Data

At the freshwater juvenile stage, abundance is monitored using rotary screw traps located near the downstream extent of spawning and rearing in each sub-basin (Figure C1; Gibson et al. 2024). Fish are counted as they move past the traps during the two primary periods of juvenile movement: as parr in the fall prior to over-wintering (i.e., only fall migrants trapped) and as smolt in the spring after surviving the winter (i.e., only spring migrants trapped). Trap capture efficiency is estimated from mark-recapture trials throughout the sampling period and is used to expand the raw trap counts to estimates of total passage.

The abundance of adults returning to natal streams each year is estimated based on a combination of expansions from redd (i.e., nest) counts and (when a weir is present) mark-recapture estimates using fish marked at the weir and later recovered as carcasses on the spawning grounds (Bliesner et al. 2020; Feldhaus et al. 2022). In populations with a hatchery supplementation program (i.e., CAT, LOS, and UGR), returning adults are trapped at a weir, where some fish are passed upstream and allowed to spawn naturally, while other fish are removed for broodstock or to limit the proportion of hatchery-origin fish on the spawning grounds. The total return-to-river estimates we supplied to the model describe abundance before any losses that occur within the natal stream, including harvest, broodstock removals, and pre-spawn mortality.

C2.2.2 Survival Rate Data

The model uses numerous empirical estimates of survival rates from different time periods during the Chinook salmon life cycle. All survival rate estimates are based on detections of fish implanted with passive integrated transponder (PIT) tags, which uniquely identify individual fish but are not always detected upon passing a receiver array. Although several years of sampling have been missed, the survival data time series are quite continuous since the initiation of the program in the early 1990s (Figure D2).

Groups of natural-origin (NOR) juveniles are PIT-tagged at four separate capture events during the freshwater juvenile phase within each population (Gibson et al. 2024, Figure C2): (*i*) in the summer, as parr of all migrant types rearing in the headwaters; (*ii*) in the fall, as fall migrant parr moving past the rotary screw trap; (*iii*) in early winter, as spring migrant parr over-wintering in the headwaters (not available for MIN population); and (*iv*) in the spring, as migrant smolt moving past the screw trap. For each tag group, the probability of survival from the time of tagging to arrival at Lower Granite Dam (LGR) – the first in a series of eight hydroelectric dams encountered during out-migration through the Snake and Columbia rivers – is estimated using a Cormack-Jolly-Seber model based on PIT-tag detections at LGR and other mainstem dams. For hatchery-origin (HOR) juveniles, there is only a single tag group for each population, representing survival from the time of smolt release in the spring to arrival at LGR (Feldhaus et al. 2022).

Downstream of LGR, survival rates for juvenile fish moving through the hydrosystem (i.e., from LGR to Bonneville Dam [BON] – the furthest downstream dam) are calculated by the Comparative Survival Study (McCann et al. 2022). We used these estimates as a data source in the model and expressed them as varying by year and origin, but common across populations. The data we used for HOR juveniles were from the CAT population, whereas those for NOR juveniles were based on an aggregate of fish from throughout the Snake River basin to obtain an adequate sample size of tagged NOR fish.

For adult fish returning from the ocean, the probability of detecting PIT-tagged fish as they move upstream past mainstem dams has been near 100% since the early 2000s (Crozier et al. 2016), meaning that the proportion of the PIT-tagged adults detected at BON in a given year that are subsequently detected at LGR contains information about survival along this portion of the spawning migration (DART 2023). We intended for this data source to integrate all sources of loss experienced during this time, including those due to harvest, straying, predation, and environmental conditions.

C2.2.3 Mean Length Data

When NOR juveniles are captured for PIT-tagging at one of the four seasonal capture events, all fish captured are also measured for fork length (Gibson et al. 2024); however, we only used data from the summer parr and spring smolt sampling events. We used annual mean fork length of all captured fish to represent mean body size in each event, which we treat as an index of early-life growth. We found that inter-annual variability in the timing of summer sampling created variability in parr mean length, and so we devised and applied a sample timing standardization (Staton et al. 2023) prior to supplying these data to the SSM. For the spring tag group (i.e., passive capture in the screw trap), variability in the timing of length sampling is driven by migration timing rather than by scheduling, so we did not apply a standardization.

C2.2.4 Age/Origin Composition Data

Total age (expressed as the number of winters experienced, including as an embryo) and origin (i.e., NOR vs. HOR) is recorded for all adults handled at weirs and, when possible, for carcasses recovered on the spawning grounds (Feldhaus et al. 2022). Age was assigned using a hierarchy of methods (in decreasing order according to their reliability): (*i*) parentage-based tagging, (*ii*) coded wire tags, (*iii*) PIT-tags, (*iv*) scale reads, or (*v*) age-length keys, as available. We constructed the SSM to assume that fish processed at weirs represented unbiased samples of the full adult population returning to each natal tributary. Carcass recoveries, however, are known to be biased with respect to fish size (and therefore age; Murdoch et al. 2010); thus, we allowed the SSM to estimate parameters that treated discrepancies between weir and carcass age compositions as observation errors (see Appendix D, Section D4.2.3).

C2.2.5 Auxiliary Information

There were several quantities known to vary annually for which information was available; however, we aimed to only include the variability in the SSM, not explain it using process model equations. An example is fecundity-at-age – data are available annually and they show variation that could be relevant for explaining variability later in the life cycle (e.g., in egg-to-parr survival rates). Rather than build process model equations to obtain true fecundity for linking to observed fecundity in the joint likelihood (as in all previously mentioned data sources), we simply used their values in model calculations as-is (e.g., model-predicted total egg production was the sum-product of female spawners-at-age and fecundity-at-age). Although this practice has disadvantages of (*i*) assuming the values are known without error and (*ii*) requiring non-missing values in every year/population/age, we deemed these of little concern given the amount of stochasticity elsewhere in the model and the relatively little amount of imputation needed. All auxiliary information sources are displayed as time series in Supplemental Material, Section 15[1].

Several data sets describing direct manipulation of fish populations are reported as known quantities. The number of HOR smolt released each year is measured as fish are transported to acclimation sites (Feldhaus et al. 2022). Harvest rates of returning adult age-4 and age-5 fish downstream of BON were compiled from run reconstruction information (S. Ellis, pers. comm.) and varied by year and origin; we assumed the harvest rate for age-3 fish was half that of age-4 and age-5 fish to account for gillnet selectivity. Numbers of adult fish (by age and origin) removed at the weir are essentially census counts (Crump et al. 2024; Simmons et al. 2023). Similarly, we assumed numbers of fish by age and origin removed in tribal and sport harvest from the natal tributaries were

[1]The "Supplemental Material" is a web document submitted alongside the manuscript and contains a wealth of additional model output too extensive to be displayed in the manuscript itself. Please contact the authors for a copy of this document.

known without error (unpublished data from Nez Perce Tribe Fisheries and Confederated Tribes of the Umatilla Indian Reservation Fisheries, as well as Lance et al. 2023).

For two other auxiliary information sources used in the SSM, we estimated values externally based on existing data sources, then supplied the results to the model as known quantities. The pre-spawn survival rate for adult fish (i.e., the probability of survival from the start of the spawning period until successful spawning) is typically estimated based on the spawn status of female carcasses recovered on the spawning grounds (Bowerman et al. 2021). Using the carcass recovery data set, we fitted population-specific logistic regression models that assumed a time-constant mean with annual random effects to predict pre-spawn survival rates by year and population. For the fecundity data set, we estimated the number of eggs produced each year as a function of the mean length of returning adult females. Data from spawning fish in a hatchery setting show that the number of eggs produced is directly related to fish size (ODFW, unpublished data). To account for varying age composition and size-at-age among populations and years, we used hatchery spawning data from Grande Ronde populations to fit a linear relationship between female fork length and fecundity. We then calculated mean length by age of the returning adult females each year from weir and carcass data, and used these mean lengths to predict mean fecundity per female by age, population, and year.

C2.2.6 Weighted Usable Habitat

We developed an index of the total quantity of high quality habitat available to rearing parr in each population. Such a metric could be useful to (*i*) standardize abundance estimates to the density scale, which enables estimating coefficients of density-dependent relationships on a common scale and (*ii*) link population dynamics parameters (e.g., rearing capacity) to available information about habitat. Development of the index (summarized in greater detail in Appendix D; described fully in Justice et al. 2021) involved predicting the relative ability of 100 m stream reaches to hold rearing parr based on local habitat characteristics, such that different reaches could be assigned weights. We fitted negative binomial generalized linear mixed models relating reach-level abundance estimates (snorkel counts corrected for partial detection and unsurveyed habitat units; Staton et al. 2022; White et al. 2012) to habitat characteristics. Models included random effects for year and a zero-inflation component for sites outside the current Chinook salmon spawning extent. Habitat metrics assessed (e.g., frequency of pools and large wood, river complexity index, maximum weekly water temperatures, flow) were collected using the Columbia Habitat Monitoring Program protocol (CHaMP 2016). Following model selection, we obtained reach weights as the model-predicted abundance for each reach divided by that of the reach with the highest abundance across all reaches, such that a weight of 0 represented habitat incapable of rearing fish and 1 represented the best potential habitat available in the basin. Our index of habitat availability – which we term "weighted usable habitat length" (WUL) – was then the sum-product of reach-specific weights and lengths,

calculated separately for each population. Our use of WUL rather than the more commonly used weighted usable area (Bovee 1982; Maret et al. 2006) accounts for the observation that (*i*) Chinook salmon parr use either shoreline or thalweg areas which are more linear stream features, rather than being uniformly dispersed across the stream channel, and (*ii*) better fit of fish density to stream length vs. stream area.

C2.3 Model Description

The SSM tracked the cohort-specific abundance of fish through various life stages and linked these state variables across cohorts via a production relationship (e.g., spawners produce eggs) and within-cohort transition probabilities that capture survival (e.g., a proportion of parr become smolt after surviving the winter) and movement (e.g., a proportion of ocean juveniles return to spawn each year, Figure C2). The SSM was structured to group and track fish by their demographic attributes of interest, including (*i*) spawning population (CAT, LOS, MIN, UGR), (*ii*) juvenile migratory strategy (fall vs. spring migrants), (*iii*) rearing origin type (NOR vs. HOR), and (*iv*) age of adult return (total age of 3, 4, or 5 years). Process and observation model equations were mostly identical for all populations, migratory strategies, origins, and ages, but the parameters governing them varied, which enabled estimating and capturing demographic heterogeneity (e.g., differences in average survival by population or origin type). We provide a narrative description of the model in the following sections; all process and observation model states and equations (represented by boxes and arrows in Figure C2, respectively) and assumed stochastic processes are described fully in Appendix D.

While it is possible to simultaneously estimate process and observation variability using state-space models (de Valpine and Hastings 2002), we had independent estimates of observation error for most data sets, allowing us to fix these variance parameters during state-space estimation. This has computational and statistical advantages relative to estimating both forms of variability (Polansky et al. 2021), especially when estimating density-dependent relationships (Knape 2008). With the exception of two processes (egg-to-parr survival and year-1 ocean survival), we assumed temporally independent process noise. We accounted for synchrony among populations by modeling process noise terms as outcomes of multivariate (log- or logit-) normal random processes (e.g., eq. D1), which involved estimating the covariance matrices (one per process) that stored the variances for each population and covariances among population pairs (eq. D2, D3; Riecke et al. 2019). Covariance estimates will tend to be positive if population pairs tend to share years in which the actual value was above the expected value.

C2.3.1 Freshwater Juvenile Processes

We initiated the life cycle at the egg stage, where the number of eggs for a given population was the product of female spawner abundance and age-specific fecundity from the previous year (eq.

D4). We modeled the expected proportion of eggs that survive to the summer parr stage as a density-dependent process following Beverton-Holt dynamics (Moussalli and Hilborn 1986, eq. D5) with serially autocorrelated process noise (via a lag-1 autoregressive process; eq. D7). We estimated the Beverton-Holt productivity parameter, in this case representing theoretical maximum egg-to-parr survival, independently across populations. However we modeled parr recruitment capacity as a linear function of basin-specific weighted usable habitat length (WUL) with a zero-valued intercept and log-normal error (eq. D6). Total parr recruitment was then the product of total egg production and this density-dependent egg-to-parr survival (eq. D8).

Freshwater juvenile survival rates also exhibit density dependence for Snake River spring Chinook salmon populations (Achord et al. 2003; Walters et al. 2013), including those in the Grande Ronde (Cooney et al. 2017; Staton et al. 2023). Further, growth rates of juvenile salmonids in freshwater have also been widely observed to be density-dependent (Grant and Imre 2005; Grossman and Simon 2020) and juvenile size is important for survival (Zabel and Achord 2004; Hostetter et al. 2015). To capture delayed effects of density-dependent growth on survival later in life, we linked several process model equations together and informed them with available monitoring data in the form of mean length, survival, and abundance estimates. First, we modeled expected parr mean length as a power function of egg density (expressed as eggs per km WUL) to represent density-dependent growth (eq. D9). Second, we used parr mean length as a predictor variable to derive expected over-winter survival (logit-linear model; eq. D13) and expected growth (multiplicative change in mean length) from the parr to smolt life stages (eq. D16). Finally, we used smolt mean length to derive expected migration survival to Lower Granite Dam (LGR; logit-linear model; eq. D19). Recognizing that extrinsic factors also affect growth and survival rates, we included process noise for all four of these deterministic processes (density-dependent growth to parr stage: eq. D10; size-based over-winter survival: eq. D14; size-based over-winter growth: D17, and size-based out-migration survival: D20).

To account for juvenile life history diversity, we modeled the expected probability that parr take on the fall migrant strategy as being time constant and obtained the number of parr that adopted each migratory strategy (eq. D11) after adding process noise (eq. D12). Modeling these two migratory strategies was supported by previous analyses suggesting differential survival rates (Cooney et al. 2017; Staton et al. 2023) and enabled building a more explicit observation model (e.g., eqs. D24 and D25). Following smolt out-migration to arrival to LGR, the SSM no longer tracked juvenile migratory strategy and instead pooled fall and spring migrants together as NOR fish for tracking separately from HOR fish (Figure C2).

HOR smolts are released in the spring prior to out-migration, and we used the number of smolt released each year by population (except MIN, which has no hatchery supplementation) to

initialize the process model calculations for HOR fish. We then tracked HOR abundance separately from NOR fish for all subsequent life stages. Thus, whereas the model included time linkages for NOR fish to previous generations through natural spawning, we simply introduced hatchery smolts into the population without process equations to explain variability in their abundance. We did not model density-dependent or size-dependent survival processes for HOR fish.

Survival along the downstream migration through the mainstem Snake and Columbia rivers was the first process for which the data did not allow modeling population heterogeneity. We assumed a time-constant expected value for each origin type and allowed the realized value to vary as a result of process noise (eq. D22). We obtained the number of smolts reaching the estuary as the product of smolt abundance reaching LGR (eq. D21) and this downstream migration survival rate (eq. D23).

C2.3.2 Ocean Processes

After reaching the estuary, ocean juveniles can mature and return as either total age-3, age-4, or age-5 after spending 1, 2, or 3 winters at sea, respectively. Accordingly, we modeled ocean dynamics using two demographic rates: survival and maturation (Figure C2). After surviving the first winter at sea, fish had the option to mature at age-3, those that did not mature must survive a second winter before the option to mature at age-4, and those that did not must survive a third winter and at which point all survivors returned as age-5 (see eqs. D37 and D38). All parameters in a "full model" (i.e., time-varying survival for year-1, year-2, and year-3 and maturity after year-1 and year-2, by origin) were not estimable, so we made several simplifying assumptions. With respect to survival, we assumed only year-1 was time-varying, and included serially autocorrelated process noise around the time-constant, but population-specific, expected value (eq. D34) to account for ocean conditions that may affect survival in a temporally non-independent fashion (e.g., Mantua et al. 1997). We forced time-constant year-2 and year-3 survival. Further, we assumed that inter-annual process noise in NOR and HOR year-1 ocean survival was perfectly correlated but estimated a difference in survival magnitude that was time-constant but varied by population (eq. D35); this estimated difference applied to year-2 and year-3 survival as well. With respect to maturation rates, we estimated time-constant expected values for both year-1 and year-2 by population and origin and introduced inter-annual process noise (eq. D36). We chose to simplify parameter structure in survival rather than in maturity because of the availability of commonly assumed values for ocean survival (CTC 1988), which we used as strongly informative priors suggesting survival rates of 0.6 and 0.7 for NOR year-2 and year-3, respectively. The output of the ocean process model was the number of mature fish (including age-3, age-4, and age-5, which we term collectively "adults") returning to the Columbia River estuary by year, population, age, and origin.

C2.3.3 Freshwater Adult Processes

Adults experience multiple sources of mortality upon return to the estuary and along their upstream migration to natal spawning tributaries. First, we subjected fish to an exploitation rate below BON (eq. D40). We did not partition mortality due to sea lion predation below BON (e.g., Rub et al. 2019) due to the lack of time series information, which in effect places that mortality into the ocean survival parameters. Second, we subjected fish to an upstream survival rate that represented all losses experienced on the migration between BON and LGR. We modeled upstream migration survival just as we did downstream survival through this corridor: time- and population-constant expected values by origin type, with inter-annual noise introduced via a multivariate logit-normal distribution allowing non-zero covariance among origin types (eq. D39). Third, upon reaching the Grande Ronde Basin, we subtracted the number of fish harvested by tributary fisheries or removed at the weirs (Crump et al. 2024; Simmons et al. 2023, eq. D41). Fourth, upon reaching the spawning grounds, we applied a time- and population-varying pre-spawn survival rate that accounted for mortality experienced prior to successful spawning (eq. D42). We assumed all surviving fish then contributed to spawning, such that 0% of age-3 spawners and 50% of age-4 and age-5 spawners were female and were assigned time-varying fecundity-at-age values based on mean length data (Supplemental Material, Section 15.5). We intended for this to account for potential declines in size (Ohlberger et al. 2018) which may have implications for egg production at population scales (Ohlberger et al. 2020) and the reliability of our egg-to-parr survival estimates. To complete the life cycle and initiate calculations for the next cohort, we obtained total annual egg production as the sum-product of female spawners-at-age and fecundity-at-age (eq. D4).

C2.3.4 Observation Model

We linked observed outcomes to model-predicted latent states through the observation model – this is the joint likelihood function that provides information to estimate unknown parameters. In our case, this involved assuming the data are randomly distributed around the modeled latent state with known magnitude of variability (e.g., screw trap passage: eqs. D24 and D25; PIT-tag-derived survival estimates: eqs. D26 – D30). To represent the stochastic processes for observing abundance and mean length we used log-normal distributions, and for survival rate data we used logit-normal distributions, where the standard deviation was the standard error of the observed value for that year (e.g., from Cormack-Jolly-Seber modeling; Gibson et al. 2024). We used binomial distributions to represent the stochastic process for observation of tags (i.e., as adults to inform survival from BON to LGR; eq. D44) and multinomial distributions for frequencies of adults by age and origin observed at weirs (eq. D46) and during carcass surveys (eq. D51), such that the magnitude of assumed observation error was a function of the sample size. In most cases, we linked observed values directly to latent states in this fashion (assuming unbiased sampling), but in the case of

fitting to age/origin frequencies in the carcass recovery data, we estimated correction factors that accommodated biased carcass counts relative to weir counts with respect to age (eqs. D47 – D50). States and transitions with data sources informing them through the observation model are denoted in Figure C2 by numbered circles.

C2.4 Model Fitting

C2.4.1 Bayesian Computation

We fitted the model to data using the Bayesian framework, which is advantageous for integrating over the multiple layers of uncertainty in SSMs (i.e., process vs. observational variability; de Valpine and Hilborn 2005). Posterior distributions of estimated parameters provided a seamless method to propagate uncertainty in quantities derived from estimated parameters. We used JAGS (v4.3.1; Plummer 2003) to perform Markov Chain Monte Carlo (MCMC) calculations, invoked through Program R (R Core Team 2023) and the 'jagsUI' package (Kellner 2021). We used the 'postpack' package (Staton 2022) to perform all posterior summarization, with the exception of the 'posterior' package (Bürkner et al. 2023) for MCMC convergence and sampling diagnostics (Vehtari et al. 2021). Our MCMC simulations involved four chains, each 150,000 iterations long with a burn-in period of 50,000 and a post-burn-in thinning rate of 25 (16,000 samples retained for inference). MCMC diagnostics included the $\hat{R}$ statistic to diagnose convergence (we deemed values $\leq$ 1.01, <1.05, <1.1, and >1.1 to be "ideal", "no issue", "acceptable", and "concerning", respectively), effective sample size to assess whether enough independent information exists to estimate posterior quantiles with precision (values >400 ideal), and MCMC coefficients of variation (expressed as MCMC standard error divided by mean) to assess the precision of posterior summaries; see Vehtari et al. (2021) for more details. We summarized MCMC diagnostics by relevant attributes (e.g., life stage, population, and origin) as the percent of values failing to meet a specific threshold, and we visualized MCMC traceplots for quantities with high $\hat{R}$ (Supplemental Material, Section 2). We report posterior summaries as the posterior mean and 95% equal-tailed credible limits (CRL).

C2.4.2 Priors

Our intent was to be as objective as possible, allowing the data to primarily shape the posterior; as such, we used flat priors in most cases (Table D3). However, we provided *a priori* information to constrain parameters when there was insufficient information in the data to either (*a*) heavily downweight biologically implausible values for identifiable parameters (e.g., maximum egg-to-parr survival rates >0.5) or (*b*) estimate an otherwise unidentifiable parameter (e.g., ocean survival in year-2 and year-3). We constructed priors for covariance matrices using scaled inverse-Wishart distributions (Gelman et al. 2014) that suggested smaller values (e.g., <0.5 or 1) were more likely for standard deviation terms, recognizing that these reflect variability on the log- or logit-scale; our scaled inverse-Wishart parameterization also gave Uniform(-1,1) distributions on all correlation

terms (Plummer 2017). Comparisons of non-flat priors to the posteriors (Supplemental Material, Section 14) implied that posteriors were shaped by the data and not the priors alone, unless this was their intended purpose (use case *b*, above).

C2.4.3 Model Fit Diagnostics

We used two primary methods to assess conformance of the data with model assumptions and both relied on the posterior predictive distribution. First, we performed a posterior predictive check as an overall index of fit (Supplemental Material, Section 12; Gelman et al. 2014). We simulated data from the model to calculate a Bayesian *p*-value: the proportion of MCMC iterations in which the observed data fitted more poorly than the simulated data (values near 0.5 are ideal; values >0.5 indicate a degree of over-dispersion). We calculated Bayesian *p*-values for each year within a given process and summarized them as the median, 2.5% and 97.5% percentiles, and the proportion of years with "extreme" *p*-values (i.e., <0.05 or >0.95).

Second, we used quantile-standardized residuals (Dunn and Smyth 1996) to investigate more detailed patterns in model-estimated noise terms (Supplemental Material, Section 11), given posterior predictive checks did not evaluate time trends or cycles in lack of fit. We used the posterior predictive distribution to calculate the cumulative probability of the realized (latent or observed) value such that values <0.5 corresponded to outcomes below model-expected values and those >0.5 above expectations. Across replicates of the same random process (i.e., years), we should expect these residuals to be distributed Uniform(0,1), with a mean of 0.5, a standard deviation equal to $\sqrt{1/12}$, and lack any time series trends (assessed as the difference in averages of the first and last halves of the time series) or cycles. Unlike Bayesian *p*-values, quantile-standardized residuals use the same fit statistic for all (observed and unobserved) stochastic values regardless of the assessed random process (e.g., logit-normal vs. binomial), providing a unified framework for assessing patterns in variability and conformance with model assumptions about stochasticity.

C2.5 Analyses of Hypotheticals

We performed two post-hoc "hypothetical" analyses to further demonstrate the utility of the model and samples from its joint posterior: (*i*) increased habitat availability and (*ii*) the loss of fall migrants. These are comparatively rudimentary examples of prospective uses of model output – future plans involve stochastic simulation of population trajectories under climate change and habitat restoration scenarios.

We constructed the model such that availability of high-quality habitat affected parr capacity (eq. D6) and density-dependent growth (eq. D9), which we then used as a predictor of survival during over-winter rearing (eqs. D13) and out-migration to LGR (eq. D19). Thus, we can demonstrate the expected change in freshwater juvenile survival and production resulting from

hypothetical increases in WUL (by 50%, 100%, and 200%) relative to their current values. We used process model equations and posterior draws to calculate expected values (i.e., without process noise) of freshwater juvenile processes at a range of fixed egg production values (converted to spawner abundance for interpretability). We compared the shape of resulting density-dependent curves for (*a*) survival from egg to smolt at LGR, (*b*) survival from parr to smolt at LGR, and (*c*) total smolt reaching LGR across hypothetical habitat levels.

Life history diversity in the timing of migration out of natal summer rearing locations and in the location of over-winter rearing may bolster freshwater production (Copeland et al. 2014) through portfolio effects that stabilize inter-annual variability (Thorson et al. 2014). We performed a simple evaluation of the contribution of the fall migrant strategy to production and stability by assuming historical parr recruitment and post-recruitment (including process noise) was identical as previously occurred, but that all parr became spring migrants (i.e., setting $\pi_{y,i=\text{fall},j} = 0$ in eq. D11). We performed post-hoc calculations using posterior draws and compared the total mean and inter-annual CV of smolt abundance arriving at LGR (within and aggregated across populations) between this hypothetical "no fall migrants" scenario and the unaltered posterior estimates. We expected that this simulated reduction in life history variability would change the magnitude of smolt production (resulting from different fall and spring migrant survival rates) and increase the CV (due to increased of synchrony).

C3 Results

C3.1 MCMC Convergence and Model Fit

We achieved overall good convergence (Supplemental Material, Section 2) despite the complexity of the model: 99% of unobserved stochastic quantities (i.e., parameters) fell into our "ideal/no issue" categories ($\hat{R} < 1.05$), 1% were deemed "acceptable" ($1.05 < \hat{R} < 1.1$) and 4 parameters (<1%) were deemed "concerning" ($\hat{R} > 1.1$). Parameters with $\hat{R} > 1.01$ were most often the latent states, though some variance and correlation parameters met this criterion, as did a few coefficients of demographic relationships. Most parameters achieved an effective sample size of >400 for estimating 2.5$^{\text{th}}$ and 97.5$^{\text{th}}$ posterior percentiles whereas it was more common to have fewer effective samples for estimating the mean.

Fit to the data was good as well, as evidenced by plots of observed vs. predicted values (Figure C3), quantile-standardized residuals (Supplemental Material, Section 11), and posterior predictive checks (Supplemental Material, Section 12). Among all data sets, fits to the age/origin composition data (weir and carcass) were the poorest according to both quantile-standardized residuals and posterior predictive checks, including some evidence for time trends in the of lack of fit (Supplemental Material, Section 11.2.4).

C3.2 Life Cycle Parameter Summary

C3.2.1 Freshwater Juvenile Phase

Posterior mean egg-to-parr survival rates were low relative to most other survival rates estimated by the model but variable, averaging ~0.15 and ranging ~0.01-0.42 across years and populations (Figure C4a). Theoretical maximum average survival (i.e., in the absence of density dependence) ranged from 0.14 (0.07-0.24; UGR)[2] to 0.21 (0.11-0.34; CAT) and parr rearing capacity ranged from 120,931 (59,600-247,271; CAT) to 975,795 (331,771-2,511,090; MIN). Parr rearing capacity was estimated to increase on average by 18,224 (5,259-31,069) for every 1 km increase in WUL (Figure C5). Assuming the time series average for eggs-per-spawner (~1,750), 100 spawners per population (of all ages/sexes) translated to expected parr recruits-per-spawner of 217 (116-331) for UGR, 255 (167-369) for LOS, 266 (154-363) for CAT, and 300 (197-427) for MIN. Reducing spawner abundance to 50 under these same conditions resulted in nearly a 15% (5-27%) increase in parr per spawner for CAT, but the other populations had increases of 6% or less. Process noise around the survival relationship implied by the Beverton-Holt function was moderately auto-correlated (Supplemental Material, Sections 4.1 and 4.2), with AR(1) coefficients averaging 0.49 (0.2-0.73) across populations.

Following recruitment, the majority of parr exhibited the spring migrant life history strategy (Figure C6a), with the fall migrant strategy ranging from an average of 9% (7-12%; UGR) of parr to 37% (32-43%; CAT). However, estimated over-winter rearing survival was consistently higher for fall migrants (average: ~0.5-0.6) than for spring migrants (average: 0.2-0.3; Figure C4b). Posterior mean over-winter survival for spring migrants exceeded that of fall migrants in only two brood years (2002 and 2003) for one population (UGR), although 95% CRLs overlapped for 66% of years – other populations ranged from no years of overlap (LOS) to 44% of years (CAT). Survival of NOR smolts migrating to LGR was more variable across populations, with CAT and UGR each averaging ~0.4 and LOS and MIN each averaging ~0.6. For populations with hatchery supplementation (CAT, LOS, and UGR), average out-migration survival to LGR (Figure C4c) was similar between HOR and NOR smolts, but survival through the hydrosystem in the average year (Figure C4d) was higher for HOR smolts at 0.57 (0.48-0.66) compared to NOR smolts at 0.52 (0.46-0.57). Although hydrosystem survival was highly variable across years (Figure C4d), it lacked any major time trend (Supplemental Material, Section 3.2.5). Time series of juvenile abundance and survival outcomes are shown in Supplemental Material, Sections 3-6, and composite rates showing conversions across multiple life stages are shown in Supplemental Material, Section 9.

[2]Ranges in parentheses immediately following a number indicate 95% credible limits, except where otherwise noted.

C3.2.2 Ocean Phase

Relative to other survival rates estimated by the model (except that from egg-to-parr), survival during the first year at sea was low: for NOR fish, across-year means ranged from 0.08 (0.05-0.12; UGR) to 0.13 (0.09-0.17; CAT), yet varied widely inter-annually, with some rare years seeing posterior mean survival rates of <0.05 or >0.3 (Figure C4e). Year-1 ocean survival was lower still for HOR fish (Figure C4e) – the odds of survival for HOR fish was 0.37 (0.33-0.4) times that of NOR fish for CAT, though somewhat higher for LOS at 0.55 (0.5-0.59) and UGR at 0.52 (0.47-0.57). Few fish that survived the first year at sea matured and returned at age-3: <10% matured in the average year for NOR fish across all populations with a consistent pattern of higher year-1 maturation rates in HOR fish (Figure C6b). In contrast, most fish that survived a second year at sea matured at age-4: >75% in the average year and again we found a pattern of higher maturation rates for HOR fish (Figure C6c) – i.e., HOR fish tended to return at younger ages than NOR fish. Maturation rates were quite variable among years, with posterior means ranging from <0.01-0.3 for year-1 and 0.3-0.99 for year-2 (Figure C6c).

C3.2.3 Freshwater Adult Phase

Survival along the upstream migration from BON to LGR was high relative to other survival terms in the model – ~80% of fish survived this migration in the average year and the rate was relatively consistent over time with values ranging 0.7 to 0.85 (Figure C4d). All other adult survival terms came in the form of auxiliary data sources (Supplemental Material, Section 15) and included (*i*) harvest rates below BON (<5% annually for NOR fish and 10-15% for HOR fish), (*ii*) harvest in tributaries (nearly exclusively in LOS, majority of years <10% of total return to river harvested, but one year [2015] nearing 40%, primarily HOR and age-4 harvested), (*iii*) weir removals (all populations except MIN, 20-30% of total return removed on average, mostly HOR, and age-3 and age-4), and (*iv*) pre-spawn mortality (lowest on average for MIN [0.02] and CAT [0.05], then LOS [0.14], and highest for UGR [0.22]). When incorporating all sources of loss and mortality, composite average adult survival rates from the estuary to successful spawning ranged from 0.36-0.77, depending on origin and population (Supplemental Material, Section 9.5) – overall, survival was higher for NOR fish (all-year, all-population average: 0.63) than HOR fish (0.39). Considering all ages versus only age-4 and age-5 did not substantially affect these estimates.

C3.3 Demographic Relationships

The magnitude of density dependence in egg-to-parr survival ranged from moderate to strong depending on the population, as evidenced by declining survival with increasing egg production (Figure C7a). Parr growth rates, indexed by parr mean length (Figure C7c), were also estimated to be strongly density-dependent – years with the largest sizes (~75mm) corresponded to those with the lowest total egg production, and years of smaller sizes (~60-65mm) corresponded to those with

higher densities. Over-winter survival was positively related to parr mean length for all populations except CAT (Figure C7d): for each 1 SD increase in mean length (~5mm), the odds of survival increased by a factor of 1.16 (1.09-1.24; LOS), 1.14 (0.86-1.53; UGR), and 1.35 (1.19-1.51; MIN) – these rates were assumed to apply equally to fall and spring migrants. The change in mean length from parr to smolt was negatively related to parr size (i.e., greatest multiplicative change for smaller initial lengths; Supplemental Material, Section 5.2.2), but years with larger parr still coincided with years of larger smolt size (Figure C7e). NOR smolt survival during out-migration to LGR was positively related to smolt mean length, such that a 1 SD increase in smolt mean length was associated with a change in the odds of survival by a factor of 1.23 (1.13-1.34) for the average population. For example, in a year with smolt mean length equal to 85mm, NOR out-migration survival for CAT was expected to be 0.34 (0.28-0.39), compared to 0.5 (0.42-0.6) in a year with smolt mean length of 95mm.

C3.4 Synchrony in Population Dynamics

Year-specific parameter estimates, which accounted for environmental variability (i.e., process noise) unexplained by demographic relationships, had correlations among population pairs that were overwhelmingly positive (Figure C8). This indicates that years of higher-than-expected outcomes (e.g., better-than-average survival) were shared to some degree among populations. For example, variability in egg-to-parr survival not explained by Beverton-Holt dynamics or the AR(1) process had a correlation coefficient of 0.25 (0.04-0.6) averaged across all population pairs (Figure C8), with some populations more correlated such as CAT and MIN with a posterior mean of 0.54 (0-0.9) than others, such as LOS and UGR at 0.07 (-0.42-0.52; Supplemental Material, Section 10.2.2). The three processes with the highest correlations were those that occurred in the shared ocean environment: year-1 survival and year-1/year-2 maturation rates – the average correlation across population pairings for these processes had posterior means all >0.5, and no population pairing had posterior mean correlation <0.25 (Figure C8). Survival through the hydrosystem, both as out-migrating smolt and returning adults, had positive but uncertain estimated correlations, and were the two processes modeling correlation among origins rather than populations. Among survival processes, over-winter rearing survival from parr to smolt showed the lowest correlations. The only process that had predominately negative correlation coefficients was the probability that parr become fall migrants (Figure C8).

C3.5 Analyses of Hypotheticals

C3.5.1 Increased Habitat Availability

We found that increasing habitat availability (i.e., WUL) in each sub-basin had the effect of reducing density dependence in growth and survival processes during the freshwater juvenile phase for their respective populations, including higher estimated survival from egg-to-smolt (Figure C9a-d)

and parr-to-smolt (Figure C9e-h). The former incorporates density effects that are both direct (i.e., Beverton-Holt recruitment dynamics) and indirect (i.e., delayed effects – size affects survival, and size is density-dependent), whereas the latter shows only indirect effects. Converted to a relationship between LGR smolts and parental spawners (Figure C9i-l), increasing WUL increased smolt production per spawner; notably, gains in the number of smolts arriving at LGR were minor at low spawner densities but more substantial at high spawner densities.

C3.5.2 Loss of Fall Migrants

We found that the number of smolts arriving at LGR would be lower and more variable if all parr had become spring migrants, rather than the observed mixture (Table C1). The CAT, LOS, and MIN populations would all have produced 25-30% fewer smolts, and UGR would have produced 8% fewer smolts (26% reduction totaled across all populations) – the difference among populations is due to the smaller actual contribution of fall migrants to UGR (Figure C6a). Two of the four populations showed increased inter-annual CVs with our hypothetical removal of this life history diversity, with CAT increasing from 51% to 59% and MIN from 51% to 57% (Table C1). However, the two other populations showed little change (1% change in CV) and the CV of the aggregation of all populations only increased from 44% to 46% (Table C1).

C4 Discussion

We have constructed a multi-population integrated SSM for Grande Ronde spring Chinook salmon by combining data on life stage-specific survival, abundance, and age/origin composition and linked population dynamics parameters to freshwater habitat availability. Instead, our purpose was to obtain a parameterized model that represents hypothesized population processes (e.g., density dependence, size-based survival) specific to each life stage, decomposed into deterministic (i.e., fixed relationships) and stochastic (i.e., unexplained inter-annual variability) components. With respect to the stochastic components, the SSM further decomposed variability into biological/environmental process noise – which we have demonstrated is correlated among populations – and observational measurement error. Our use of the Bayesian framework provided a joint posterior distribution from which we can sample for parameterizing specific post-hoc analyses, two of which we demonstrated here. Perhaps the most useful follow-up application will be for populating stochastic simulation models for probabilistic evaluation of hypothetical futures under various restoration and other interventional scenarios. Had we used a simpler analytical framework, we would have less confidence in the estimates used to populate these follow-up applications.

The model integrated a wide variety of data sources (including biological and physical habitat), as well as multiple populations, juvenile life histories (fall vs. spring migrants), rearing types (NOR vs. HOR), and adult ages-of-return. This integration – enabled by the extensive monitoring efforts

initiated in the early 1990s and facilitated by the state-space framework – allowed rigorous estimation of many different demographic parameters and relationships among them. Some inferences from the model solidified previously known patterns (e.g., HOR fish tend to mature earlier and have lower smolt-to-adult survival rates than NOR fish), whereas others highlighted previously unquantified patterns for these populations (e.g., synchrony in demographic rates among populations at a variety of life stages and the large discrepancy between fall and spring migrant survival). Furthermore, our application of the SSM enabled more statistically rigorous estimation of previously quantified relationships for these populations (e.g., the Beverton-Holt recruitment function, size-based survival; Cooney et al. 2017; Staton et al. 2023) by acknowledging the time series and measurement error properties of the data sets.

C4.1 Biological Implications of Findings

The direct density-dependent processes we modeled in the freshwater juvenile phase included survival and growth from the egg to the parr stage. We modeled the capacity term that mediated egg-to-parr survival as a function of available quality habitat (WUL; Figure C5) and early-life growth rates as a function of density. We indexed this growth rate by parr size upon capture in late-summer, which then facilitated building size-based survival relationships. Taken together, the strength and directionality of these relationships indicated that increased population density early in life resulted in lower egg-to-parr survival (Figure C7a) and growth rates (parr size; Figure C7c), which translated into lower survival as over-wintering parr (Figure C7d) and out-migrating smolt (Figure C7f). This represents evidence of indirect and delayed effects of density dependence. Many other studies have found evidence of early-life density-dependent effects on growth and survival (e.g., Walters et al. 2013; Grossman and Simon 2020); however, ours is the first – to our knowledge – to incorporate these dynamics explicitly into a stochastic retrospective salmon population dynamics model.

Because we tied the strength of the direct density-dependent processes to WUL, we now have estimates of how available habitat mediates the effect of density on parr rearing capacity (and thus, density-specific egg-to-parr survival) and growth rates. In one hypothetical post-hoc analysis, we used these relationships to illustrate how additional quality habitat (e.g., via intense restoration actions) could weaken freshwater density dependence and result in higher per capita productivity (e.g., smolt reaching LGR per spawner). However, the +50%, +100%, and +200% WUL scenarios showed much less dramatic differences in overall smolt production at low spawner densities than at high densities (Figure C9i-l). This finding reveals that we should not expect habitat restoration alone to boost population abundance in the near term, but rather that the greatest benefits of increased freshwater habitat will be seen under higher spawner densities. However, there were clear linkages between juvenile size and survival, thus restoration actions that diversity and increase prey resources

(Flitcroft et al. 2022; Rossi et al. 2024) may increase growth, size, and size-based survival even at low spawner densities.

Our integrated SSM facilitated the joint analysis of biological diversity in these populations, reinforcing and uncovering knowledge about how heterogeneity in demographic rates among these populations and population subcomponents contribute to dynamics at aggregated scales (Schindler et al. 2010). Juvenile fall out-migrants are outnumbered at the parr stage (comprising roughly 25-35% of all parr in the average year for the CAT, LOS, and MIN populations, ~10% for UGR; Figure C6a) but make a comparatively larger contribution to total smolt out-migrants reaching LGR (roughly 40-60% on average for CAT, LOS, and MIN, ~15% for UGR) due to higher survival during over-winter rearing and/or spring out-migration to LGR. This conclusion, facilitated by our joint analysis of the freshwater juvenile and adult monitoring data, highlights the importance of life history diversity for Grande Ronde spring Chinook salmon populations. Baker et al. (2025) reported similar findings in a more southern population of coho salmon (*O. kisutch*), wherein the early-migrating juvenile life history strategy was less prevalent, but displayed higher survival and thus contributed comparatively more to the adult abundance than their later-migrating counterparts. This heterogeneous survival also sheds light on a potentially fruitful area for restoration activities: if spring migrant over-winter survival was increased through restoration actions, the number of smolts reaching LGR would increase by a larger amount than would result from proportional increases in fall migrant survival. Similar heterogeneity was captured by integrating the analysis of HOR and NOR fish, and we were able to draw similar conclusions within the same inferential framework. Upon arrival at LGR, HOR smolts vastly outnumber NOR smolts, and although HOR adults still outnumber NOR adults returning to tributaries, the magnitude is diminished in the average year (CAT: 90% of LGR smolt vs. 68% of returning adults; LOS: 87% vs. 75%; UGR: 91% vs. 83%) due to lower out-of-basin survival of HOR fish, particularly at sea.

Among the most novel findings from our integrated analysis was related to the extent of synchronous variability among populations. It has been noted previously that adult salmon returns to Columbia River sub-basins appear to follow similar patterns (i.e., years with above-average returns are shared among populations; Jorgensen et al. 2016; Crozier et al. 2021), however no previous analyses for Grande Ronde populations have sought to evaluate which processes and life stages show the greatest synchrony. We found broad evidence of positive correlations in the process noise surrounding demographic rates throughout the entire life cycle. Although the magnitude varied among processes, the only process for which the correlation was predominately negative was the apportionment rate of parr to become either spring or fall migrants (Figure C8). This finding of primarily positive correlations throughout life implies that inter-annual variability in population-level demographic rates is in part driven by some broader scale factors that jointly affect all populations.

Because these populations spawn within different tributaries of the same watershed, they are likely to experience similar hydrologic conditions – the inter-annual fluctuations of which appear to have similar population-level responses throughout the basin. The strongest correlations we quantified were for those processes occurring in the shared ocean environment: year-1 ocean survival and maturation rates. These inferences are intuitive and give us confidence in interpreting not only the directionality of the correlations we estimate, but also their comparative magnitudes.

The positive correlations in demographic rates among these populations have two important implications. First, we should not expect to see a strong portfolio effect for the aggregate return to Grande Ronde Basin arising from the multiple populations, as portfolio effects are caused by asynchronous dynamics. Second, to the extent that the shared hydrologic and oceanographic conditions that operate to force these synchronous dynamics will be affected (presumably negatively; Crozier et al. 2021; Gallagher et al. 2022) by climate change, we should expect similar responses from the multiple populations.

C4.2 Weaknesses and Caveats

The rigorous modeling effort and development of this SSM yielded many benefits, but there are weaknesses and caveats worth expanding upon. With a model as complex as this (MCMC monitored 21,543 quantities, 1,995 of which were "unobserved stochastic quantities", i.e., estimated parameters), there are truly thousands of possible model designs and substructures. We considered many different structures during development of the model (many are described in the development history documented on GitHub; archived under Staton 2025); however, we viewed these as steps towards constructing a final model, rather than alternative models from which to base inference. This, of course, is an oversimplification and an area for potential improvement to our work – of all the types of uncertainty the model quantified, we did not consider model uncertainty. As a baseline assumption, for example, the model allowed nearly all quantities to vary by population and year, and did not consider the possibility that some populations may have the same parameter values guiding their population dynamics. We made this "fully heterogeneous" assumption to allow comparisons among populations and other levels of organization, as forcing common parameters would preclude such comparisons. Our expectation was that if parameters were similar enough as to be considered functionally identical, then this would arise in the posterior as informed by the data. Still, the model may allow more heterogeneity than is actually warranted by variability in the data and as a result, some parameters will be more uncertain than under simpler model structures.

As complex as the model is, there are several places where we chose to simplify real complexity. Good examples are found in the downstream and upstream migrations through the hydrosystem and in the ocean survival/maturation components. A primary goal of this modeling effort was to develop a model capable of evaluating impacts of restoration and other management actions in tributary

habitats on future population status. Therefore, we chose the model structures for the mainstem migration and ocean phase to be minimally complex while still capturing variability between the two freshwater tributary phases of the life cycle (juvenile and adult). We chose to allow year-1 ocean survival to vary annually, forced year-2 and year-3 ocean survival terms to be time-constant, and allowed the maturation parameters to vary annually. Because we forced time-constant late-ocean survival, some of the variability quantified in the parameters describing the probability of maturing at age-4 includes variability in survival as well. While there is much complexity that could be added to these model structures, we did not feel that more complexity could be reliably estimated given the data set. Ultimately, the model received high quality information about annual smolt-to-adult return rates – as informed by the total number of smolts (by population and origin) arriving to LGR and the number of adults returning to tributaries (by population, origin, and age) – and we believe we selected a model structure sufficient to capture variability in the data while partitioning it into biologically meaningful parameters.

In modeling the correlation structures among time-varying parameters, we made a critical assumption that covariance occurs across populations (or in some cases, origin types) for a given life stage. An alternative way to model correlation would have been to assume parameters covary within each population, rather than across populations. For example, the model assumed that the process noise terms for egg-to-parr survival and growth covary across populations, but that these terms are independent of one another within a given population. If the same environmental conditions affect both processes, then perhaps we should expect the realizations of these processes to covary within populations. If evidence exists for this in the data, the process noise terms for historical realizations will be correlated; however, this property would not be reflected in the model structure and will not propagate to any simulations produced from this model. This has potential ramifications for the variance of the composite of nonadjacent processes; for example, if the survival from life stages *A* to *B* truly has positive covariance with the survival from stages *B* to *C*, a simulation model that assumes independence will result in higher variance in the composite survival rate from *A* to *C* than should actually exist. This could have important ramifications for the distributions of outcomes from such a simulation model (i.e., being less confident in the range of outcomes) and thus perhaps warrants further exploration.

C4.3 Advancements and Future Work

We believe this model represents an advancement in the application of integrated SSMs to Pacific salmon time series data. With respect to naturally produced freshwater juveniles, we separated density dependence into direct (early life survival and growth) and indirect (size-based survival) effects, which are consistent with observations in the Grande Ronde Basin (Cooney et al. 2017; Staton et al. 2023) and elsewhere in the Columbia River Basin at large (Walters et al. 2013; Zabel and

Achord 2004). Further, we tied the strength of these effects to available habitat (WUL), providing a framework to evaluate how alternative habitat restoration scenarios may affect population dynamics. We incorporated HOR fish by modeling their dynamics directly from the time of release to their return alongside the NOR fish, which is more comprehensive than other approaches that may only model population dynamics of NOR fish, for example by inserting adult HOR returns such that they can be accounted for in natural spawning but not including their juvenile life stages. Hatchery supplementation in the Grande Ronde Basin is intended to maintain and enhance natural production, with HOR fish contributing to natural spawning each year. The ability to realistically model returning HOR adults each year alongside NOR fish is critical for assessing the impact of future restoration scenarios on naturally spawning populations. Tracking HOR fish throughout the life cycle also provided additional information to better inform NOR dynamics, namely in year-1 ocean survival. Beyond the model structure, we also applied two detailed and comprehensive model checking frameworks for evaluating whether the model agreed well with the data (quantile-standardized residuals and posterior predictive checks; Supplemental Material, Sections 11 and 12) in addition to the simple and more commonly applied diagnostic shown in Figure C3.

Our next steps will be to use the output of this model to populate a stochastic simulation model that can be subjected to future scenarios including alternative restoration, hatchery operation, and climate change actions. By partitioning the life cycle into fine-scale growth and survival processes for individual life stages, we will be able to apply hypothetical changes to these processes as influenced by external drivers. We designed the WUL metric to be especially useful for this purpose. It is derived from reach-level habitat attributes, so restoration scenarios can be spatially structured depending on which actions are planned in which areas. Via the relationships we have modeled currently, changes to WUL will affect only parr rearing capacity and growth rates to the parr stage (and subsequent size-based survival). However, this will not preclude us from evaluating other restoration actions that may increase growth and survival in other life stages, such as over-winter rearing, migration out of the basin, or adult pre-spawn survival. Just as restoration is expected to increase habitat quantity and quality, we can also evaluate projected deleterious impacts of climate change on available habitat and pre-spawn survival (e.g., Bowerman et al. 2021), as well as devise scenarios reflecting negative out-of-basin effects. In short, the retrospective population model we developed will be a useful parameterized blueprint for prospective modeling aimed at evaluating the likely effects of management interventions on future population status.

Development of this integrated SSM for Grande Ronde spring Chinook salmon populations required a substantial undertaking. However, with this framework in place and the code and data to fit the model publicly accessible (Staton 2025; Gibson 2025), far less effort would be required to adapt and apply the model to other populations, species, and locations in which similar data are

available. In particular, there are several other systems within the Columbia River Basin (e.g., spring Chinook salmon populations in the John Day River) with similar monitoring frameworks providing opportunities for further learning and testing of the hypotheses upon which the version applied to Grande Ronde spring Chinook salmon populations is based.

Acknowledgments

We first thank D. A. McCullough, formerly of the Columbia River Inter-Tribal Fish Commission, for initiating the proposal and pilot fieldwork which were the origins of this large scale, long-term project. We are grateful to the countless field personnel – employed primarily by the Confederated Tribes of the Umatilla Indian Reservation, Nez Perce Tribe, and the Oregon Department of Fish and Wildlife – who worked to collect the wealth of monitoring data upon which this modeling work depended. Gratitude is also due to T. Cooney, as the freshwater juvenile portion of our model was informed by some of his ideas and research. R. Lessard and T. Garrison gave important input regarding the out-of-basin portions of our model, especially surrounding mainstem and ocean survival. We thank S. Ellis and K. Self for their assistance in obtaining harvest rate estimates downstream of Bonneville Dam. We thank the internal agency reviewers and journal-appointed reviewers for their feedback, which ultimately improved the manuscript.

Funding Sources

Funding for data collection was provided by Bonneville Power Administration and the Lower Snake River Compensation Plan. Model development was supported by the Bonneville Power Administration as part of the Columbia Basin Fish Accords Agreement (Project #2009-004-00). The funding organization had no involvement in the study design, collection, analysis and interpretation of data, writing of the manuscript, or any other decisions regarding publication.

Competing Interests

The authors declare no competing interests.

Data Availability

Data used to fit the model are available in the GitHub repository at https://www.github.com/gibsonpp/GR-sslcm-data (archived under Gibson 2025). The code for model fitting, including the JAGS model definition, data formatting, and posterior summarization is available in the GitHub repository at https://www.github.com/bstaton1/GR-sslcm (archived under Staton 2025)[3].

CRediT Author Roles

- **B.A. Staton** (conceptualization, formal analysis, investigation, methodology, software, validation, visualization, writing – original draft, writing – review and editing)

[3]These repositories will be archived using Zenodo upon manuscript acceptance and archival DOIs will be created at that time.

- **P.P. Gibson** (conceptualization, data curation, formal analysis, investigation, methodology, visualization, writing – original draft, writing – review and editing)
- **M. Liermann** (conceptualization, formal analysis, investigation, methodology, writing – review and editing)
- **C. Justice** (conceptualization, data curation, formal analysis, funding acquisition, investigation, methodology, project administration, supervision, writing – review and editing)
- **M.J. Kaylor** (conceptualization, investigation, methodology, writing – original draft, writing – review and editing)
- **R. Sharma** (conceptualization, formal analysis, investigation, methodology)
- **S.M. White** (conceptualization, funding acquisition, investigation, methodology, project administration, supervision, writing – review and editing)

References

Achord, S., Levin, P. S., and Zabel, R. W. 2003. Density-dependent mortality in Pacific salmon: The ghost of impacts past? *Ecology Letters*, 6(4):335–342. doi:10.1046/j.1461-0248.2003.00438.x.

Auger-Méthé, M., Newman, K., Cole, D., Empacher, F., Gryba, R., King, A. A., Leo-Barajas, V., Flemming, J. M., Nielsen, A., Petris, G., and Thomas, L. 2021. A guide to state–space modeling of ecological time series. *Ecological Monographs*, 91(4):e01470. doi:10.1002/ecm.1470.

Baker, H. K., Obedzinski, M., Grantham, T. E., and Carlson, S. M. 2025. Variation in salmon migration phenology bolsters population stability but is threatened by drought. *Ecology Letters*, 28(2):e70081. e70081 ELE-01115-2024.R3. doi:10.1111/ele.70081.

Beckerman, A., Benton, T. G., Ranta, E., Kaitala, V., and Lundberg, P. 2002. Population dynamic consequences of delayed life-history effects. *Trends in Ecology & Evolution*, 17(6):263–269. doi:10.1016/S0169-5347(02)02469-2.

Bjørnstad, O. N., Ims, R. A., Lambin, X., Bjørnstad, O. N., Ims, R. A., Lambin, X., Bjørnstad, O. N., Ims, R. A., Lambin, X., Bjørnstad, O. N., Ims, R. A., Lambin, X., Bjørnstad, O. N., Ims, R. A., and Lambin, X. 1999. Spatial population dynamics: Analyzing patterns and processes of population synchrony. *Trends in Ecology & Evolution*, 14(11):427–432. doi:10.1016/S0169-5347(99)01677-8.

Bliesner, K. L., Craft, N. M., Feldhaus, J. W., and Ruzycki, J. R. 2020. A compendium of viable salmonid population abundance and productivity field and analysis methods for natural origin adult Chinook salmon populations in the Snake River spring/summer-run ESU of northeast Oregon from 1949-2019. Technical report, Oregon Department of Fish and Wildlife, East Region Fish Research. URL: https://nrimp.dfw.state.or.us/DataClearinghouse/default.aspx?p=202&XMLname=1151.xml.

Bouchard, C., Buoro, M., Lebot, C., and Carlson, S. M. 2022. Synchrony in population dynamics of juvenile Atlantic salmon: Analyzing spatiotemporal variation and the influence of river flow and demography. *Canadian Journal of Fisheries and Aquatic Sciences*, 79(5):782–794. doi:10.1139/cjfas-2021-0017.

Bourret, S. L., Caudill, C. C., and Keefer, M. L. 2016. Diversity of juvenile Chinook salmon life history pathways. *Reviews in Fish Biology and Fisheries*, 26(3):375–403. doi:10.1007/s11160-016-9432-3.

Bovee, K. D. 1982. Guide to stream habitat analysis using the instream flow incremental methodology. Instream Flow Information Paper FWS/OBS-82/26, U.S. Fish and Wildlife Service, Springfield, VA.

Bowerman, T. E., Keefer, M. L., and Caudill, C. C. 2021. Elevated stream temperature, origin, and individual size influence Chinook salmon prespawn mortality across the Columbia River Basin. *Fisheries Research*, 237:105874. doi:10.1016/j.fishres.2021.105874.

Bürkner, P.-C., Gabry, J., Kay, M., and Vehtari, A. 2023. posterior: Tools for working with posterior distributions. R package version 1.4.1. URL: https://mc-stan.org/posterior/.

CHaMP 2016. *Scientific Protocol for Salmonid Habitat Surveys within the Columbia Habitat Monitoring Program*. Columbia Habitat Monitoring Program. URL: https://www.champmonitoring.org/Program/RetrieveProgramDocumentFile/Tab/1126.

Chen, E. K., Satterthwaite, W. H., Kormos, B. J., Johnson, R. C., Phillis, C. C., and Carlson, S. M. 2023. Age structure of natural versus hatchery-origin endangered Chinook salmon and implications for fisheries management in California. *Marine Ecology Progress Series*, 723:37–55. doi:10.3354/meps14446.

Connors, B. M., Siegle, M. R., Harding, J., Rossi, S., Staton, B. A., Jones, M. L., Bradford, M. J., Brown, R., Bechtol, B., Doherty, B., Cox, S., and Sutherland, B. J. G. 2022. Chinook salmon diversity contributes to fishery stability and trade-offs with mixed-stock harvest. *Ecological Applications*, 32(8):e2709. doi:10.1002/eap.2709.

Cooney, T. D., Jonasson, B. C., Sedell, E. R., Hoffnagle, T. L., and Carmichael, R. W. 2017. Grande Ronde spring Chinook populations: Juvenile based models. In *NOAA Fisheries' Interior Columbia Basin Life-Cycle Modeling*, pages 1–30.

Copeland, T. and Venditti, D. A. 2009. Contribution of three life history types to smolt production in a Chinook salmon (*Oncorhynchus tshawytscha*) population. *Canadian Journal of Fisheries and Aquatic Sciences*, 66(10):1658–1665. doi:10.1139/F09-110.

Copeland, T., Venditti, D. A., and Barnett, B. R. 2014. The importance of juvenile migration tactics to adult recruitment in stream-type Chinook salmon populations. *Transactions of the American Fisheries Society*, 143(6):1460–1475. doi:10.1080/00028487.2014.949011.

Crozier, L., Dorfmeier, E., Marsh, T., Sandford, B., and Widener, D. 2016. Refining our understanding of early and late migration of adult Upper Columbia spring and Snake River spring/summer Chinook salmon: Passage timing, travel time, fallback and survival. Technical report, Fish Ecology Division, NMFS Northwest Fisheries Science Center,

Seattle, WA. URL: https://www.webapps.nwfsc.noaa.gov/assets/11/9043_02102017_113115_Crozier%20et%20al%202016%20Chinook%20adult%20mig%20timing%20survival-Mar08_2016.pdf.

Crozier, L. G., Burke, B. J., Chasco, B. E., Widener, D. L., and Zabel, R. W. 2021. Climate change threatens Chinook salmon throughout their life cycle. *Communications Biology*, 4(1):1–14. doi:10.1038/s42003-021-01734-w.

Crump, C., Naylor, L., Van Sickle, A., Kennedy, J., Cottingham, M., and Shippentower, G. 2024. Monitoring and evaluation of supplemented spring Chinook salmon and life histories of wild summer steelhead in the Grande Ronde Basin. Annual Report for BPA Project #2007-083-00, Confederated Tribes of the Umatilla Indian Reservation, Pendleton, OR. URL: https://www.cbfish.org/Document.mvc/Viewer/P208816.

CTC 1988. Exploitation rate analysis - Appendix 2 to Chinook technical committee 1987 annual report. Technical Report TCCHINOOK (88)-2, CTC Analytical Work Group. URL: https://www.psc.org/download/35/chinook-technical-committee/2150/tcchinook88-2app2.pdf.

Cunningham, C. J., Westley, P. A. H., and Adkison, M. D. 2018. Signals of large scale climate drivers, hatchery enhancement, and marine factors in Yukon River Chinook salmon survival revealed with a Bayesian life history model. *Global Change Biology*, 24(9):4399–4416. doi:10.1111/gcb.14315.

DART 2023. PIT tag adult returns conversion rate. URL: https://www.cbr.washington.edu/dart/query/pitadult_conrate.

de Valpine, P. and Hastings, A. 2002. Fitting population models incorporating process noise and observation error. *Ecological Monographs*, 72(1):57–76. doi:10.1890/0012-9615(2002)072[0057:FPMIPN]2.0.CO;2.

de Valpine, P. and Hilborn, R. 2005. State-space likelihoods for nonlinear fisheries time-series. *Canadian Journal of Fisheries and Aquatic Sciences*, 62(9):1937–1952. doi:10.1139/f05-116.

Dunn, P. K. and Smyth, G. K. 1996. Randomized quantile residuals. *Journal of Computational and Graphical Statistics*, 5(3):236–244. doi:10.1080/10618600.1996.10474708.

Feldhaus, J., Brandt, E., Tattam, I., Vatland, S., Crump, C., and Naylor, L. 2022. 2022 Grande Ronde and Imnaha River basin spring Chinook salmon hatchery review. Technical report, Oregon Department of Fish and Wildlife; Nez Perce Tribe; Confederated Tribes of the Umatilla Indian Reservation. URL: https://www.fws.gov/sites/default/files/documents/2A%20-%202022%20Grande%20Ronde%20and%20Imnaha%20Basin%20Spring%20Chinook%20ISRP%20review.pdf.

Fleischman, S. J., Catalano, M. J., Clark, R. A., and Bernard, D. R. 2013. An age-structured state-space stock–recruit model for Pacific salmon (*Oncorhynchus* spp.). *Canadian Journal of Fisheries and Aquatic Sciences*, 70(3):401–414. doi:10.1139/cjfas-2012-0112.

Flitcroft, R. L., Brignon, W. R., Staab, B., Bellmore, J. R., Burnett, J., Burns, P., Cluer, B., Giannico, G., Helstab, J. M., Jennings, J., Mayes, C., Mazzacano, C., Mork, L., Meyer, K., Munyon, J., Penaluna, B. E., Powers, P., Scott, D. N., and Wondzell, S. M. 2022. Rehabilitating valley floors to a Stage 0 condition: A synthesis of opening outcomes. *Frontiers in Environmental Science*, 10. doi:10.3389/fenvs.2022.892268.

Ford, M. J. 2022. Biological viability assessment update for Pacific salmon and steelhead listed under the Endangered Species Act: Pacific Northwest. Technical Report 171, NMFS Northwest Fisheries Science Center. URL: https://doi.org/10.25923/kq2n-ke70.

Gallagher, B. K., Geargeoura, S., and Fraser, D. J. 2022. Effects of climate on salmonid productivity: A global meta-analysis across freshwater ecosystems. *Global Change Biology*, 28(24):7250–7269. doi:10.1111/gcb.16446.

Gelman, A., Carlin, J. B., Stern, H. S., Dunson, D. B., Vehtari, A., and Rubin, D. B. 2014. *Bayesian Data Analysis*. Texts in Statistical Science. Chapman & Hall/CRC, Boca Raton, FL, 3 edition.

Gibson, P. 2025. GR-sslcm-data: Github repository storing data to fit the Grande Ronde Basin state-space life cycle model for spring Chinook salmon. Archival DOI not yet available. URL: https://github.com/gibsonpp/GR-sslcm-data.

Gibson, P. P., Drascic, F. J., and Lemanski, J. R. 2024. Investigations into the life history of naturally produced spring Chinook salmon and summer steelhead in the Grande Ronde River subbasin, 2023. BPA Annual Report for Project 1992-026-04, Oregon Department of Fish and Wildlife, La Grande, OR. URL: https://nrimp.dfw.state.or.us/DataClearinghouse/default.aspx?p=202&XMLname=42802.xml.

González-Megías, A., Gómez, J. M., and Sánchez-Piñero, F. 2005. Consequences of spatial autocorrelation for the analysis of metapopulation dynamics. *Ecology*, 86(12):3264–3271. doi:10.1890/05-0387.

Grant, J. W. A. and Imre, I. 2005. Patterns of density-dependent growth in juvenile stream-dwelling salmonids. *Journal of Fish Biology*, 67(sB):100–110. doi:10.1111/j.0022-1112.2005.00916.x.

Grossman, G. D. and Simon, T. N. 2020. Density-dependent effects on salmonid populations: A review. *Ecology of Freshwater Fish*, 29(3):400–418. doi:10.1111/eff.12523.

Hansen, B. B., Grøtan, V., Herfindal, I., and Lee, A. M. 2020. The Moran effect revisited: Spatial population synchrony under global warming. *Ecography*, 43(11):1591–1602. doi:10.1111/ecog.04962.

Heino, M., Kaitala, V., Ranta, E., and Lindström, J. 1997. Synchronous dynamics and rates of extinction in spatially structured populations. *Proceedings of the Royal Society of London. Series B: Biological Sciences*, 264(1381):481–486. doi:10.1098/rspb.1997.0069.

Hilborn, R. and Mangel, M. 1997. *The Ecological Detective: Confronting Models with Data*. Number 28 in Monographs in Population Biology. Princeton University Press, Princeton, New Jersey.

Hostetter, N. J., Evans, A. F., Loge, F. J., O'Connor, R. R., Cramer, B. M., Fryer, D., and Collis, K. 2015. The influence of individual fish characteristics on survival and detection: Similarities across two salmonid species. *North American Journal of Fisheries Management*, 35(5):1034–1045. doi:10.1080/02755947.2015.1077176.

Isaak, D. J., Thurow, R. F., Rieman, B. E., and Dunham, J. B. 2003. Temporal variation in synchrony among chinook salmon (*Oncorhynchus tshawytscha*) redd counts from a wilderness area in central Idaho. *Canadian Journal of Fisheries and Aquatic Sciences*, 60(7):840–848. doi:10.1139/f03-073.

Jacobs, G. R., Thurow, R. F., Petrosky, C. E., Osenberg, C. W., and Wenger, S. J. 2023. Life-cycle modeling reveals high recovery potential of at-risk wild Chinook salmon via improved migrant survival. *Canadian Journal of Fisheries and Aquatic Sciences*. doi:10.1139/cjfas-2023-0167.

Jorgensen, J. C., Ward, E. J., Scheuerell, M. D., and Zabel, R. W. 2016. Assessing spatial covariance among time series of abundance. *Ecology and Evolution*, 6(8):2472–2485. doi:10.1002/ece3.2031.

Justice, C., Staton, B., White, S., Kaylor, M., and Burns, L. 2021. Developing an index of Chinook Salmon parr capacity in the Grande Ronde River basin. In *Assessing the Status and Trends of Spring Chinook Habitat in the Upper Grande Ronde River and Catherine Creek: Annual Report 2020*, Annual Report for BPA Project #2009-004-00, pages 82–94. Columbia River Inter-Tribal Fish Commission, Portland, OR. URL: https://critfc.org/reports/assessing-the-status-and-trends-of-spring-chinook-habitat-in-the-upper-grande-ronde-river-and-catherine-creek-annual-report-2020/.

Justice, C., White, S. M., McCullough, D. A., Graves, D. S., and Blanchard, M. R. 2017. Can stream and riparian restoration offset climate change impacts to salmon populations? *Journal of Environmental Management*, 188:212–227. doi:10.1016/j.jenvman.2016.12.005.

Kellner, K. 2021. *jagsUI: A Wrapper Around 'rjags' to Streamline 'JAGS' Analyses*. R package version 1.5.2. URL: https://CRAN.R-project.org/package=jagsUI.

Knape, J. 2008. Estimability of density dependence in models of time series data. *Ecology*, 89(11):2994–3000. doi:10.1890/08-0071.1.

Lance, M. E., Brandt, E. J., and Bratcher, K. W. 2023. Lower Snake River Compensation Plan: Oregon spring Chinook harvest monitoring, 2023 annual progress report. Science Bulletin 2023-11, Oregon Department of Fish and Wildlife, Salem, OR. URL: http://www.fws.gov/lsnakecomplan/Reports/ODFWreports.html.

Lindén, A. and Knape, J. 2009. Estimating environmental effects on population dynamics: Consequences of observation error. *Oikos*, 118(5):675–680. doi:10.1111/j.1600-0706.2008.17250.x.

Mantua, N. J., Hare, S. R., Zhang, Y., Wallace, J. M., and Francis, R. C. 1997. A Pacific Interdecadal climate oscillation with impacts on salmon production. *Bulletin of the American Meteorological Society*, 78(6):1069–1080. doi:10.1175/1520-0477(1997)078<1069:APICOW>2.0.CO;2.

Maret, T. R., Hortness, J. E., and Ott, D. S. 2006. Instream flow characterization of upper Salmon River Basin streams, central Idaho, 2005. Technical Report 2006-5230, U.S. Geological Survey.

McCann, J., Chockley, B., Cooper, E., Scheer, G., Haeseker, S., Lessard, B., Copeland, T., Ebel, J., Storch, A., and Rawding, D. 2022. Comparative survival study of PIT-tagged spring/summer/fall Chinook, summer steelhead, and sockeye, 2022. Annual Report BPA Contract #19960200, CSS Oversight Committee and Fish Passage Center, Portland, OR. URL: https://www.fpc.org/documents/CSS/CSS%20Final%20Revised%202022.pdf.

Moussalli, E. and Hilborn, R. 1986. Optimal stock size and harvest rate in multistage life history models. *Canadian Journal of Fisheries and Aquatic Sciences*, 43(1):135–141. doi:10.1139/f86-014.

Murdoch, A. R., Pearsons, T. N., and Maitland, T. W. 2010. Estimating the spawning escapement of hatchery- and natural-origin spring Chinook salmon using redd and carcass data. *North American Journal of Fisheries Management*, 30(2):361–375. doi:10.1577/M09-071.1.

Myers, R. A. and Barrowman, N. J. 1995. Time series bias in the estimation of density-dependent mortality in stock-recruitment models. *Canadian Journal of Fisheries and Aquatic Sciences*, 52(1):223–232. doi:10.1139/f95-022.

Newman, K., King, R., Elvira, V., de Valpine, P., McCrea, R. S., and Morgan, B. J. T. 2023. State-space models for ecological time-series data: Practical model-fitting. *Methods in Ecology and Evolution*, 14(1):26–42. doi:10.1111/2041-210X.13833.

Ohlberger, J., Schindler, D. E., Brown, R. J., Harding, J. M. S., Adkison, M. D., Munro, A. R., Horstmann, L., and Spaeder, J. 2020. The reproductive value of large females: Consequences of shifts in demographic structure

for population reproductive potential in Chinook salmon. *Canadian Journal of Fisheries and Aquatic Sciences*, 77(8):1292–1301. doi:10.1139/cjfas-2020-0012.

Ohlberger, J., Ward, E. J., Schindler, D. E., and Lewis, B. 2018. Demographic changes in Chinook salmon across the Northeast Pacific Ocean. *Fish and Fisheries*, 19(3):533–546. doi:10.1111/faf.12272.

Perry, R. W., Plumb, J. M., Hance, D. J., and Tiffan, K. F. 2020. Using a state-space life-cycle model to simulate population trajectories of natural-origin Snake River Basin fall Chinook slamon under the 2020 biological opinion proposed action. In Tiffan, K. F. and Perry, R. W., editors, *Research, Monitoring, and Evaluation of Emerging Issues and Measures to Recover the Snake River Fall Chinook Salmon ESU*, BPA Annual Report for Project #199102900, pages 82–120. United States Geological Survey, Cook, WA. URL: https://doi.org/10.13140/RG.2.2.23170.30406.

Plummer, M. 2003. JAGS: A program for analysis of Bayesian graphical models using Gibbs sampling. *3rd International Workshop on Distributed Statistical Computing (DSC 2003); Vienna, Austria*, 124. URL: https://www.r-project.org/conferences/DSC-2003/Drafts/Plummer.pdf.

Plummer, M. 2017. JAGS Version 3.4.0 User Manual. URL: https://sourceforge.net/projects/mcmc-jags/.

Polansky, L., Newman, K. B., and Mitchell, L. 2021. Improving inference for nonlinear state-space models of animal population dynamics given biased sequential life stage data. *Biometrics*, 77(1):352–361. doi:10.1111/biom.13267.

Punt, A. E., Butterworth, D. S., de Moor, C. L., Oliveira, J. A. A. D., and Haddon, M. 2016. Management strategy evaluation: Best practices. *Fish and Fisheries*, 17(2):303–334. doi:10.1111/faf.12104.

R Core Team 2023. *R: A Language and Environment for Statistical Computing*. R Foundation for Statistical Computing, Vienna, Austria. R Version 4.3.0. URL: https://www.R-project.org/.

Ranta, E., Kaitala, V., Lindström, J., and Helle, E. 1997. The Moran effect and synchrony in population dynamics. *Oikos*, 78(1):136–142. doi:10.2307/3545809.

Reed, J. M., Mills, L. S., Dunning Jr., J. B., Menges, E. S., McKelvey, K. S., Frye, R., Beissinger, S. R., Anstett, M.-C., and Miller, P. 2002. Emerging issues in population viability analysis. *Conservation Biology*, 16(1):7–19. doi:10.1046/j.1523-1739.2002.99419.x.

Riecke, T. V., Sedinger, B. S., Williams, P. J., Leach, A. G., and Sedinger, J. S. 2019. Estimating correlations among demographic parameters in population models. *Ecology and Evolution*, 9(23):13521–13531. doi:10.1002/ece3.5809.

Rivot, E., Prévost, E., Parent, E., and Baglinière, J. L. 2004. A Bayesian state-space modelling framework for fitting a salmon stage-structured population dynamic model to multiple time series of field data. *Ecological Modelling*, 179(4):463–485. doi:10.1016/j.ecolmodel.2004.05.011.

Rose, K. A., Cowan, J. H., Winemiller, K. O., Myers, R. A., and Hilborn, R. 2001. Compensatory density dependence in fish populations: Importance, controversy, understanding and prognosis. *Fish and Fisheries*, 2(4):293–327. doi:10.1046/j.1467-2960.2001.00056.x.

Rossi, G. J., Bellmore, J. R., Armstrong, J. B., Jeffres, C., Naman, S. M., Carlson, S. M., Grantham, T. E., Kaylor, M. J., White, S., Katz, J., and Power, M. E. 2024. Foodscapes for salmon and other mobile consumers in river networks. *BioScience*, 74(9):586–600. doi:10.1093/biosci/biae064.

Rub, A. M. W., Som, N. A., Henderson, M. J., Sandford, B. P., Doornik, D. M. V., Teel, D. J., Tennis, M. J., Langness, O. P., van der Leeuw, B. K., and Huff, D. D. 2019. Changes in adult Chinook salmon (*Oncorhynchus tshawytscha*) survival within the lower Columbia River amid increasing pinniped abundance. *Canadian Journal of Fisheries and Aquatic Sciences*, 76(10):1862–1873. doi:10.1139/cjfas-2018-0290.

Schindler, D. E., Armstrong, J. B., and Reed, T. E. 2015. The portfolio concept in ecology and evolution. *Frontiers in Ecology and the Environment*, 13(5):257–263. doi:10.1890/140275.

Schindler, D. E., Hilborn, R., Chasco, B., Boatright, C. P., Quinn, T. P., Rogers, L. A., and Webster, M. S. 2010. Population diversity and the portfolio effect in an exploited species. *Nature*, 465(7298):609–612. doi:10.1038/nature09060.

Simmons, B. W., Espinosa, N., Arnsberg, B., Cleary, P., Nelson, D., Rabe, C., and Sublett, M. 2023. Snake River Basin adult Chinook salmon and steelhead monitoring, 2022. Annual Report, Nez Perce Tribe, Department of Fisheries Resources Management, Research Division, Lapwai, ID. URL: https://www.researchgate.net/publication/373923696.

Staton, B. 2022. *postpack: Utilities for Processing Posterior Samples Stored in 'mcmc.lists'*. R package version 0.5.4. URL: https://CRAN.R-project.org/package=postpack.

Staton, B. 2025. GR-sslcm: Github repository storing code to fit the Grande Ronde Basin state-space life cycle model for spring Chinook salmon. Archival DOI not yet available. URL: https://github.com/bstaton1/GR-sslcm.

Staton, B., Justice, C., Kaylor, M., and Ringelman, A. 2023. Objective E-1: Grande Ronde phase 12 - development of a spring Chinook statistical estimation life cycle model. In *Evaluating Salmonid and Stream Ecosystem Response to Conservation Measures and Environmental Stressors in the Columbia River Basin*, Annual Report for BPA Project #2009-004-00, pages 69–83. Columbia River Inter-Tribal Fish Commission, Portland, OR. URL:

https://critfc.org/wp-content/uploads/2023/07/23_03.pdf.

Staton, B. A., Catalano, M. J., Connors, B. M., Jr, L. G. C., Jones, M. L., Walters, C. J., Fleischman, S. J., and Gwinn, D. C. 2020. Evaluation of methods for spawner–recruit analysis in mixed-stock Pacific salmon fisheries. *Canadian Journal of Fisheries and Aquatic Sciences*, 77(7):1149–1162. doi:10.1139/cjfas-2019-0281.

Staton, B. A., Catalano, M. J., and Fleischman, S. J. 2017. From sequential to integrated Bayesian analyses: Exploring the continuum with a Pacific salmon spawner-recruit model. *Fisheries Research*, 186:237–247. doi:10.1016/j.fishres.2016.09.001.

Staton, B. A., Catalano, M. J., Fleischman, S. J., and Ohlberger, J. 2021. Incorporating demographic information into spawner–recruit analyses alters biological reference point estimates for a western Alaska salmon population. *Canadian Journal of Fisheries and Aquatic Sciences*, 78(12):1755–1769. doi:10.1139/cjfas-2020-0478.

Staton, B. A., Justice, C., White, S., Sedell, E. R., Burns, L. A., and Kaylor, M. J. 2022. Accounting for uncertainty when estimating drivers of imperfect detection: An integrated approach illustrated with snorkel surveys for riverine fishes. *Fisheries Research*, 249:106209. doi:10.1016/j.fishres.2021.106209.

Su, Z. 2023. Evaluation of management performance of a new state-space model for pink salmon (*Oncorhynchus gorbuscha*) stock–recruitment analysis. *Canadian Journal of Fisheries and Aquatic Sciences*, 80(8):1268–1288. doi:10.1139/cjfas-2022-0262.

Su, Z. and Peterman, R. M. 2012. Performance of a Bayesian state-space model of semelparous species for stock-recruitment data subject to measurement error. *Ecological Modelling*, 224(1):76–89. doi:10.1016/j.ecolmodel.2011.11.001.

Tattam, I. A., Ruzycki, J. R., McCormick, J. L., and Carmichael, R. W. 2015. Length and condition of wild Chinook Salmon smolts influence age at maturity. *Transactions of the American Fisheries Society*, 144(6):1237–1248. doi:10.1080/00028487.2015.1082503.

Thorson, J. T., Scheuerell, M. D., Buhle, E. R., and Copeland, T. 2014. Spatial variation buffers temporal fluctuations in early juvenile survival for an endangered Pacific salmon. *Journal of Animal Ecology*, 83(1):157–167. doi:10.1111/1365-2656.12117.

Vehtari, A., Gelman, A., Simpson, D., Carpenter, B., and Bürkner, P.-C. 2021. Rank-normalization, folding, and localization: An improved Rhat for assessing convergence of MCMC (with discussion). *Bayesian Analysis*, 16(2):667–718. doi:10.1214/20-BA1221.

Walters, A. W., Copeland, T., and Venditti, D. A. 2013. The density dilemma: Limitations on juvenile production in threatened salmon populations. *Ecology of Freshwater Fish*, 22(4):508–519. doi:10.1111/eff.12046.

Walters, C. J. 1985. Bias in the estimation of functional relationships from time series data. *Canadian Journal of Fisheries and Aquatic Sciences*, 42(1):147–149. doi:10.1139/f85-018.

Walters, C. J. and Martell, S. J. D. 2004. *Fisheries Ecology and Management*. Princeton University Press, Princeton, New Jersey.

White, S., Justice, C., and McCullough, D. 2012. Protocol for snorkel surveys of fish densities. Technical report, Columbia River Inter-Tribal Fish Commission. URL: https://critfc.org/wp-content/uploads/2023/03/ReportPost_White_etal2012.pdf.

White, S. M., Brandy, S., Justice, C., Morinaga, K. A., Naylor, L., Ruzycki, J., Sedell, E. R., Steele, J., Towne, A., Webster, J. G., and Wilson, I. 2021. Progress towards a comprehensive approach for habitat restoration in the Columbia Basin: Case study in the Grande Ronde River. *Fisheries*, 46(5):229–243. doi:10.1002/fsh.10562.

White, S. M., Justice, C., Kelsey, D. A., McCullough, D. A., and Smith, T. 2017. Legacies of stream channel modification revealed using General Land Office surveys, with implications for water temperature and aquatic life. *Elementa: Science of the Anthropocene*, 5:3. doi:10.1525/elementa.192.

Zabel, R. W. and Achord, S. 2004. Relating size of juveniles to survival within and among populations of Chinook salmon. *Ecology*, 85(3):795–806. doi:10.1890/02-0719.

Zabel, R. W. and Levin, P. S. 2002. Simple assumptions on age composition lead to erroneous conclusions on the nature of density dependence in age-structured populations. *Oecologia*, 133(3):349–355. doi:10.1007/s00442-002-1051-0.

Zabel, R. W., Scheuerell, M. D., McClure, M. M., and Williams, J. G. 2006. The interplay between climate variability and density dependence in the population viability of Chinook salmon. *Conservation Biology*, 20(1):190–200. doi:10.1111/j.1523-1739.2005.00300.x.

Table C1. Inter-annual mean and coefficient of variation (%CV) of NOR smolt reaching LGR in the presence (real) and hypothetical absence of the fall migrant life history type. Findings indicate that smolt abundance would have been lower on average and more variable across years if all parr had been spring migrants.

	Inter-Annual Mean			Inter-Annual %CV	
	Real[1,3]	**All Spring[2,3]**	**%Δ**	**Real[1]**	**All Spring[2]**
CAT	5.5 (0.3)	3.9 (0.2)	-30% (3%)	51% (8%)	59% (9%)
LOS	16.4 (0.9)	11.1 (0.6)	-32% (2%)	58% (8%)	59% (7%)
MIN	23.2 (1.3)	17.3 (1.1)	-25% (2%)	51% (5%)	57% (6%)
UGR	6.5 (0.5)	5.9 (0.5)	-8% (1%)	80% (10%)	79% (11%)
Total	51.6 (1.9)	38.3 (1.5)	-26% (1%)	44% (4%)	46% (4%)

Posterior summaries represented as mean (standard deviation).

[1] Based on the observed time series, in which both spring and fall migrants were present.

[2] Based on the hypothetical case where no parr recruits were fall migrants – calculated after model fitting by assuming all parr recruits experience the higher mortality rates of the spring migrant life history type.

[3] Abundance expressed as thousands of natural-origin smolt reaching Lower Granite Dam.

FIGURE C1. Map of the Grande Ronde Basin. Shown are the watersheds for the four populations we model, the location of fish monitoring infrastructure, and the extent of Chinook salmon spawning in each tributary. Map credit: Nadine Craft, ODFW.

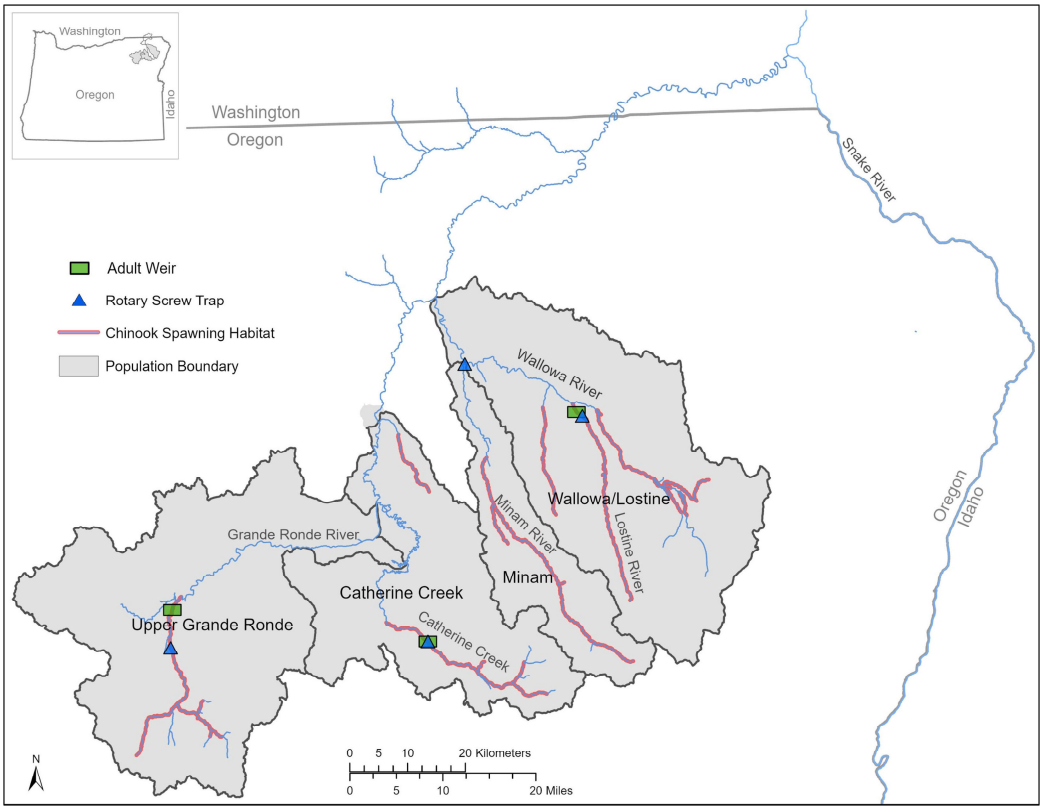

Figure C2. Schematic of the life stages and transitions captured in the state-space model. Diagram shows one generation for one population. Boxes represent abundances of fish (states), arrows represent changes (rates) among stages, and circled numbers represent quantities with data sources informing them. Blue states have associated mean length, and blue arrows are expressed as functions of mean length.

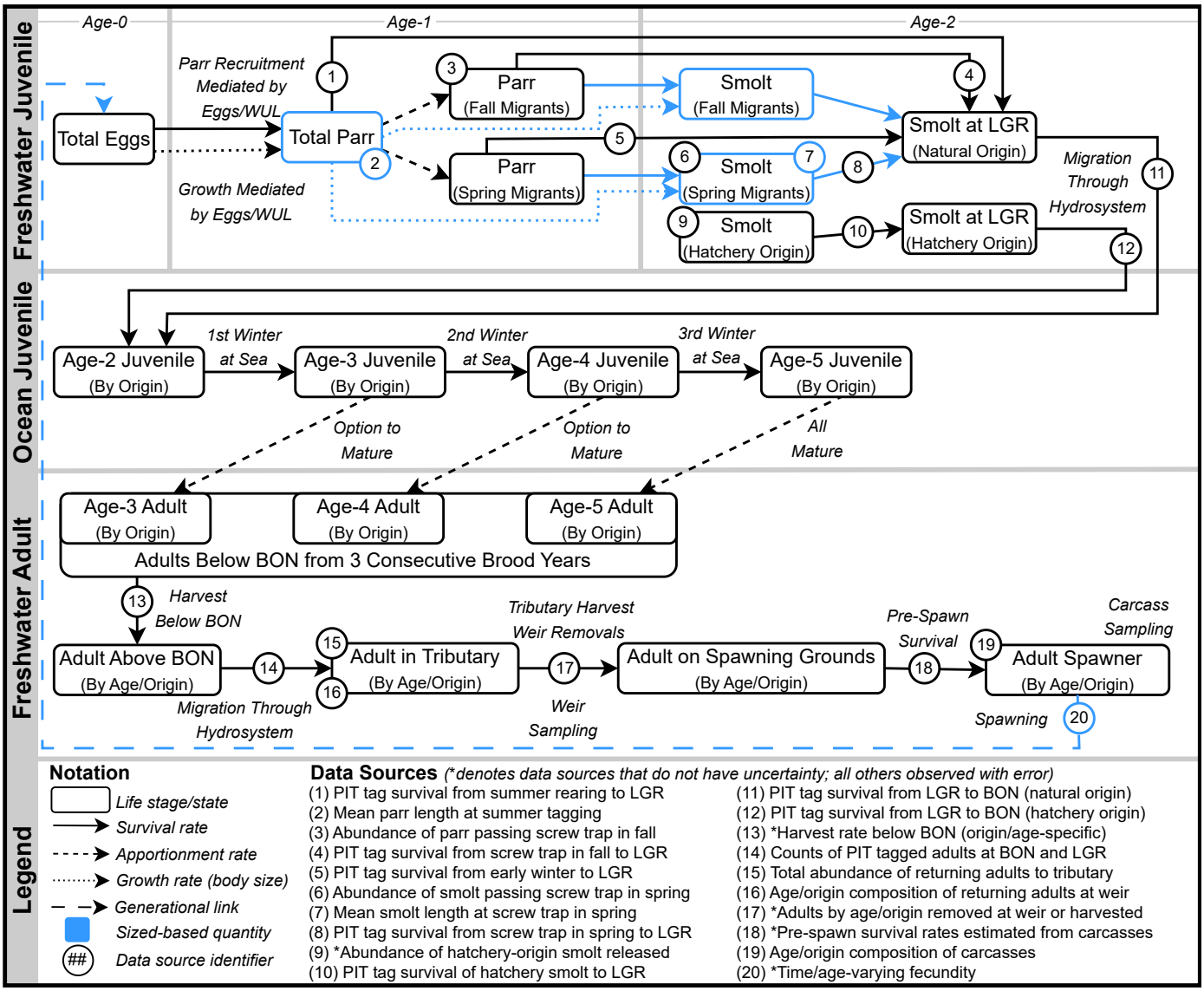

Figure C3. Consistency between fitted values and data points. Nearly all data sources with an explicit likelihood function are shown; only parr and smolt mean length data have been omitted here for space. Each data point is one year for one population (posterior means on y-axis), with the exceptions of panels g, h, and i, which display values for both NOR and HOR survival rates, and in the cases of h and i, these rates apply equally to all populations. More detailed visualizations of model fit are shown in the Supplement (Section 3: model fits as time series with magnitude of observation uncertainty shown; Section 11: diagnostics based on quantile-standardized residuals; Section 12: posterior predictive checks).

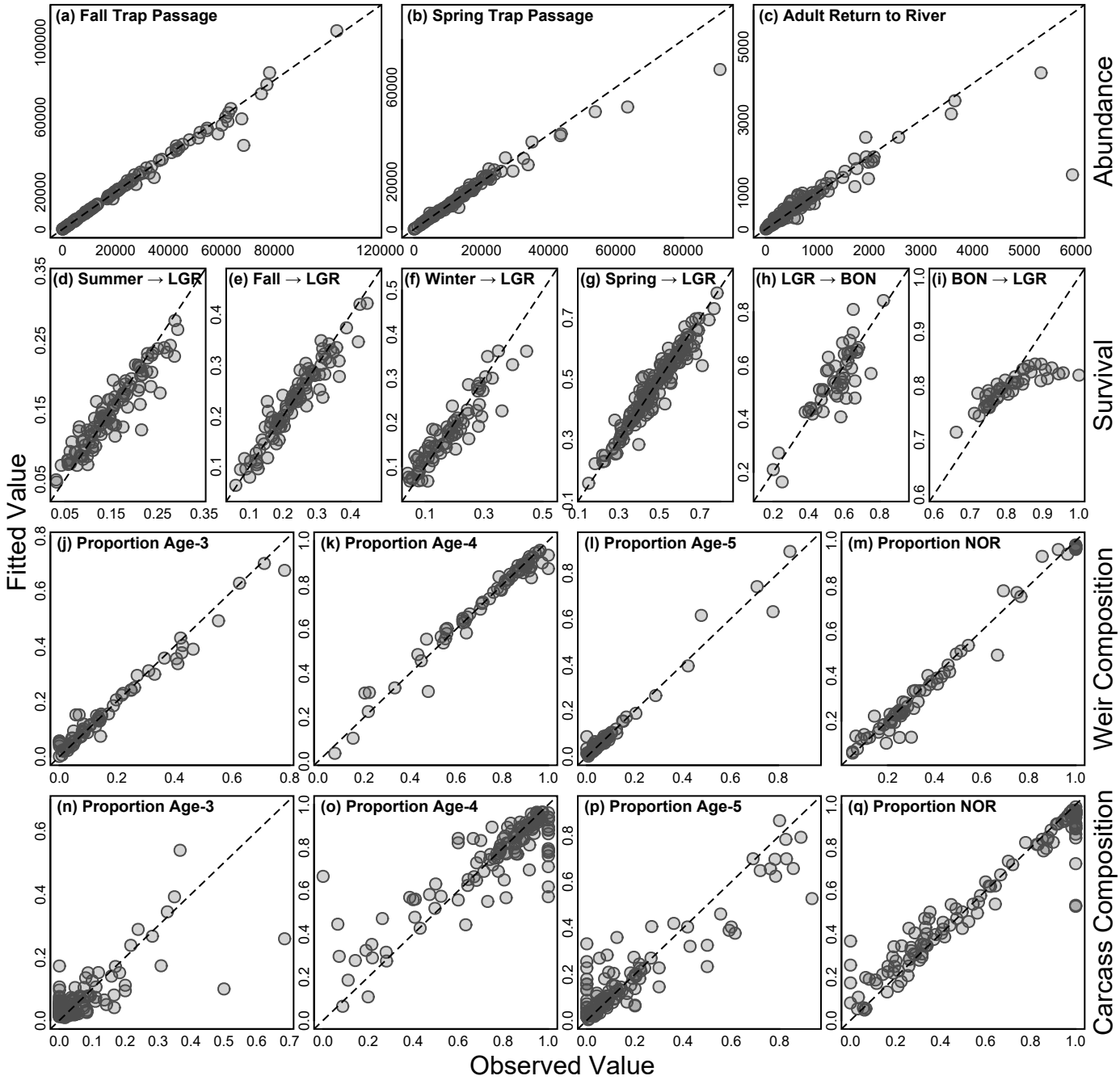

Figure C4. Survival probability parameters estimated by the state-space model. Estimates are separated by population, migratory type, and origin where applicable. Small points show posterior means of year-specific latent values (jitter for visual effect only) and large points show the average across years. Information about mortality due to sources/stages not displayed here was either assumed known without error (e.g., pre-spawn mortality) or expressed as strong prior information with no inter-annual variability (i.e., mortality experienced in ocean-1 → ocean-2 and ocean-2 → ocean-3).

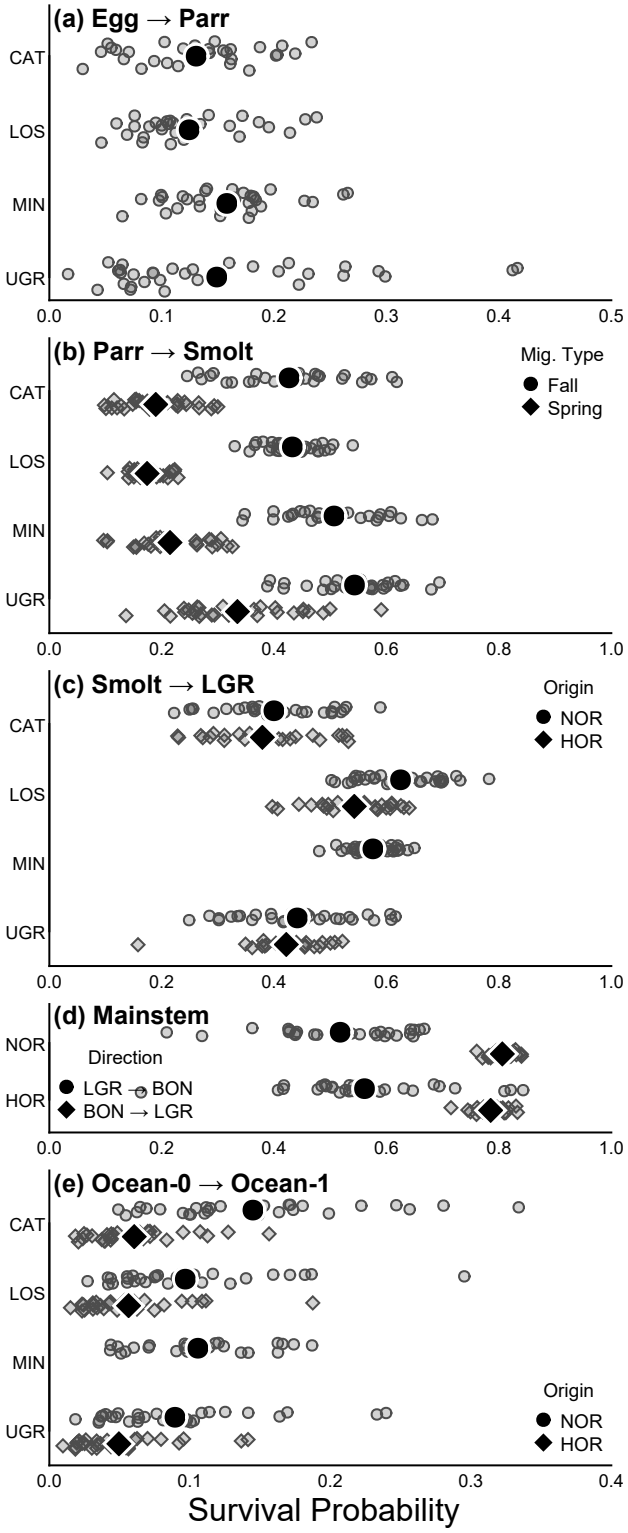

Figure C5. Estimated relationship between parr capacity and weighted usable habitat length (WUL). Darker gray/thicker error bars represent 80% credible regions and lighter gray/thinner error bars represent 95% credible regions.

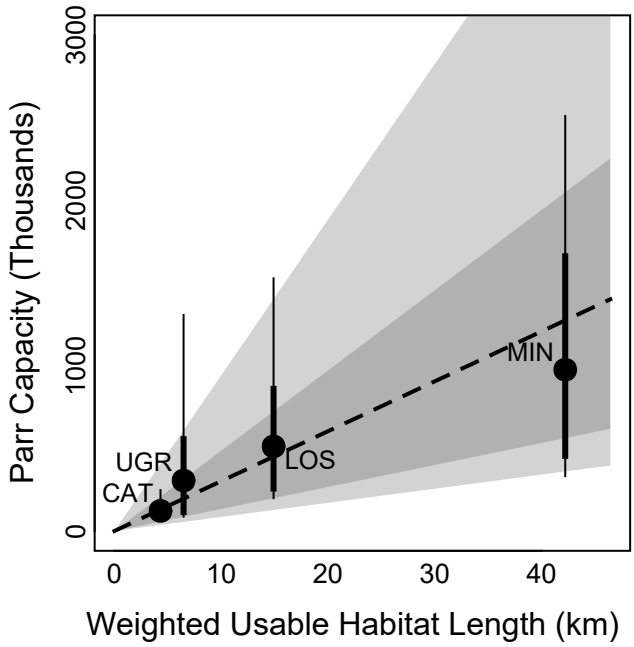

Figure C6. Non-survival transition probability parameters estimated by the state-space model. Estimates are separated by life stage, population, and origin where applicable. Small points show posterior means of year-specific latent values (jitter for visual effect only) and large points show the average across years.

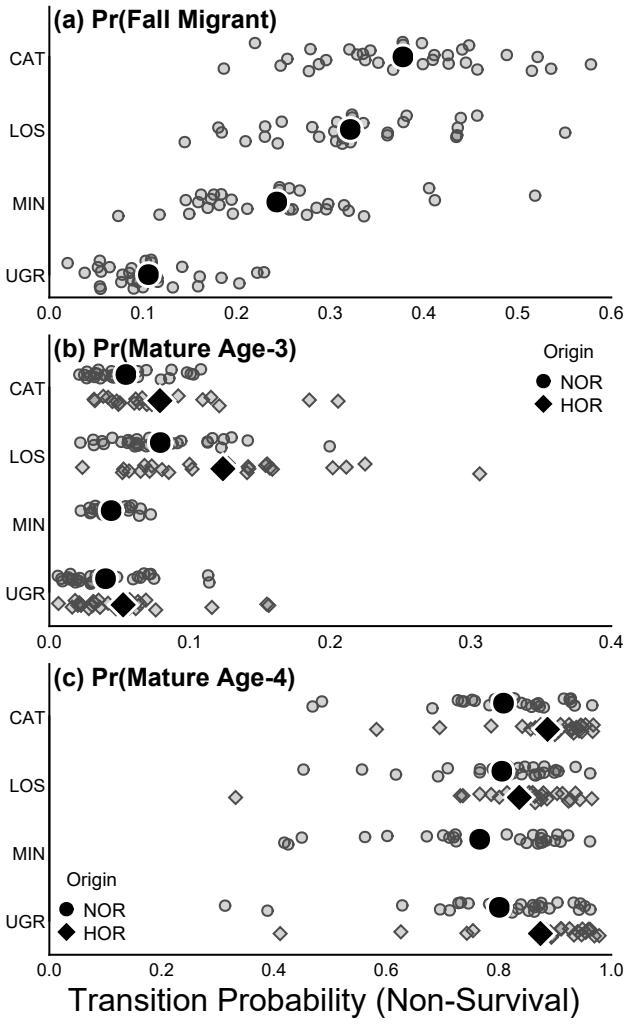

FIGURE C7. Demographic relationships estimated by the state-space model. Relationships include those showing density effects on recruitment (panels *a* and *b*) and mean length (panel *c*), and length effects on future length (panel *e*) and survival (panels *d* and *f*). Process model deterministic relationships are shown as the posterior mean (thick line) and 95% credible region (shaded region); points show latent values. Panels within the same row show the process model relationship for each of the four populations; *x*- and *y*-axis limits are identical for all panels within a row.

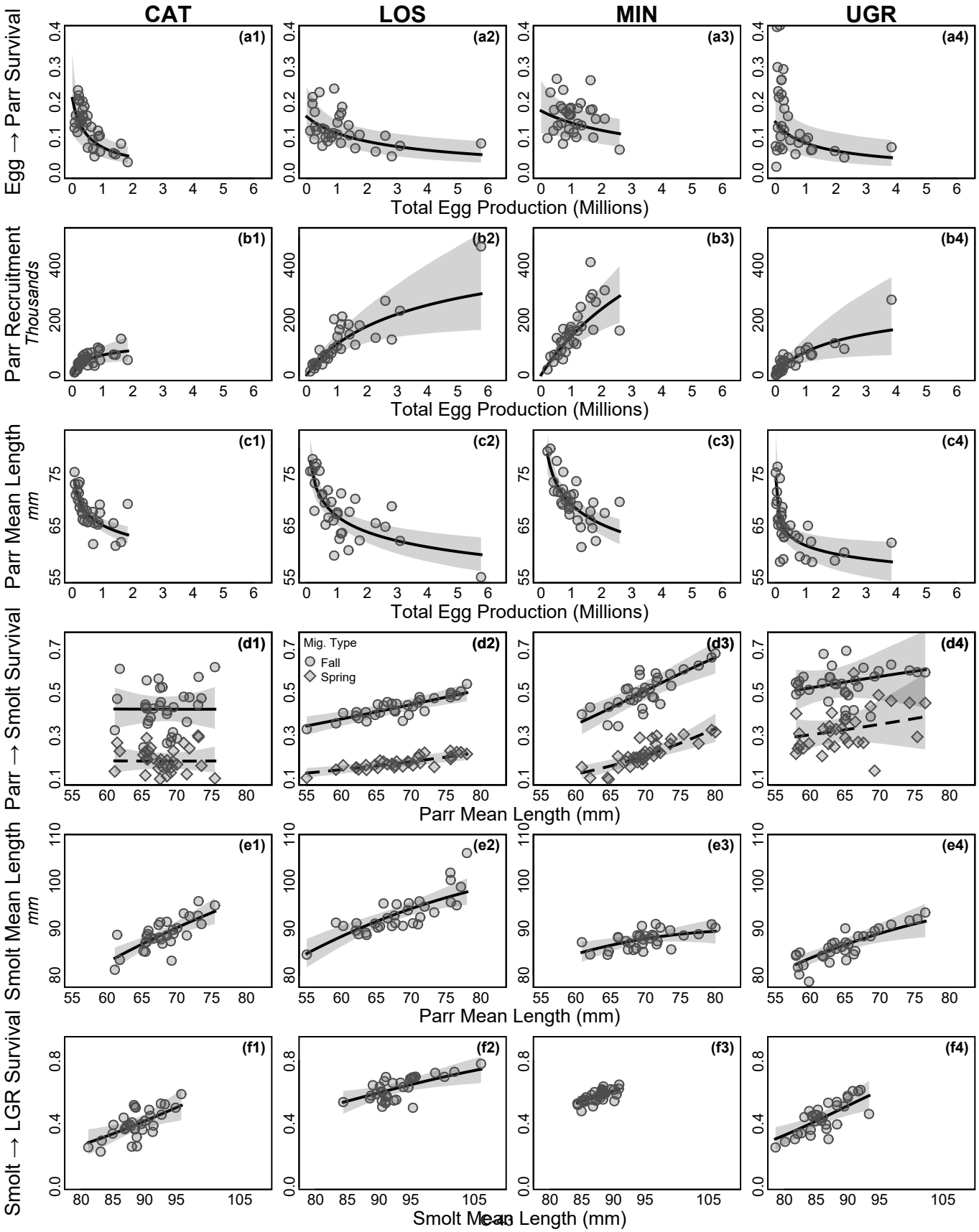

Figure C8. Correlation terms estimated by the state-space model representing synchrony in process variability. Posterior means of population pair-specific correlations are displayed as points and the posterior of the average of the 6 pairs is summarized in black (thin lines are 95% CRIs, thick lines 50% CRIs, and cross marks are means). Survival processes are denoted by $x \rightarrow y$, whereas non-survival transition processes are denoted by $\Pr(x)$. The correlation in survival processes representing the migration downstream and upstream through the mainstem (LGR → BON and BON → LGR, respectively) represent among-origin correlation, hence the lack of points.

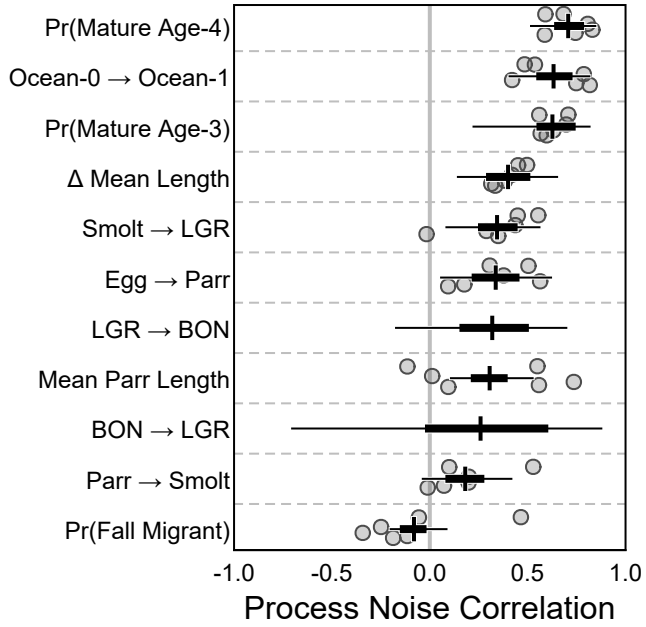

Figure C9. Freshwater juvenile density-dependent relationships under current and increased weighted usable habitat (WUL). Panels (*a-d*): composite survival from egg-to-smolt at LGR including both direct (i.e., egg density affects egg survival via Beverton-Holt dynamics) and indirect (i.e., egg density affects growth rates, size affects parr and smolt survival) density effects; panels (*e-h*): composite survival from parr-to-smolt at LGR which includes only indirect effects; panels (*i-l*): smolt reaching LGR. Calculations operate based on density of eggs – *x*-axis converted to approximate spawner abundance (all ages, origins, and sexes) for ease of interpretation. Gray bands show the 95% credible region for the current relationship only; lines show posterior means.

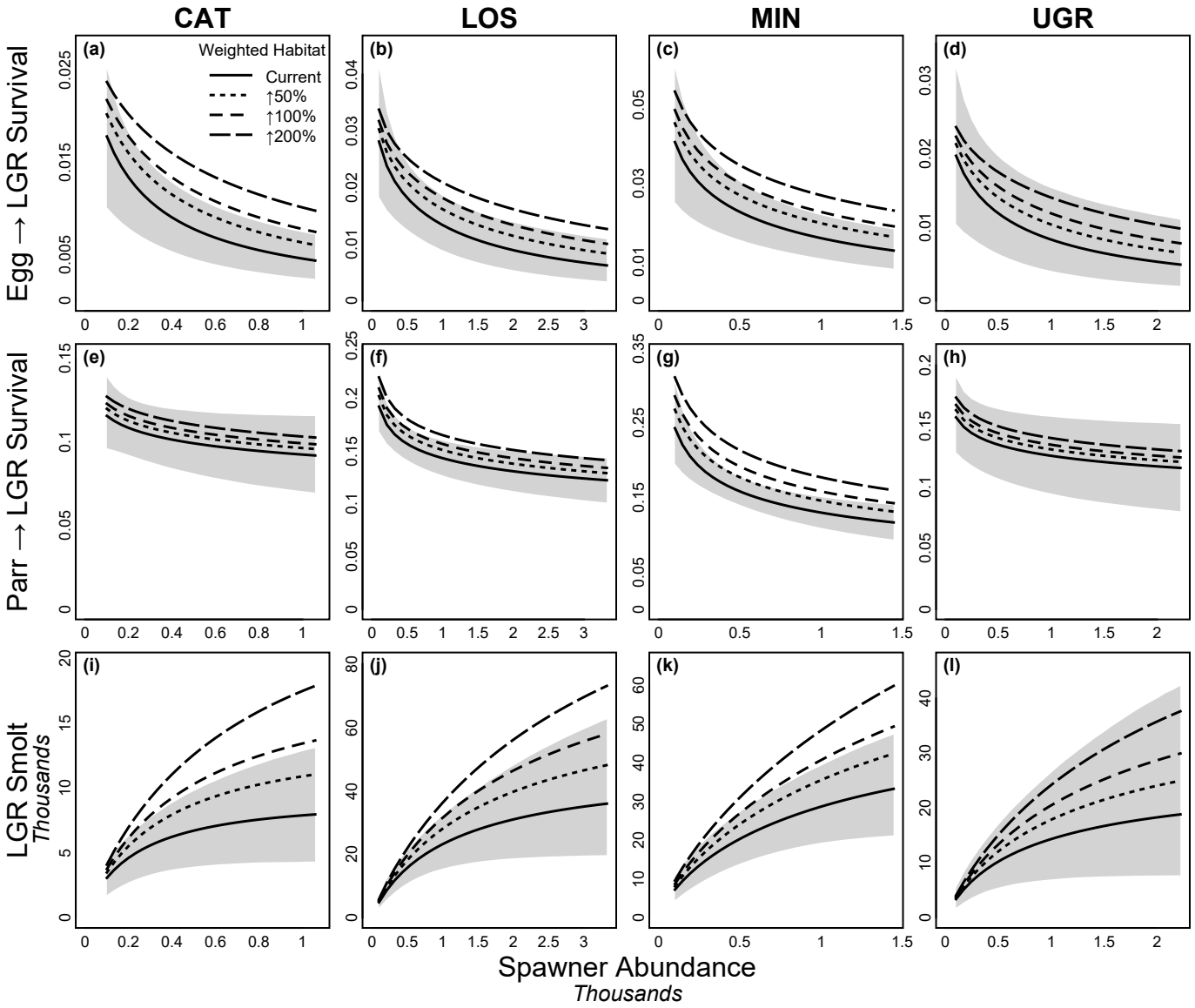

Appendix D Grande Ronde LCM Math Description

Appendix D: Mathematical Model Description

A state-space model to quantify density dependence, demographic heterogeneity, and spatial synchrony in Grande Ronde Basin Chinook salmon populations

Authors: Benjamin A. Staton, Polly P. Gibson, Martin Liermann, Casey Justice, Matthew J. Kaylor, Rishi Sharma, and Seth M. White

This document is a supplement to the state-space model manuscript, included as Appendix C of this report.

Table of Contents

D1 Syntactical and Statistical Conventions

The state-space life cycle model symbology aims for consistency in mathematical representation of quantities. This, however, has created some conventions that require devoted explanation. All quantities are defined in Tables D1 (indices and dimensional constants), D2 (states and rates), D3 (free parameters), and D4 (data sources) and a catalog of all equations is provided in Table D5. A schematic of the model is displayed in Figure D1 and a representation of which years and populations had specific kinds of monitoring data available is displayed in Figure D2.

(1) For simplicity, the term "adult" is used to refer to any mature individual returning to spawn, including age-3 "jacks".

(2) Life stage-specific states are defined by capital letters, these include: eggs (E), parr (P), smolt (M), ocean juveniles (O), adults returning to river (R), or adults with potential to spawn (S).

(3) Parameters (e.g., survival terms, non-survival transition probabilities, coefficients in relationships, etc.) are predominately denoted by Greek symbols and are used consistently where possible, e.g., ϕ for survival rates or ψ for maturation rates.

(4) Subscripts denote placement of a quantity in a larger array (i.e., the index), e.g., y denotes a specific year and j a specific population (see Table D1).

(5) Superscripts are most often used syntactically to further describe the quantity, not in a mathematical sense. E.g., M^b represents smolt abundance *before* out-of-basin migration and M^a represents smolt abundance *after* out-of-basin migration. As such, M^b is not "M raised to the power b"; if the quantity M^b must be raised to the power c, it will be written $(M^b)^c$.

(6) Survival terms to transition from state A to state B in year y for population j are denoted by $\phi_{y,j}^{A\rightarrow B}$.

(7) The expected value of a stochastic process is expressed by a dot, e.g., $\dot{\phi}_j^{A\rightarrow B}$ – this is the value expected in the absence of process (biological/environmental) variability.

(8) In some cases, calculations are performed on vectors rather than scalars. Vectors are denoted via boldface, and the dimension of the vector is denoted using $1{:}n$ syntax. E.g., $\boldsymbol{\phi}_{y,1:n_j}^{A\rightarrow B}$ represents a vector of parameters representing the transition (survival) probability from state A to state B in year y, where each element stores the value for each population.

(9) Mathematical operations performed on two vectors $\boldsymbol{C}$ and $\boldsymbol{D}$ are performed in an element-wise fashion, and the resulting vector will have identical dimensions to both $\boldsymbol{C}$ and $\boldsymbol{D}$.

(10) In some cases, a calculation is performed differently for a subset of the possible index values. For example, to denote that k should take on only the values of 1 and 3 (not 2), we would write, $k \in [1, 3]$.

(11) $\log(x)$ represents the natural logarithm of x and it is implied that the constraint $x > 0$ is satisfied.

(12) logit(p) represents the log odds of p (i.e., $\log[p/(1-p)]$) and it is implied that the constraint $0 < p < 1$ is satisfied.

(13) All observed quantities used in a likelihood component are denoted by a "hat", e.g., a survival term ($\hat{\phi}_{y,j}^{A\to B}$) and its logit-normal standard error ($\hat{\sigma}_{\phi_{y,j}^{A\to B}}$, which is used as a direct estimate of observation error variability).

(14) Stochastic processes are represented by $x_y \sim \mathrm{F}(\theta_1, \theta_2)$, where x_y is a random variable, F() is some probability density (mass) function (N() for univariate normal, MVN() for multivariate normal, B() for binomial, b() for beta, M() for multinomial, D() for Dirichlet, SIW() for scaled inverse-Wishart, and U() for uniform), and θ_1 and θ_2 are parameters of the probability distribution.

Process noise was modeled by assuming year-specific values are multivariate logit-normal random variables around the deterministic value. This enabled modeling covariability in demographic rates (Riecke et al. 2019; Bouchard et al. 2022) among populations or origins, which is advantageous for estimation involving incompletely overlapping time series (Staton et al. 2020) and provides useful ecological insights by quantifying synchrony in demographic rates (Thorson et al. 2014). The covariance matrices of these random variables are denoted by Σ, and have a common structure for all model components. Take the hypothetical survival term $\phi_{y,j}^{A\to B}$ as an example. The random process introducing inter-annual variability and inter-population covariability is expressed as:

$$\mathrm{logit}\left(\boldsymbol{\phi}_{y,1:n_j}^{A\to B}\right) \sim \mathrm{MVN}\left[\mathrm{logit}\left(\dot{\boldsymbol{\phi}}_{y,1:n_j}^{A\to B}\right), \Sigma_{\phi^{A\to B}}\right] \tag{D1}$$

where $\Sigma_{\phi^{A\to B}}$ is an $n_j \times n_j$ matrix constructed of population-specific variance terms $\left(\sigma_{\phi_j^{A\to B}}\right)^2$ and correlation terms specific to each pair of populations j and j' $\rho_{\phi_{j,j'}^{A\to B}}$:

$$\begin{bmatrix} \left(\sigma_{\phi_{j=1}^{A\to B}}\right)^2 & \sigma_{\phi_{j=1}^{A\to B}} \cdot \sigma_{\phi_{j=2}^{A\to B}} \cdot \rho_{\phi_{j=1,j'=2}^{A\to B}} & \dots & \sigma_{\phi_{j=1}^{A\to B}} \cdot \sigma_{\phi_{j=n_j}^{A\to B}} \cdot \rho_{\phi_{j=1,j'=n_j}^{A\to B}} \\ \sigma_{\phi_{j=2}^{A\to B}} \cdot \sigma_{\phi_{j=1}^{A\to B}} \cdot \rho_{\phi_{j=2,j'=1}^{A\to B}} & \left(\sigma_{\phi_{j=2}^{A\to B}}\right)^2 & \dots & \sigma_{\phi_{j=2}^{A\to B}} \cdot \sigma_{\phi_{j=n_j}^{A\to B}} \cdot \rho_{\phi_{j=2,j'=n_j}^{A\to B}} \\ \vdots & \vdots & \ddots & \vdots \\ \sigma_{\phi_{j=n_j}^{A\to B}} \cdot \sigma_{\phi_{j=1}^{A\to B}} \cdot \rho_{\phi_{j=n_j,j'=1}^{A\to B}} & \sigma_{\phi_{j=n_j}^{A\to B}} \cdot \sigma_{\phi_{j=2}^{A\to B}} \cdot \rho_{\phi_{j=n_j,j'=2}^{A\to B}} & \dots & \left(\sigma_{\phi_{j=n_j}^{A\to B}}\right)^2 \end{bmatrix} \tag{D2}$$

In cases where a quantity varies annually and covaries by origin but is identical across populations, $\Sigma_{\phi^{A\to B}}$ would have dimensions $n_o \times n_o$:

$$\begin{bmatrix} \left(\sigma_{\phi^{A\to B}_{o=1}}\right)^2 & \sigma_{\phi^{A\to B}_{o=1}} \cdot \sigma_{\phi^{A\to B}_{o=2}} \cdot \rho_{\phi^{A\to B}} \\ \sigma_{\phi^{A\to B}_{o=2}} \cdot \sigma_{\phi^{A\to B}_{o=1}} \cdot \rho_{\phi^{A\to B}} & \left(\sigma_{\phi^{A\to B}_{o=2}}\right)^2 \end{bmatrix} \tag{D3}$$

Covariance matrices have certain constraints, which makes them difficult to estimate (Barnard et al. 2000). One solution is to use an inverse-Wishart distribution – random variables from which meet the positive definite constraint – as a prior for modeling covariance matrices (Gelman and Hill 2007; Gelman et al. 2014). Although Riecke et al. (2019) recommend against the use of this prior distribution, they provided an alternative "separation strategy" only for the case of 2×2 covariance matrices; Barnard et al. (2000) proposed a strategy for the general $n \times n$ case. As most matrices used were 4×4, the Barnard et al. (2000) approach was attempted, however the MCMC sampler would not permit it, and it would have been very computationally inefficient even if possible. Thus, the more convenient scaled inverse-Wishart distribution was used as the prior, which solves some of the issues of the unscaled version (Gelman and Hill 2007; Gelman et al. 2014; Plummer 2017, Table D3). Although the stochastic process requires the full covariance matrix, the component σ and ρ terms were the parameters used for inference regarding magnitude of inter-annual variability and synchrony, respectively.

D2 Freshwater Juvenile Phase

D2.1 Process Model

D2.1.1 Egg Production, Parr Recruitment, and Parr Mean Length

The life cycle begins at the egg stage immediately after spawning. Total egg production was the sum product of age-specific spawner abundance ($S^a_{y,k,o,j}$, from eq. D42, below), proportion female-at-age (Ω_k), and fecundity-at-age ($f_{y,k,j}$):

$$E_{y,j} = \sum_{o}^{n_o} \sum_{k}^{n_k} S^a_{y,k,o,j} \cdot \Omega_k \cdot f_{y,k,j} \tag{D4}$$

Spawners of age-4 or age-5 were assumed to be 50% female and age-3 spawners were assumed 100% male (i.e., $\Omega_{k=1} = 0$; $\Omega_{k\in[2,3]} = 0.5$; approximately equal to values estimated from carcass data). Fecundity was predicted from length-fecundity relationships based on Grande Ronde-origin hatchery broodstock and time-varying mean length-at-age data (ODFW, unpublished data). Both Ω_k and $f_{y,k,j}$ were assumed known without error.

Expected egg-to-parr survival was assumed to be a density-dependent process following Beverton-Holt dynamics with productivity parameter α_j (i.e., theoretical maximum egg-to-parr

survival probability, in the absence of density effects) and capacity parameter β_j (i.e., theoretical maximum parr recruitment abundance):

$$\dot{\phi}_{y,j}^{E\rightarrow P^b} = \frac{1}{\frac{1}{\alpha_j} + \frac{E_{y,j}}{\beta_j}} \tag{D5}$$

To facilitate later analyses (not documented here) investigating the effects of habitat restoration and climate change on population dynamics, parr capacity was modeled as a function of weighted usable habitat length specific to each population (WUL_j; derivation summarized in Appendix 1 of this document):

$$\log\left(\beta_j\right) \sim \mathrm{N}\left[\log\left(\lambda \cdot \mathrm{WUL}_j\right), \sigma_\beta\right] \tag{D6}$$

where λ is the expected change in parr capacity per 1 km change in weighted usable habitat length, and σ_β is the log-normal standard deviation of variability in this relationship not captured by WUL values.

Realized (i.e., with process noise) egg-to-parr survival was a multivariate logit-normal random variable around the expected value ($\dot{\phi}_{y,j}^{E\rightarrow P^b}$) from eq. D5. Rather than assume egg-to-parr survival anomalies (i.e., inter-annual variability in egg-to-parr survival beyond that explained by density dependence) are completely random across years, a lag-1 autoregressive process [AR(1); coefficient denoted $\kappa_j^{E\rightarrow P^b}$] was used to account for serial autocorrelation:

$$\mathrm{logit}\left(\boldsymbol{\phi}_{y,1:n_j}^{E\rightarrow P^b}\right) \sim \mathrm{MVN}\left\{\mathrm{logit}\left(\dot{\boldsymbol{\phi}}_{y,1:n_j}^{E\rightarrow P^b}\right) + \boldsymbol{\kappa}_{1:n_j}^{E\rightarrow P^b} \cdot \left[\mathrm{logit}\left(\boldsymbol{\phi}_{y-1,1:n_j}^{E\rightarrow P^b}\right) - \mathrm{logit}\left(\dot{\boldsymbol{\phi}}_{y-1,1:n_j}^{E\rightarrow P^b}\right)\right], \Sigma_{\phi^{E\rightarrow P^b}}\right\} \tag{D7}$$

Thus, the covariance matrix $\Sigma_{\phi^{E\rightarrow P^b}}$ captures variability in the white noise (i.e., non-correlated) portion of the survival anomaly. Total parr recruitment ($P_{y,j}^b$) was then the product of total egg production and egg-to-parr survival:

$$P_{y,j}^b = \phi_{y,j}^{E\rightarrow P^b} \cdot E_{y,j} \tag{D8}$$

In addition to density-dependent egg-to-parr survival (eq. D5), there was reason to expect that parr growth/size is density-dependent, both from the literature on salmonid early life history (Grant and Imre 2005; Copeland and Venditti 2009; Walters et al. 2013; Myrvold and Kennedy 2015; Grossman and Simon 2020) and previous analyses on Grande Ronde spring Chinook salmon populations (Cooney et al. 2017; Staton et al. 2023). Given the established relationships between size and survival (Zabel and Achord 2004; Hostetter et al. 2015), growth and density (e.g., Grant and Imre 2005),

and survival and density (Achord et al. 2003; Walters et al. 2013), it is possible that growth could be a useful mechanism to model density effects on post-recruitment juvenile survival. Expected parr mean length ($\dot{L}^{P^b}_{y,j}$, mm fork length) was modeled as a power function of egg density, which expressed on the logarithmic scale was:

$$\log\left(\dot{L}^{P^b}_{y,j}\right) = \omega_{0,j} + \omega_{1,j} \cdot \log\left(\frac{E_{y,j}}{\mathrm{WUL}_j}\right) \tag{D9}$$

and the realized parr mean length as being multivariate log-normally distributed around $\dot{L}^{P^b}_{y,j}$ with covariance matrix $\Sigma_{L^{P^b}}$:

$$\log\left(\boldsymbol{L}^{P^b}_{y,1:n_j}\right) \sim \mathrm{MVN}\left[\log\left(\dot{\boldsymbol{L}}^{P^b}_{y,1:n_j}\right), \Sigma_{L^{P^b}}\right] \tag{D10}$$

D2.1.2 Migratory Strategy Apportionment

Like many populations of stream-type spring Chinook salmon in the Columbia River Basin, those in the Grande Ronde Basin display life history diversity with respect to juvenile migratory phenology and over-winter rearing habitat use (Copeland et al. 2014). Some portion of parr recruits ($P^b_{y,j}$) migrate from the headwaters rearing areas in the fall and rear over-winter farther downstream (termed "fall migrants" and indexed by i = fall) and the remaining portion migrate the following spring during the out-of-basin migration (termed "spring migrants" and indexed by i = spring). Due to this difference in migratory phenology, these two groups of fish are monitored separately (Gibson et al. 2024) depending on when they pass the rotary screw trap located in each tributary. Separate abundance and survival data in the observation model required that the process model track fish using these strategies separately, thus they were apportioned:

$$P^a_{y,i,j} = P^b_{y,j} \cdot \pi_{y,i,j} \tag{D11}$$

where $P^a_{y,i,j}$ is migratory strategy-specific parr abundance and $\pi_{y,i,j}$ is the proportion that take on each migratory strategy. The expected value of the proportion of fall migrants ($\dot{\pi}_{i=\mathrm{fall},j}$) was assumed to be time-constant and the realized values were modeled as having a multivariate logit-normal distribution with covariance matrix $\Sigma_{\pi_{i=\mathrm{fall}}}$:

$$\mathrm{logit}\left(\boldsymbol{\pi}_{y,i=\mathrm{fall},1:n_j}\right) \sim \mathrm{MVN}\left[\mathrm{logit}\left(\dot{\boldsymbol{\pi}}_{i=\mathrm{fall},1:n_j}\right), \Sigma_{\pi_{i=\mathrm{fall}}}\right] \tag{D12}$$

With only two migratory strategies, the proportion that were spring migrants was obtained as the complement: $\pi_{y,i=\mathrm{spring},j} = 1 - \pi_{y,i=\mathrm{fall},j}$.

D2.1.3 Survival to Smolt Stage and Smolt Mean Length

The model assumed that some inter-annual variability in over-winter survival (i.e., the transition from age-1 parr to age-2 smolt prior to out-migration) can be explained by parr mean length[1]. This was achieved by modeling expected over-winter survival (denoted by $\dot{\phi}_{y,i,j}^{P^a \to M^b}$) as a logit-linear function of parr mean length:

$$\text{logit}\left(\dot{\phi}_{y,i,j}^{P^a \to M^b}\right) = \gamma_{0,i,j} + \gamma_{1,j} \cdot L_{y,j}^{*P^b} \tag{D13}$$

where $L_{y,j}^{*P^b}$ is parr mean length centered and scaled based on the mean and standard deviation of observed mean lengths (denoted $\hat{L}_{y,j}^{P^b}$) across years for population j, respectively. Thus, $\gamma_{0,i,j}$ represents the expected log-odds of survival for type i in population j in a year with average parr mean length, and $\gamma_{1,j}$ represents the expected change in the log-odds for every additional standard deviation increase in parr mean length. Then, for each migratory strategy separately, realized over-winter survival was a multivariate logit-normal random variable around the expected value with covariance matrix $\Sigma_{\phi^{P^a \to M^b}}$ (assumed common among migratory strategies):

$$\text{logit}\left(\boldsymbol{\phi}_{y,i,1:n_j}^{P^a \to M^b}\right) \sim \text{MVN}\left[\text{logit}\left(\dot{\boldsymbol{\phi}}_{y,i,1:n_j}^{P^a \to M^b}\right), \Sigma_{\phi^{P^a \to M^b}}\right] \tag{D14}$$

The abundance of natural origin smolt (indexed by o = NOR, hatchery-origin smolt releases described in Section D2.1.4) before out-migration was then:

$$M_{y,i,o=\text{NOR},j}^{b} = P_{y,i,j}^{a} \cdot \phi_{y,i,j}^{P^a \to M^b} \tag{D15}$$

Similar to the use of parr mean length to explain inter-annual variability in over-winter survival, smolt mean length ($L_{y,j}^{M^b}$) may be useful for explaining inter-annual variability in out-migration survival. Only spring migrant smolt have been measured for mean length (as they pass the screw trap), thus the i subscript is omitted from quantities related to smolt mean length.

Preliminary analyses on the observed mean length data revealed that smolt mean length was positively related with parr mean length, but that the relationship was non-linear (Staton et al. 2023). This non-linearity was captured by modeling the expected multiplicative change in mean length from the parr to smolt stages as a log-linear function of (scaled and centered) parr mean length:

$$\log\left(\dot{\Delta}_{y,j}^{L^{P^b} \to L^{M^b}}\right) = \theta_{0,j} + \theta_{1,j} \cdot L_{y,j}^{*P^b} \tag{D16}$$

[1]The assumption that parr length is related to over-winter survival can be relaxed by forcing $\gamma_{1,j}$ in eq. D13 to zero rather than assigning it an uninformative prior distribution; in this case over-winter survival would be assumed to fluctuate around a time-constant expected value.

The realized multiplicative change in mean length was multivariate log-normally distributed around $\dot{\Delta}_{y,j}^{L^{Pb}\to L^{Mb}}$ with covariance matrix $\Sigma_{\Delta^{L^{Pb}\to L^{Mb}}}$:

$$\log\left(\boldsymbol{\Delta}_{y,1:n_j}^{L^{Pb}\to L^{Mb}}\right) \sim \text{MVN}\left[\log\left(\dot{\boldsymbol{\Delta}}_{y,1:n_j}^{L^{Pb}\to L^{Mb}}\right), \Sigma_{\Delta^{L^{Pb}\to L^{Mb}}}\right] \tag{D17}$$

Smolt mean length was then the product:

$$L_{y,j}^{Mb} = L_{y,j}^{Pb} \cdot \Delta_{y,j}^{L^{Pb}\to L^{Mb}} \tag{D18}$$

D2.1.4 Hatchery Inputs

For populations with hatchery supplementation (CAT, LOS, and UGR), hatchery-origin smolt releases (Feldhaus et al. 2022, assumed known without error) were stored in the variable $M_{y,i=\text{spring},o=\text{HOR},j}^{b}$; the very rare occasions in which hatchery-origin parr were released the prior year were ignored, thus $M_{y,i=\text{fall},o=\text{HOR},j}^{b} = 0$ for all y and j. Abundance (and often survival) of hatchery-origin fish was tracked separately from natural-origin fish for all subsequent life stages.

D2.1.5 Seaward Migration

The model separates mortality sources experienced during seaward migration into two stages: (*a*) from the natal tributary to Lower Granite Dam (LGR), the first in a series of eight hydroelectric dams encountered during the downstream migration through the Snake and Columbia rivers, and (*b*) from LGR to the ocean. Mortality source (*a*) was not identifiable when separated by migratory strategy, thus it was assumed identical between natural-origin fall and spring migrants (i.e., $\phi_{y,i=\text{fall},o=\text{NOR},j}^{M^b\to M^a} = \phi_{y,i=\text{spring},o=\text{NOR},j}^{M^b\to M^a}$ for all j and y); the i dimension is thus omitted when defining these quantities below. Both mortality sources were separable by origin type (see Section D2.2.2)

Expected out-of-basin migration survival for natural-origin smolt was a logit-linear function of smolt mean length:

$$\text{logit}\left(\dot{\phi}_{y,o=\text{NOR},j}^{M^b\to M^a}\right) = \tau_{0,j} + \tau_{1,j} \cdot L_{y,j}^{*M^b} \tag{D19}$$

where $L_{y,j}^{*M^b}$ has been centered and scaled on the measured smolt mean length values ($\hat{L}_{y,j}^{M^b}$), just as for $L_{y,j}^{*P^b}$ in eqs. D13 and D16. For hatchery-origin smolt, expected out-of-basin survival was assumed to be time-constant (i.e., all $\dot{\phi}_{y,o=\text{HOR},j}^{M^b\to M^a}$ were equal within a population). For each origin separately, realized out-of-basin migration survival was a multivariate logit-normal random variable around the expected value with covariance matrix $\Sigma_{\phi^{M^b\to M^a}}$ (assumed common across origin types):

$$\text{logit}\left(\boldsymbol{\phi}^{M^b \to M^a}_{y,o,1:n_j}\right) \sim \text{MVN}\left[\text{logit}\left(\dot{\boldsymbol{\phi}}^{M^b \to M^a}_{y,o,1:n_j}\right), \Sigma_{\phi^{M^b \to M^a}}\right] \tag{D20}$$

and the abundance of smolt reaching LGR after surviving the migration out-of-basin was:

$$M^a_{y,i,o,j} = M^b_{y,i,o,j} \cdot \phi^{M^b \to M^a}_{y,o,j} \tag{D21}$$

Survival during the downstream migration through the hydrosystem on the Snake and Columbia rivers was modeled as a single survival rate, specific to each year and origin but shared among populations ($\phi^{M^a \to O^0}_{y,o}$). Realized survival rates were multivariate logit-normal random variables around a time-constant expected value ($\dot{\phi}^{M^a \to O^0}_{o}$) with covariance matrix $\Sigma_{\phi^{M^a \to O^0}}$:

$$\text{logit}\left(\boldsymbol{\phi}^{M^a \to O^0}_{y,1:n_o}\right) \sim \text{MVN}\left[\text{logit}\left(\dot{\boldsymbol{\phi}}^{M^a \to O^0}_{1:n_o}\right), \Sigma_{\phi^{M^a \to O^0}}\right] \tag{D22}$$

and the abundance of fish reaching the ocean by origin and population was:

$$O^0_{y,o,j} = \phi^{M^a \to O^0}_{y,o} \sum_{i}^{n_i} M^a_{y,i,o,j} \tag{D23}$$

The summation across migration strategies (i) in eq. D23 indicates that the fates of fish with differing migratory strategies were not tracked separately after the $M^a_{y,i,o,j}$ stage.

D2.2 Observation Model

The observation model components for the freshwater juvenile life stage were fitted to three primary data types: (a) abundance of juveniles passing rotary screw traps (located in each tributary; Gibson et al. 2024) in either the fall or spring, (b) survival of juveniles from several PIT-tagging events to LGR (Feldhaus et al. 2022; Gibson et al. 2024), and (c) the mean length of sampled individuals during two of the PIT-tagging events (Gibson et al. 2024). For all data types, the information supplied to the model were externally compiled estimates (e.g., survival from Cormack-Jolly-Seber models) and the estimated standard error was supplied to the model as a measure of observation error variability.

An even more fully integrated model would involve constructing the joint likelihood based on the frequency of PIT-tag detection histories. This was deemed unnecessary given (a) external estimates have been pre-compiled as well as their estimates of uncertainty (thus the model is consistent with published/established estimates), (b) much additional observational model complexity would be needed (e.g., detection probabilities), and (c) it would be unlikely to lead to greater parameter identifiability in the process model (e.g., allowing $\phi^{M^b \to M^a}_{y,i=\text{fall},o=\text{NOR},j} \neq \phi^{M^b \to M^a}_{y,i=\text{spring},o=\text{NOR},j}$). The practice

of performing estimation based on pre-compiled estimates that are treated as data versus on raw data is discouraged, especially if the uncertainty in pre-compiled estimates cannot be acknowledged (Brooks and Deroba 2015). However, Staton et al. (2017) investigated this topic in the context of state-space (adult-to-adult age-structured spawner-recruit) models and found little difference in inferences between models that were integrated to varying degrees with respect to the extent of data pre-compilation, so long as uncertainty from the pre-compilation step is accounted for.

D2.2.1 Abundance Data Sources

Fish with the fall migratory strategy pass the screw trap in the fall as parr and fish with the spring migratory strategy pass the screw trap the following spring as smolt. The estimated passage abundances during these time periods were used in log-normal likelihoods by assuming:

$$\log\left(\hat{P}^{a}_{y,i=\text{fall},j}\right) \sim \text{N}\left[\log\left(P^{a}_{y,i=\text{fall},j}\right), \hat{\sigma}_{P^{a}_{y,i=\text{fall},j}}\right] \tag{D24}$$

for the fall screw trap estimate and

$$\log\left(\hat{M}^{b}_{y,i=\text{spring},o=\text{NOR},j}\right) \sim \text{N}\left[\log\left(M^{b}_{y,i=\text{spring},o=\text{NOR},j}\right), \hat{\sigma}_{M^{b}_{y,i=\text{spring},o=\text{NOR},j}}\right] \tag{D25}$$

for the spring screw trap estimate.

D2.2.2 Survival Data Sources

Natural-origin juveniles have been PIT-tagged during four separate events in most years and populations: (*a*) in summer prior to migratory strategy divergence, (*b*) as fall migrant parr that pass the screw trap in the fall, (*c*) in early winter in the headwaters (after fall migrants leave, thus applies only to spring migrants; also not available for MIN), and (*d*) as spring migrant smolt pass the screw trap. Hatchery-origin smolt released in the spring were also PIT-tagged prior to release. All five of these tag groups have their survival estimated from the time of tagging to their arrival at LGR. These estimates (and their associated standard errors) were used in logit-normal likelihoods by assuming the following for each tag group.

Summer tag group:

$$\text{logit}\left(\hat{\phi}^{P^{b}\rightarrow M^{a}}_{y,j}\right) \sim \text{N}\left[\text{logit}\left(\frac{\sum_{i}^{n_i} M^{a}_{y,i,o=\text{NOR},j}}{P^{b}_{y,j}}\right), \hat{\sigma}_{\phi^{P^{b}\rightarrow M^{a}}_{y,j}}\right] \tag{D26}$$

Fall tag group:

$$\text{logit}\left(\hat{\phi}^{P^{a}\rightarrow M^{a}}_{y,i=\text{fall},j}\right) \sim \text{N}\left[\text{logit}\left(\frac{M^{a}_{y,i=\text{fall},o=\text{NOR},j}}{P^{a}_{y,i=\text{fall},j}}\right), \hat{\sigma}_{\phi^{P^{a}\rightarrow M^{a}}_{y,i=\text{fall},j}}\right] \tag{D27}$$

Winter tag group:

$$\text{logit}\left(\hat{\phi}^{P^a \to M^a}_{y,i=\text{spring},j}\right) \sim \text{N}\left[\text{logit}\left(\frac{M^a_{y,i=\text{spring},o=\text{NOR},j}}{P^a_{y,i=\text{spring},j} \cdot \phi^{P^b \to P^a}_j}\right), \hat{\sigma}_{\phi^{P^a \to M^a}_{y,i=\text{spring},j}}\right] \tag{D28}$$

(where $\phi^{P^b \to P^a}_j$ is a time-constant model-estimated survival from summer tagging to winter tagging for parr that ultimately become spring migrants and $j \in [\text{CAT}, \text{LOS}, \text{UGR}]$).

Spring tag group:

$$\text{logit}\left(\hat{\phi}^{M^b \to M^a}_{y,i=\text{spring},o=\text{NOR},j}\right) \sim \text{N}\left[\text{logit}\left(\phi^{M^b \to M^a}_{y,i=\text{spring},o=\text{NOR},j}\right), \hat{\sigma}_{\phi^{M^b \to M^a}_{y,i=\text{spring},o=\text{NOR},j}}\right] \tag{D29}$$

Hatchery smolt tag group:

$$\text{logit}\left(\hat{\phi}^{M^b \to M^a}_{y,i=\text{spring},o=\text{HOR},j}\right) \sim \text{N}\left[\text{logit}\left(\phi^{M^b \to M^a}_{y,i=\text{spring},o=\text{HOR},j}\right), \hat{\sigma}_{\phi^{M^b \to M^a}_{y,i=\text{spring},o=\text{HOR},j}}\right] \tag{D30}$$

for hatchery-origin smolt releases ($j \in [\text{CAT}, \text{LOS}, \text{UGR}]$).

Much research has been devoted to studying the survival of Chinook salmon smolt migrating through the hydrosystem on the Snake and Columbia rivers. In particular, the Comparative Survival Study has tracked the downstream survival of a variety of tagging groups going back to the early 2000s; estimates from a recent report (McCann et al. 2022, Table A.1) were used as empirical observations (with estimates of uncertainty) to inform this component of our model. Provided by McCann et al. (2022) are annual estimates of in-stream survival along the migration from LGR through Bonneville Dam (BON); separate time series are available for natural-origin (we used the "Aggregate Wild Chinook" estimates as none were available for Grande Ronde populations only, denoted $\hat{\phi}^{M^a \to O^0}_{y,o=\text{NOR}}$ here) and for hatchery-origin (we used the "Catherine Creek AP" estimates, denoted $\hat{\phi}^{M^a \to O^0}_{y,o=\text{HOR}}$ here). These estimates were treated as representative of the survival for each population, which implies an assumption that the different populations experienced similar conditions during this migration and attributes all variability to either random process or observation noise (i.e., no factors known to influence hydrosystem survival such as fish size, proportion of fish transported, or timing of flood pulses were included). Similar to the other survival data sets, these estimates were assumed to have been made with logit-normal random error around the process model values to build the likelihood:

$$\text{logit}\left(\hat{\phi}^{M^a \to O^0}_{y,o}\right) \sim \text{N}\left[\text{logit}\left(\phi^{M^a \to O^0}_{y,o}\right), \hat{\sigma}_{\phi^{M^a \to O^0}_{y,o}}\right] \tag{D31}$$

D2.2.3 Mean Length Data Sources

Individual fish lengths have been measured upon capture for PIT-tagging (Gibson et al. 2024). The mean fork length of all captured fish (tagged and untagged; only fish ≥ 55mm can receive a PIT-tag) was used in log-normal likelihoods by assuming:

$$\log\left(\hat{L}_{y,j}^{P^b}\right) \sim \mathrm{N}\left[\log\left(L_{y,j}^{P^b}\right), \hat{\sigma}_{L_{y,j}^{P^b}}\right] \tag{D32}$$

for mean length data for the summer parr tagging group and

$$\log\left(\hat{L}_{y,j}^{M^b}\right) \sim \mathrm{N}\left[\log\left(L_{y,j}^{M^b}\right), \hat{\sigma}_{L_{y,j}^{M^b}}\right] \tag{D33}$$

for mean length data for the smolt tagging group. Because each population had approximately 1,000 fish tagged and measured during each tagging event, the log-scale standard errors on the mean length estimates were quite small (on the order of 0.001-0.005) – to give the model a small amount of flexibility around fitting to these data, we set the values of the $\hat{\sigma}_{L_{y,j}^{P^b}}$ and $\hat{\sigma}_{L_{y,j}^{M^b}}$ terms equal to 0.01.

Preliminary analyses revealed that parr mean length estimates had inter-annual variability attributable to the median sample date (capture method is active), so a standardization was devised and applied prior to model fitting (Staton et al. 2023, Figure 26 therein). All uses of $\hat{L}_{y,j}^{P^b}$ in this document refer to the standardized version. Although timing has varied for smolt mean length estimates ($\hat{L}_{y,j}^{M^b}$), it was caused by migratory timing rather than sample timing, thus should treated as process noise.

D3 Ocean Phase

D3.1 Process Model

Spring Chinook salmon in the Grande Ronde Basin migrate to sea as age-2 smolt and can return as either age-3, age-4, or age-5 adults. That is, ocean juveniles spend between 1 and 3 winters at sea and some fraction makes the return migration as adults after each winter. Thus, ocean dynamics were divided into two types of demographic rates: survival and maturation. Attempting to freely estimate all desired parameters (i.e., time varying year-1, year-2, and year-3 survival rates and maturation rates after year-1 and year-2) revealed that these parameters were confounded given the available data, requiring more simplifying assumptions and stronger prior information than in other parts of the model.

D3.1.1 Survival Rates

Year-1 natural-origin[2] ocean survival was modeled as a multivariate logit-normal random variable around a time-constant expected value ($\dot{\phi}^{O^0\to O^1}_{o=\text{NOR},j}$) with covariance matrix $\Sigma_{\phi^{O^0\to O^1}}$, but included a lag-1 autoregressive process as a means to account for ocean conditions that may affect survival in a temporally non-independent fashion (e.g., Mantua et al. 1997):

$$\text{logit}\left(\boldsymbol{\phi}^{O^0\to O^1}_{y,o,1:n_j}\right) \sim \text{MVN}\left\{\text{logit}\left(\dot{\boldsymbol{\phi}}^{O^0\to O^1}_{o,1:n_j}\right) + \boldsymbol{\kappa}^{O^0\to O^1}_{1:n_j} \cdot \left[\text{logit}\left(\boldsymbol{\phi}^{O^0\to O^1}_{y-1,o,1:n_j}\right) - \text{logit}\left(\dot{\boldsymbol{\phi}}^{O^0\to O^1}_{o,1:n_j}\right)\right], \Sigma_{\phi^{O^0\to O^1}}\right\} \tag{D34}$$

The first simplifying assumption surrounding ocean survival rates was that process variation was negligible in year-2 and year-3, thus we forced the values of $\phi^{O^1\to O^2}_{y,o=\text{NOR},j}$ and $\phi^{O^2\to O^3}_{y,o=\text{NOR},j}$ to take on the same value for all years (i.e., $\dot{\phi}^{O^1\to O^2}_{o=\text{NOR},j}$ and $\dot{\phi}^{O^2\to O^3}_{o=\text{NOR},j}$, respectively). Further, it was discovered that reasonably strong priors would be needed to inform $\dot{\phi}^{O^1\to O^2}_{o=\text{NOR},j}$ and $\dot{\phi}^{O^2\to O^3}_{o=\text{NOR},j}$ to allow identifiability of the maturity parameters (Table D3); priors were used for ocean survival rather than maturity parameters because commonly assumed values were available for the former (CTC 1988). The second simplifying assumption was that natural- and hatchery-origin ocean survival rates were perfectly correlated across years within populations, but offset by a time-constant log-odds ratio (δ_j):

$$\begin{aligned}
\text{logit}\left(\phi^{O^0\to O^1}_{y,o=\text{HOR},j}\right) &= \text{logit}\left(\phi^{O^0\to O^1}_{y,o=\text{NOR},j}\right) + \delta_j \\
\text{logit}\left(\phi^{O^1\to O^2}_{y,o=\text{HOR},j}\right) &= \text{logit}\left(\phi^{O^1\to O^2}_{y,o=\text{NOR},j}\right) + \delta_j \\
\text{logit}\left(\phi^{O^2\to O^3}_{y,o=\text{HOR},j}\right) &= \text{logit}\left(\phi^{O^2\to O^3}_{y,o=\text{NOR},j}\right) + \delta_j
\end{aligned} \tag{D35}$$

D3.1.2 Maturation Rates

Realized maturation rates (i.e., the proportion of fish from a given brood year alive and in the ocean at the beginning of a year that make the return migration that year) were modeled as multivariate logit-normal random variables around time-constant expected values ($\dot{\psi}^{O^w}_{o,j}$; w is the number of winters spent in the ocean) with covariance matrix $\Sigma_{\psi^{O^w}}$ (assumed common across origins):

$$\begin{aligned}
\text{logit}\left(\boldsymbol{\psi}^{O^1}_{y,o,1:n_j}\right) &\sim \text{MVN}\left[\text{logit}\left(\dot{\boldsymbol{\psi}}^{O^1}_{o,1:n_j}\right), \Sigma_{\psi^{O^1}}\right] \\
\text{logit}\left(\boldsymbol{\psi}^{O^2}_{y,o,1:n_j}\right) &\sim \text{MVN}\left[\text{logit}\left(\dot{\boldsymbol{\psi}}^{O^2}_{o,1:n_j}\right), \Sigma_{\psi^{O^2}}\right]
\end{aligned} \tag{D36}$$

[2]All o = NOR in eq. D34, omitted for brevity.

Since age-5 was the last modeled age of maturity, all fish alive and in the ocean after the third year at sea mature and return that year (i.e., all $\psi^{O^3}_{y,o,j} = 1$).

D3.1.3 Return to Columbia River

Based on the sources of process variation modeled in eqs. D34, D35, and D36 and the initial abundance of ocean juveniles ($O^0_{y,o,j}$, eq. D23), the abundance of ocean juveniles after a given number of winters (w, superscripts in all O^w symbols) was modeled as a sequence of survival, maturation of surviving fish, and survival of non-maturing fish:

$$\begin{aligned} O^1_{y,o,j} &= O^0_{y,o,j} \cdot \phi^{O^0 \to O^1}_{y,o,j} \\ O^2_{y,o,j} &= O^1_{y,o,j} \cdot (1 - \psi^{O^1}_{y,o,j}) \cdot \phi^{O^1 \to O^2}_{y,o,j} \\ O^3_{y,o,j} &= O^2_{y,o,j} \cdot (1 - \psi^{O^2}_{y,o,j}) \cdot \phi^{O^2 \to O^3}_{y,o,j} \end{aligned} \tag{D37}$$

That is, fish reaching the ocean as age-2 juveniles ($O^0_{y,o,j}$) must survive one winter to become age-3 ocean juveniles ($O^1_{y,o,j}$); if they do not mature at age-3 (with probability $1 - \psi^{O^1}_{y,o,j}$), then they must survive another winter to become age-4 ocean juveniles ($O^2_{y,o,j}$), and if they do not mature at that point (with probability $1 - \psi^{O^2}_{y,o,j}$), they must survive a third winter to become age-5 ocean juveniles ($O^3_{y,o,j}$).

The abundances of ocean juveniles ($O^1_{y,o,j}$, $O^2_{y,o,j}$, and $O^3_{y,o,j}$) from a given cohort were organized by brood year, however they returned in different years and ages to spawn. Returning mature fish were placed into the correct year and age of return to the mouth of the Columbia River before the upstream migration ($R^b_{y,k,o,j}$) based on the following rule: members of the cohort spawned in brood year y returned at the k^{th} possible age of maturity to produce the cohort for brood year $y + A_{\min} + k - 1$. As an example, fish spawned in brood year $y = 2000$ returned in 2003 as age-3 ($k = 1$), in 2004 as age-4 ($k = 2$), or in 2005 as age-5 ($k = 3$) – see Table D6 for a visual of this example. Thus, the abundance of fish spawned in brood year y returning as age-3, age-4, and age-5, respectively, was:

$$\begin{aligned} R^b_{y+A_{\min}+1-1,1,o,j} &= O^1_{y,o,j} \cdot \psi^{O^1}_{y,o,j} \\ R^b_{y+A_{\min}+2-1,2,o,j} &= O^2_{y,o,j} \cdot \psi^{O^2}_{y,o,j} \\ R^b_{y+A_{\min}+3-1,3,o,j} &= O^3_{y,o,j} \cdot \psi^{O^3}_{y,o,j} \end{aligned} \tag{D38}$$

This, however, leaves 12 ($\sum_k^{n_k} A_{\min} + k - 1$) age/year combinations per origin unpopulated with returning adults (the first 3 missing years for age-3 returns, first 4 missing years for age-4 returns, and first 5 missing years for age-5 returns; see Table D6). This occurs because no juvenile process model outcomes existed that would ultimately become these $R^b_{y,k,o,j}$ values in these early years.

Thus, to initialize the adult returns for natural-origin fish, these 12 year/age return abundances were estimated as unknown parameters with fairly restrictive priors (Table D3) with boundaries loosely informed by the ranges of adult returns-at-age observed in the early years of the data time series. Initial abundances of age-specific hatchery-origin returns were handled by the "straying model" (see Section D4.1.2, below).

D3.2 Observation Model

No data sources were used to inform population dynamics occurring in the ocean phase – estimation of these quantities was enabled by (*a*) reasonably precise information about the abundance and composition of fish entering the ocean and returning to natal tributaries, (*b*) the simplifying assumptions described above (i.e., time-constant second and third year ocean survival and perfectly correlated but offset origin-specific survival), and (*c*) through the use of reasonably strong priors for second and third year ocean survival (Table D3).

D4 Freshwater Adult Phase

D4.1 Process Model

There are a variety of mortality sources that occur along the upstream migration from the mouth of the Columbia River to the point of spawning in natal tributaries in Grande Ronde Basin. For ease of presentation, we separate these processes into three categories depending on where they occur spatiotemporally: (*a*) downstream of Bonneville Dam (BON) at the beginning of the upstream migration, (*b*) along the upstream migration in the mainstem Columbia and Snake rivers between BON and LGR, and (*c*) after arrival to the natal tributaries and up until the point of spawning.

D4.1.1 Processes Downstream of BON

Prior to reaching BON, returning adults are subjected to harvest mortality from fisheries (harvest rate denoted by $U_{y,k,o}$). These estimates were supplied to the model as known without error (i.e., non-stochastic; used in eq. D40, below).

D4.1.2 Processes Between BON and LGR

Upon arrival to BON, survival to LGR has been monitored (since 2000; $y = 10$) via PIT-tags with high (>0.95) detection probabilities, enabling estimation of survival along this portion of the migration. The survival rate between BON and LGR was assumed to vary by origin (but not by population) as multivariate logit-normal random variables around expected values ($\dot{\phi}_o^{R^b \rightarrow R^a}$) with covariance matrix $\Sigma_{\phi^{R^b \rightarrow R^a}}$. In years without these PIT-tag counts, however, the survival from BON to LGR was found to be confounded with ocean survival; this was resolved by using the expected value rather than estimating the value for these years:

$$\text{logit}\left(\boldsymbol{\phi}_{y,1:n_o}^{R^b \to R^a}\right) \begin{cases} = \text{logit}\left(\dot{\boldsymbol{\phi}}_{1:n_o}^{R^b \to R^a}\right) & \text{if } y < 10 \\ \sim \text{MVN}\left[\text{logit}\left(\dot{\boldsymbol{\phi}}_{1:n_o}^{R^b \to R^a}\right), \Sigma_{\phi^{R^b \to R^a}}\right] & \text{if } y \geq 10 \end{cases} \tag{D39}$$

Examination of the adult composition data indicated that hatchery-origin adults returned to Grande Ronde populations in early years that could not be attributed to conventional hatchery-origin smolt releases to these populations. Further, the Minam River population (which has no hatchery supplementation program) has had hatchery adults found in carcass surveys in many of the years since monitoring began. Without a process model adjustment, the observation model would treat these unexpected non-zero hatchery-origin counts as impossible. This model component is referred to as the "straying model" (total abundance of entering strays denoted $G_{y,o,j}$), and it applied only in years/populations in which the presence of non-zero hatchery-origin returning adults could not otherwise be explained due to zero-valued conventional hatchery-origin smolt releases. Thus, all $G_{y,o=\text{NOR},j} = 0$ and all $G_{y,o=\text{HOR},j} = 0$ in years where non-zero hatchery-origin smolt releases to population j could have explained non-zero hatchery-origin adult returns in year y at age k. The age composition of these strays was assumed to be time-constant ($p_{k,j}^G$; where $\sum_k^{n_k} p_{k,j}^G = 1$) and was used to apportion $G_{y,o,j}$.

The abundance of adults arriving to natal spawning tributaries by age and origin ($R_{y,k,o,j}^a$) was:

$$R_{y,k,o,j}^a = R_{y,k,o,j}^b \cdot (1 - U_{y,k,o}) \cdot \phi_{y,o}^{R^b \to R^a} + \left(G_{y,o,j} \cdot p_{k,j}^G\right) \tag{D40}$$

D4.1.3 Processes in Natal Tributary

Upon arrival to the natal tributary, populations with a weir and hatchery supplementation program (all populations except the Minam River, indexed by $j = \text{MIN}$) have some number of adults removed each year for broodstock and as a means to control the number of hatchery-origin fish that spawn naturally. These weir removals (denoted by $B_{y,k,o,j}$; all $B_{y,k,o,j=\text{MIN}} = 0$) were supplied to the model as known without error, as were the number of fish estimated to have been harvested in the natal tributaries prior to spawning (Lance et al. 2023). Thus, the abundance of potential spawners was:

$$S_{y,k,o,j}^b = \max\left(R_{y,k,o,j}^a - B_{y,k,o,j} - H_{y,k,o,j}, 1\right) \tag{D41}$$

The maximum constraint was used to ensure all $S_{y,k,o,j}^b > 0$.

It is well-known that some potential spawners die prior to spawning (e.g., Bowerman et al. 2021); these "pre-spawn survival" outcomes are denoted by $\phi_{y,j}^{S^b \to S^a}$. The initial desire was to allow for the model to internally estimate time-varying pre-spawn survival probabilities, but it

was discovered that the observational data (counts of spawned vs. gravid female carcasses) were not informative enough for all populations to prevent parameter confounding with egg-to-parr survival. As an alternative, binary logistic regression models were fitted that included year-specific random effects around a time-constant expected value (one per population; success represented by year-specific counts of spawned female carcasses, trials represented by total female carcasses examined) and the resulting time- and population-varying estimates were supplied to the model as known without error. The abundance of adults spawning successfully was then:

$$S^{a}_{y,k,o,j} = S^{b}_{y,k,o,j} \cdot \phi^{S^b \rightarrow S^a}_{y,j} \tag{D42}$$

This $S^{a}_{y,k,o,j}$ value was used to calculate total egg production ($E_{y,j}$) in eq. D4 to link the spawner abundance to the parr recruitment abundance in the next generation.

D4.2 Observation Model

The adult observation model relied on three primary data types: (*a*) total abundance of adult returns to the natal tributaries, (*b*) information about survival on the upstream migration between LGR and BON, and (*c*) composition data to inform the relative abundance of adults of different ages and origins returning each year.

D4.2.1 Abundance Data Source

Total tributary return abundance has been estimated annually external to the model using a combination of weir counts, mark-recapture methods, and spawning ground surveys (Bliesner et al. 2020; Feldhaus et al. 2022). For each population and year, these have been compiled into a point estimate ($\hat{R}^{a}_{y,j}$; the lack of o or k indices indicates the estimate is aggregated across the origin and age dimensions) and an estimate of observation uncertainty ($\hat{\sigma}_{R^{a}_{y,j}}$, expressed as a log-normal standard error). The model assumed the point estimate is made with log-normal observation error around the model-predicted total returns to the tributary to build the likelihood for this component:

$$\log\left(\hat{R}^{a}_{y,j}\right) \sim \mathrm{N}\left[\log\left(\sum_{o}^{n_o}\sum_{k}^{n_k} R^{a}_{y,k,o,j}\right), \hat{\sigma}_{R^{a}_{y,j}}\right] \tag{D43}$$

D4.2.2 Survival Data Sources

The model fitted to counts of PIT-tag detections of known Grande Ronde-origin fish passing BON ($\hat{x}^{\mathrm{BON}}_{y,o}$) and LGR ($\hat{x}^{\mathrm{LGR}}_{y,o}$) to inform the migratory survival rate between these two locations (DART 2023; exact query settings used described in Gibson 2025). The latter was assumed to be a binomial random variable to build the likelihood component for this data set:

$$\hat{x}_{y,o}^{\mathrm{LGR}} \sim \mathrm{B}\left(\phi_{y,o}^{R^b \to R^a}, \hat{x}_{y,o}^{\mathrm{BON}}\right) \tag{D44}$$

D4.2.3 Composition Data Sources

Since the model is both age- and origin-structured, it required data to inform the relative abundance of adults returning according to these different classes. These data took the form of two sources: (*a*) those collected at weirs located within three of the four populations ($\hat{x}_{y,ko,j}^{R^a}$) and (*b*) those collected from carcasses recovered during spawning ground surveys ($\hat{x}_{y,ko,j}^{S^{a'}}$), given the Minam River population does not have a weir (Crump et al. 2024; Simmons et al. 2023; Feldhaus et al. 2022). The weirs were assumed to have sampled fish representatively with respect to age and origin composition and both data sources were fitted to by assuming multinomial sampling in which there were $n_{ko} = 6$ possible outcomes: $n_k = 3$ ages of return by $n_o = 2$ origins. Further, the observed sample size ($\sum_{ko}^{n_{ko}} \hat{x}_{y,ko,j}^{R^a}$) was used as the multinomial sample size rather than attempting to adjust it for non-independent sampling (Maunder 2011); alternative sample size selections would likely be arbitrary, and past analyses have suggested that inferences are robust to rational alternatives (see Supplement A of Staton et al. 2021). The model-expected composition by age and origin ($p_{y,ko,j}^{R^a}$) was calculated from the return abundance by age and origin, reorganized such that age and origin fell along the same array dimension ($R_{y,ko,j}^{a}$) rather than along two dimensions as shown in the process model ($R_{y,k,o,j}^{a}$):

$$p_{y,ko,j}^{R^a} = \frac{R_{y,ko,j}^{a}}{\sum_{ko}^{n_{ko}} R_{y,ko,j}^{a}} \tag{D45}$$

which was used as the multinomial expected frequency to build the likelihood:

$$\hat{\boldsymbol{x}}_{y,1:n_{ko},j}^{R^a} \sim \mathrm{M}\left(\boldsymbol{p}_{y,1:n_{ko},j}^{R^a}, \sum_{ko}^{n_{ko}} \hat{x}_{y,ko,j}^{R^a}\right) \tag{D46}$$

Preliminary analyses revealed an age sampling bias of examined carcasses relative to weir sampling, which required a correction to ensure reliable fits to all data sets while recovering unbiased true age composition data for the Minam River population, which had only carcass composition data (and other populations prior to weir operations, or in years of otherwise missing weir data, Figure D2). For the three populations with paired composition data (i.e., $j \in [\mathrm{CAT}, \mathrm{LOS}, \mathrm{UGR}]$), correction factors were estimated in a hierarchical fashion:

$$z_{k,j} \sim \mathrm{N}\left(\dot{z}_k, \sigma_{z_k}\right) \tag{D47}$$

where $k = 1$ or $k = 3$ ($k = 2$ was treated as the baseline category), $z_{k,j}$ are age- and population-specific coefficients, $\dot{z}_k$ are their expectations across populations, and σ_{z_k} are their standard deviations across populations. These coefficients were used in the following log-linear model to derive the correction factors ($\zeta_{k,j}$):

$$\log(\zeta_{k,j}) = z_{k=1,j} \cdot \text{age3}_k + z_{k=3,j} \cdot \text{age5}_k \tag{D48}$$

where $k \in [1, 2, 3]$, $\mathbf{age3}_{1:n_k} = [1\ 0\ 0]$ is a dummy variable indicating whether each value of k corresponds to age-3, and $\mathbf{age5}_{1:n_k} = [0\ 0\ 1]$ is a dummy variable indicating whether each value of k corresponds to age-5. These correction factors were averaged across populations to obtain the correction factors for the Minam River population:

$$\zeta_{k,j=\text{MIN}} = \text{mean}\left(\zeta_{k,j\in[\text{CAT,LOS,UGR}]}\right) \tag{D49}$$

These correction factors were used to calculate the expected proportions by age and origin for carcass surveys ($p^{S^{a'}}_{y,ko,j}$):

$$p^{S^{a'}}_{y,ko,j} = \frac{S^{a}_{y,ko,j} \cdot \zeta_{k,j}}{\sum_{ko}^{n_{ko}} S^{a}_{y,ko,j} \cdot \zeta_{k,j}} \tag{D50}$$

which was used as the multinomial expected frequency to build the likelihood by assuming:

$$\hat{\boldsymbol{x}}^{S^{a'}}_{y,1:n_{ko},j} \sim \text{M}\left(\boldsymbol{p}^{S^{a'}}_{y,1:n_{ko},j}, \sum_{ko}^{n_{ko}} \hat{x}^{S^{a'}}_{y,ko,j}\right) \tag{D51}$$

References

Achord, S., Levin, P. S., and Zabel, R. W. 2003. Density-dependent mortality in Pacific salmon: The ghost of impacts past? *Ecology Letters*, 6(4):335–342. doi:10.1046/j.1461-0248.2003.00438.x.

Barnard, J., McCulloch, R., and Meng, X.-L. 2000. Modeling covariance matrices in terms of standard deviations and correlations, with application to shrinkage. *Statistica Sinica*, 10(4):1281–1311. URL: https://www.jstor.org/stable/24306780.

Bliesner, K. L., Craft, N. M., Feldhaus, J. W., and Ruzycki, J. R. 2020. A compendium of viable salmonid population abundance and productivity field and analysis methods for natural origin adult Chinook salmon populations in the Snake River spring/summer-run ESU of northeast Oregon from 1949-2019. Technical report, Oregon Department of Fish and Wildlife, East Region Fish Research. URL: https://nrimp.dfw.state.or.us/DataClearinghouse/default.aspx?p=202&XMLname=1151.xml.

Bouchard, C., Buoro, M., Lebot, C., and Carlson, S. M. 2022. Synchrony in population dynamics of juvenile Atlantic salmon: Analyzing spatiotemporal variation and the influence of river flow and demography. *Canadian Journal of Fisheries and Aquatic Sciences*, 79(5):782–794. doi:10.1139/cjfas-2021-0017.

Bovee, K. D. 1982. Guide to stream habitat analysis using the instream flow incremental methodology. Instream Flow Information Paper FWS/OBS-82/26, U.S. Fish and Wildlife Service, Springfield, VA.

Bowerman, T. E., Keefer, M. L., and Caudill, C. C. 2021. Elevated stream temperature, origin, and individual size influence Chinook salmon prespawn mortality across the Columbia River Basin. *Fisheries Research*, 237:105874. doi:10.1016/j.fishres.2021.105874.

Brooks, E. N. and Deroba, J. J. 2015. When "data" are not data: The pitfalls of post hoc analyses that use stock assessment model output. *Canadian Journal of Fisheries and Aquatic Sciences*, 72(4):634–641. doi:10.1139/cjfas-2014-0231.

CHaMP 2016. *Scientific Protocol for Salmonid Habitat Surveys within the Columbia Habitat Monitoring Program*. Columbia Habitat Monitoring Program. URL: https://www.champmonitoring.org/Program/RetrieveProgramDocumentFile/Tab/1126.

Cooney, T. D., Jonasson, B. C., Sedell, E. R., Hoffnagle, T. L., and Carmichael, R. W. 2017. Grande Ronde spring Chinook populations: Juvenile based models. In *NOAA Fisheries' Interior Columbia Basin Life-Cycle Modeling*, pages 1–30.

Copeland, T. and Venditti, D. A. 2009. Contribution of three life history types to smolt production in a Chinook salmon (*Oncorhynchus tshawytscha*) population. *Canadian Journal of Fisheries and Aquatic Sciences*, 66(10):1658–1665. doi:10.1139/F09-110.

Copeland, T., Venditti, D. A., and Barnett, B. R. 2014. The importance of juvenile migration tactics to adult recruitment in stream-type Chinook salmon populations. *Transactions of the American Fisheries Society*, 143(6):1460–1475. doi:10.1080/00028487.2014.949011.

Crump, C., Naylor, L., Van Sickle, A., Kennedy, J., Cottingham, M., and Shippentower, G. 2024. Monitoring and evaluation of supplemented spring Chinook salmon and life histories of wild summer steelhead in the Grande Ronde Basin. Annual Report for BPA Project #2007-083-00, Confederated Tribes of the Umatilla Indian Reservation, Pendleton, OR. URL: https://www.cbfish.org/Document.mvc/Viewer/P208816.

CTC 1988. Exploitation rate analysis - Appendix 2 to Chinook technical committee 1987 annual report. Technical Report TCCHINOOK (88)-2, CTC Analytical Work Group. URL: https://www.psc.org/download/35/chinook-technical-committee/2150/tcchinook88-2app2.pdf.

DART 2023. PIT tag adult returns conversion rate. URL: https://www.cbr.washington.edu/dart/query/pitadult_conrate.

Dorazio, R. M., Gotelli, N. J., and Ellison, A. M. 2011. Modern methods of estimating biodiversity loss from presence-absence surveys. In Grillo, O., editor, *Biodiversity Loss in a Changing Planet*, pages 277–302. InTech. URL: https://www.intechopen.com/books/biodiversity-loss-in-a-changing-planet/modern-methods-of-estimating-biodiversity-from-presence-absence-surveys.

Feldhaus, J., Brandt, E., Tattam, I., Vatland, S., Crump, C., and Naylor, L. 2022. 2022 Grande Ronde and Imnaha River basin spring Chinook salmon hatchery review. Technical report, Oregon Department of Fish and Wildlife; Nez Perce Tribe; Confederated Tribes of the Umatilla Indian Reservation. URL: https://www.fws.gov/sites/default/files/documents/2A%20-%202022%20Grande%20Ronde%20and%20Imnaha%20Basin%20Spring%20Chinook%20ISRP%20review.pdf.

Gelman, A., Carlin, J. B., Stern, H. S., Dunson, D. B., Vehtari, A., and Rubin, D. B. 2014. *Bayesian Data Analysis*.

Texts in Statistical Science. Chapman & Hall/CRC, Boca Raton, FL, 3 edition.

Gelman, A. and Hill, J. 2007. *Data Analysis Using Regression and Multilevel and Hierarchical Models*. Cambridge University Press, New York.

Gibson, P. 2025. GR-sslcm-data: Github repository storing data to fit the Grande Ronde Basin state-space life cycle model for spring Chinook salmon. Archival DOI not yet available. URL: https://github.com/gibsonpp/GR-sslcm-data.

Gibson, P. P., Drascic, F. J., and Lemanski, J. R. 2024. Investigations into the life history of naturally produced spring Chinook salmon and summer steelhead in the Grande Ronde River subbasin, 2023. BPA Annual Report for Project 1992-026-04, Oregon Department of Fish and Wildlife, La Grande, OR. URL: https://nrimp.dfw.state.or.us/DataClearinghouse/default.aspx?p=202&XMLname=42802.xml.

Grant, J. W. A. and Imre, I. 2005. Patterns of density-dependent growth in juvenile stream-dwelling salmonids. *Journal of Fish Biology*, 67(sB):100–110. doi:10.1111/j.0022-1112.2005.00916.x.

Grossman, G. D. and Simon, T. N. 2020. Density-dependent effects on salmonid populations: A review. *Ecology of Freshwater Fish*, 29(3):400–418. doi:10.1111/eff.12523.

Hartig, F. 2022. Dharma: Residual diagnostics for hierarchical (multi-level / mixed) regression models. R package version 0.4.6. URL: https://CRAN.R-project.org/package=DHARMa.

Hostetter, N. J., Evans, A. F., Loge, F. J., O'Connor, R. R., Cramer, B. M., Fryer, D., and Collis, K. 2015. The influence of individual fish characteristics on survival and detection: Similarities across two salmonid species. *North American Journal of Fisheries Management*, 35(5):1034–1045. doi:10.1080/02755947.2015.1077176.

Justice, C., Staton, B., White, S., Kaylor, M., and Burns, L. 2021. Developing an index of Chinook Salmon parr capacity in the Grande Ronde River basin. In *Assessing the Status and Trends of Spring Chinook Habitat in the Upper Grande Ronde River and Catherine Creek: Annual Report 2020*, Annual Report for BPA Project #2009-004-00, pages 82–94. Columbia River Inter-Tribal Fish Commission, Portland, OR. URL: https://critfc.org/reports/assessing-the-status-and-trends-of-spring-chinook-habitat-in-the-upper-grande-ronde-river-and-catherine-creek-annual-report-2020/.

Lance, M. E., Brandt, E. J., and Bratcher, K. W. 2023. Lower Snake River Compensation Plan: Oregon spring Chinook harvest monitoring, 2023 annual progress report. Science Bulletin 2023-11, Oregon Department of Fish and Wildlife, Salem, OR. URL: http://www.fws.gov/lsnakecomplan/Reports/ODFWreports.html.

Mantua, N. J., Hare, S. R., Zhang, Y., Wallace, J. M., and Francis, R. C. 1997. A Pacific Interdecadal climate oscillation with impacts on salmon production. *Bulletin of the American Meteorological Society*, 78(6):1069–1080. doi:10.1175/1520-0477(1997)078<1069:APICOW>2.0.CO;2.

Maret, T. R., Hortness, J. E., and Ott, D. S. 2006. Instream flow characterization of upper Salmon River Basin streams, central Idaho, 2005. Technical Report 2006-5230, U.S. Geological Survey.

Maunder, M. N. 2011. Review and evaluation of likelihood functions for composition data in stock-assessment models: Estimating the effective sample size. *Fisheries Research*, 109(2):311–319. doi:10.1016/j.fishres.2011.02.018.

McCann, J., Chockley, B., Cooper, E., Scheer, G., Haeseker, S., Lessard, B., Copeland, T., Ebel, J., Storch, A., and Rawding, D. 2022. Comparative survival study of PIT-tagged spring/summer/fall Chinook, summer steelhead, and sockeye, 2022. Annual Report BPA Contract #19960200, CSS Oversight Committee and Fish Passage Center, Portland, OR. URL: https://www.fpc.org/documents/CSS/CSS%20Final%20Revised%202022.pdf.

Myrvold, K. M. and Kennedy, B. P. 2015. Density dependence and its impact on individual growth rates in an age-structured stream salmonid population. *Ecosphere*, 6(12):1–16. doi:10.1890/ES15-00390.1.

Plummer, M. 2017. JAGS Version 3.4.0 User Manual. URL: https://sourceforge.net/projects/mcmc-jags/.

Riecke, T. V., Sedinger, B. S., Williams, P. J., Leach, A. G., and Sedinger, J. S. 2019. Estimating correlations among demographic parameters in population models. *Ecology and Evolution*, 9(23):13521–13531. doi:10.1002/ece3.5809.

Simmons, B. W., Espinosa, N., Arnsberg, B., Cleary, P., Nelson, D., Rabe, C., and Sublett, M. 2023. Snake River Basin adult Chinook salmon and steelhead monitoring, 2022. Annual Report, Nez Perce Tribe, Department of Fisheries Resources Management, Research Division, Lapwai, ID. URL: https://www.researchgate.net/publication/373923696.

Staton, B., Justice, C., Kaylor, M., and Ringelman, A. 2023. Objective E-1: Grande Ronde phase 12 - development of a spring Chinook statistical estimation life cycle model. In *Evaluating Salmonid and Stream Ecosystem Response to Conservation Measures and Environmental Stressors in the Columbia River Basin*, Annual Report for BPA Project #2009-004-00, pages 69–83. Columbia River Inter-Tribal Fish Commission, Portland, OR. URL: https://critfc.org/wp-content/uploads/2023/07/23_03.pdf.

Staton, B. A., Catalano, M. J., Connors, B. M., Jr, L. G. C., Jones, M. L., Walters, C. J., Fleischman, S. J., and Gwinn, D. C. 2020. Evaluation of methods for spawner–recruit analysis in mixed-stock Pacific salmon fisheries. *Canadian*

Journal of Fisheries and Aquatic Sciences, 77(7):1149–1162. doi:10.1139/cjfas-2019-0281.

Staton, B. A., Catalano, M. J., and Fleischman, S. J. 2017. From sequential to integrated Bayesian analyses: Exploring the continuum with a Pacific salmon spawner-recruit model. *Fisheries Research*, 186:237–247. doi:10.1016/j.fishres.2016.09.001.

Staton, B. A., Catalano, M. J., Fleischman, S. J., and Ohlberger, J. 2021. Incorporating demographic information into spawner–recruit analyses alters biological reference point estimates for a western Alaska salmon population. *Canadian Journal of Fisheries and Aquatic Sciences*, 78(12):1755–1769. doi:10.1139/cjfas-2020-0478.

Thorson, J. T., Scheuerell, M. D., Buhle, E. R., and Copeland, T. 2014. Spatial variation buffers temporal fluctuations in early juvenile survival for an endangered Pacific salmon. *Journal of Animal Ecology*, 83(1):157–167. doi:10.1111/1365-2656.12117.

Walters, A. W., Copeland, T., and Venditti, D. A. 2013. The density dilemma: Limitations on juvenile production in threatened salmon populations. *Ecology of Freshwater Fish*, 22(4):508–519. doi:10.1111/eff.12046.

White, S., Justice, C., and McCullough, D. 2012. Protocol for snorkel surveys of fish densities. Technical report, Columbia River Inter-Tribal Fish Commission. URL: https://critfc.org/wp-content/uploads/2023/03/ReportPost_White_etal2012.pdf.

Zabel, R. W. and Achord, S. 2004. Relating size of juveniles to survival within and among populations of Chinook salmon. *Ecology*, 85(3):795–806. doi:10.1890/02-0719.

FIGURE D1. Schematic of the life stages and transitions captured in the state-space life cycle model for Grande Ronde spring Chinook Salmon. Diagram shows one generation for one population. Boxes represent abundances of fish (states), arrows represent changes (rates) among stages, and circled numbers represent quantities with data sources informing them. Blue states have associated mean length, and blue arrows are expressed as functions of mean length. Duplicated from Figure 1 of the article main text for completeness.

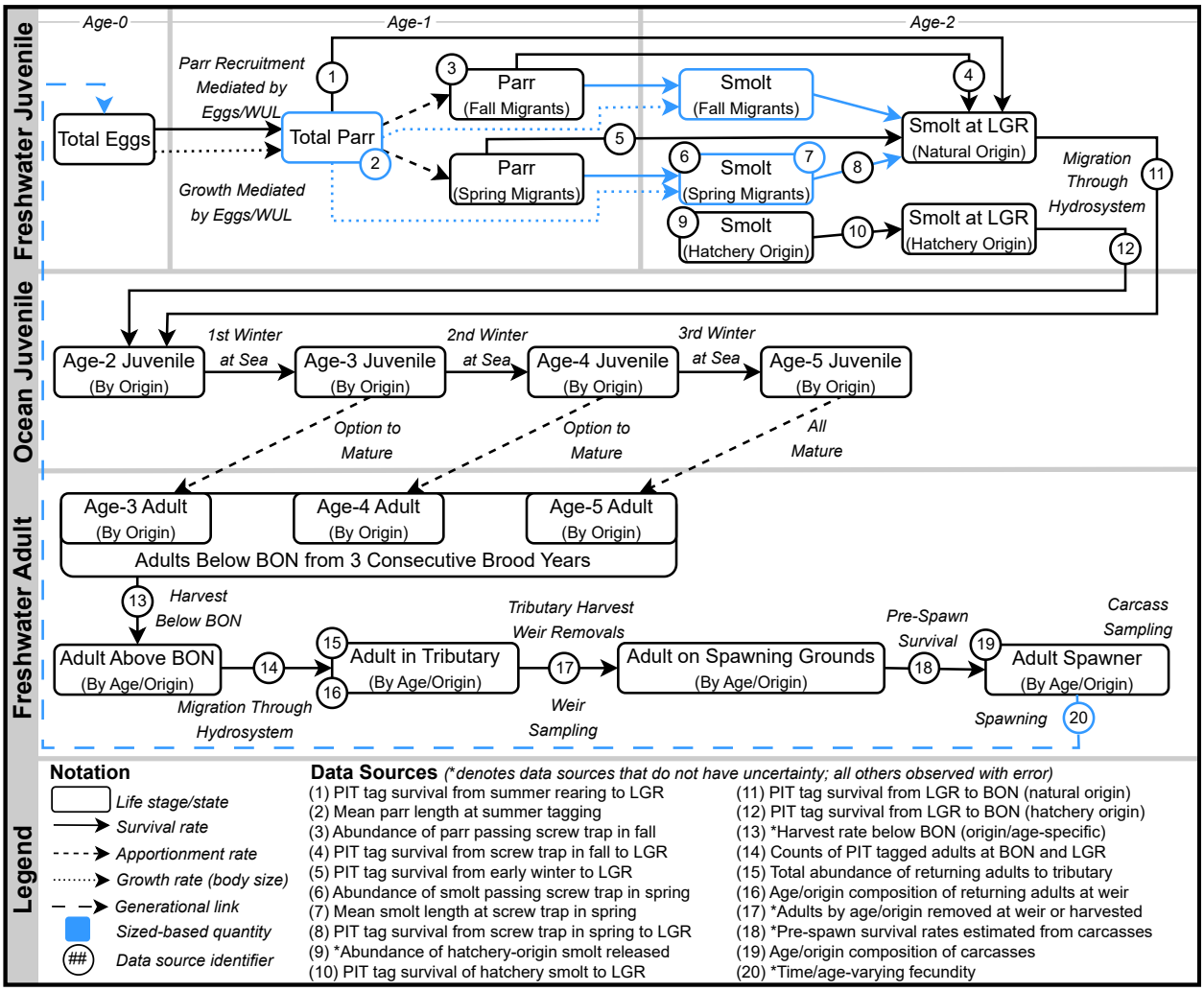

FIGURE D2. Visual representation of the years in which data of each type were available for each population and/or origin type. For juvenile life stages (i.e., panels *a-j*), year represents the brood year whereas for adult life stages (i.e., panels *k-n*) year represents the return year. The number in brackets in each panel title denotes the numbered data source in Figure D1.

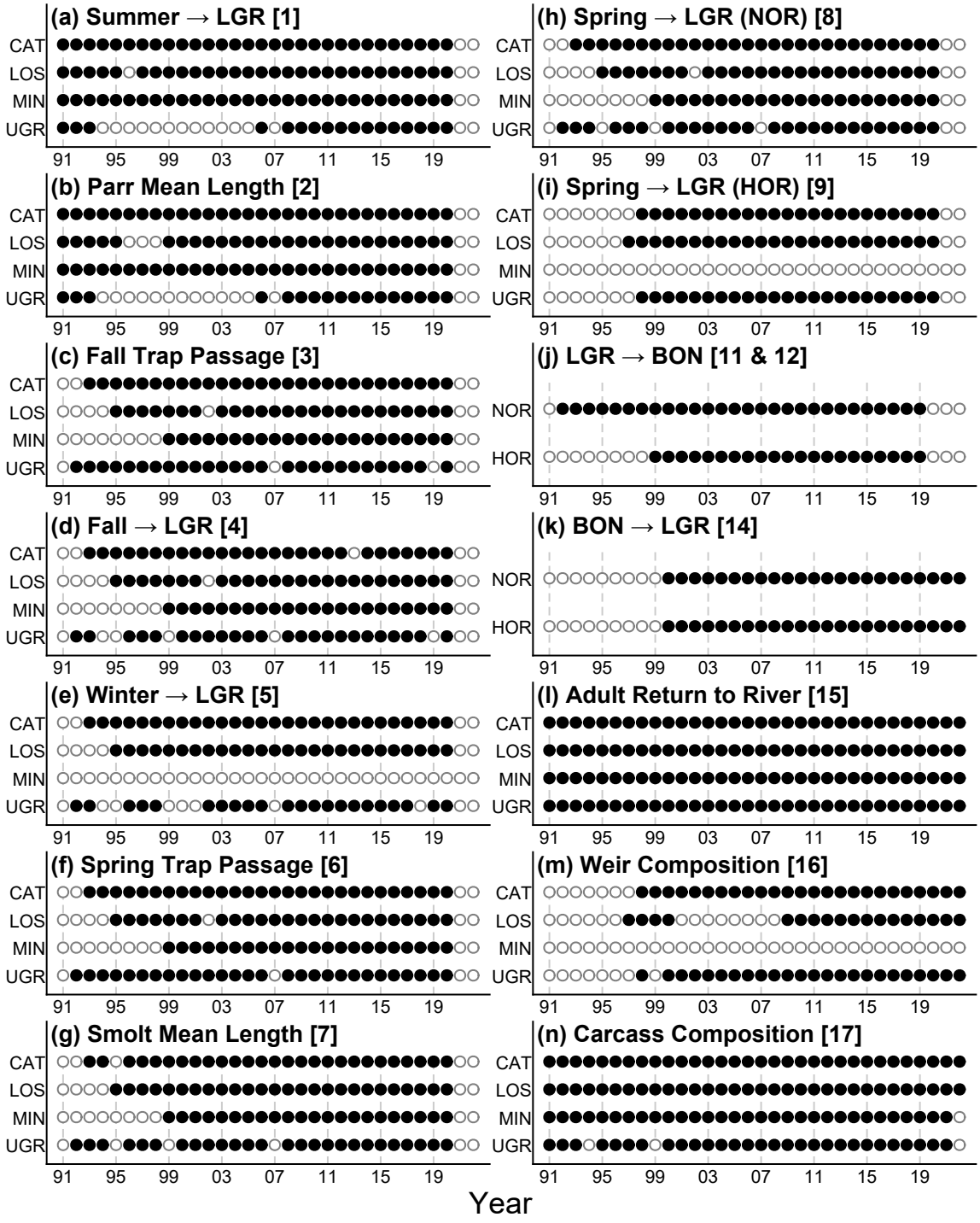

TABLE D1. Various indices and dimensional constants used in defining the structure and scope for the state-space life cycle model for Grande Ronde spring Chinook salmon.

Type	Symbol	Description
Indices	j	[1]Population; $j \in [\text{CAT}, \text{LOS}, \text{MIN}, \text{UGR}]$
	y	[2]Year; $y \in [1, \ldots, n_y]$
	k	[3]Age of maturation; $k \in [1, \ldots, n_k]$
	i	[4]Juvenile migratory strategy; $i \in [\text{fall}, \text{spring}]$
	o	[5]Origin type; either natural- or hatchery-origin; $o \in [\text{NOR}, \text{HOR}]$
	ko	[6]Unique age/origin combinations; $ko \in [1, \ldots, n_{ko}]$
	w	Number of winters spent at sea prior to maturation; $w \in [1, 2, 3]$
Scoping Constants	y_{min}	[2]First year modeled; equal to 1991 here; first brood year with juvenile data
	y_{max}	[2]Last year modeled; equal to 2022 here; last return year with adult data
	A_{min}	[3]Minimum total age of maturation; equal to 3 here
	A_{max}	[3]Maximum total age of maturation; equal to 5 here
Dimensional Constants	n_j	[1]Number of populations modeled; equal to 4 here
	n_y	[2]Number of years modeled; equal to 32 here
	n_k	[3]Number of ages at maturation modeled; equal to 3 here
	n_i	[4]Number of migratory strategies modeled; equal to 2 here
	n_o	[5]Number of origins modeled; equal to 2 here
	n_{ko}	[6]Number of unique age/origin combinations

[1] "Population" is used to distinguish among the tributaries within the Grande Ronde Basin with sufficient data to model complete life cycle population dynamics. Abbreviations are: Catherine Creek (CAT), Lostine River (LOS), Minam River (MIN), and Upper Grande Ronde River (UGR).

[2] "Year" refers to the year of spawning; for juvenile phases this is the year fish were spawned (i.e., brood year) and for adult phases this is the year of return (i.e., calendar year).

[3] "Age" refers to the total age, i.e., the number of winters experienced (including the winter spent as an egg). For example, eggs fertilized in brood year 2000 were age-0 until they hatched in spring of 2001 (age-1), migrated to sea in spring/summer of 2002 (age-2), and returned to spawn in one of 2003 (age-3), 2004 (age-4), or 2005 (age-5). $k = 1$ is the first age of maturation (age-3) and $k = 3$ is the last age of maturation (age-5).

[4] "Migratory strategy" refers to the timing of migration from headwaters rearing areas – either as fall (as age-1) or spring (age-2) migrants. Regardless, all fish make the out-of-basin migration at age-2.

[5] "Origin" refers to the rearing type: natural-origin (NOR) vs. hatchery-origin (HOR).

[6] Most quantities treat age (k) and origin (o) as two separate dimensions of a larger array. However, for fitting to compositional data by age and origin, we collapse these two dimensions into one. $ko \in [1, 2, 3]$ represents age-3, age-4, and age-5 for natural-origin fish, respectively, and $ko \in [4, 5, 6]$ represents these same ages for hatchery-origin fish, respectively.

TABLE D2. Symbology used to represent the key states (i.e., abundance at life stage/group) and rates (i.e., transition probabilities among states) in the presentation of the state-space life cycle model for Grande Ronde spring Chinook salmon. The majority of rates presented in this table are hierarchically structured/estimated, where the population- and/or origin-specific expected value and standard deviation are free parameters (or a function of free parameters) presented in Table D3. Equation numbers reference any equation that uses that quantity.

Type	Symbol	Eq(s).	Description
Freshwater Juvenile			
States	$E_{y,j}$	D4, D5, D8	Total egg production
	$P^{b}_{y,j}$	D8, D11, D26	Parr abundance at end of summer (*before* migratory strategy apportionment)
	$P^{a}_{y,i,j}$	D11, D13, D15, D27, D28	Parr abundance *after* migratory strategy apportionment
	$M^{b}_{y,i,o,j}$	D15, D21, D25	In-basin smolt abundance, immediately following over-winter mortality and *before* migration out of basin; hatchery-origin smolt releases introduced here
	$M^{a}_{y,i,o,j}$	D21, D23, D26, D27, D28, D29, D30	Smolt abundance at Lower Granite Dam *after* migration out of basin
	$L^{P^b}_{y,j}$	D10, D13, D16, D18, D32	Parr mean length at end of summer ($L^{*P^b}_{y,j}$ is scaled and centered on the observed time series $\hat{L}^{P^b}_{y,j}$)
	$L^{M^b}_{y,j}$	D18, D19, D33	Smolt mean length before migration out of basin ($L^{*M^b}_{y,j}$ is scaled and centered on the observed time series $\hat{L}^{M^b}_{y,j}$)
Rates	$\phi^{E\rightarrow P^b}_{y,j}$	D7, D8	Survival rate from egg to end of summer parr
	$\pi_{y,i,j}$	D11, D12	Proportion of parr at end of summer that have migratory strategy i
	$\phi^{P^a\rightarrow M^b}_{y,i,j}$	D14, D15	Over-winter survival from parr year to smolt year; i.e., to move from total age-1 to total age-2
	$\phi^{M^b\rightarrow M^a}_{y,i,o,j}$	D20, D21, D29, D30	Migration survival from within basin to Lower Granite Dam
	$\phi^{M^a\rightarrow O^0}_{y,o}$	D22, D23, D31	Migration survival downstream through hydrosystem to reach ocean

TABLE D2. Symbology used to represent the key states (i.e., abundance at life stage/group) and rates (i.e., transition probabilities among states) in the presentation of the state-space life cycle model for Grande Ronde spring Chinook salmon. The majority of rates presented in this table are hierarchically structured/estimated, where the population- and/or origin-specific expected value and standard deviation are free parameters (or a function of free parameters) presented in Table D3. Equation numbers reference any equation that uses that quantity. *(continued)*

Type	Symbol	Eq(s).	Description
Ocean			
States	$O^{w}_{y,o,j}$	D23, D37, D38	Abundance of ocean juveniles after experiencing w winter(s) at sea, where $w \in [0, 1, 2, 3]$
Rates	$\phi^{O^w \rightarrow O^{w+1}}_{y,o,j}$	D34, D35, D37	Survival of ocean juveniles from the end of winter w to the end of winter $w + 1$ at sea, where $w \in [0, 1, 2]$
	$\psi^{O^w}_{y,o,j}$	D36, D37, D38	Proportion of ocean juveniles alive at the end of winter w at sea that make spawning migration before winter $w + 1$, where $w \in [1, 2, 3]$
Freshwater Adult			
States	$R^{b}_{y,k,o,j}$	D38, D40	Abundance of adults (i.e., mature) arriving at the estuary (*before* upstream main-stem migration)
	$R^{a}_{y,k,o,j}$	D40, D41, D43, D45	Abundance of adults arriving at their natal tributary (*after* upstream main-stem migration)
	$G_{y,k,o,j}$	D40	Abundance of adult strays
	$B_{y,k,o,j}$	D41	Abundance of adults removed at weir, primarily for broodstock
	$H_{y,k,o,j}$	D41	Abundance of adults harvested within tributaries
	$S^{b}_{y,k,o,j}$	D41, D42	Abundance of adults following weir removals (e.g., for hatchery broodstock but *before* pre-spawn mortality)
	$S^{a}_{y,k,o,j}$	D4, D42, D50	Abundance of spawning adults *after* pre-spawn mortality
Rates	$U_{y,k,o}$	D40	Fishery harvest rate downstream of Bonneville Dam
	$\phi^{R^b \rightarrow R^a}_{y,o}$	D40, D44	Survival from all mortality sources during the migration between Bonneville Dam and arrival to natal tributaries
	$\phi^{S^b \rightarrow S^a}_{y,j}$	D42	Pre-spawn survival rate
	Ω_k	D4	Proportion of spawners that are female by age
	$f_{y,k,j}$	D4	Eggs per female spawner

TABLE D3. Free parameters (i.e., that have a prior that is not function of other free parameters) estimated by the state-space life cycle model for Grande Ronde spring Chinook salmon. Distributions and their parameterizations are defined in the footnotes.

Symbol	Prior[1,2,3,4,5,6]	Eq.	Description
Freshwater Juvenile			
α_j	$\mathrm{b}(2, 8)$	D5	Maximum expected egg-to-parr survival rate; Beverton-Holt productivity
σ_β	$\mathrm{U}(0, 5)$	D6	Among-population SD of parr capacity not explained by WUL_j
λ	$\mathrm{N}\left(0, 1 \times 10^{-8}\right)$	D6	Expected change in parr capacity per 1 km change in WUL_j; prior bounded by $(0, \infty)$
$\Sigma_{\phi_j^{E \to P^b}}$	$\mathrm{SIW}(0.30, 2)$	D7	Covariance matrix for egg-to-parr survival rate (white noise portion only); constructed of $\sigma_{\phi_j^{E \to P^b}}$ and $\rho_{\phi_{j,j'}^{E \to P^b}}$ following eq. D2
$\kappa_j^{E \to P^b}$	$\mathrm{U}(-1, 1)$	D7	Lag-1 autoregressive coefficient for egg-to-parr survival rate
$\omega_{0,j}$	$\mathrm{N}\left(0, 1 \times 10^{-3}\right)$	D9	Intercept of density-dependent parr size relationship
$\omega_{1,j}$	$\mathrm{N}\left(0, 1 \times 10^{-3}\right)$	D9	Slope of density-dependent parr size relationship
$\Sigma_{L^{P^b}}$	$\mathrm{SIW}(0.10, 2)$	D10	Covariance matrix for variability in parr mean length not explained by egg density; constructed of $\sigma_{L_j^{P^b}}$ and $\rho_{L_{j,j'}^{P^b}}$ following eq. D2
$\dot{\pi}_{i=\mathrm{fall},j}$	$\mathrm{b}(1, 1)$	D12	Expected proportion of summer parr that are fall migrants
$\Sigma_{\pi_{i=\mathrm{fall}}}$	$\mathrm{SIW}(0.30, 2)$	D12	Covariance matrix for variability in the proportion of summer parr that are fall migrants; constructed of $\sigma_{\pi_{i=\mathrm{fall},j}}$ and $\rho_{\pi_{i=\mathrm{fall},j,j'}}$ following eq. D2
$\phi_j^{P^b \to P^a}$	$\mathrm{b}(1, 1)$	D28	Survival from summer tagging to winter tagging for summer parr that are spring migrants
$\gamma_{0,i,j}$	$\mathrm{t}\left(0, 1.57^{-2}, 7.76\right)$	D13	Intercept of over-winter survival vs. parr size relationship
$\gamma_{1,j}$	$\mathrm{t}\left(0, 1.57^{-2}, 7.76\right)$	D13	Slope of over-winter survival vs. parr size relationship
$\Sigma_{\phi^{P^a \to M^b}}$	$\mathrm{SIW}(0.30, 2)$	D14	Covariance matrix for variability in over-winter survival not explained by parr mean length; constructed of $\sigma_{\phi_j^{P^a \to M^b}}$ and $\rho_{\phi_{j,j'}^{P^a \to M^b}}$ following eq. D2
$\theta_{0,j}$	$\mathrm{N}\left(0, 1 \times 10^{-3}\right)$	D16	Intercept of change in parr to smolt mean length vs. parr mean length relationship

TABLE D3. Free parameters (i.e., that have a prior that is not function of other free parameters) estimated by the state-space life cycle model for Grande Ronde spring Chinook salmon. Distributions and their parameterizations are defined in the footnotes. *(continued)*

Symbol	Prior[1,2,3,4,5,6]	Eq.	Description
$\theta_{1,j}$	$\mathrm{N}(0, 1 \times 10^{-3})$	D16	Slope of change in parr to smolt mean length vs. parr mean length relationship
$\Sigma_{\Delta^{L^{Pb}\to L^{Mb}}}$	SIW(0.15, 2)	D17	Covariance matrix for variability in the change in mean length from parr to smolt not explained by parr mean length; constructed of $\sigma_{\Delta_j^{L^{Pb}\to L^{Mb}}}$ and $\rho_{\Delta_{j,j'}^{L^{Pb}\to L^{Mb}}}$ following eq. D2
$\tau_{0,j}$	$\mathrm{t}(0, 1.57^{-2}, 7.76)$	D19	Intercept of smolt migration survival to LGR vs. smolt mean length relationship
$\tau_{1,j}$	$\mathrm{t}(0, 1.57^{-2}, 7.76)$	D19	Slope of smolt migration survival to LGR vs. smolt mean length relationship
$\Sigma_{\phi^{M^b\to M^a}}$	SIW(0.30, 2)	D20	Covariance matrix for variability in smolt migration survival to LGR not explained by smolt mean length; constructed of $\sigma_{\phi_j^{M^b\to M^a}}$ and $\rho_{\phi_{j,j'}^{M^b\to M^a}}$ following eq. D2
$\dot{\phi}_o^{M^a\to O^0}$	b(1, 1)	D22	Expected migration survival from LGR to ocean
$\Sigma_{\phi^{M^a\to O^0}}$	SIW(0.30, 2)	D22	Covariance matrix for variability in smolt migration survival from LGR to ocean; constructed of $\sigma_{\phi_o^{M^a\to O^0}}$ and $\rho_{\phi^{M^a\to O^0}}$ following eq. D3
Ocean			
$\dot{\phi}_{o=\mathrm{NOR},j}^{O^0\to O^1}$	b(1, 9)	D34	Expected first year ocean survival for natural origin fish
$\Sigma_{\phi^{O^0\to O^1}}$	SIW(0.30, 2)	D34	Covariance matrix for variability in first year ocean survival (white noise portion only); constructed of $\sigma_{\phi_j^{O^0\to O^1}}$ and $\rho_{\phi_{j,j'}^{O^0\to O^1}}$ following eq. D2
$\kappa_j^{O^0\to O^1}$	U(−1, 1)	D34	Lag-1 autoregressive coefficient for first year ocean survival
$\dot{\phi}_{o=\mathrm{NOR},j}^{O^1\to O^2}$	b(60, 40)		Expected second year ocean survival for natural origin fish
$\dot{\phi}_{o=\mathrm{NOR},j}^{O^2\to O^3}$	b(70, 30)		Expected third year ocean survival for natural origin fish

TABLE D3. Free parameters (i.e., that have a prior that is not function of other free parameters) estimated by the state-space life cycle model for Grande Ronde spring Chinook salmon. Distributions and their parameterizations are defined in the footnotes. *(continued)*

Symbol	Prior[1,2,3,4,5,6]	Eq.	Description
δ_j	$\mathrm{t}(0, 1.57^{-2}, 7.76)$	D35	Log-odds ratio to convert natural origin to hatchery origin ocean survival
$\dot{\psi}^{O^1}_{o,j}$	$\mathrm{b}(1, 9)$	D36	Expected maturation rate after $w = 1$ winter at sea
$\dot{\psi}^{O^2}_{o,j}$	$\mathrm{b}(8.5, 1.5)$	D36	Expected maturation rate after $w = 2$ winters at sea
$\Sigma_{\psi^{O^1}}$	$\mathrm{SIW}(0.15, 2)$	D36	Covariance matrix for variability in maturation rate after $w = 1$ winter at sea; constructed of $\sigma_{\psi^{O^1}_j}$ and $\rho_{\psi^{O^1}_{j,j'}}$ following eq. D2
$\Sigma_{\psi^{O^2}}$	$\mathrm{SIW}(0.30, 2)$	D36	Covariance matrix for variability in maturation rate after $w = 2$ winters at sea; constructed of $\sigma_{\psi^{O^2}_j}$ and $\rho_{\psi^{O^2}_{j,j'}}$ following eq. D2
Freshwater Adult			
$R^b_{y,k=1,y,o,j}$	$\mathrm{U}(0, 50)$		Return abundance of natural-origin age-3 fish in years without process model link; only for $y \in [1, 2, 3]$ and o = NOR
$R^b_{y,k=2,y,o,j}$	$\mathrm{U}(0, 200)$		Return abundance of natural-origin age-4 fish in years without process model link; only for $y \in [1, 2, 3, 4]$ and o = NOR
$R^b_{y,k=3,y,o,j}$	$\mathrm{U}(0, 200)$		Return abundance of natural-origin age-5 fish in years without process model link; only for $y \in [1, 2, 3, 4, 5]$ and o = NOR
$\dot{\phi}^{R^b \to R^a}_o$	$\mathrm{b}(1, 1)$	D39	Expected adult migration survival from BON to LGR
$\Sigma_{\phi^{R^b \to R^a}}$	$\mathrm{SIW}(0.30, 2)$	D40	Covariance matrix for variability in migration survival from BON to LGR; constructed of $\sigma_{\phi^{R^b \to R^a}_o}$ and $\rho_{\phi^{R^b \to R^a}}$ following eq. D3
$G_{y,o,j}$	$\mathrm{U}(0, 500)$	D40	Total hatchery-origin "strays"; only for o = HOR and y where presence of HOR adults could not be explained by non-zero smolt releases
$p^G_{k,j}$	$\mathrm{D}(1, 1, 1)$	D40	Age composition of hatchery-origin "strays"
$\dot{z}_k$	$\mathrm{U}(-10, 10)$	D47	Across-population expected coefficient of log-linear carcass composition correction model; only for $k \in [1, 3]$

σ_{z_k}	U(0, 5)	D47	Across-population SD for coefficients of log-linear carcass composition correction model; only for $k \in [1, 3]$

Prior Distribution Parameterizations in Table D3

[1] Beta Distribution: $\mathrm{b}(\mathrm{shape}_1, \mathrm{shape}_2)$

[2] Normal Distribution: N(mean, precision)

[3] Uniform Distribution: U(lower, upper)

[4] t-Distribution: t(mean, precision, degrees of freedom); this specific $\mathrm{t}(0, 1.57^{-2}, 7.76)$ prior results in approximately a U(0, 1) prior after inverse-logit transformation (Dorazio et al. 2011).

[5] Dirichlet Distribution: $\mathrm{D}(\mathrm{shape}_1, \mathrm{shape}_2, \mathrm{shape}_3)$

[6] Scaled Inverse-Wishart Distribution: SIW($\mathbf{S}$, degrees of freedom); $\mathbf{S}$ is a vector of scale parameters for scaled-Wishart; see Plummer (2017) page 62 for details on this prior. Briefly, the scale parameters of 0.10 - 0.30 places higher prior weight on small values of the component σ parameters, which was intentional because these represent variability on the log- or logit-scale. Setting the degrees of freedom to 2 results in a U$(-1, 1)$ prior on the ρ components.

TABLE D4. Symbology used to represent the data sources in the presentation of observation model components of the state-space life cycle model for Grande Ronde spring Chinook salmon. All data sources listed here have an explicit likelihood component and were thus assumed to be observed with error.

Type	Symbol	Eq.	Description
Freshwater Juvenile			
Abundance	$\hat{P}^{a}_{y,i=\text{fall},j}$	D24	Estimated smolt trap passage of parr in the fall
	$\hat{\sigma}_{P^{a}_{y,i=\text{fall},j}}$	D24	Log-normal SE of estimated smolt trap passage of parr in the fall
	$\hat{M}^{b}_{y,i=\text{spring},o=\text{NOR},j}$	D25	Estimated smolt trap passage of smolt in the spring
	$\hat{\sigma}_{M^{b}_{y,i=\text{spring},o=\text{NOR},j}}$	D25	Log-normal SE of estimated smolt trap passage of smolt in the spring
Survival	$\hat{\phi}^{P^{b}\rightarrow M^{a}}_{y,j}$	D26	Estimated survival from summer tagging to LGR
	$\hat{\sigma}_{\phi^{P^{b}\rightarrow M^{a}}_{y,j}}$	D26	Logit-normal SE of estimated survival from summer tagging to LGR
	$\hat{\phi}^{P^{a}\rightarrow M^{a}}_{y,i=\text{fall},j}$	D27	Estimated survival from fall tagging to LGR
	$\hat{\sigma}_{\phi^{P^{a}\rightarrow M^{a}}_{y,i=\text{fall},j}}$	D27	Logit-normal SE of estimated survival from fall tagging to LGR
	$\hat{\phi}^{P^{a}\rightarrow M^{a}}_{y,i=\text{spring},j}$	D28	Estimated survival from winter tagging to LGR
	$\hat{\sigma}_{\phi^{P^{a}\rightarrow M^{a}}_{y,i=\text{spring},j}}$	D28	Logit-normal SE of estimated survival from winter tagging to LGR
	$\hat{\phi}^{M^{b}\rightarrow M^{a}}_{y,i=\text{spring},o=\text{NOR},j}$	D29	Estimated survival from spring tagging to LGR
	$\hat{\sigma}_{\phi^{M^{b}\rightarrow M^{a}}_{y,i=\text{spring},o=\text{NOR},j}}$	D29	Logit-normal SE of estimated survival from spring tagging to LGR
	$\hat{\phi}^{M^{b}\rightarrow M^{a}}_{y,i=\text{spring},o=\text{HOR},j}$	D30	Estimated survival of hatchery-origin smolt releases to LGR
	$\hat{\sigma}_{\phi^{M^{b}\rightarrow M^{a}}_{y,i=\text{spring},o=\text{HOR},j}}$	D30	Logit-normal SE of estimated survival of hatchery-origin smolt releases to LGR
	$\hat{\phi}^{M^{a}\rightarrow O^{0}}_{y,o}$	D31	Estimated aggregate survival of smolt through hydrosystem
	$\hat{\sigma}_{\phi^{M^{a}\rightarrow O^{0}}_{y,o}}$	D31	Logit-normal SE of estimated aggregate survival of smolt through hydrosystem
	$\hat{L}^{P^{b}}_{y,j}$	D32	Estimated parr mean length (mm fork length) at summer tagging
	$\hat{\sigma}_{L^{P^{b}}_{y,j}}$	D32	Log-normal SE of estimated parr mean length at summer tagging

TABLE D4. Symbology used to represent the data sources in the presentation of observation model components of the state-space life cycle model for Grande Ronde spring Chinook salmon. All data sources listed here have an explicit likelihood component and were thus assumed to be observed with error. *(continued)*

Type	Symbol	Eq.	Description
Length	$\hat{L}_{y,j}^{M^b}$	D33	Estimated smolt mean length (mm fork length) at spring tagging
	$\hat{\sigma}_{L_{y,j}^{M^b}}$	D33	Log-normal SE of estimated smolt mean length at spring tagging
Freshwater Adult			
Abundance	$\hat{R}_{y,j}^{a}$	D43	Estimated total adult return to tributary (all ages/origins)
	$\hat{\sigma}_{R_{y,j}^{a}}$	D43	Log-normal SE of estimated total adult return to tributary
Survival	$\hat{x}_{y,o}^{\text{BON}}$	D44	Count of Grande Ronde-origin PIT-tagged adults detected at BON
	$\hat{x}_{y,o}^{\text{LGR}}$	D44	Count of Grande Ronde-origin PIT-tagged adults detected at LGR
Composition	$\hat{x}_{y,ko,j}^{R^a}$	D46	Count of sampled adults returning to tributary by age/origin; only for $j \in [\text{CAT}, \text{LOS}, \text{UGR}]$
	$\hat{x}_{y,ko,j}^{S^{a'}}$	D51	Count of sampled carcasses by age/origin

TABLE D5. Catalog of all equations presented, separated by life phase (freshwater juvenile, ocean, or freshwater adult) and model component (process model or observation model).

Model	Eq.	Description
Generic		
	D1	Syntax for quantities assumed to follow a multivariate logit-normal distribution
	D2	Covariance structure for quantities that vary across populations
Syntax	D3	Covariance structure for quantities that vary across origins, not populations
Freshwater Juvenile		
	D4	Obtain total egg production
	D5	Obtain expected egg-to-parr survival as a function of egg density
	D6	Obtain parr capacity as a function of weighted usable habitat length
	D7	Add stochasticity to egg-to-parr survival
	D8	Obtain total parr recruitment
	D9	Obtain expected parr mean length as a function of egg density
	D10	Add stochasticity to parr mean length
	D11	Obtain migratory strategy-specific parr abundance
	D12	Add stochasticity to migratory strategy apportionment rates
	D13	Obtain expected over-winter survival; related to parr mean length
	D14	Add stochasticity to over-winter survival
	D15	Obtain natural-origin smolt abundance prior to out-of-basin migration
	D16	Obtain expected multiplicative change in mean length from parr to smolt
	D17	Add stochasticity to multiplicative change in mean length from parr to smolt
	D18	Obtain smolt mean length
	D19	Obtain expected migration survival from in-basin to LGR
	D20	Add stochasticity to migration survival from in-basin to LGR
	D21	Obtain smolt abundance at LGR
	D22	Add stochasticity to migration survival from LGR to ocean
Process	D23	Obtain initial abundance of ocean juveniles
	D24	Assumption for fall screw trap count data likelihood
	D25	Assumption for spring screw trap count data likelihood
	D26	Assumption for summer tagging event survival data likelihood
	D27	Assumption for fall tagging event survival data likelihood
	D28	Assumption for winter tagging event survival data likelihood
	D29	Assumption for spring tagging event survival data likelihood (NOR)
	D30	Assumption for spring tagging event survival data likelihood (HOR)
	D31	Assumption for migration through hydrosystem survival data likelihood
	D32	Assumption for parr mean length data likelihood
Observation	D33	Assumption for smolt mean length data likelihood
Ocean		

TABLE D5. Catalog of all equations presented, separated by life phase (freshwater juvenile, ocean, or freshwater adult) and model component (process model or observation model). *(continued)*

Model	Eq.	Description
	D34	Add stochasticity to first year ocean survival
	D35	Obtain HOR ocean survival
	D36	Add stochasticity to maturation rates
	D37	Obtain abundance of ocean juveniles by ocean age
	D38	Obtain return abundance of adults by total age
Freshwater Adult		
	D39	Add stochasticity to migration survival from BON to LGR
	D40	Obtain return abundance to natal tributary
	D41	Obtain abundance of potential spawners reaching spawning grounds
Process	D42	Obtain abundance of successful spawners
	D43	Assumption for natal tributary return abundance data likelihood
	D44	Assumption for migration from BON to LGR survival data likelihood
	D45	Obtain expected composition by age and origin of adults counted at weirs
	D46	Assumption for age and origin composition at weir data likelihood
	D47	Add stochasticity to carcass composition correction factor coefficients
	D48	Obtain correction factors for populations with weir and carcass data
	D49	Obtain correction factors for population with carcass composition data only
	D50	Obtain expected composition by age and origin of carcasses
Observation	D51	Assumption for age and origin carcass composition data likelihood

TABLE D6. Year of return based on age of return and brood year. For example, adults that were progeny of spawners in 2000 (their brood year) returned to spawn in 2003 as age-3, 2004 as age-4, and 2005 as age-5 (shown in blue). The return years with red brood years show the age-specific return abundances that were estimated because no previous states (e.g., parr, smolt) were available for these early brood years (see Section D3.1.3 for more details).

	Brood Year of Returning Adults by Age		
Return Year	**Age-3**	**Age-4**	**Age-5**
1991	1988	1987	1986
1992	1989	1988	1987
1993	1990	1989	1988
1994	1991	1990	1989
1995	1992	1991	1990
1996	1993	1992	1991
⋮	⋮	⋮	⋮
2003	2000	1999	1998
2004	2001	2000	1999
2005	2002	2001	2000
⋮	⋮	⋮	⋮
2022	2019	2018	2017

Derivation of Weighted Usable Habitat Length

We analyzed local empirical estimates of Chinook salmon parr abundance and physical habitat to provide an index of available habitat quantity and quality that was used to scale density-dependent parr capacity and growth functions in the state-space model and provide a means for evaluating impacts of restoration and climate change scenarios in forthcoming prospective models. Specifically, we used paired snorkel and habitat survey data collected via multiple visits to 121 sites in the Upper Grande Ronde and Minam River basins in NE Oregon between 2011 and 2017, totaling 294 unique site-year observations. A detailed description of this analysis is provided in (Justice et al. 2021).

Snorkel surveys were used to count Chinook salmon parr during summer (July 1 – September 15) at each site using methods described in White et al. (2012) and physical habitat data was collected using the Columbia Habitat Monitoring Program protocol (CHaMP 2016). We expanded snorkel counts to abundance estimates using a detection probability model informed by local paired snorkel counts and mark-recapture abundance data (Staton et al. 2021).

We selected a limited set of environmental covariates representing *a priori* hypotheses about the ecological processes influencing Chinook salmon parr abundance. In-stream habitat covariates included pool frequency, large wood frequency (log-transformed), river complexity index, and maximum weekly maximum water temperature. Population-level spawner abundance during the prior year (standardized to mean 0 and SD of 1) was included account for effects of adult run size on juvenile abundance. We used an indicator variable (1 or 0) to denote whether the site was within the current Chinook salmon spawning extent and to account for excessive zeros in non-natal rearing habitats. Mean summer flow (log transformed) and gradient (and its quadratic term) were used to capture variation in fish abundance related to intrinsic channel characteristics.

The count of juvenile Chinook salmon per 100 meters for each observation was modeled using a zero-inflated negative binomial mixed-effects model, with random effects for site and year. We used a negative binomial model to account for high among-observation variability and the zero-inflated component was required to accommodate excessive zero counts. We fitted an initial "global model" using the full set of fixed effect covariates and random effects. We then generated a set of candidate models consisting of all subsets of the fixed-effect covariates from the global model with random effects for site and year held fixed for all models. We used Akaike's Information Criterion (AIC_c) to select the best fitting model and assessed model goodness-of-fit using residual diagnostic plots generated with the 'DHARMa' package (Hartig 2022).

We used the best fitting model to make spatially continuous predictions of fish density across all Chinook salmon-bearing stream reaches within each study population using the National Hydrography Dataset (NHD) high resolution (1:24K) stream layer as the basis for reach designations

and the most current habitat measurements as covariates. We set annual spawner abundance to 2 standard deviations above the mean to reflect expected juvenile densities under high seeding levels (i.e., approximating carrying capacity).

To translate predicted fish densities into an index of habitat suitability, we calculated a weight for each stream reach (W_i) scaled between 0 and 1 by dividing the predicted parr density in each reach (μ_i; vector of values across all reaches: $\boldsymbol{\mu}$) by the maximum predicted parr density ($W_i = \mu_i / \max(\boldsymbol{\mu})$). Then we calculated weighted usable length for each population (WUL_j) as the sum-product of reach-specific weights and lengths ($\text{WUL}_j = \sum_{i=1}^{n_{\text{reaches}}} W_i \times \text{Length}_i$). Our use of WUL rather than the more commonly used weighted usable area (Bovee 1982; Maret et al. 2006) accounts for the observation that Chinook salmon parr use either shoreline or thalweg areas which are more linear stream features, rather than being uniformly dispersed across the stream channel, and better fit to data of fish density to stream length vs. stream area.